NASA CR-72341
PWA FR-2552

INTERIM REPORT

SPACE STORABLE REGENERATIVE COOLING INVESTIGATION

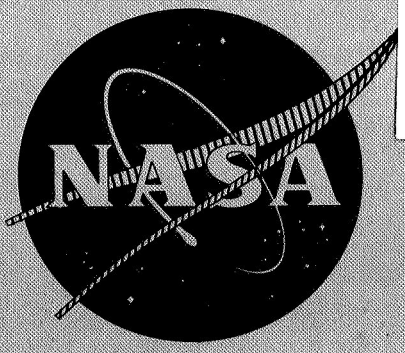
GPO PRICE $ _____

CFSTI PRICE(S) $ _____

Hard copy (HC) 3.00

Microfiche (MF) .65

ff 653 July 65



Prepared for

NATIONAL AERONAUTICS AND SPACE ADMINISTRATION

CONTRACT NAS3-11190

FACILITY FORM 602

N68-29458 (ACCESSION NUMBER)

231 (PAGES)

CR-72341 (NASA CR OR TMX OR AD NUMBER)

(THRU) 1

(CODE) 27

(CATEGORY)

AUG 1968
RECEIVED
NASA STI FACILITY
INPUT BRANCH

Pratt & Whitney Aircraft DIVISION OF UNITED AIRCRAFT CORPORATION
FLORIDA RESEARCH AND DEVELOPMENT CENTER
BOX 2691, WEST PALM BEACH, FLORIDA 33402

Printed in the United States of America

NOTICE

This report was prepared as an account of Government sponsored work. Neither the United States, nor the National Aeronautics and Space Administration (NASA), nor any person acting on behalf of NASA:

A.) Makes any warranty or representation, expressed or implied, with respect to the accuracy, completeness, or usefulness of the information contained in this report, or that the use of any information, apparatus, method, or process disclosed in this report may not infringe privately owned rights; or

B.) Assumes any liabilities with respect to the use of, or for damages resulting from the use of any information, apparatus, method or process disclosed in this report.

As used above, "person acting on behalf of NASA" includes any employee or contractor of NASA, or employee of such contractor, to the extent that such employee or contractor of NASA, or employee of such contractor prepares, disseminates, or provides access to, any information pursuant to his employment or contract with NASA, or his employment with such contractor.

Requests for copies of this report should be referred to

National Aeronautics and Space Administration
Office of Scientific and Technical Information
Attention: AFSS-A
Washington, D.C. 20546

NASA CR-72341
PWA FR-2552

INTERIM REPORT

SPACE STORABLE REGENERATIVE COOLING INVESTIGATION

Prepared for
NATIONAL AERONAUTICS AND SPACE ADMINISTRATION
CONTRACT NAS3-11190
26 JULY 1968

PRATT & WHITNEY AIRCRAFT
PROGRAM MANAGER
J.P. MITCHELL

TECHNICAL MANAGEMENT
JOHN W. GREGORY
LIQUID ROCKET TECHNOLOGY BRANCH
NASA LEWIS RESEARCH CENTER
CLEVELAND, OHIO

Pratt & Whitney Aircraft DIVISION OF UNITED AIRCRAFT CORPORATION
FLORIDA RESEARCH AND DEVELOPMENT CENTER
BOX 2691, WEST PALM BEACH, FLORIDA 33402

Printed in the United States of America

FOREWORD

This report was prepared by the Pratt & Whitney Aircraft Division of United Aircraft Corporation under Contract NAS3-11190, which is sponsored by the NASA Lewis Research Center. The NASA project manager is Mr. J. W. Gregory.

This is an interim report covering the results obtained under Task I of the contract. The period of performance was 1 July to 30 September 1967.

The following personnel at the Pratt & Whitney Aircraft Research and Development Center contributed to the technical effort and preparation of the report: W. R. Kaminski, J. Neal, D. J. Stout, M. L. Johnson, D. L. Elmore, T. M. Rhodes, J. Quinn, T. E. Bailey and J. P. Mitchell.

PRECEDING PAGE BLANK NOT FILMED.

ABSTRACT

An analytical study was made to evaluate the regenerative cooling capabilities of light hydrocarbon fuels when used with fluorinated oxidizers. Regenerative cooling feasibility limits for methane, a methane-ethane blend, ethane, propane, and butene-1 were established based on the thermodynamic heat capacities of the fuels and overall thrust chamber heat transfer rates over the 1000- to 20,000-lb thrust range and the 100- to 1000-psia chamber pressure range. Subsequently, regenerative cooling limits for selected propellant combinations at thrust levels of 1000, 5000, and 20,000 lb were examined in more detail with consideration of coolant passage design and local chamber heat fluxes.

PRECEDING PAGE BLANK NOT FILMED.

CONTENTS

SECTION		PAGE
	ILLUSTRATIONS	ix
	NOMENCLATURE	xv
I	INTRODUCTION	1
II	SUMMARY	5
III	CONCLUSIONS AND RECOMMENDATION	13
	A. Conclusions	13
	B. Recommendation	14
IV	FEASIBILITY STUDY	15
	A. Approach	15
	B. Regenerative Cooling Limits	39
	C. Summary of Results	51
V	DETAILED HEAT TRANSFER STUDY	55
	A. Approach	55
	B. Regenerative Cooling Chamber Pressure Limits	68
	C. Summary of Results	98
VI	ENGINE CYCLE STUDIES	103
	A. Introduction	103
	B. Turbo-Expander Cycle	103
	C. Gas Generator Cycle	105
	D. Performance Comparison	108
VII	REFERENCES	111
	APPENDIX A - Thermal Skin$_{TM}$ Chambers	A-1
	APPENDIX B - Heat Transfer Reduction Due To Carbon Deposition On Chamber Walls	B-1
	APPENDIX C - Thermal Decomposition of Fuels	C-1
	APPENDIX D - Feasibility Study - Method of Analysis	D-1
	APPENDIX E - Detailed Heat Transfer Study - Method of Analysis	E-1
	APPENDIX F - Fuel Thermodynamic and Transport Properties	F-1
	APPENDIX G - Theoretical Performance Curves	G-1
	APPENDIX H - Distribution List for Interim Report NASA CR-72341 Contract NAS3-11190	H-1

PRECEDING PAGE BLANK NOT FILMED.

ILLUSTRATIONS

FIGURE		PAGE
1	Effect of Fuel Hydrogen-To-Carbon Ratio on Total Engine Heat Transfer.	17
2	Variation in Combustion Chamber Fuel Enthalpy Rise With Thrust and Chamber Contraction Ratio	18
3	Variation in Nozzle Fuel Enthalpy Rise With Thrust and Nozzle Expansion Ratio.	18
4	Variation of Wall Temperature Correction Factor With Chamber Pressure for Chamber Fuel Enthalpy Rise	19
5	Variation of Wall Temperature Correction Factor With Chamber Pressure for Nozzle Fuel Enthalpy Rise.	19
6	Variation of Fuel Type Correction Factor With Propellant Mixture Ratio for Fuel Enthalpy Rise . . .	20
7	Variation of Fuel Type Correction Factor With Propellant Mixture Ratio for Fuel Enthalpy Rise . . .	20
8	Enthalpy - Temperature Diagram for Methane.	23
9	Enthalpy - Temperature Diagram for 55% Methane - 45% Ethane.	24
10	Enthalpy - Temperature Diagram for Ethane	25
11	Enthalpy - Temperature Diagram for Propane.	26
12	Enthalpy - Temperature Diagram for Butene-1	27
13	Determination of Enthalpy Rise From Basic Curves. . .	28
14	Coolant Outlet State for Methane With Flox as a Function of Chamber Pressure, Thrust, and Mixture Ratio	29
15	Coolant Outlet State for 55% Methane - 45% Ethane With Flox as a Function of Chamber Pressure, Thrust, and Mixture Ratio	30
16	Coolant Outlet State for Ethane With Flox as a Function of Chamber Pressure, Thrust, and Mixture Ratio	31
17	Coolant Outlet State for Propane With Flox as a Function of Chamber Pressure, Thrust, and Mixture Ratio	32
18	Coolant Outlet State for Butene-1 With Flox as a Function of Chamber Pressure, Thrust, and Mixture Ratio	33
19	Coolant Outlet State for Methane With OF_2 as a Function of Chamber Pressure, Thrust, and Mixture Ratio	34

ILLUSTRATIONS (Continued)

FIGURE		PAGE
20	Coolant Outlet State for 55% Methane - 45% Ethane With OF_2 as a Function of Chamber Pressure, Thrust, and Mixture Ratio.	35
21	Coolant Outlet State for Ethane With OF_2 as a Function of Chamber Pressure, Thrust, and Mixture Ratio.	36
22	Coolant Outlet State for Propane With OF_2 as a Function of Chamber Pressure, Thrust, and Mixture Ratio.	37
23	Coolant Outlet State for Butene-1 With OF_2 as a Function of Chamber Pressure, Thrust, and Mixture Ratio.	38
24	Feasibility Study Results - Chamber Pressure Regenerative Cooling Limits vs Wall Temperature. . . .	43
25	Feasibility Study Results - Chamber Pressure Regenerative Cooling Limits vs Mixture Ratio	43
26	Feasibility Study Results - Chamber Pressure Regenerative Cooling Limits vs Expansion Ratio	44
27	Feasibility Study Results - Chamber Pressure Regenerative Cooling Limits vs Contraction Ratio . . .	44
28	Feasibility Study Results - Chamber Pressure Regenerative Cooling Limits as a Function of Thrust for Q_m/Q_p = Average	45
29	Feasibility Study Results - Chamber Pressure Regenerative Cooling Limits as a Function of Thrust for Q_m/Q_p = 1.0	46
30	Feasibility Study Results - Minimum Chamber Pressure Regenerative Cooling Limits With Flox for Subcritical Coolant Pressures.	48
31	Feasibility Study Results - Minimum Chamber Pressure Regenerative Cooling Limits With OF_2 for Subcritical Coolant Pressures.	49
32	Feasibility Study Regenerative Cooling Limits: P_{out}/P_c = 2.0, Q_m/Q_p = Average	52
33	Feasibility Study - Regenerative Cooling Limits: ϵ_c = 4, ϵ_e = 100, T_w = 1700°F, r = Optimum, Q_m/Q_p = Average.	53
34	Thermal $Skin_{TM}$ Passage Dimensions.	61
35	Variation in Coolant Passage Width at Throat and Injector: Flox/Methane, 1000-lb Thrust	64

ILLUSTRATIONS (Continued)

FIGURE		PAGE
36	Variation in Coolant Passage Width at Throat and Injector: Flox/Methane, 5000-lb Thrust.	65
37	Variation in Coolant Passage Width at Throat and Injector: Flox/Methane, 20,000-lb Thrust.	66
38	Coolant Passage Geometry and Pressure Drop Iteration	67
39	Procedure Used to Determine Chamber Pressure Limit for Supercritical Coolant Pressures	67
40	Variation of Regenerative Cooling Chamber Pressure Limits With Thrust: Flox/Methane.	73
41	Regenerative Cooling Chamber Pressure Limits: Flox/Methane 1000-lb Thrust	74
42	Regenerative Cooling Chamber Pressure Limits: Flox/Methane, 5000-lb Thrust.	75
43	Regenerative Cooling Chamber Pressure Limits: Flox/Methane, 20,000-lb Thrust.	75
44	Throat Heat Flux at the Upper Chamber Pressure Limit for Regenerative Cooling.	76
45	Regenerative Cooling Chamber Pressure Limits: OF_2/55% Methane-45% Ethane, 5000-lb Thrust.	77
46	Throat Station Heat Flux Comparison	79
47	Regenerative Cooling Study Results for 1000-lb Thrust, OF_2/Butene-1 Thrust Chamber	79
48	Regenerative Cooling Study Results for a 1000-lb Thrust, OF_2/Butene-1, Thermal Barrier Coated Chamber	81
49	Effect of Heat Reduction Factor on Regenerative Cooling Chamber Pressure Limits	82
50	Effect of Chamber Contraction Ratio on Regenerative Cooling Chamber Pressure Limits	82
51	Effect of Cycle Considerations (P_{in}/P_c) on Regenerative Cooling Chamber Pressure Limits.	83
52	Effect of L* on Regenerative Cooling Chamber Pressure Limits	84
53	Variation of Combustion-Side Wall Temperature With Chamber Location	85
54	Coolant Passage Pressure Drop Comparison for Optimized and Unoptimized Coolant Passage Configurations.	86

ILLUSTRATIONS (Continued)

FIGURE		PAGE
55	Increased Chamber Pressure With Fabrication Improvements	87
56	Wall Temperature Profile for Various Thermal Skin Channel Designs	89
57	Required Coolant Pressure Drop at P_c = 1000 psia.	90
58	Variation in Thrust and Cooling Jacket Pressure Drop With Chamber Pressure for a Fixed Thrust Chamber Configuration: Flox/Methane	92
59	Variation in Throat Wall and Coolant Discharge Temperatures With Chamber Pressure for a Fixed Thrust Chamber Configuration: Flox/Methane	92
60	Variation in Thrust and Cooling Jacket Pressure Drop With Chamber Pressure for a Fixed Thrust Chamber Configuration: OF_2/55% Methane - 45% Ethane	93
61	Variation in Throat Wall and Coolant Discharge Temperatures With Chamber Pressure for a Fixed Thrust Chamber Configuration: OF_2/55% Methane - 45% Ethane	93
62	Variation in Thrust and Cooling Jacket Pressure Drop With Chamber Pressure for a Fixed Thrust Chamber Configuration: OF_2/Propane.	94
63	Variation in Throat Wall and Coolant Discharge Temperatures With Chamber Pressure for a Fixed Thrust Chamber Configuration: OF_2/Propane.	94
64	Comparison of Actual Throat and Maximum Nucleate Boiling Heat Fluxes: OF_2/Butene-1	97
65	Comparison of Actual Throat and Maximum Nucleate Boiling Heat Fluxes: OF_2/Propane.	97
66	Regenerative Cooling Limits at 1000-lb Thrust for Flox/Methane and OF_2/Butene-1	98
67	Regenerative Cooling Limits at 5000-lb Thrust for Flox/Methane and OF_2/55% Methane - 45% Ethane	99
68	Regenerative Cooling Limits at 20,000-lb Thrust for Flox/Methane and OF_2/Propane.	99
69	Regenerative Cooling Limits for Q_m/Q_p = 1, Flox/Methane and OF_2/55% Methane - 45% Ethane.	100
70	Permissible Regenerative Cooling Region for Flox/Methane.	100
71	Turbo-Expander Schematic.	104
72	Effect of Heat Transfer On Expander Cycle Limit	105
73	Gas Generator Schematic	106

ILLUSTRATIONS (Continued)

FIGURE		PAGE
74	Variation in Impulse Loss With Chamber Pressure for Gas Generator Cycles at Average Q_m/Q_p.	107
75	Variation in Impulse Loss With Chamber Pressure for Gas Generator Cycles at Q_m/Q_p = 1.0.	107
76	Theoretical Performance Comparison of 5K Thrust Level Expander and Gas Generator Cycles at Average Q_m/Q_p.	109
77	Theoretical Performance Comparison of 5K Thrust Level Expander and Gas Generator Cycles at Q_m/Q_p = 1.0.	109

PRECEDING PAGE BLANK NOT FILMED.

NOMENCLATURE

Symbol	Description	Units
A	Area	$in.^2$, ft^2
A_s	Surface Area	$in.^2$, ft^2
$\bar{A}$	Average Chamber Area	$in.^2$, ft^2
AR	Proportion of Back Wall Area that Conducts Heat	none
$A(\epsilon^*)$	Frictional Similarity Parameter	none
C_p	Specific Heat	$Btu/lb_m \cdot °R$
$c^{*'}$	Theoretical Characteristic Exhaust Velocity	ft/sec
C_s	Nozzle Stream Thrust Coefficient	dimensionless
D	Diameter	in., ft
D*	Thrust Chamber Throat Diameter	in., ft
D_h	Coolant Passage Hydraulic Diameter	in., ft
E	Young's Modulus	psi
F	Thrust	lb_f
f	Isothermal Friction Factor	none
f_h	Friction Factor with Heat Transfer	none
g_c	Gravitational Constant	$lb_m \cdot ft/lb_f \cdot sec^2$
H, ΔH	Coolant Enthalpy and Coolant Enthalpy Rise	Btu/lb
ΔH_c	Coolant Enthalpy Rise in Combustion Chamber	Btu/lb
ΔH_e	Coolant Enthalpy Rise in Nozzle	Btu/lb
h_c	Coolant-Side Heat Transfer Coefficient	$Btu/hr \cdot ft^2 \cdot °R$
h_g	Combustion-Side Heat Transfer Coefficient	$Btu/hr \cdot ft^2 \cdot °R$
I'_{vac}	Theoretical Vacuum Specific Impulse	$lb_f \cdot sec/lb_m$
J	Conversion Factor (778.16)	$ft \cdot lb_f/lb_m$
k	Thermal Conductivity	$Btu/hr \cdot ft \cdot °R$
L*	Characteristic Chamber Length	in.
ℓ	Coolant Passage Depth	in.
M	Mach Number	none
N_s	Number of Cooling Passage	none
P	Pressure	psia
P_c	Chamber Pressure	psia

NOMENCLATURE (Continued)

Symbol	Description	Units
P_{out}/P_c	Ratio of Coolant Jacket Outlet Pressure to Chamber Pressure	none
P_{in}/P_c	Ratio of Coolant Jacket Inlet Pressure to Chamber Pressure	none
Pr	Prandtl Number	none
Q	Total Heat Transferred to Wall of the Thrust Chamber	Btu/hr
Q_m/Q_p	Ratio of Experimentally Measured to Theoretically Predicted Thrust Chamber Heat Transfer	none
q	Heat Flux	$Btu/ft^2 \cdot hr$
$\mathcal{R}$	Recovery Factor	none
R	Radius	in., ft
R_c	Chamber Radius at Injector	in., ft
R*	Thrust Chamber Throat Radius	in., ft
Re	Reynolds Number	none
s	Web Thickness Between Coolant Passages	in.
s_t	Web Thickness Based on Braze Tensile Stress	in.
St	Stanton Number	none
t	Time, Coating Thickness	sec, in.
T	Temperature	°R
T'_c	Theoretical Combustion Temperature	°R
T_o	Total Temperature	°R
T_s	Static Temperature	°R
T_{aw}	Adiabatic Wall Temperature	°R
T_w	Combustion-Side Wall Temperature	°R
T_{wc}	Coolant-Side Wall Temperature	°R
U	Coolant Bulk Velocity	ft/sec
V	Combustion Chamber Volume	in^3
w	Coolant Passage Width	in.
$\dot{w}_f$	Fuel Flow Rate	lb_m/sec
$\dot{w}_p$	Propellant Flow Rate	lb_m/sec
x	Distance Along Coolant Passage	in.
α	Coefficient of Thermal Expansion	in./in.·°R

NOMENCLATURE (Continued)

Symbol	Description	Units
δ	Wall Thickness	in.
δ_b	Required Wall Thickness Based on Bending Stress Calculations	in.
δ_s	Required Wall Thickness Based on Shear Stress Calculations	in.
δ_{th}	Required Wall Thickness Based on Thermal Stress Calculations	in.
ΔT	Difference in Ambient and Wall Temperature	°R
ϵ	Absolute Passage Surface Roughness	in.
ϵ_c	Chamber Contraction Ratio	none
ϵ_e	Nozzle Expansion Ratio	none
ϵ^*	Friction Similarity Parameter	none
η_{c^*}	Characteristic Exhaust Velocity Efficiency	none
η_{fin}	Coolant Passage Fin Efficiency	none
η_{CF}	Chamber Thrust Coefficient Efficiency	none
μ	Viscosity	$lb_m/ft \cdot sec$
ρ	Density	lb_m/ft^3
σ_T	Material Tensile Strength	psi
σ_y	Material Yield Strength	psi
τ_w	Wall Viscous Force Acting on Coolant	lb_f/ft^2

Subscripts

b	Property Evaluated at Bulk Temperature
f	Property Evaluated at Film Temperature
w	Property Evaluated at Wall Temperature

SECTION I
INTRODUCTION

Interest in the space storable class of propellants for application in future planetary exploratory missions is expanding. Space storable fuels and oxidizers are typically cryogenic with overlapping liquid ranges and liquid temperatures sufficiently high to permit thermal equilibrium to be established in the near-planet space environment. There are a number of space storable propellant combinations that show promise, and NASA has sponsored investigations of these combinations, but mostly at chamber pressures in the range suitable for pressure-fed engine systems. Although the exact requirements for future propulsion systems have not been completely established, it is apparent from review of possible missions that not only high performance, but also small engine envelope dimensions will be required in some applications. With these requirements, high chamber pressure, pump-fed engines are most attractive and thus technology must be developed in this area.

The light hydrocarbon fuels with either flox or OF_2 are the only space storable propellant combinations that provide the active thrust chamber cooling capability that is necessary for reliable operation at high chamber pressures, and consequently these are the most promising candidate space storable propellant combinations for many future missions.

Programs to investigate the performance and cooling capability of the light hydrocarbon fuels with flox mixtures have been proceeding since 1964 under Contracts NAS3-4195, NAS3-6296, and NAS3-7950. Under the first two contracts, tests were made with several of the flox/hydrocarbon fuels at 100-psia chamber pressure and 5000-lb thrust (References 1*and 2). Under Contract NAS3-7950, a program to demonstrate the feasibility of a pump-fed engine system with flox and methane using modified RL10 engines is in progress. The chamber pressure level for this latter effort is 250 psia and the thrust level is 12,500 lb.

For future applications, chamber pressures of primary interest are 500 to 1000 psia at thrust levels in the range from 1000 to 20,000 lb. For these conditions, regenerative cooling and performance are being

* References are given on page 111.

investigated under this current contract, NAS3-11190. The contracted program is to be accomplished in the following five tasks:

Task I - Regenerative Cooling Analysis
Task II - Hardware Analysis and Design
Task III - Injector Development Tests
Task IV - Water-Cooled Chamber Altitude Tests
Task V - Regenerative Cooled Chamber Tests

The first task, which is the subject of this interim report, requires an analytical study to determine regenerative cooling limits for selected light hydrocarbon fuels with both flox and OF_2. The limits obtained in the Task I study together with mission considerations external to the study form the basis for selecting the design point for hardware to be designed in Task II and tested in Tasks III, IV, and V.

The regenerative cooling study was conducted in two parts. The first part was an evaluation of cooling feasibility based on comparisons of the integrated or total heat transfer to the thrust chamber and the heat absorption capacity of the fuel. Regenerative cooling feasibility was thus determined for five fuels with both flox and OF_2 over a wide range of thrusts, chamber pressures, and design variables.

In the second part of the study (referred to as the detailed heat transfer study) effects of local heat flux variations along the thrust chamber and of coolant passage design were considered for two selected oxidizer/fuel combinations at each of three thrust levels, 1000, 5000, and 20,000 lb. A new thrust chamber concept, referred to as "Thermal Skin$_{TM}$" was considered exclusively. Thermal Skin construction features small, carefully controlled cooling passages that can be tailored to provide required cooling film coefficients at all chamber locations. Thermal Skin chambers have been demonstrated in combustion firing tests with fluorine/hydrogen propellants at chamber pressures up to 820 psia and throat heat fluxes to 32 Btu/in^2 sec (see Appendix A), a level greater than the computed throat heat fluxes for any of the flox/light hydrocarbon fuels at 1000-psia chamber pressure.

In both parts of the study, experimental heat transfer results obtained in previous combustion firing tests with the flox/light hydrocarbon propellant combinations were factored into the analysis. Specifically, the combustion-side film coefficients were reduced by a measured-to-predicted heat transfer rate ratio (Q_m/Q_p) based on available test data to account for effects of carbon deposition on chamber walls.

The results of the feasibility analysis and the detailed heat transfer study are reported separately in Sections IV and V. The results of cycle studies that were conducted concurrently with and in support of the heat transfer study are presented in Section VI. A report summary is presented in Section II and the conclusions and recommendation are given in Section III.

PRECEDING PAGE BLANK NOT FILMED.

SECTION II
SUMMARY

The objective of the heat transfer studies described in this interim report was to define the regenerative cooling capabilities and limits for light hydrocarbon fuels with fluorinated oxidizers over a range of chamber pressures from 100 to 1000 psia and at thrust levels from 1000 to 20,000 lb. Although the study was analytical, results obtained in previous NASA-sponsored experimental programs were factored into the analysis. Specifically, the theoretical predicted heat flux values were adjusted by an experimentally determined factor, Q_m/Q_p, to account for the heat reduction due to carbon deposition on the chamber walls.

The study was conducted in two parts. In the first part, the feasibility of regenerative cooling for wide ranges of conditions was investigated for five fuels and two oxidizers. Limits were established by comparing computed thrust chamber heat transfer rates to the allowable fuel heat absorption capability. In the second part of the study, coolant passage design was analyzed in detail for a selected number of cases so that the effects of local heat fluxes could be studied and practical limitations on thrust chamber regenerative cooling could be obtained.

The fuels and variables considered in the feasibility part of the study were as follows:

Fuels: Methane, 55% Methane - 45% Ethane, Ethane, Propane, and Butene-1

Oxidizers: Flox (Optimum Mixture) and OF_2

Chamber Pressure Range: 100 to 1000 psia

Thrust Range: 1000, 2500, 5000, 10,000, and 20,000 lb

Mixture Ratio Range: 70% to 100% of Optimum

Contraction Ratio Range: 2, 3, and 4

Chamber Characteristic Length (L*): 30 in.

c* Efficiency: 96% of Theoretical Shifting Equilibrium

Nozzle Expansion Ratios: 40, 60, and 100

Wall Temperatures (Combustion Side): 1700°, 2100°, and 3200°F

Individual treatment of each of the 27,000 cases, which combinations of the variables in the preceding table could produce, was not considered practicable. However, by grouping the variables according to their relative effects on heat transfer to the thrust chamber, it was possible to summarize in six sets of parametric curves all the heat transfer data necessary to determine the enthalpy rise of the regenerative coolant for any combination. These six curves plus the temperature-enthalpy diagrams for each of the fuels were used to establish regenerative cooling limits. They also provide a set of curves that can be used by the reader to compute the coolant outlet temperature and state point for any particular case (see Section IV).

At supercritical coolant pressures, regenerative cooling limits were set by upper coolant temperature limits established for the respective fuels based on considerations of (1) fuel thermal decomposition (cracking) and (2) allowable operating temperatures for engine components downstream of the jacket (e.g. the chamber coolant exit manifold and the injector) which are in contact with the hot coolant. At subcritical coolant pressures, bulk boiling considerations established the regenerative cooling limits.

The feasibility study results indicated that if the heat reduction due to carbon deposition on the chamber walls is as great as observed in previous experimental testing, all the fuels evaluated have adequately high heat capacities for application as regenerative coolants at all thrust levels from 1000 to 20,000-lb, if design variables are properly selected. At supercritical coolant pressures, cooling limits were less than 1000 psia only at the lowest thrust levels, 1000 and 2500 lb, and then only with the combination of conditions that yield the highest coolant enthalpy rise (i.e. for $\epsilon_c = 2$, $\epsilon_e = 100$, $T_w = 1700°F$ and r = optimum). At subcritical pressures, only butene-1 can be used at all thrust levels (1000 to 20,000 lb) without encountering bulk boiling.

The values of Q_m/Q_p used in the study were averages, establishment of which was based on experimental data obtained in combustion firing tests. The data indicate that Q_m/Q_p is primarily a function of the fuel hydrogen-to-carbon atomic ratio, being greatest (i.e., having the least reduction) for methane, and lowest for butene-1. Both the relative and absolute effects of the values used are significant.

Computations made with $Q_m/Q_p = 1.0$ showed completely different trends, i.e., whereas methane had shown more restricted upper limits with the average values, the greatest restriction was on butene-1 when no reduction due to carbon formation was assumed. On an absolute basis, using the example of flox/methane for 2000 lb thrust, $\epsilon_c = 2$, $\epsilon_e = 100$, and $T_w = 2100°F$, a chamber pressure limit of 915 psia was found with Q_m/Q_p equal to the average value of 0.765; the corresponding limit for $Q_m/Q_p = 1$ was 425 psia.

In the detailed heat transfer study, regenerative cooling limits were investigated for two oxidizer/fuel combinations at each of three thrust levels as indicated below:

1000 lb	5000 lb	20,000 lb
Flox/Methane	Flox/Methane	Flox/Methane
OF_2/Butene-1	OF_2/55% Methane-45% Ethane	OF_2/Propane

In addition, the effects of operating thrust chambers designed for 8000-lb thrust at 500 psia chamber pressure at off-design chamber pressures were evaluated for three oxidizer/fuel combinations: flox/methane, OF_2/55% methane - 45% ethane, and OF_2/propane.

For the study of chamber pressure cooling limits at the 1000-, 5000-, and 20,000-lb thrust levels, the primary variables for evaluation were expansion ratio and mixture ratio, as well as the thrust chamber wall material. Contraction ratio (ϵ_c), the coolant jacket inlet pressure-to-chamber pressure ratio (P_{in}/P_c), and the factor Q_m/Q_p were assumed constant for most of the study. Average experimentally determined values of Q_m/Q_p were used for the particular fuels; P_{in}/P_c ratios were established for the respective propellant combinations based on engine cycle considerations ; and a contraction ratio of 4 was selected based on injector considerations that indicated that for chamber pressures of primary interest (500 to 1000 psia) contraction ratios of at least 4 will be required to keep the injector thrust per element size in a range conducive to high performance. A limited number of calculations was made at the 5000-lb thrust level to investigate the effects of changes in the assumed values for these parameters; these results are presented in Section V.

Thermal Skin thrust chamber design, which utilizes bonded sandwich plates with preformed internal cooling passages, formed into thrust chamber contours, was considered exclusively in the detailed heat transfer study. Because the passages are created by a photochemical milling process, great latitude in design is possible, and chamber pressure levels at which regenerative cooling can be employed are maximized. Counterflow cooling was used at all thrust levels because it provides larger coolant passages than parallel flow.

The regenerative cooling limits were dictated, based on the following considerations:

1. Film boiling caused by either bulk boiling or high heat fluxes that exceed the upper limit heat flux for transition from nucleate to film boiling
2. Coolant temperatures in excess of structural-based limits
3. Thermal decomposition of the coolant because of high coolant-side wall temperatures
4. Pressure drop through the coolant passages
5. Feasibility of fabricating the required coolant dimensions.

Considerations 2 through 5 are applicable to supercritical coolant pressures at upper chamber pressure limits.

It was found that the limits defined in the detailed heat transfer study (which are associated with local heat flux conditions and coolant passage design and set by a coolant pressure drop limit of one-half of chamber pressure) are lower than those determined in the feasibility study (and which are related only to coolant heat capacity). Table I summarizes the upper regenerative cooling limits obtained in the detailed study. In all instances in which the cooling limit is less than 1000 psia, the coolant pressure drop was the limiting criterion. Note in table I that the cooling limits for OF_2/butene-1 at 1000-lb thrust and for OF_2/propane at 20,000-lb thrust are above 1000 psia. At the 5000-lb thrust level with OF_2/55% methane - 45% ethane, the cooling limits are above 1000 psia for all thrust chamber materials except 347 stainless steel. Flox/methane, which was evaluated at all three thrust levels, was found to have cooling limits typically lower than those for the other propellants. Cooling to 1000 psia chamber pressure was indicated as possible only at the 5000- and 20,000-lb thrust levels and then only when nickel or a thermal barrier coating operating at 3200°F (not included in table I) is used. The primary reason for this result is

that the factor Q_m/Q_p is higher for methane than for the other fuels. Also, however, methane has a lower density than the other fuels and thus higher velocities (with their inherently higher coolant pressure drops) are required to cool at any given heat flux level.

Because the Thermal Skin design takes advantage of conduction in chamber walls around the coolant passages, the cooling limits are more sensitive to changes in wall materials than to changes in thrust, mixture ratio, or expansion ratio. Increases in chamber pressure cooling limits over those for stainless steel were indicated for Haynes 25 alloy operating at a high wall temperature (2100°F as compared to 1700°F) because total heat flux is reduced, but greater gains over stainless steel were shown when nickel (which has a higher thermal conductivity) was used and the wall temperature, and therefore heat flux, was unchanged.

The lower chamber pressure limits were found to depend primarily on the liquid-phase heat capacities of the individual fuels. Methane and the 55% methane - 45% ethane blend have low liquid-phase heat capacities and thus to avoid bulk boiling their use at all thrust levels is restricted to supercritical coolant pressures (jacket discharge pressures of 673 and 976 psia, respectively, which correspond to chamber pressures of approximately 233 and 330 psia for turbo-expander cycles). Propane and butene-1, on the other hand, have large liquid-phase heat capacities and therefore can be used as subcritical coolants at low chamber pressures as long as local heat fluxes are lower than the upper-limit heat flux for nucleate boiling. For example, at 1000-lb thrust, the heat flux limit for butene-1 occurs at approximately 260 psia chamber pressure, and for propane at 20,000 lb thrust, the chamber pressure limit is approximately 140 psia.

At the 8000-lb thrust level, where off-design chamber pressure operation was evaluated, results indicate that the coolant passages should be designed for the highest chamber pressure level in the operating range if permissible combustion-side wall temperatures are not to be exceeded.

Engine cycle studies were accomplished concurrently with the detailed heat transfer study. The chamber pressure cycle limits for both the turbo-expander and the gas generator cycles were determined for the 5000-lb thrust level, which was of interest for subsequent hardware design. The

propellant combinations, flox/methane, OF_2/55% methane - 45% ethane, OF_2/propane and OF_2/methane were considered in the study. The results indicate that, for chamber pressures up to 700 to 800 psia, regardless of the Q_m/Q_p ratio considered, the flox/methane expander cycle has the highest theoretical specific impulse. Based on these results, flox/methane has been recommended as the propellant combination for evaluation in the experimental phases of the contract.

Table I. Summary of Regenerative Cooling Chamber Pressure Limits (Q_m/Q_p = avg)

Thrust Level			1000 lb						5000 lb						20,000 lb					
Propellant			Flox/Methane			OF_2/Butene-1			Flox/Methane			OF_2/55% Methane-45% Ethane			Flox/Methane			OF_2/Propane		
Expansion Ratio			40	60	100	40	60	100	40	60	100	40	60	100	40	60	100	40	60	100
1700°F Nickel 200	% Optimum r	100	825	776	731	> 1000	>1000	> 1000	> 1000	>1000	989	> 1000	>1000	> 1000	> 1000	>1000	> 1000	> 1000	>1000	>1000
		90	838			> 1000			> 1000			> 1000			> 1000			> 1000		
		70	968			> 1000			> 1000			> 1000			> 1000			> 1000		
1700°F 347 Stainless Steel	% Optimum r	100			293				415	375	350	896	944	944			355			
		90							452			903								
		70							522			798								
2100°F Haynes 25	% Optimum r	100	645	625	595	>1000	>1000	>1000	830	780	730	> 1000	>1000	> 1000	825	775	736	> 1000	>1000	>1000
		90	655			>1000			860			> 1000			840			> 1000		
		70	750			>1000			884			> 1000			855			> 1000		

Notes: a. All chamber pressure limits (in psia) for Q_m/Q_p = avg, $\epsilon_c = 4$; $P_{in}/P_c = 3.0$ for flox/methane and OF_2/55% Methane-45% Ethane; $P_{in}/P_c = 1.65$ for OF_2 Butene-1, OF_2 Propane.

b. $L^* = 30$ inch

PRECEDING PAGE BLANK NOT FILMED.

SECTION III
CONCLUSIONS AND RECOMMENDATION

A. CONCLUSIONS

The following conclusions were made:

1. If the heat reduction due to carbon deposition on the chamber walls is as significant as that observed in previous flox/light hydrocarbon combustion tests, all the fuels evaluated (methane, 55% methane - 45% ethane, ethane, propane, and butene-1) have adequately high heat capacity for application as regenerative coolants at most conditions evaluated and at all thrust levels from 1000 to 20,000 lb.
2. The regenerative cooling limits for any of the light hydrocarbon fuels considered are essentially the same with either flox or OF_2 oxidizers.
3. Thermal Skin chambers can be cooled at higher chamber pressures than tubular wall chambers. Furthermore, nickel 200 operating at a wall temperature of 1700°F is an attractive material for application in Thermal Skin chambers; it provided higher regenerative cooling chamber pressure limits than either 347 stainless steel at a comparable wall temperature or Haynes 25 at 2100°F wall temperature.
4. Although the fuels have adequate heat capacity for regenerative cooling at chamber pressures to 1000 psia at the thrust levels considered, practical limits for thrust chamber design, and particularly coolant jacket pressure drop, restrict application to lower levels. However, operation of practical chambers at high pressures (between 700 and 1000 psia) is possible for the light hydrocarbon fuels.
5. The limits on maximum chamber pressure imposed by coolant pressure drop considerations occur at lower levels with methane than with most of the other fuels because the heat reduction due to carbon deposition is less (Q_m/Q_p is higher) and also because methane is less dense and therefore higher velocities and thus higher pressure drops are required for cooling a given heat load.
6. For flox/methane, regenerative cooling limits increase with decreasing expansion ratio and mixture ratio. With OF_2/55% methane - 45% ethane, the cooling limits decrease with decreases in ϵ_e (because the coolant reaches the throat region in the compressed liquid state) and mixture ratio (because the throat heat flux increases with decreasing mixture ratio).

7. Heat transfer reduction due to carbon deposition has a significant effect on the regenerative cooling chamber pressure limits. For example, at the 5000-lb thrust level and for flox/methane, the limits decreased approximately 500 psia by increasing Q_m/Q_p from its so-called average value (0.765) to 1.0 (no heat reduction due to carbon deposition on the chamber walls).

8. The regenerative cooling chamber pressure limits increase significantly with increasing chamber contraction ratio and decreasing chamber length.

9. By optimization of the coolant passage design so that the wall temperature is constant throughout the thrust chamber (i.e., by elimination of overcooled regions where coolant passages are smaller than required) regenerative cooling could be extended to levels above the limits given in the study. In one sample case for flox/methane at 5000-lb thrust, use of a constant wall temperature in the combustion chamber produced an increase in maximum chamber pressure from 989 to 1190 psia.

10. If thrust chambers are to be operated at off-design chamber pressures, the coolant passages should be designed for the highest chamber pressure, i.e., the highest heat flux level.

11. The lower chamber pressure limits, which are set by boiling consideration, depend on the liquid-phase heat capacities of the individual fuels. Methane and the 55% methane - 45% ethane have low liquid-phase heat capacities and thus their use is restricted to supercritical pressures. Propane and butene-1, on the other hand, have large liquid phase heat capacities and therefore can be used as subcritical coolants at chamber pressure where local heat fluxes in the chamber are lower than the upper-limit heat flux for nucleate boiling.

B. RECOMMENDATION

Flox/methane is recommended for evaluation in subsequent hardware phases of the contract. The detailed study of upper chamber pressure cooling limits indicated that flox/methane was more restricted than other fuels. However, flox/methane provides higher theoretical specific impulse than the other fluorinated oxidizer/light hydrocarbon fuel combinations, and methane is the best working fluid for use in turbo-expander engine cycles, which are capable of higher ideal performance than gas generator engines. The chamber pressure cooling limitation with flox/methane is not significant, and levels can be increased over those indicated in the study by thrust chamber coolant passage design optimization.

SECTION IV
FEASIBILITY STUDY

A. APPROACH

1. General

The objective of the feasibility study was to determine, for the fluorinated-oxidizer/light-hydrocarbon-fuel propellant combinations, the areas in which the fuels have adequate heat capacity for application as regenerative coolants. In the study, the heat flux values were integrated over the thrust chamber length and the integrated (or total) heat transfer rate was divided by the coolant flow rate to determine the coolant enthalpy rise. The enthalpy rise, in turn, was used to establish the coolant exit temperature, which was compared to established limits to ascertain regenerative cooling feasibility.

The fuels and parameters considered are given in table II. In addition to the fuel and oxidizer, eight other parameters were specified. Furthermore there were three additional parameters for which assumptions were necessary before regenerative cooling limits could be determined. These were (1) coolant inlet temperature, (2) coolant pressure at the outlet of the heat exchanger, and (3) heat transfer reduction due to carbon deposition on the wall.

Table II. Ranges of Operating Variables

Fuel	Methane, Ethane, 45% Ethane - 55% Methane Blend, Propane, and Butene-1
Oxidizer	Flox (optimum mixture), and OF_2
Chamber Pressure	100, 250, 500, 750, and 1000 psia
Vacuum Thrust	1000, 2500, 5000, 10,000, and 20,000 lb_f
c* Efficiency	96% of theoretical shifting equilibrium
Mixture Ratio	70%, 80%, 90% and 100% of optimum
Contraction Ratio	2:1, 3:1, and 4:1
Chamber Characteristic Length	30 in.
Nozzle Area Ratio (Regenerative Cooled Portion)	40:1, 60:1, and 100:1
Gas-Side Wall Temperature	1700°F, 2100°F, and 3200°F

2. Assumptions

The coolant inlet temperature was assumed to be 10°R above the fuel's normal freezing point. It was not necessary to specify the coolant inlet pressure because fuel enthalpy at low temperatures is not a strong function of pressure.

Coolant outlet pressure was required to determine the coolant outlet state and thus to test for bulk boiling. For the feasibility effort, the coolant outlet pressure/chamber pressure ratio (P_{out}/P_c) was assumed to be 2. With this value, all the fuels were at subcritical pressures at the 100 and 250 psia chamber pressure levels. The effect of assuming different values for P_{out}/P_c was evaluated on a limited basis.

To account for heat transfer reduction caused by carbon deposition on thrust chamber walls, theoretical heat flux predictions were altered based upon experimental results obtained in previous flox/light hydrocarbon programs. In firing tests with methane, propane, and butene-1 with flox, dramatic differences in thrust chamber heat transfer from those predicted have been consistently observed, and have been attributed to carbon deposition on the chamber walls. The effect of the carbon layer cannot be treated rigorously as an insulation phenomenon. There is not sufficient background to permit identification of the particular carbon composition that can be expected; therefore thermal conductivity, which varies widely for carbon, is not known. However, the effect can be accounted for by adjusting the gas-side film coefficient by the measured-to-predicted heat transfer ratio (Q_m/Q_p), the establishment of which is based on experimental data (see Appendix B).

Tests at 100 psia chamber pressure indicate that although the Q_m/Q_p ratio varies with injector design, it is a strong function of the fuel's hydrogen-to-carbon atomic ratio, as shown in figure 1. Fuels such as butene-1 and propane, which have low hydrogen-to-carbon atomic ratios, have large heat reductions due to carbon deposition on the chamber walls and thus low values of the Q_m/Q_p ratio. With methane, which has a higher hydrogen-to-carbon atomic ratio, the heat reduction was not as appreciable and therefore Q_m/Q_p is higher. For the studies reported herein, establishment of the average Q_m/Q_p values for methane, propane, and butene-1 were based on previous test data. Values for ethane and the 55% methane - 45% ethane blend were obtained by assuming that Q_m/Q_p is a

linear function of the fuel hydrogen-to-carbon atomic ratio (H/C). The values for Q_m/Q_p used as averages in this report are:

Fuel	H/C	Q_m/Q_p
Methane	4.0	0.765
55% Methane - 45% Ethane	3.54	0.645
Ethane	3.0	0.505
Propane	2.67	0.420
Butene-1	2.0	0.255

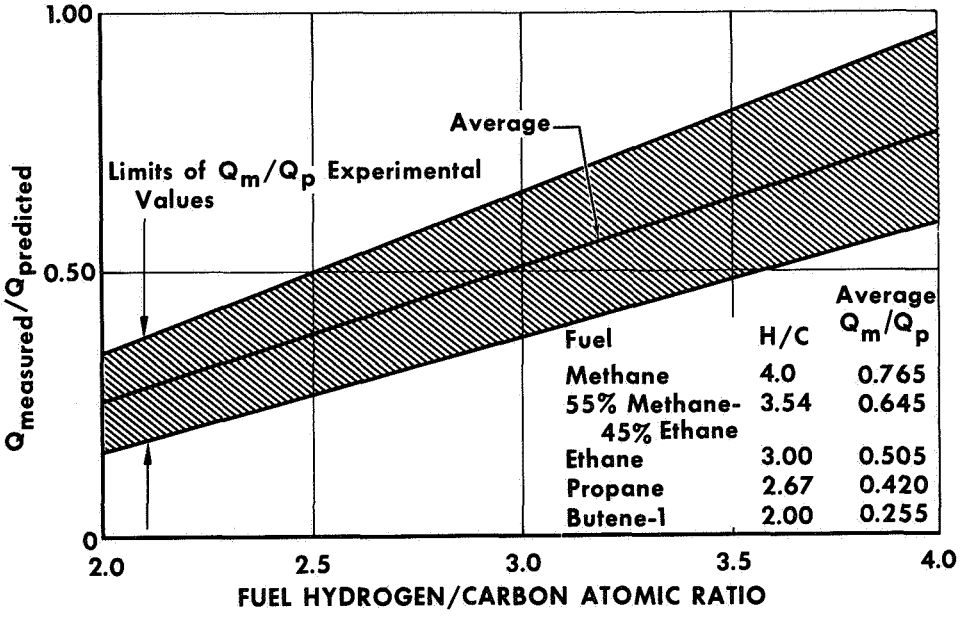


Figure 1. Effect of Fuel Hydrogen-To-Carbon Ratio GS 7015B on Total Engine Heat Transfer

To illustrate the effect of the Q_m/Q_p assumption on the results, limits were determined for the instance of no heat reduction (i.e., $Q_m/Q_p = 1$) for a few selected conditions.

3. Analysis

The number of possible combinations of the variables and propellants listed in table II is 27,000. Because the direct calculation of total heat transfer for each combination considered separately would have resulted in an excessive expenditure of engineering manpower and computer occupancy, a parametric approach was followed in the feasibility study. The approach was based upon separation of chamber and nozzle heat transfer (to account for contraction and expansion ratio effects),

and use of a baseline enthalpy rise to which adjustments for chamber pressure, wall temperature, fuel, and oxidizer variations could be made. This technique permitted development of the six sets of parametric curves shown in figures 2 through 7, which permit the determination of the coolant enthalpy rise for any combination of the variables.

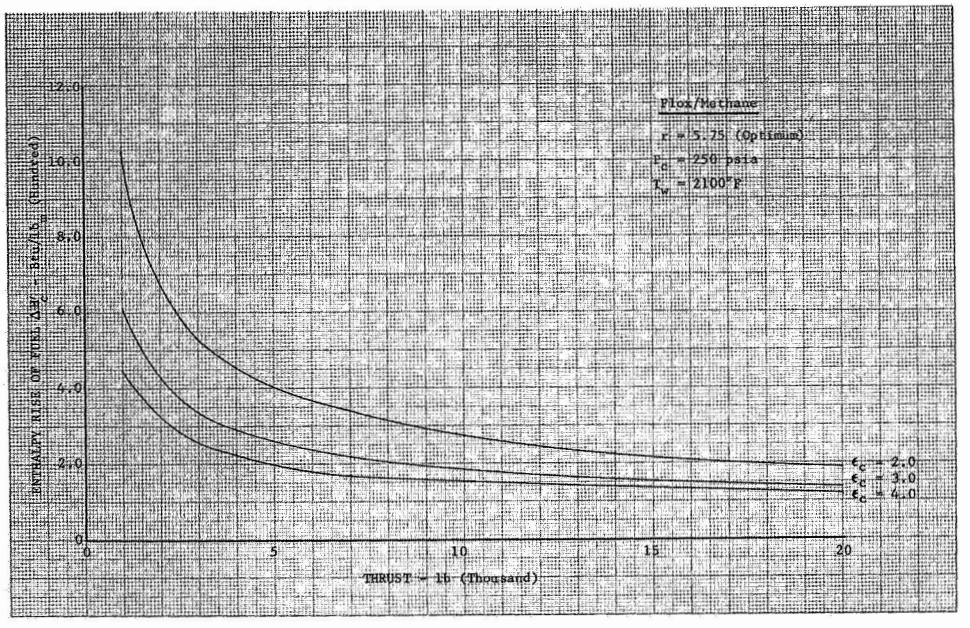


Figure 2. Variation in Combustion Chamber Fuel Enthalpy Rise With Thrust and Chamber Contraction Ratio DF 58062

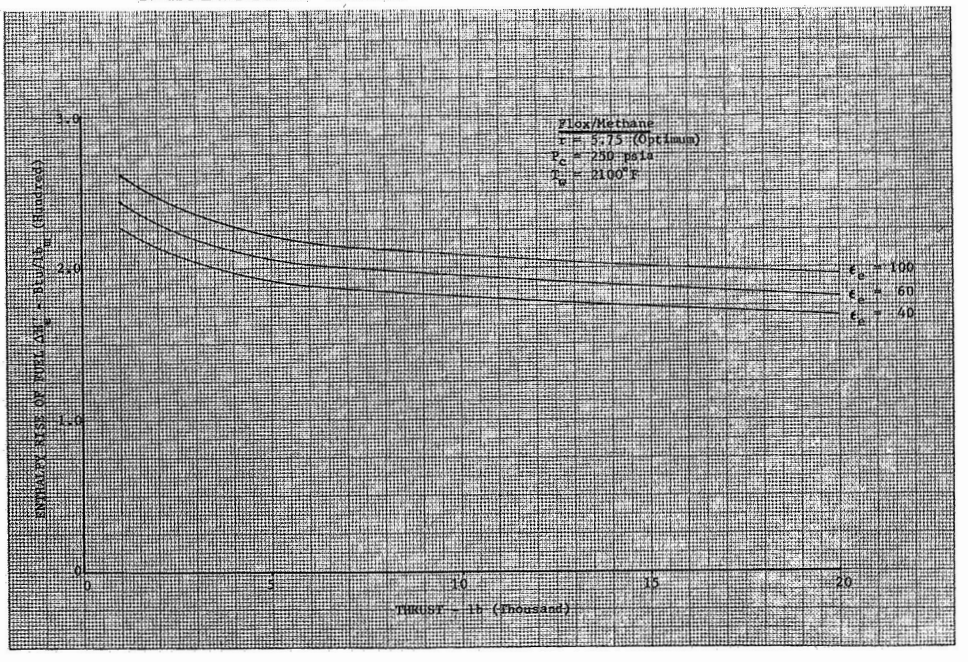


Figure 3. Variation in Nozzle Fuel Enthalpy Rise With Thrust and Nozzle Expansion Ratio DF 58063

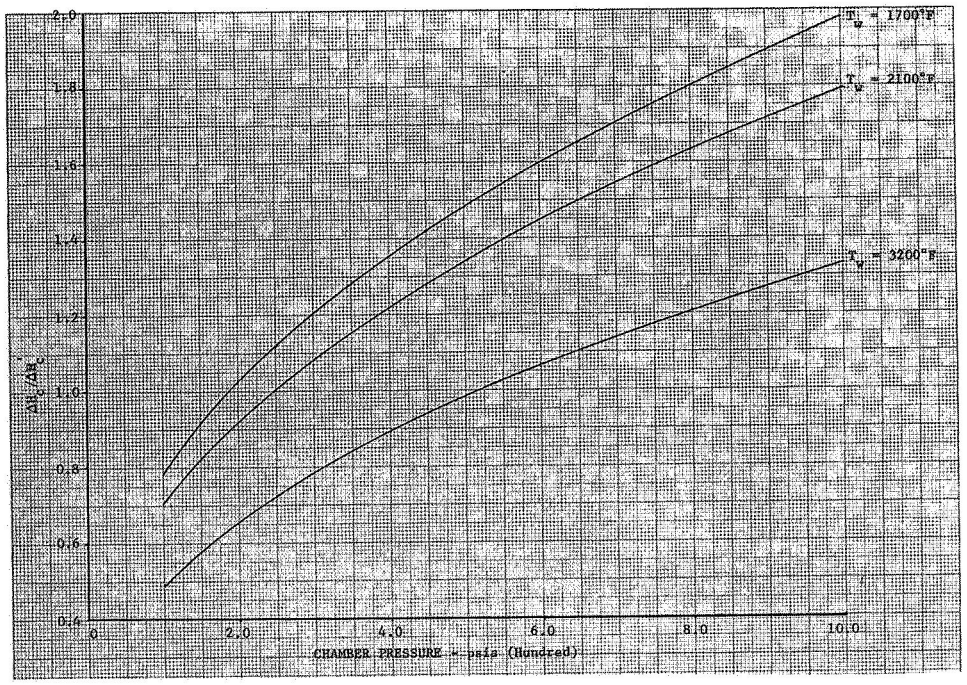


Figure 4. Variation of Wall Temperature Correction Factor With Chamber Pressure for Chamber Fuel Enthalpy Rise DF 58064

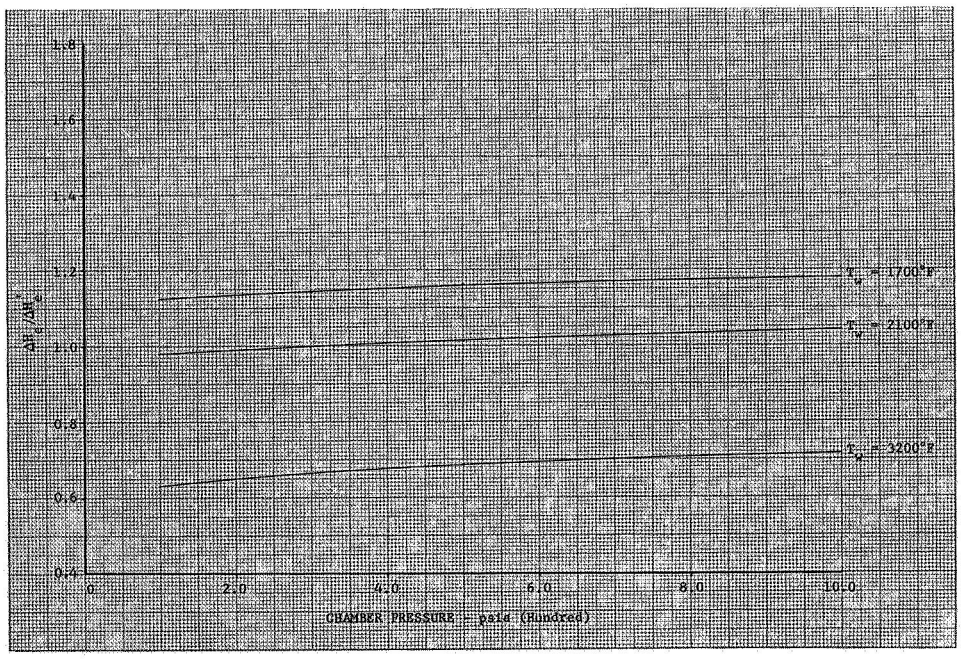


Figure 5. Variation of Wall Temperature Correction Factor With Chamber Pressure for Nozzle Fuel Enthalpy Rise DF 58065

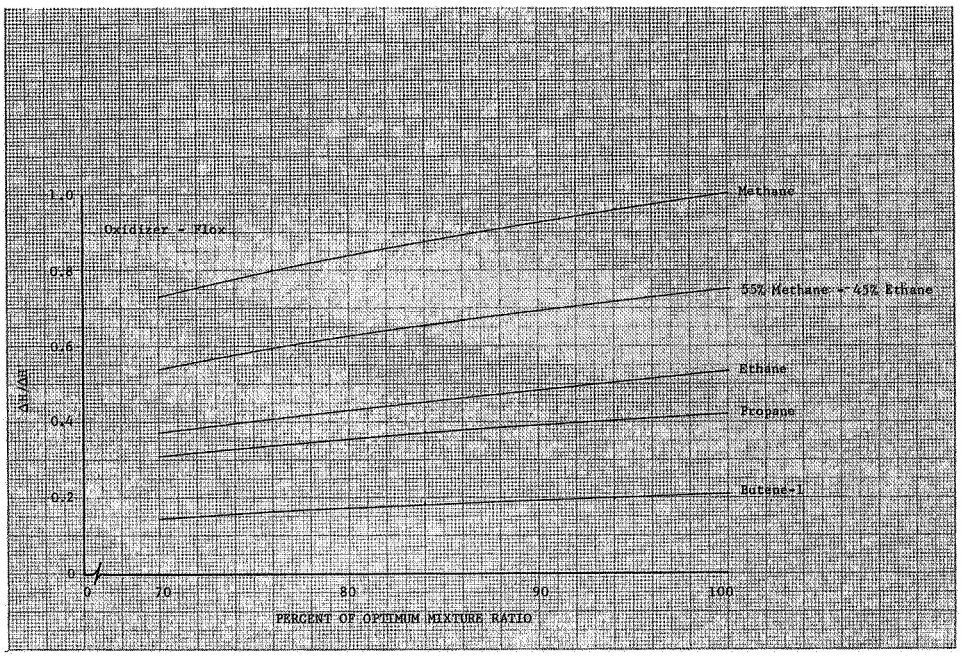


Figure 6. Variation of Fuel Type Correction Factor With Propellant Mixture Ratio for Fuel Enthalpy Rise

DF 58066

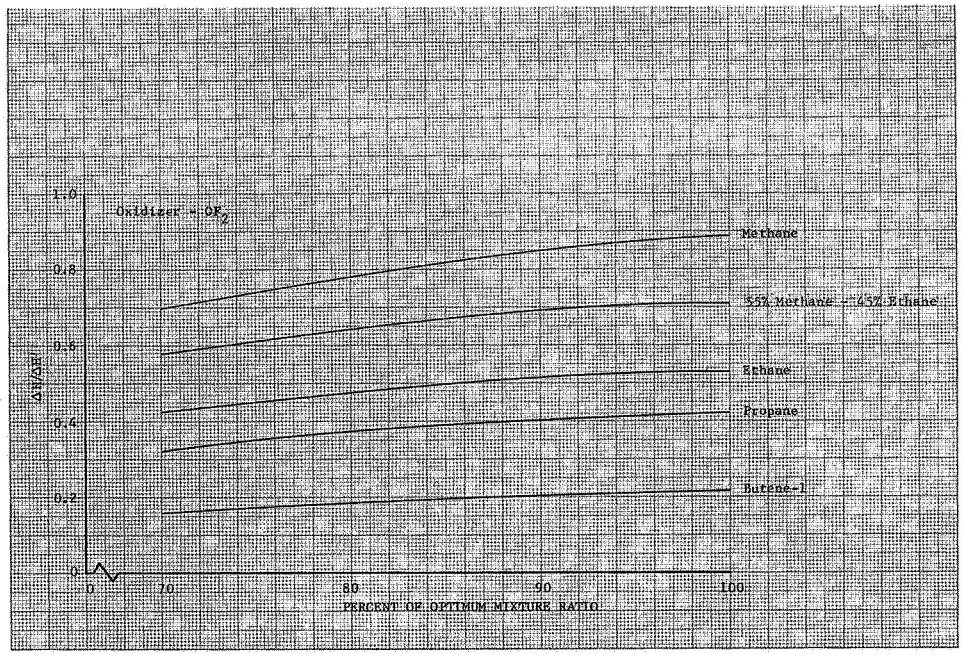


Figure 7. Variation of Fuel Type Correction Factor With Propellant Mixture Ratio for Fuel Enthalpy Rise

DF 58067

Development of these parametric curves is discussed in Appendix D. The significance of each of the curves is as follows:

1. Figure 2 presents coolant enthalpy rise ($\Delta H_c'$) for the combustion chamber as a function of thrust and contraction ratio for flox/methane at a mixture ratio of 5.75, a chamber pressure of 250 psia and a wall temperature of 2100°F.
2. Figure 3 shows the variation of the enthalpy rise ($\Delta H_e'$) in the nozzle portion of the thrust chamber, for the same set of conditions as those for figure 2, as a function of thrust and expansion ratio.
3. Figure 4 provides an adjustment factor ($\Delta H_c/\Delta H_c'$) for the enthalpy rise in the combustion chamber for changes in chamber pressure and wall temperature from the baseline values of 250 psia and 2100°F, respectively.
4. Figure 5 is a companion of figure 4; it provides an adjustment factor ($\Delta H_e/\Delta H_e'$) for the nozzle enthalpy rise for changes in chamber pressure and wall temperature from the baseline values.
5. Figure 6 provides a factor for adjustment of the total chamber enthalpy rise (determined by use of the first four figures) for fuel type and mixture ratio when flox is the oxidizer.
6. Figure 7 provides an adjustment factor to be used when OF_2 is the oxidizer.

These six parametric curves used with the temperature-enthalpy diagrams for each fuel (figures 8 through 12) form a consistent set of curves that can be used to determine the coolant outlet temperature and state point for a given set of conditions. The procedure for using the curves is illustrated in figure 13 and by the following sample calculation:

Problem

Determine the coolant jacket outlet temperature for the following conditions:

OF_2/propane

$F = 5000$ lb

$\epsilon_c = 3$

$\epsilon_e = 60$

$P_c = 500$ psia

$T_w = 2100°F$

$r = 4.74$ (optimum)

$P_{out}/P_c = 2$

Solution

From the parametric curves obtain:

$\Delta H_c' = 260$ from figure 2 for F = 5000 lb and $\epsilon_c = 3$

$\Delta H_e' = 212$ from figure 3 for F = 5000 lb and $\epsilon_e = 60$

$\Delta H_c/\Delta H_c' = 1.34$ from figure 4 for $P_c = 500$ psia and $T_w = 2100°F$

$\Delta H_e/\Delta H_e' = 1.015$ from figure 5 for $P_c = 500$ psia and $T_w = 2100°F$

$\Delta H/\Delta H' = 0.415$ from figure 7 for propane and optimum mixture ratio.

Compute:

$$\Delta H = \left[\Delta H_c' \left(\frac{\Delta H_c}{\Delta H_c'}\right) + \Delta H_e' \left(\frac{\Delta H_e}{\Delta H_e'}\right)\right] \frac{\Delta H}{\Delta H'} = \left[563\right] 0.415 = 233 \text{ Btu/lb}_m$$

With this enthalpy rise value used directly in figure 11 (note that the enthalpy of the fuels was set equal to zero at the coolant inlet temperature of 10°R above the normal freezing point) 580°R is obtained. This is the coolant outlet temperature for the average Q_m/Q_p for propane (i.e., for $Q_m/Q_p = 0.420$). The enthalpy rise can be computed for any value of Q_m/Q_p by dividing the enthalpy rise obtained by 0.420 and multiplying by the new value. As an example, for no heat reduction (i.e., for $Q_m/Q_p = 1.0$) the enthalpy rise would be

$$\Delta H = \frac{233}{0.420} \times 1.0 = 555 \text{ Btu/lb}_m$$

With this value for enthalpy rise and since for $P_{out}/P_c = 2$ the coolant outlet pressure is 1000 psia (or 68 atm), the coolant outlet temperature can be determined from figure 11 to be 965°R. Comparison of this value to 580°R, which was obtained for the average Q_m/Q_p value of 0.420, illustrates the significant effect of the carbon deposition on the chamber walls.

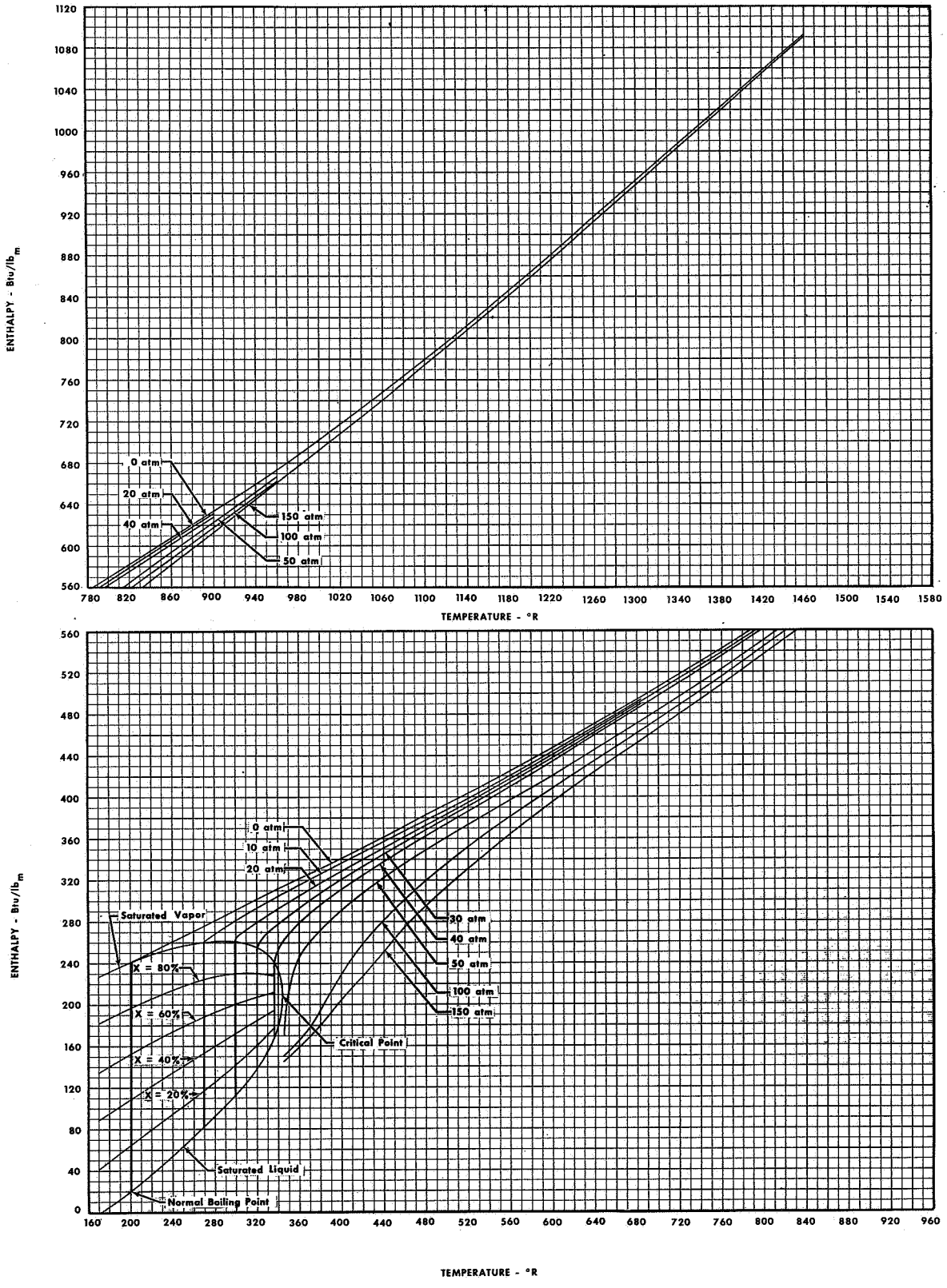


Figure 8. Enthalpy - Temperature Diagram for Methane FD 22635

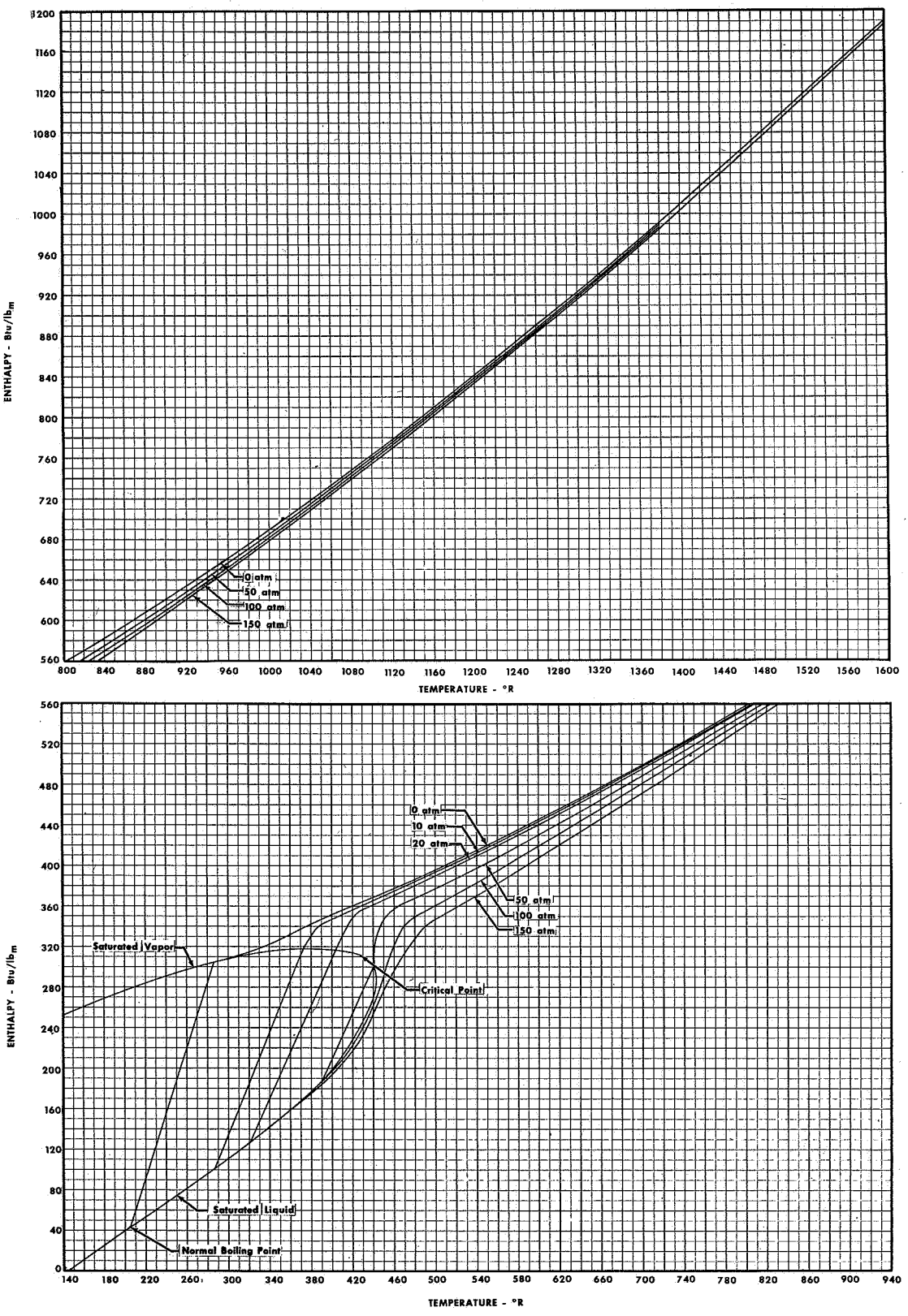


Figure 9. Enthalpy - Temperature Diagram for 55% Methane - 45% Ethane FD 22637

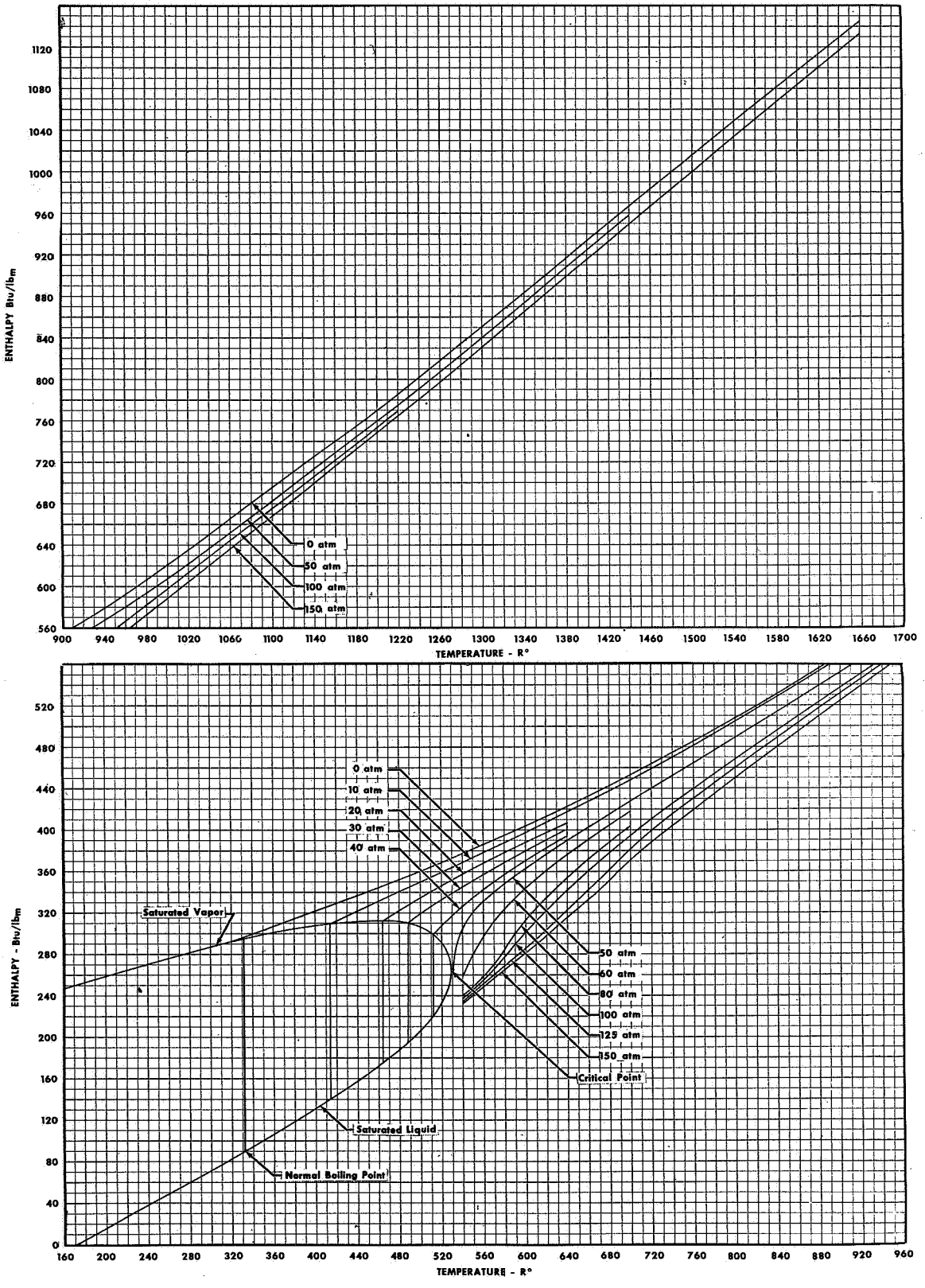


Figure 10. Enthalpy - Temperature Diagram for Ethane FD 22636

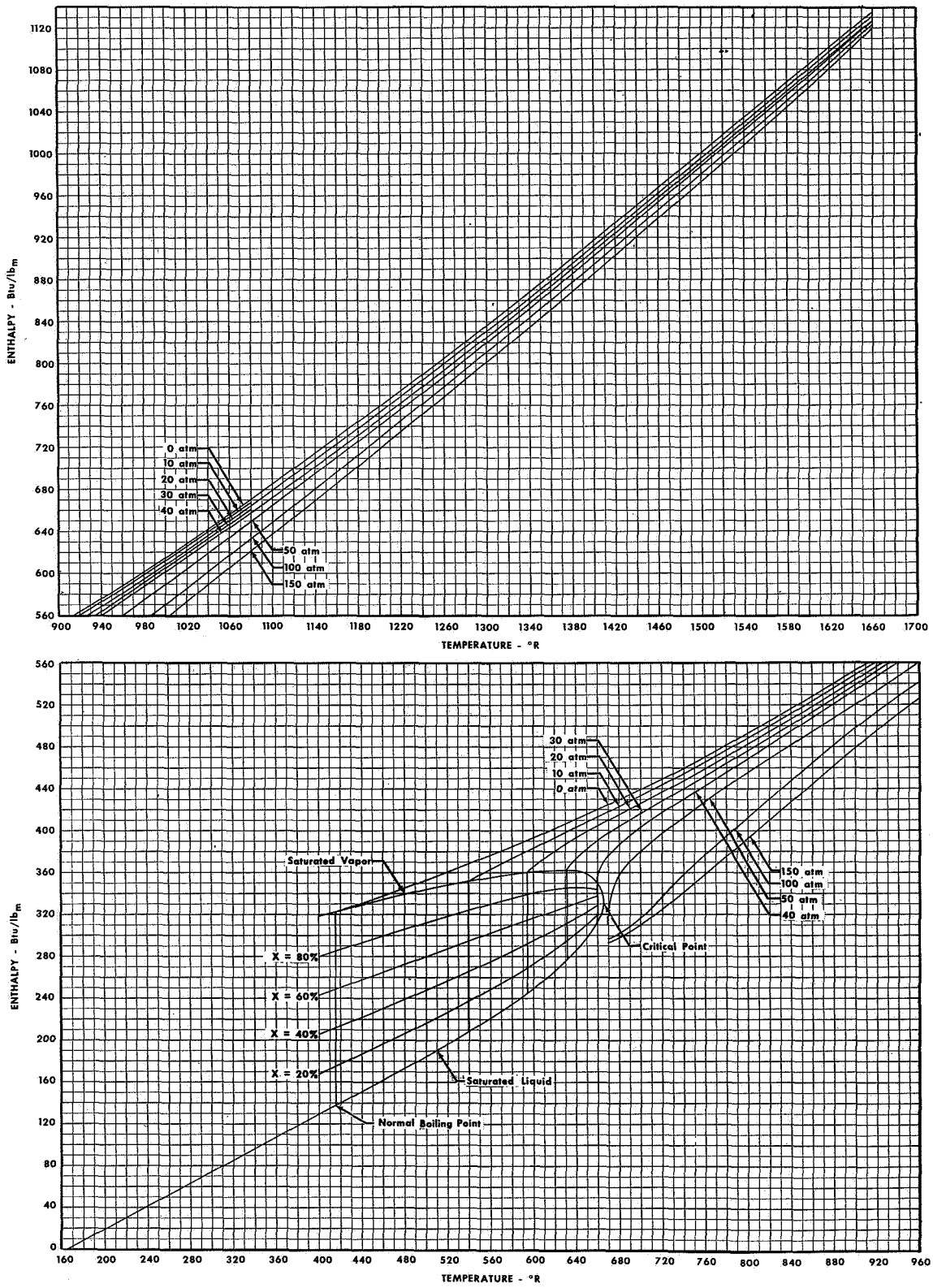


Figure 11. Enthalpy - Temperature Diagram for Propane FD 22638

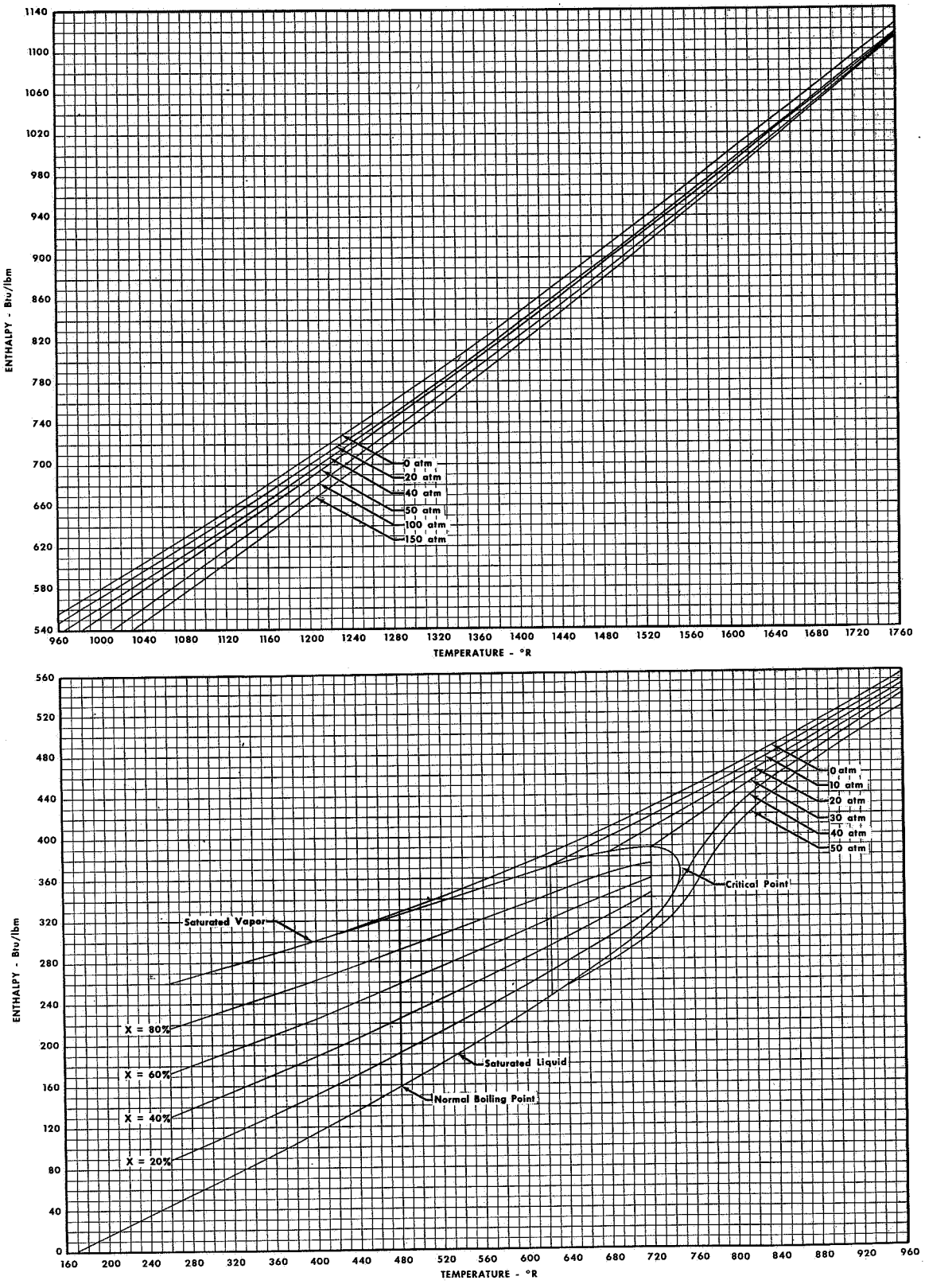


Figure 12. Enthalpy - Temperature Diagram for Butene-1

FD 22639

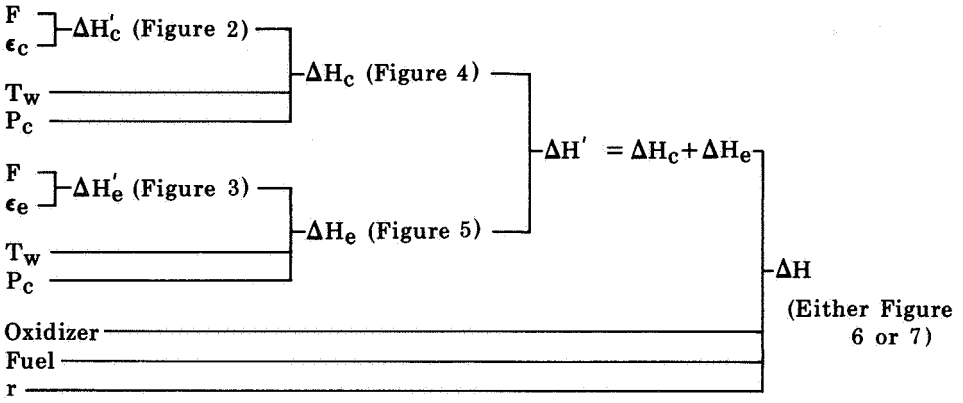


Figure 13. Determination of Enthalpy Rise From Basic Curves FD 23278

Following the procedure cited in the above example, ten typical curves were constructed, which define the fuel coolant outlet state as a function of chamber pressure and thrust for optimum and 70% optimum mixture ratios. Figures 14 through 18 present the coolant outlet conditions for each of the five fuels of table II with flox as the oxidizer; figures 19 through 23 are companion curves for OF_2. All these curves are for the midrange value of the other parameters, i.e.:

$$T_w = 2100°F$$
$$\epsilon_e = 60$$
$$\epsilon_c = 3.0$$
$$Q_m/Q_p = \text{avg.}$$
$$P_{out}/P_c = 2.0$$

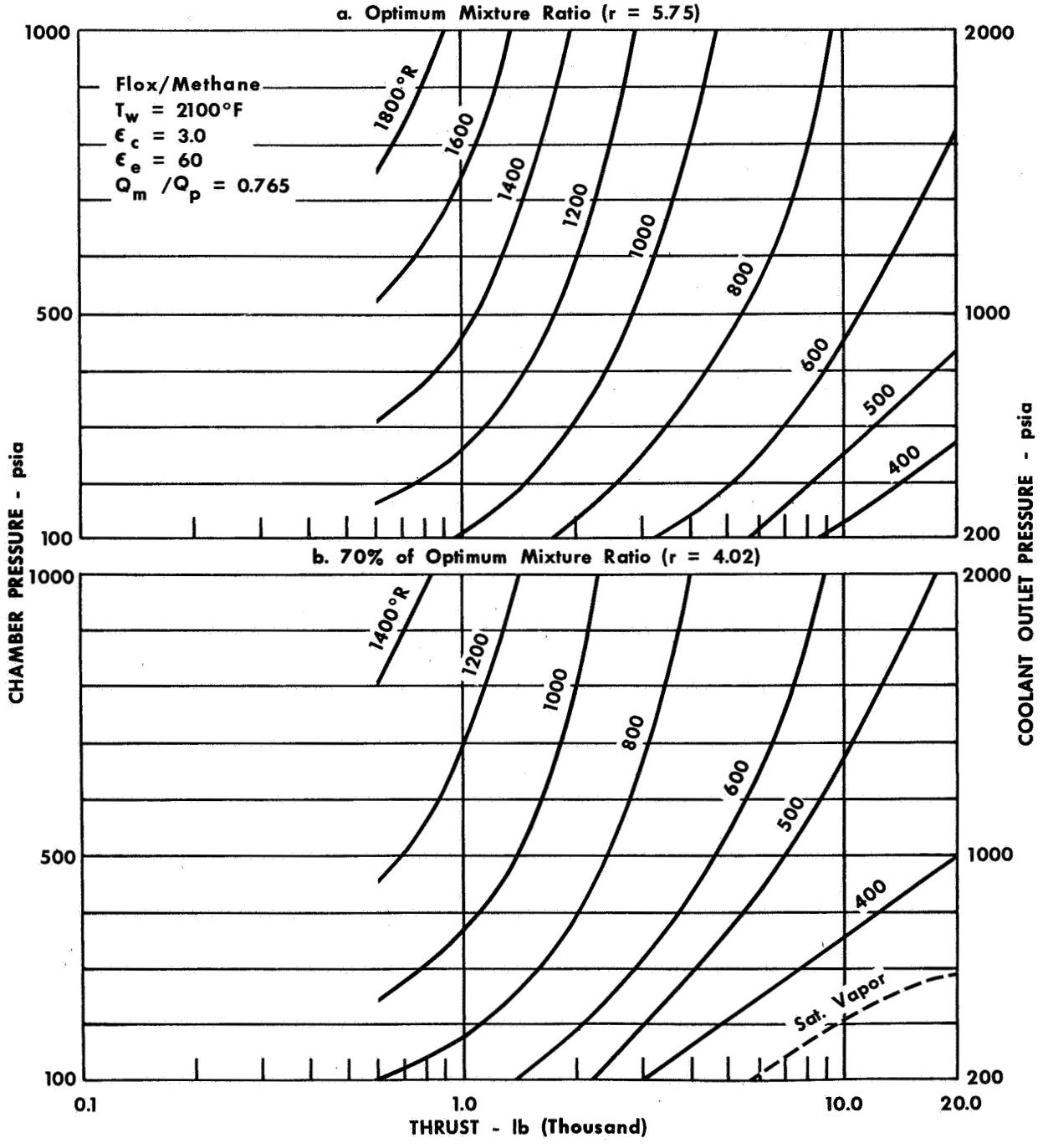


Figure 14. Coolant Outlet State for Methane With Flox as a Function of Chamber Pressure, Thrust, and Mixture Ratio GS 7463A

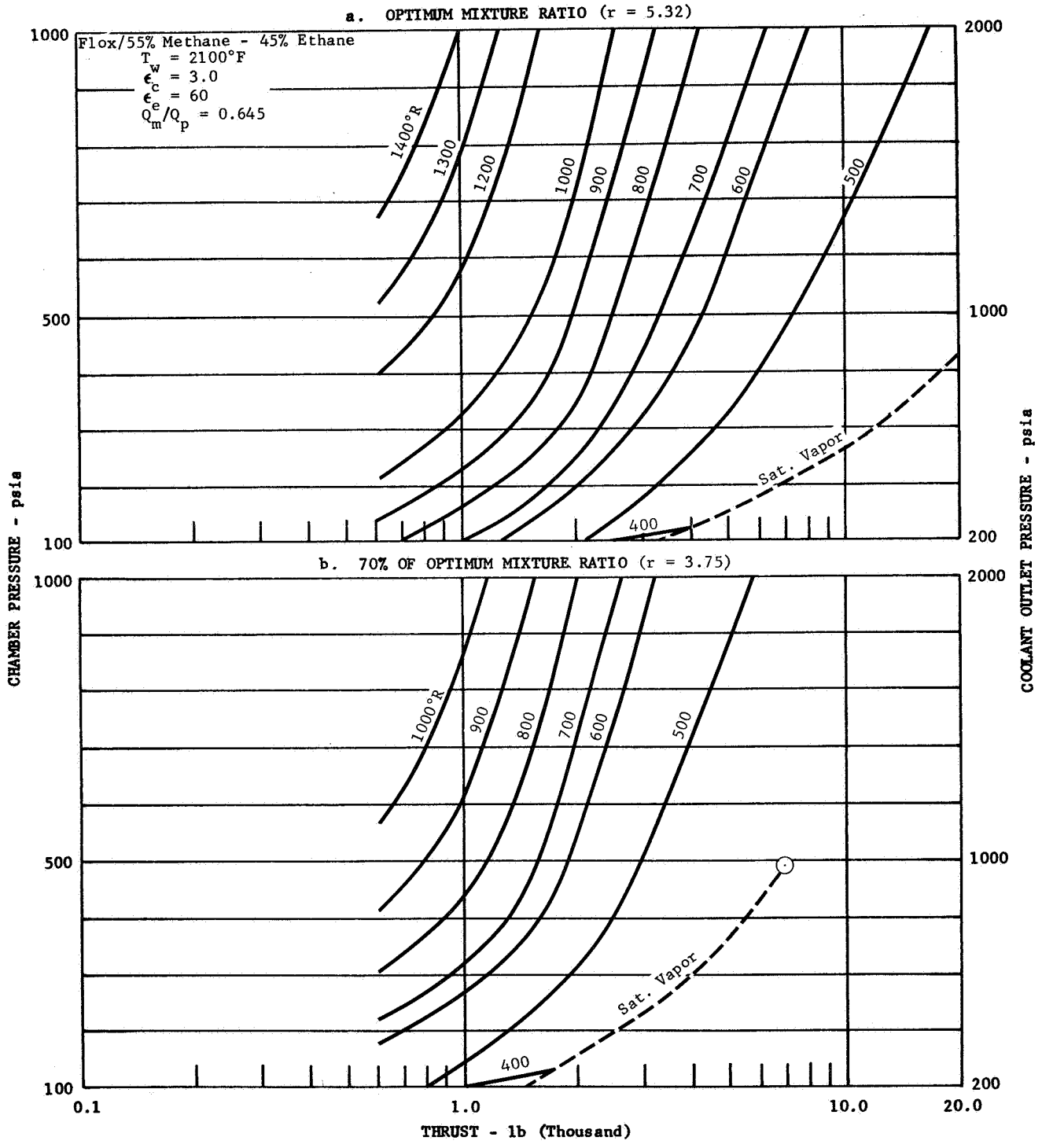


Figure 15. Coolant Outlet State for 55% Methane - 45% Ethane With Flox as a Function of Chamber Pressure, Thrust, and Mixture Ratio

FD 23475

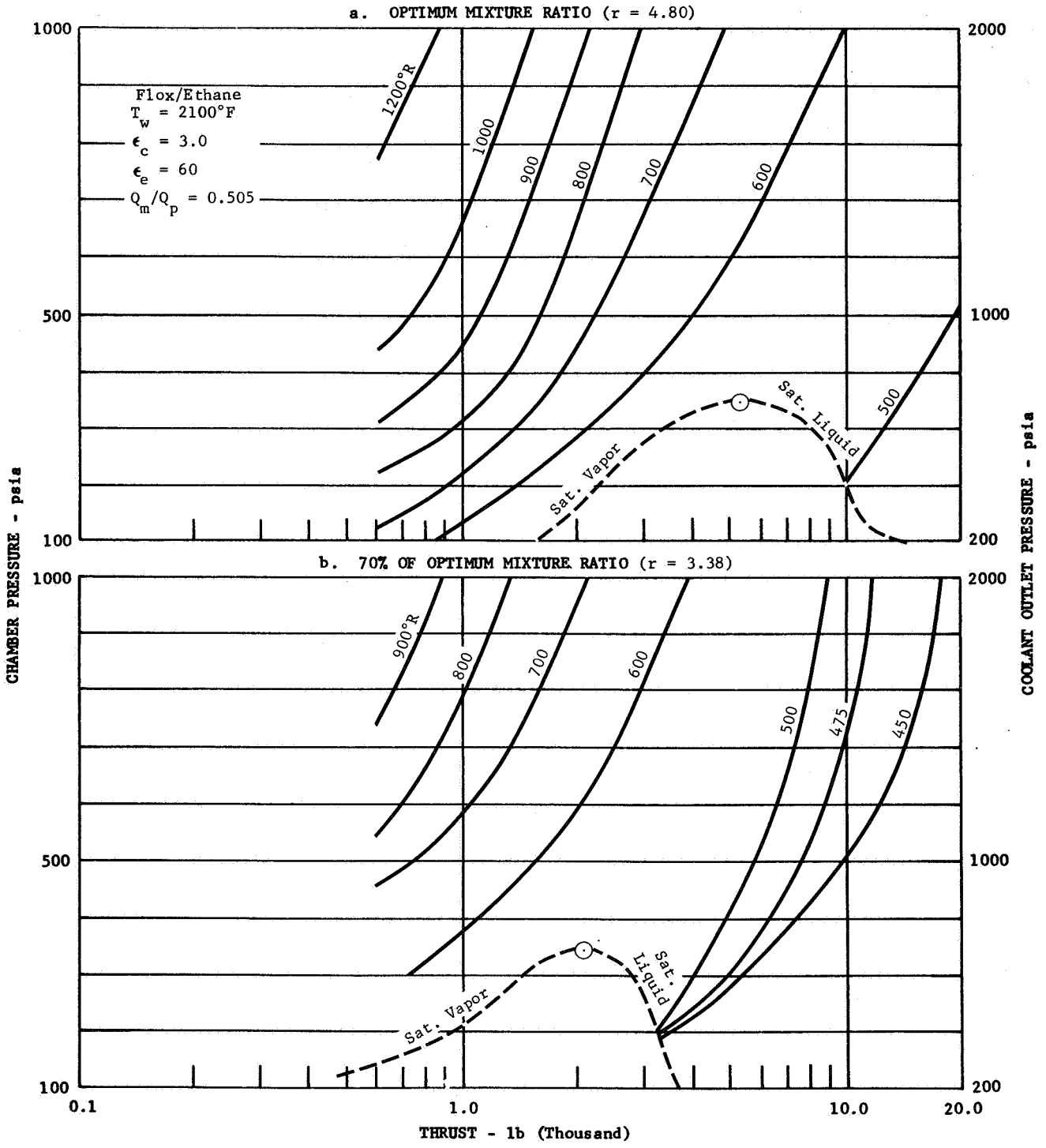


Figure 16. Coolant Outlet State for Ethane With Flox as a Function of Chamber Pressure, Thrust, and Mixture Ratio FD 23476

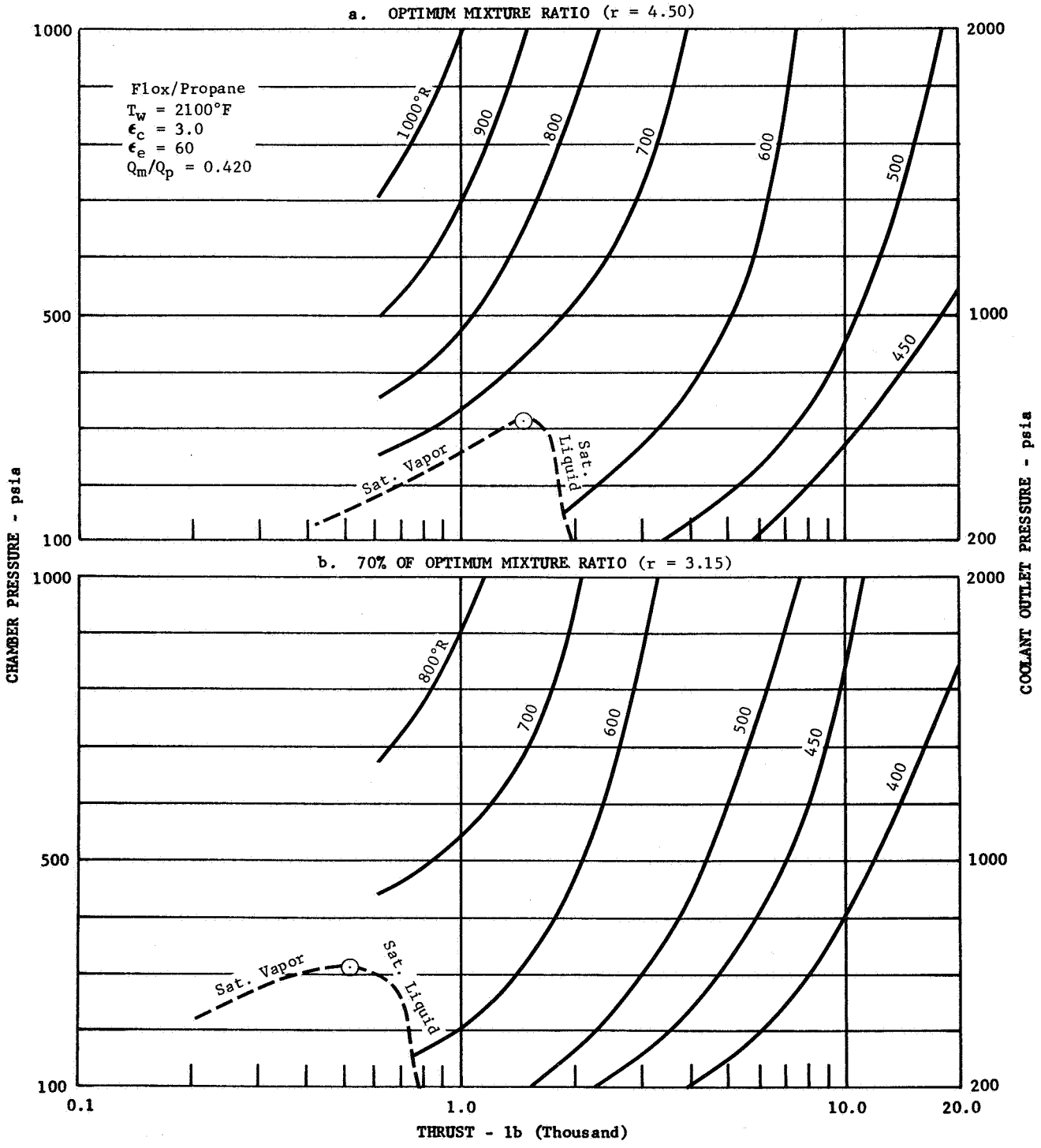


Figure 17. Coolant Outlet State for Propane With Flox as a Function of Chamber Pressure, Thrust, and Mixture Ratio FD 23477

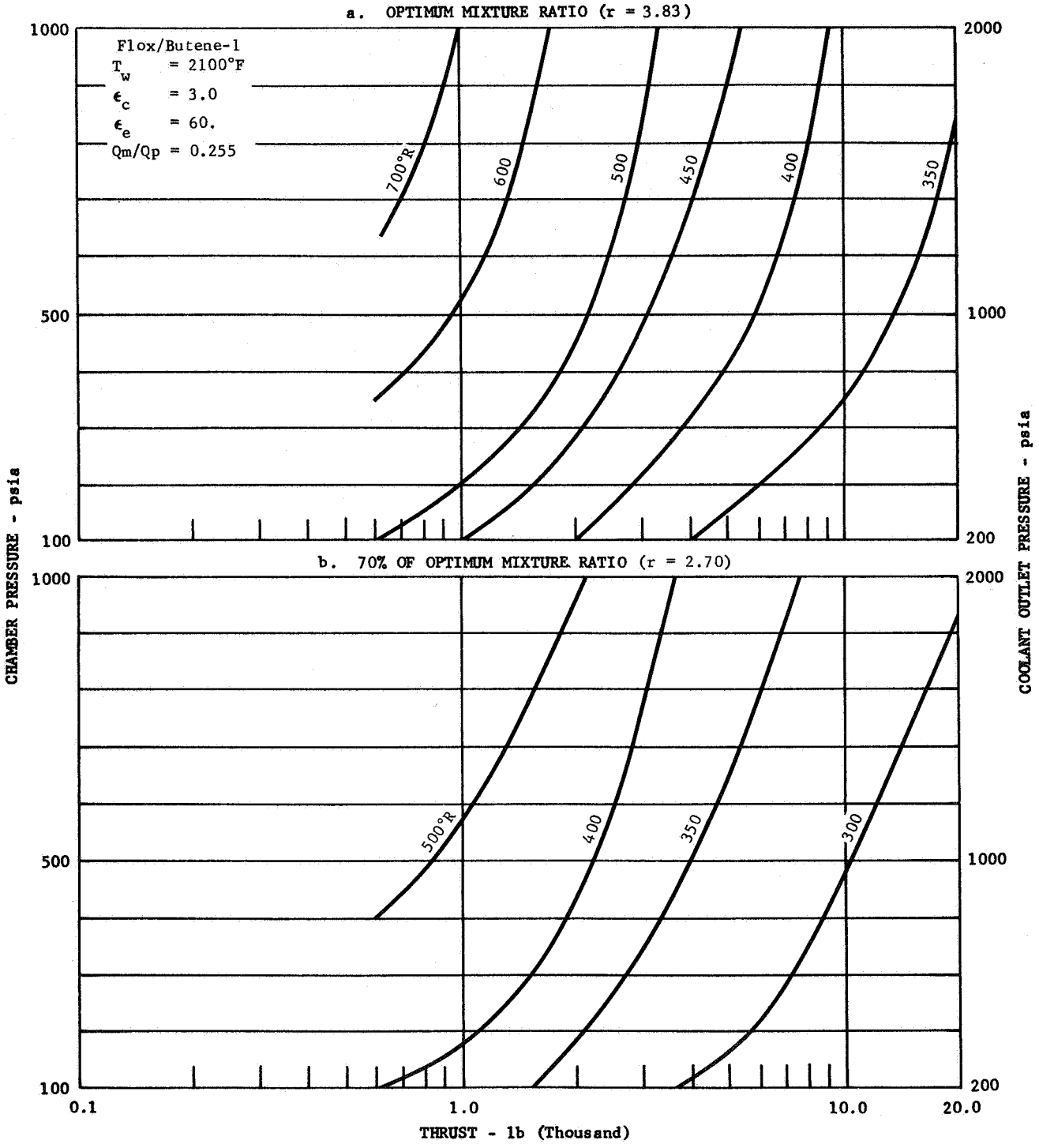


Figure 18. Coolant Outlet State for Butene-1 With Flox as a Function of Chamber Pressure, Thrust, and Mixture Ratio

FD 23478

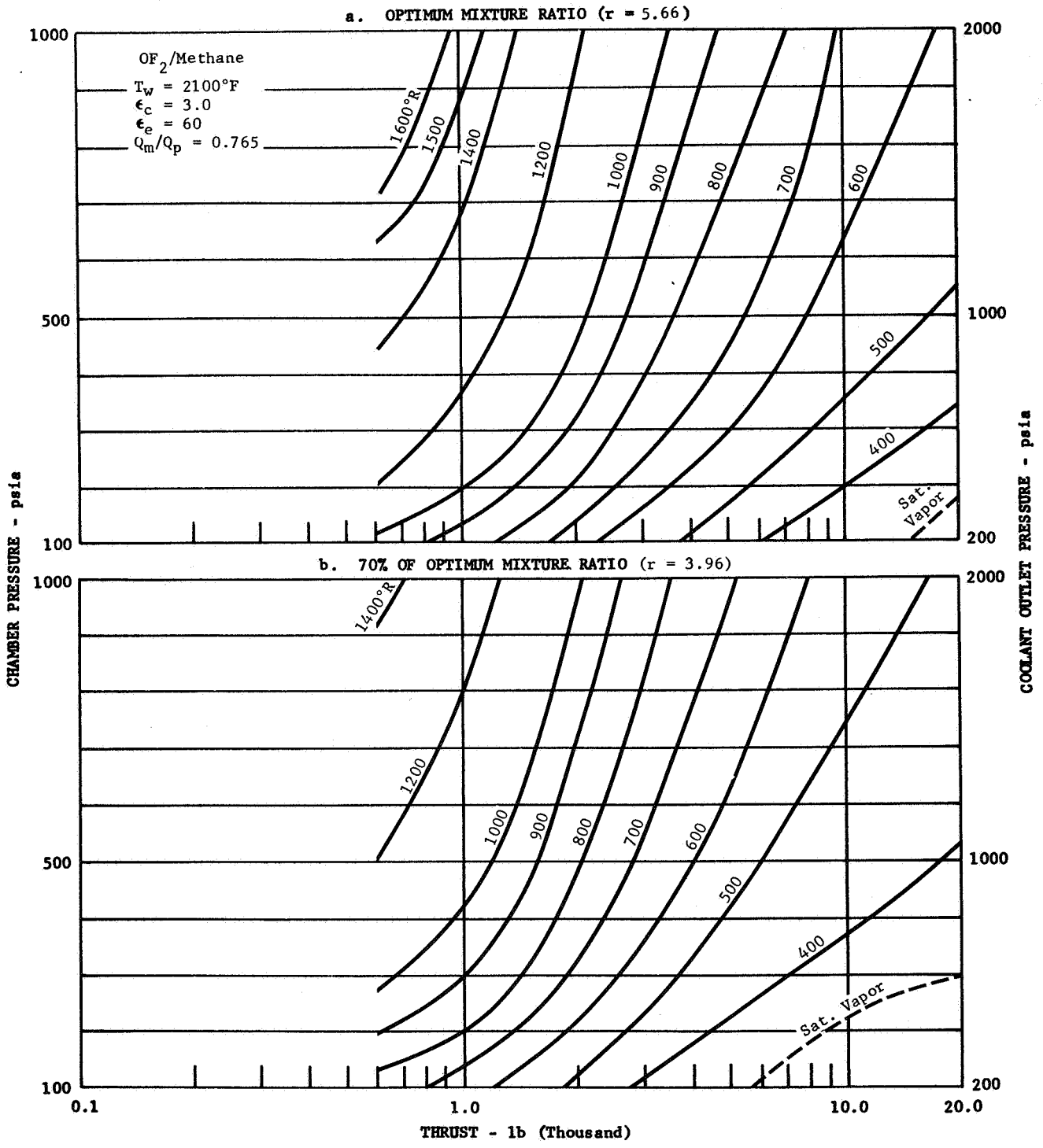


Figure 19. Coolant Outlet State for Methane With OF_2 as a Function of Chamber Pressure, Thrust, and Mixture Ratio

FD 23479

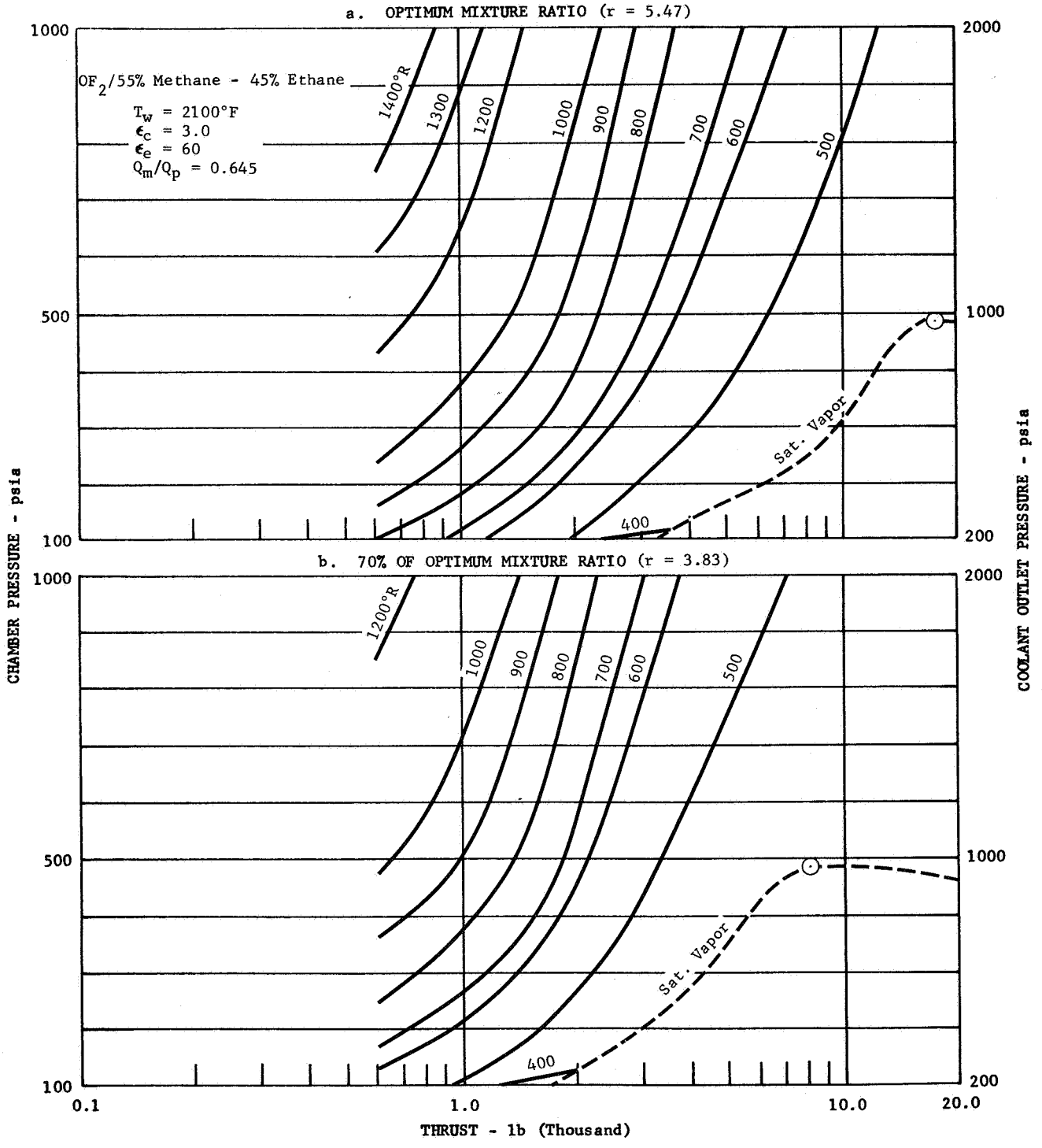


Figure 20. Coolant Outlet State for 55% Methane - 45% Ethane With OF_2 as a Function of Chamber Pressure, Thrust, and Mixture Ratio

FD 23480

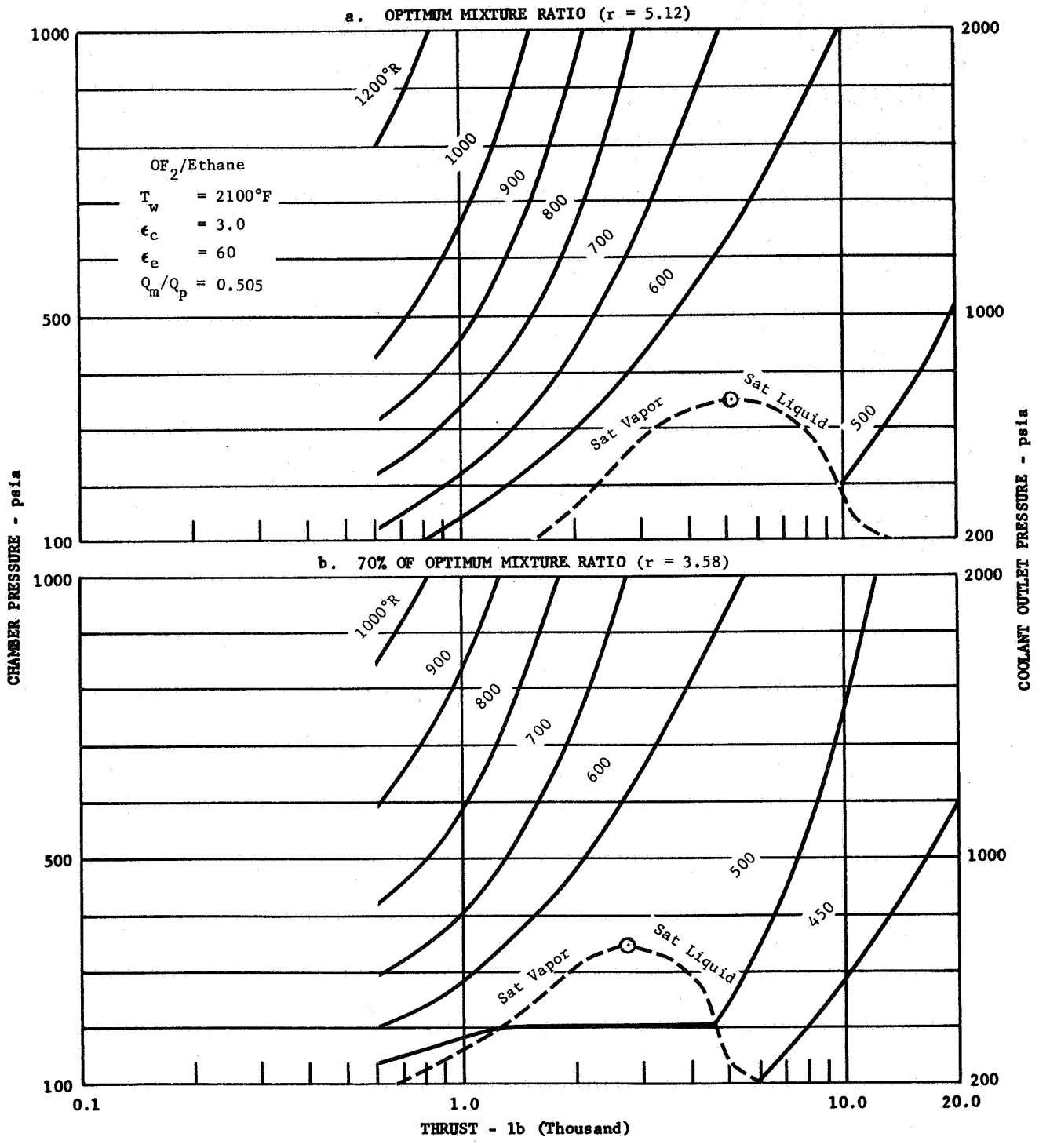


Figure 21. Coolant Outlet State for Ethane With OF_2 as a Function of Chamber Pressure, Thrust, and Mixture Ratio

FD 23481

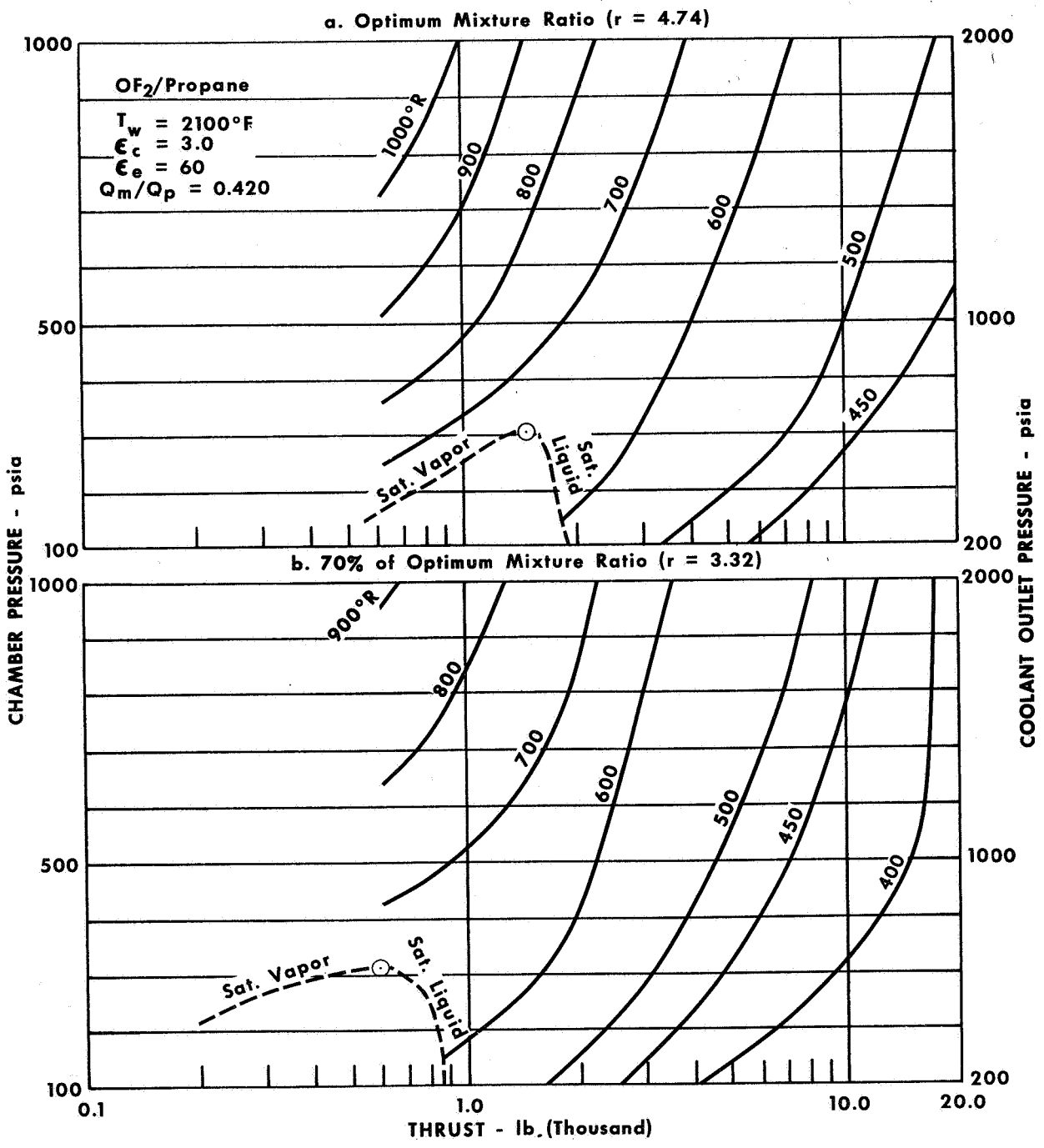


Figure 22. Coolant Outlet State for Propane With OF_2 as a Function of Chamber Pressure, Thrust, and Mixture Ratio GS 7464A

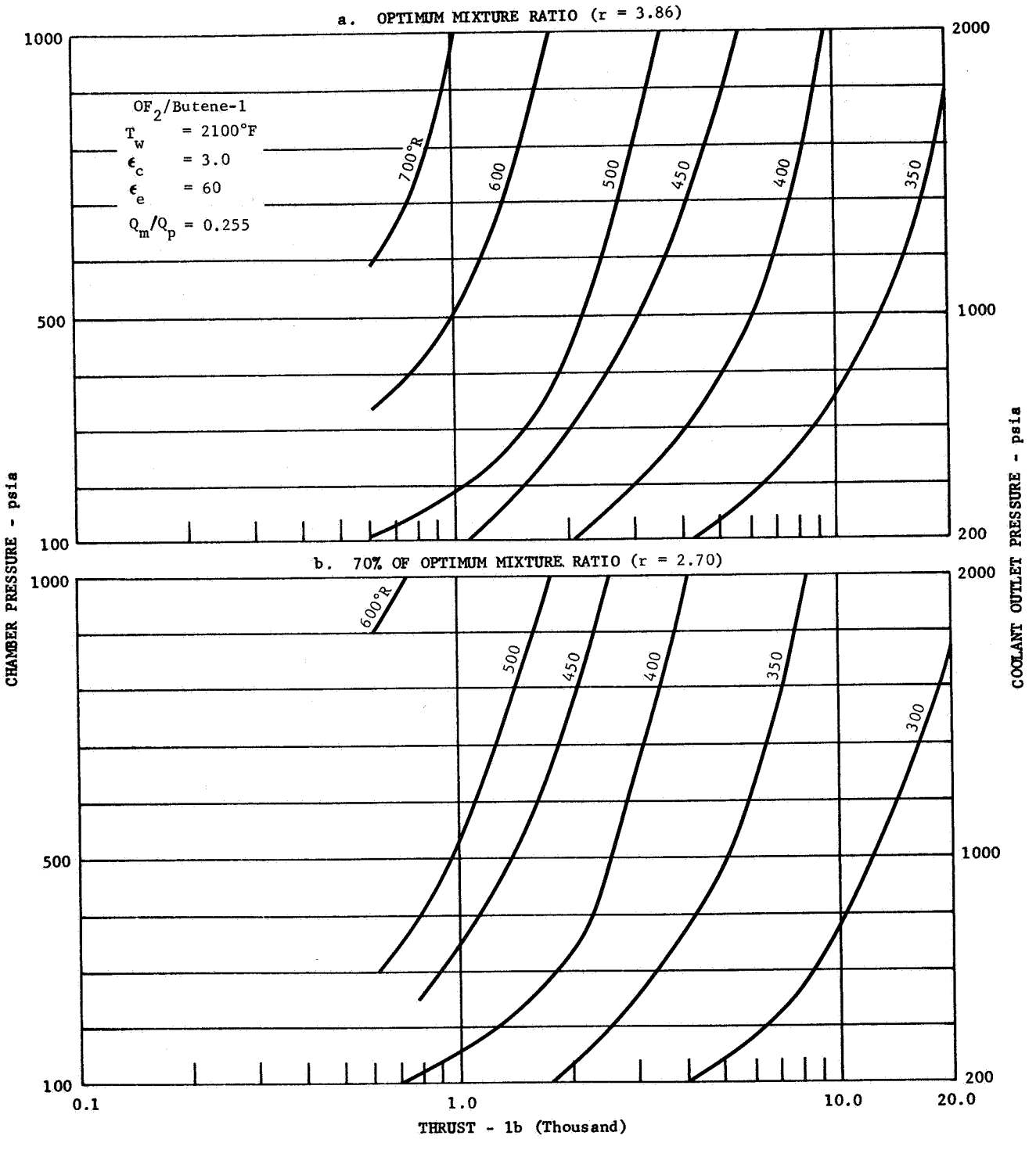


Figure 23. Coolant Outlet State for Butene-1 With OF_2 as a Function of Chamber Pressure, Thrust, and Mixture Ratio

FD 23483

For a given propellant combination, chamber pressure, thrust, and mixture ratio, figures 14 through 23 can be used to estimate the fuel coolant outlet state (gas, liquid, or two-phase), pressure, and temperature. For mixture ratios between the optimum and 70% optimum, coolant outlet conditions can be estimated by interpolation between the conditions for optimum and 70% optimum. The two-phase dome region for the majority of the fuels was included for rapid identification of the fluid outlet state. For flox/methane (figure 14), the dome region falls within the limits of the graph for 70% optimum mixture ratio but not in the graph for optimum mixture ratio; thus the coolant is in the gaseous state at all conditions. Butene-1 is in the liquid state at all thrust levels and chamber pressures with both flox and OF_2 (see figures 18 and 23).

B. REGENERATIVE COOLING LIMITS

1. Limit Criteria

For a given set of conditions, the criteria that set the regenerative cooling limits are dependent on coolant pressure, and specifically on whether the coolant pressure level is above or below critical pressure.

At supercritical pressures, considerations of (1) fuel thermal decomposition (cracking) and (2) allowable operating temperature limits for engine structural components in contact with the hot coolant established the high coolant temperature limits that are given in table III. These temperature limits, in turn, were used to establish regenerative cooling limits.

Table III. High Coolant Temperature Limits

Fuel	Temperature, °R	Limiting Criterion
Methane	1760	Structural Temperature
55% Methane - 45% Ethane	1715	Thermal Decomposition
Ethane	1400	Thermal Decomposition
Propane	1320	Thermal Decomposition
Butene-1	1160	Thermal Decomposition

Selection of the structural temperature limit of 1760°R was based on past experience. This limit is approximately the maximum temperature at which engine components such as the injector, the chamber coolant exit manifold, and plumbing (which are in contact with the hot coolant) can operate and still have acceptable life.

All the fuels with the exception of methane exhibit thermal decomposition at temperatures below 1760°R. As the fuel decomposes, carbon and tar would deposit on the coolant passage walls causing a decrease in heat transfer and an increase in wall temperature. If the deposition were allowed to continue over a period of time, wall failure could eventually occur. Although the tolerable level of carbon formation is not known for a rocket engine coolant passage, it is desirable to keep the coolant temperature at a conservatively low level so that passage fouling will not be a problem. Consequently, the incipient thermal decomposition temperature (see Appendix C) based upon a 1% decomposition rate per hour was used in the study.

At low chamber pressures, where the pressure in the thrust chamber cooling jacket is below critical pressure, boiling was the criterion that limited regenerative operation. Because the cooling passage design was not considered in the feasibility study, local chamber heat fluxes could not be compared to the upper limit heat flux for transition from nucleate to film boiling. As a result, film boiling was assumed to correspond to the inception of bulk boiling, i.e., to the point at which there is net vapor generation. The saturation state thus defined the maximum allowable coolant jacket discharge condition for the boiling criterion. Based on previous experimental work, which indicates that nucleate boiling cannot be sustained for qualities greater than 20 to 30% without having the process proceed into the film boiling regime, the assumption that film and bulk boiling are coincident is considered to be valid. Actually, film and bulk boiling could be tolerated in the low heat flux regions of the nozzle. Furthermore, a chamber could conceivably be designed in which the coolant is completely vaporized in the nozzle and reaches the high heat flux region near the throat in a gaseous state. Based on this possibility, the cooling limits obtained for the subcritical coolant pressures are somewhat conservative.

2. Regenerative Cooling Limits for Supercritical Coolant Pressures

Six variables plus the two oxidizers and five fuels were considered in the study. Regenerative cooling limits were established in terms of chamber pressure for a given set of conditions, i.e., for a selected oxidizer/fuel combination and for selected values of the remaining five variables. Thus, the limits indicate the maximum level of chamber pressure at which regenerative cooling is feasible for a given set of conditions.

Although there are several thousand sets of conditions or combinations of the variables that could be considered, there is one combination of variables that provides maximum coolant temperature rise. This set of conditions thus provides the lowest chamber pressure cooling limits. Regardless of thrust level or propellant combination, maximum coolant temperature rise occurs when (1) contraction ratio is minimum ($\epsilon_c = 2$), (2) expansion ratio is maximum ($\epsilon_e = 100$), (3) wall temperature is minimum ($T_w = 1700°F$) and (4) mixture ratio is at the optimum value. The chamber pressure cooling limits for the maximum-coolant-temperature-rise set of conditions are tabulated in table IV. Note that although this is the severest set of conditions, all the fuels have sufficient heat capacity for regenerative cooling at chamber pressures above 1000 psia for all but the 2500-lb and 1000-lb thrust levels. At 2500-lb thrust, all fuels except methane have the capacity for cooling to chamber pressures above 1000 psia.

Table IV. Feasibility Study Results - Minimum Chamber Pressure Regenerative Cooling Limits for Supercritical Coolant Pressures

$T_w = 1700°F$, $\epsilon_e = 100$, $\epsilon_c = 2.0$, r = 100% Optimum, Q_m/Q_p = Average

Propellants		Thrust Level - lb				
Fuel	Oxidizer	1000	2500	5000	10,000	20,000
Methane	Flox	270*	970	>1000	>1000	>1000
	OF_2	390	>1000	>1000	>1000	>1000
55% Methane-45% Ethane	Flox	430	>1000	>1000	>1000	>1000
	OF_2	490	>1000	>1000	>1000	>1000
Ethane	Flox	440	>1000	>1000	>1000	>1000
	OF_2	460	>1000	>1000	>1000	>1000
Propane	Flox	660	>1000	>1000	>1000	>1000
	OF_2	685	>1000	>1000	>1000	>1000
Butene-1	Flox	>1000	>1000	>1000	>1000	>1000
	OF_2	>1000	>1000	>1000	>1000	>1000

*Chamber Pressure Limits in psia.

Regenerative cooling could be extended beyond the chamber pressure limits given in table IV by changing any of the parameters to another value within the range considered in the study. For example, changing only the contraction ratio (from 2 to 4) decreases the heat transfer to the thrust chamber so drastically that there are no cooling limits below 1000 psia chamber pressure at any thrust level (table V).

Table V. Feasibility Study Results - Chamber Pressure Regenerative Cooling Limits for Supercritical Coolant Pressures

T_w = 1700°F, ϵ_e = 100, ϵ_c = 4.0, r = 100% Optimum, Q_m/Q_p = Average

Propellants		Thrust Level - lb				
Fuel	Oxidizer	1000	2500	5000	10,000	20,000
Methane	Flox	>1000*	>1000	>1000	>1000	>1000
	OF_2	>1000	>1000	>1000	>1000	>1000
55% Methane-45% Ethane	Flox	>1000	>1000	>1000	>1000	>1000
	OF_2	>1000	>1000	>1000	>1000	>1000
Ethane	Flox	>1000	>1000	>1000	>1000	>1000
	OF_2	>1000	>1000	>1000	>1000	>1000
Propane	Flox	>1000	>1000	>1000	>1000	>1000
	OF_2	>1000	>1000	>1000	>1000	>1000
Butene-1	Flox	>1000	>1000	>1000	>1000	>1000
	OF_2	>1000	>1000	>1000	>1000	>1000

*Chamber Pressure Limits in psia.

The effects of changes in contraction ratio, expansion ratio, wall temperature, and mixture ratio on the cooling limits with flox/methane at the 1000-lb thrust level are shown in figures 24 through 27. The chamber pressure cooling limits are raised when contraction ratio and wall temperature are increased and when expansion ratio is decreased. These changes have the effect of reducing total heat transfer. Decreases in mixture ratio do not necessarily reduce heat transfer, but permit cooling at higher chamber pressures because fuel flow is increased, and thus the fuel coolant temperature rise for a given chamber heat load is reduced.

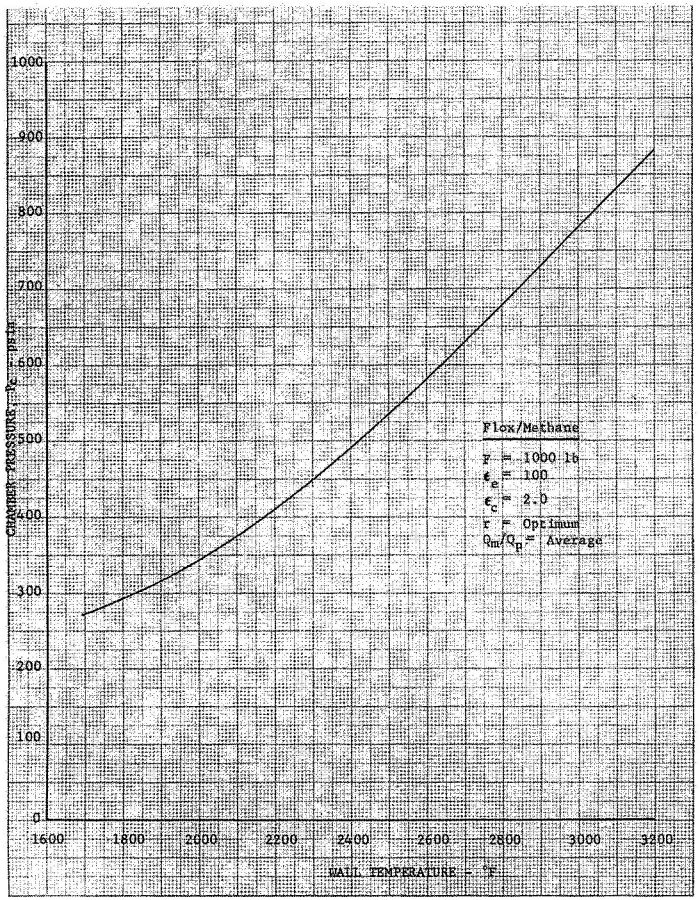


Figure 24. Feasibility Study Results - Chamber Pressure Regenerative Cooling Limits vs Wall Temperature

DF 60444

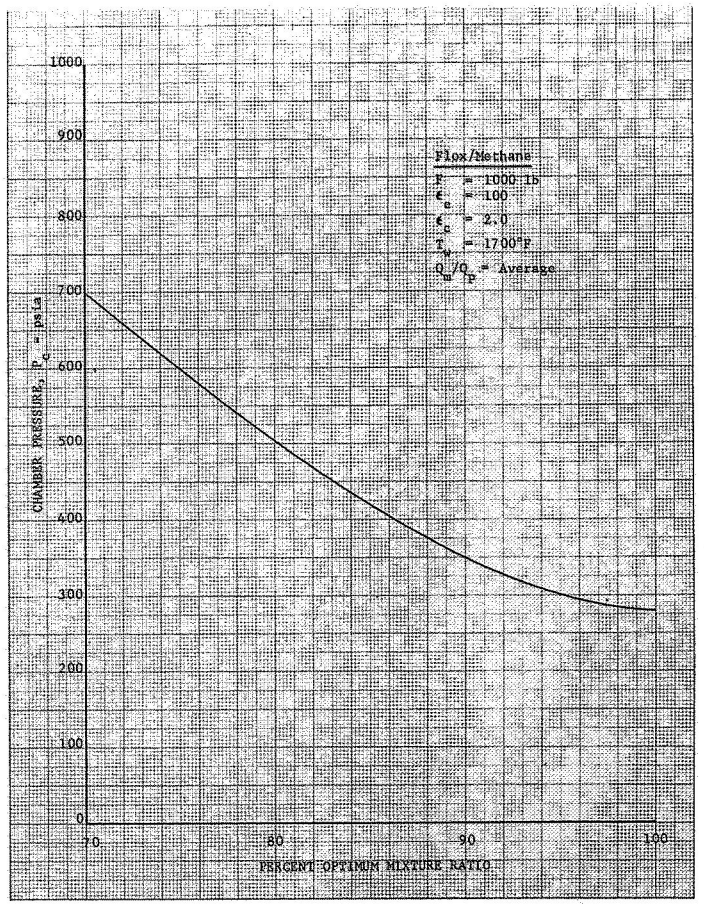
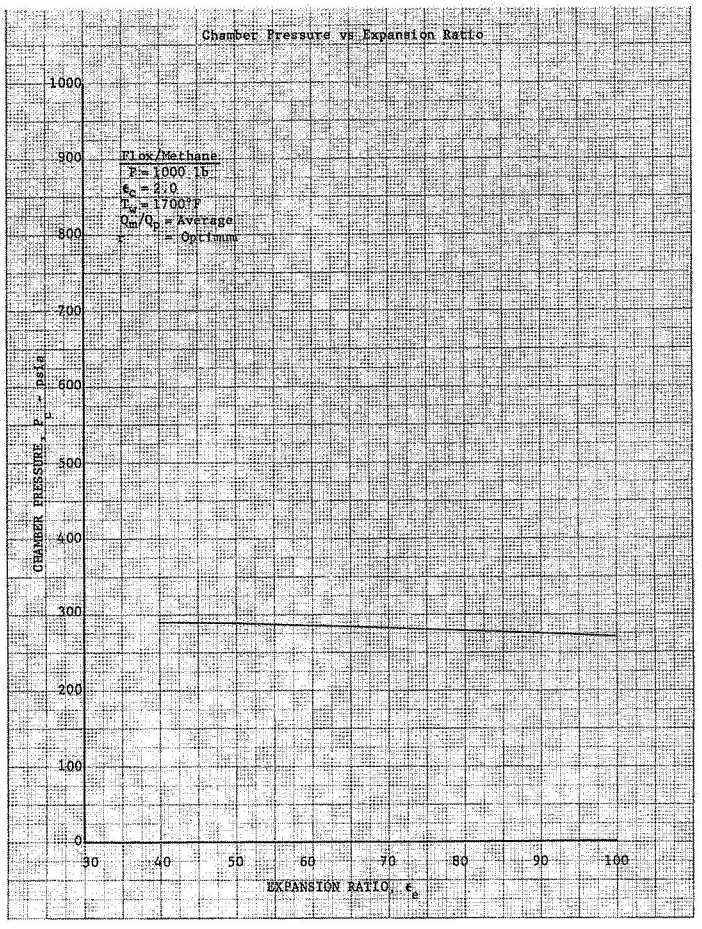
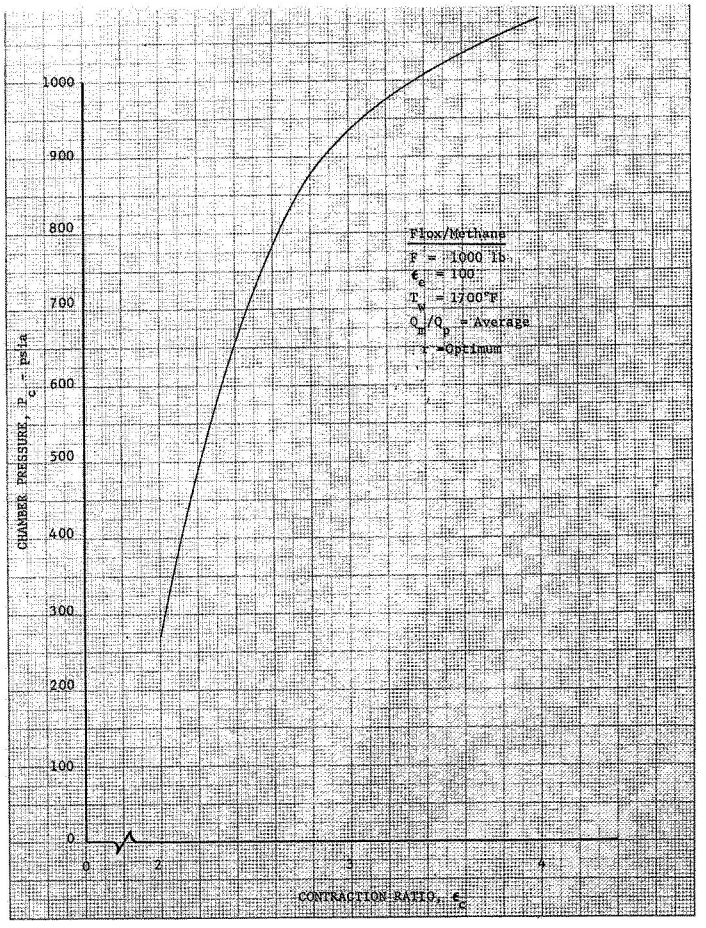


Figure 25. Feasibility Study Results - Chamber Pressure Regenerative Cooling Limits vs Mixture Ratio

DF 60445



DF 60446 Figure 26. Feasibility Study Results - Chamber Pressure Regenerative Cooling Limits vs Expansion Ratio



DF 60447 Figure 27. Feasibility Study Results - Chamber Pressure Regenerative Cooling Limits vs Contraction Ratio

The chamber pressure cooling limits for the five fuels considered (at the optimum flox mixture ratios) are plotted versus thrust in figure 28 for T_w = 2100°F, ϵ_c = 2, and ϵ_e = 100. A curve for butene-1 is not included in the illustration because under these conditions cooling is possible at chamber pressures above 1000 psia at all thrust levels with that fuel. The maximum chamber pressures attainable with methane are lower than those for the other fuels primarily because the average Q_m/Q_p ratio indicated for methane in experimental tests is higher than the Q_m/Q_p ratios for other fuels. The effect of Q_m/Q_p on chamber pressure limits was assessed at the optimum flox mixture ratio, and for the same set of conditions (T_w = 2100°F, ϵ_c = 2, and ϵ_e = 100) by assuming that Q_m/Q_p was 1.0 for all fuels (i.e. no heat reduction because of carbon deposition on the chamber walls). The resulting chamber pressure cooling limits are shown in figure 29. Note that the order of the curves is completely reversed from that obtained with the average Q_m/Q_p values. The highest chamber pressure limit is now shown for methane and the lowest for butene-1.

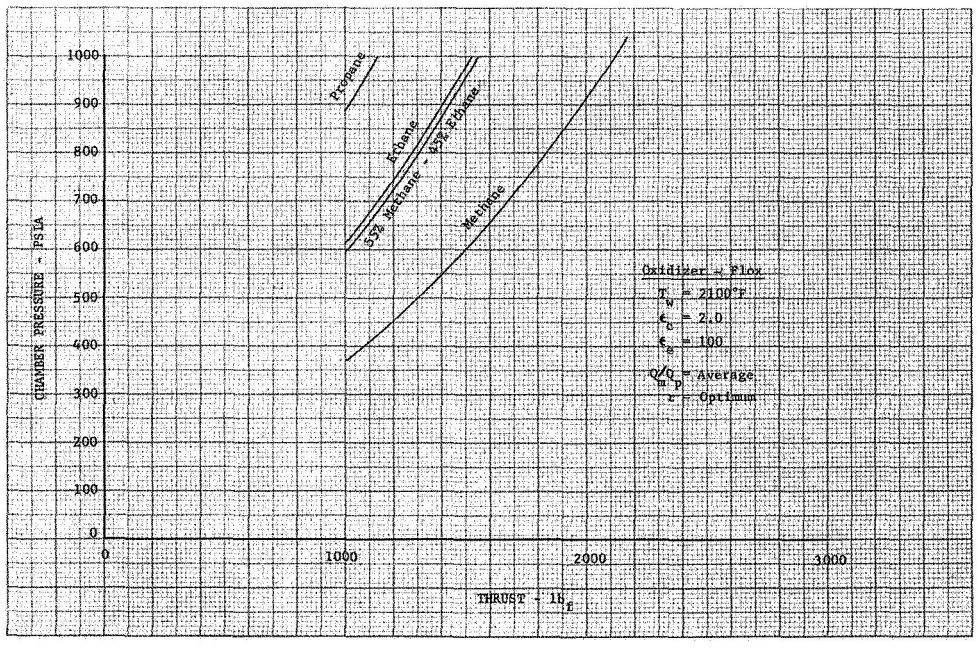


Figure 28. Feasibility Study Results - Chamber Pressure Regenerative Cooling Limits as a Function of Thrust for Q_m/Q_p = Average

DF 60107

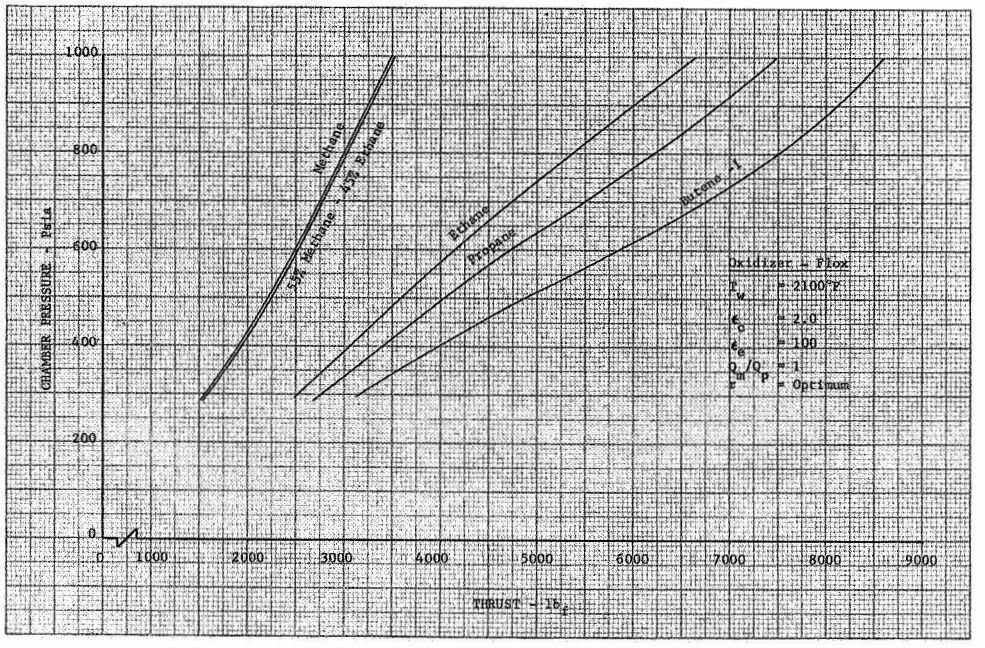


Figure 29. Feasibility Study Results - Chamber Pressure Regenerative Cooling Limits as a Function of Thrust for $Q_m/Q_p = 1.0$ DF 60108

3. Regenerative Cooling Limits for Subcritical Pressures

Regenerative cooling for subcritical pressures was also investigated for the combination of parameters that gives the highest coolant temperature rise (i.e., for $\epsilon_c = 2$, $\epsilon_e = 100$, $T_w = 1700°F$, and optimum mixture ratio). The area in which regenerative cooling is possible at these severe conditions is indicated by the shaded blocks in table VI. Note that only butene-1 can be used as a subcritical coolant at all thrust levels.

Figures 30 and 31 are graphic presentations of subcritical cooling limits for the highest-coolant-temperature-rise condition for flox and OF_2, respectively. Regenerative cooling is feasible at thrust levels to the right of the constant mixture ratio curves. Decreasing mixture ratio has the effect of reducing the lower thrust limits for the same reason as in the supercritical case: increased coolant flow.

Subcritical regenerative cooling could be extended beyond the limits shown in the same manner as that demonstrated for supercritical cooling by selecting values for the parameters that reduce the thrust chamber heat load and thus provide a lower coolant temperature rise. The coolant temperature rise will be lowest with the highest contraction ratio (4), lowest expansion ratio (40), highest wall temperature (3200°F), and lowest mixture ratio (70% optimum). With this set of conditions, ethane, propane, and butene-1 can be used at all thrust levels as subcritical regenerative coolants, as shown by the shaded blocks in table VII. Methane and the methane-ethane blend are not well suited for low chamber pressure operation because of their limited liquid range.

The foregoing results indicate that butene-1 and propane, which have the highest critical temperatures and thus the highest liquid phase heat capacities, are the best subcritical coolants. However, these fuels also have the lowest Q_m/Q_p factors. Table VIII shows the effects of nullifying the assumed Q_m/Q_p values, by assuming no heat reduction due to carbon deposition on the chamber walls at the lowest coolant temperature rise condition (T_w = 3200°F, ϵ_c = 4.0, ϵ_e = 40, and r = 70% of optimum). The shaded areas in which regenerative cooling is feasible are reduced significantly but this does not alter the conclusion that butene-1 and propane are the best subcritical coolants.

Table VI. Feasibility Study Results - Minimum Regenerative Cooling Limits for Subcritical Coolant Pressures

T_w = 1700°F, ϵ_c = 2.0, ϵ_e = 100, r - Optimum, Q_m/Q_p = Average, P_{out}/P_c = 2.0

Propellants		Thrust Level - lb									
		1000		2500		5000		10,000		20,000	
Fuel	Oxidizer	Chamber Pressure - psia									
		100	250	100	250	100	250	100	250	100	250
Methane	Flox										
	OF_2										
55% Methane 45% Ethane	Flox										
	OF_2										
Ethane	Flox										
	OF_2										
Propane	Flox										
	OF_2										
Butene-1	Flox										
	OF_2										

Regenerative Cooling Permissible

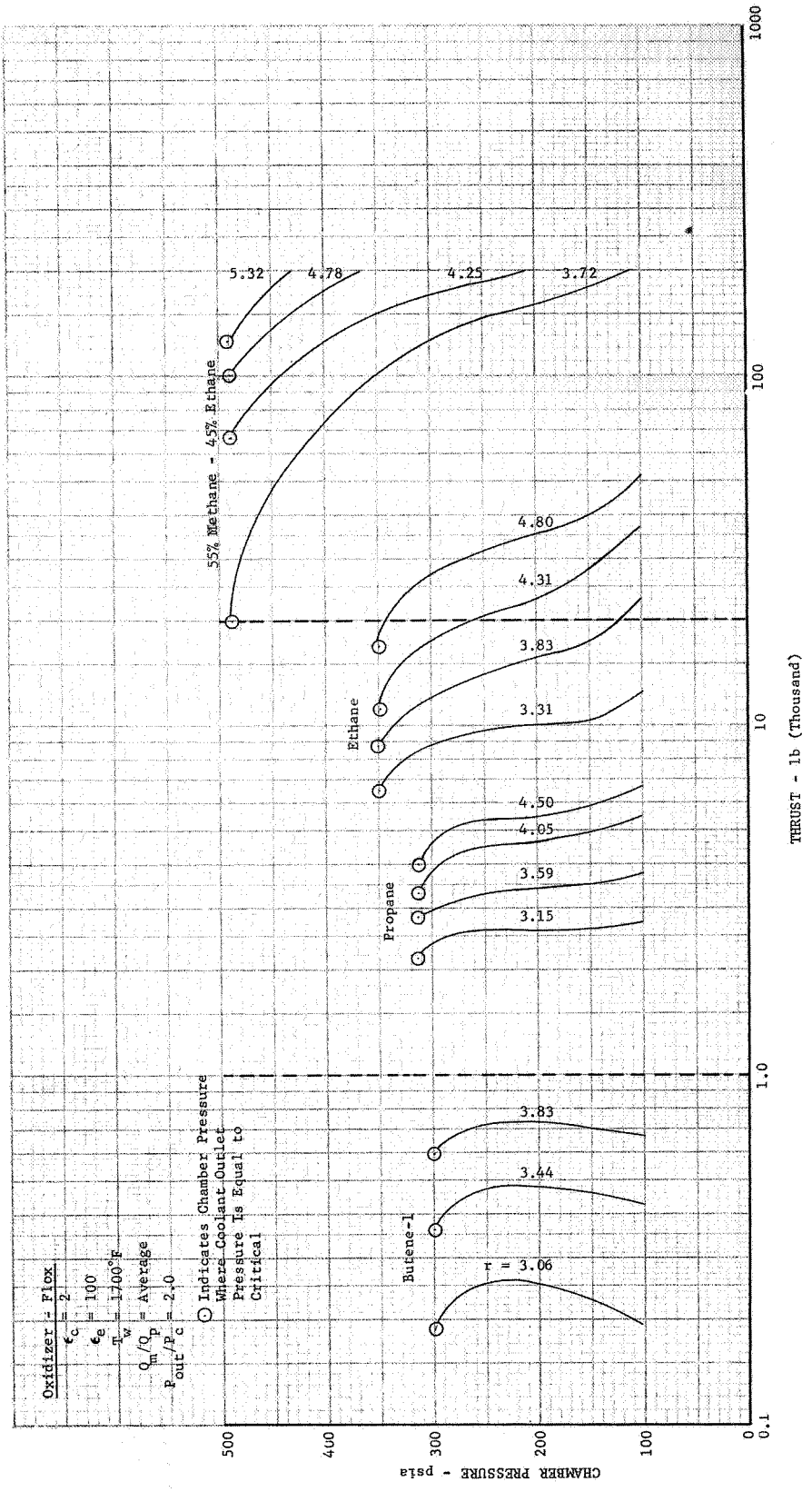


Figure 30. Feasibility Study Results - Minimum Chamber Pressure Regenerative Cooling Limits With Flox for Subcritical Coolant Pressures

DF 60109

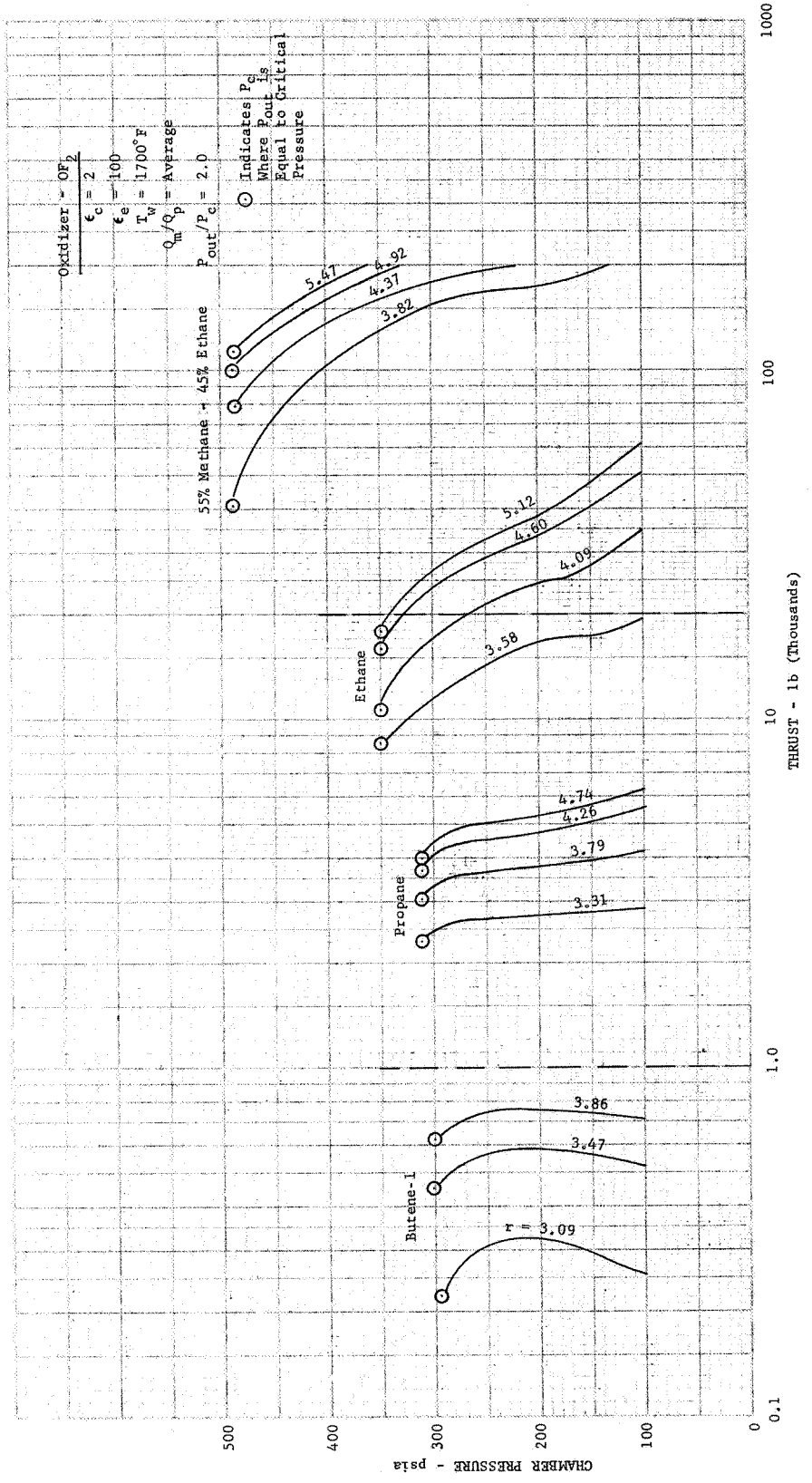


Figure 31. Feasibility Study Results - Minimum Chamber Pressure Regenerative Cooling Limits With OF_2 for Subcritical Coolant Pressures

DF 60110

Table VII. Feasibility Study Results - Chamber Pressure Regenerative Cooling Limits for Sub-Critical Coolant Pressures

$T_w = 3200°F$, $\epsilon_e = 40$, $\epsilon_c = 4.0$, r = 70% Optimum, Q_m/Q_p = Average
$P_{out}/P_c = 2.0$

Propellants		Thrust Level - lb									
		1000		2500		5000		10,000		20,000	
Fuel	Oxidizer	Chamber Pressure - psia									
		100	250	100	250	100	250	100	250	100	250
Methane	Flox										
	OF_2										
55% Methane 45% Ethane	Flox										
	OF_2										
Ethane	Flox										
	OF_2										
Propane	Flox										
	OF_2										
Butene-1	Flox										
	OF_2										

Regenerative Cooling Permissible

Table VIII. Feasibility Study Results - Regenerative Cooling Limits for Subcritical Coolant Pressures

$\epsilon_c = 4$, $\epsilon_e = 40$, $T_w = 3200$, r = 70% Optimum, $Q_m/Q_p = 1.0$
$P_{out}/P_c = 2.0$

Propellants		Thrust Level - lb									
		1000		2500		5000		10,000		20,000	
Fuel	Oxidizer	Chamber Pressure - psia									
		100	250	100	250	100	250	100	250	100	250
Methane	Flox										
	OF_2										
55% Methane 45% Ethane	Flox										
	OF_2										
Ethane	Flox										
	OF_2										
Propane	Flox										
	OF_2										
Butene-1	Flox										
	OF_2										

Regenerative Cooling Permissible

c. Summary of Results

Based on the limits determined in the feasibility study it can be concluded that, if the heat reduction due to carbon deposition on the chamber walls is as great as observed in past firing tests with flox/LPG propellants, regenerative cooling is possible in the chamber pressure range from 100 to 1000 psia at all thrust levels from 1000 to 20,000 lb if the fuel and design parameters are properly selected.

With the coolant at supercritical pressures, there are chamber pressure regenerative cooling limits only at the lowest thrust levels, 1000 and 2500 lb, when the highest-coolant-temperature rise condition (ϵ_c = 2, ϵ_e = 100, T_w = 1700°F and optimum mixture ratios) is assumed. When more nominal heat loads are considered, the thrust limit is below 1000 pounds at 1000 psia chamber pressure. At subcritical coolant pressures, the application of regenerative cooling is more restricted. Only Butene-1, which has a high critical temperature and thus a large liquid-phase heat capacity, can be used at all thrust levels and at chamber pressure down to 100 psia without the danger of bulk boiling at the maximum heating condition.

The areas where regenerative cooling is feasible for each of the fuels with the optimum flox mixture and OF_2 are shown in figure 32 for both the lowest and the highest coolant-temperature rise conditions, which are as follows:

Parameter	Maximum Coolant Temperature Rise	Minimum Coolant Temperature Rise
T_w	1700°F	3200°F
ϵ_e	100	40
ϵ_c	2.0	4.0
r	Optimum	70% Optimum

Figure 33 presents chamber-pressure-thrust limits for each of the fuels with flox at the set of conditions that was of most interest for the subsequent detailed heat transfer study (i.e., for ϵ_c = 4, ϵ_e = 100, T_w = 1700°F, and optimum mixture ratios). A contraction ratio of 4 was selected for primary evaluation in the detailed heat transfer study based on injector considerations. The wall temperature of 1700°F corresponds to the maximum level considered for nickel Thermal Skin thrust chambers. The other conditions, ϵ_e = 100 and optimum mixture ratio, were selected for performance reasons.

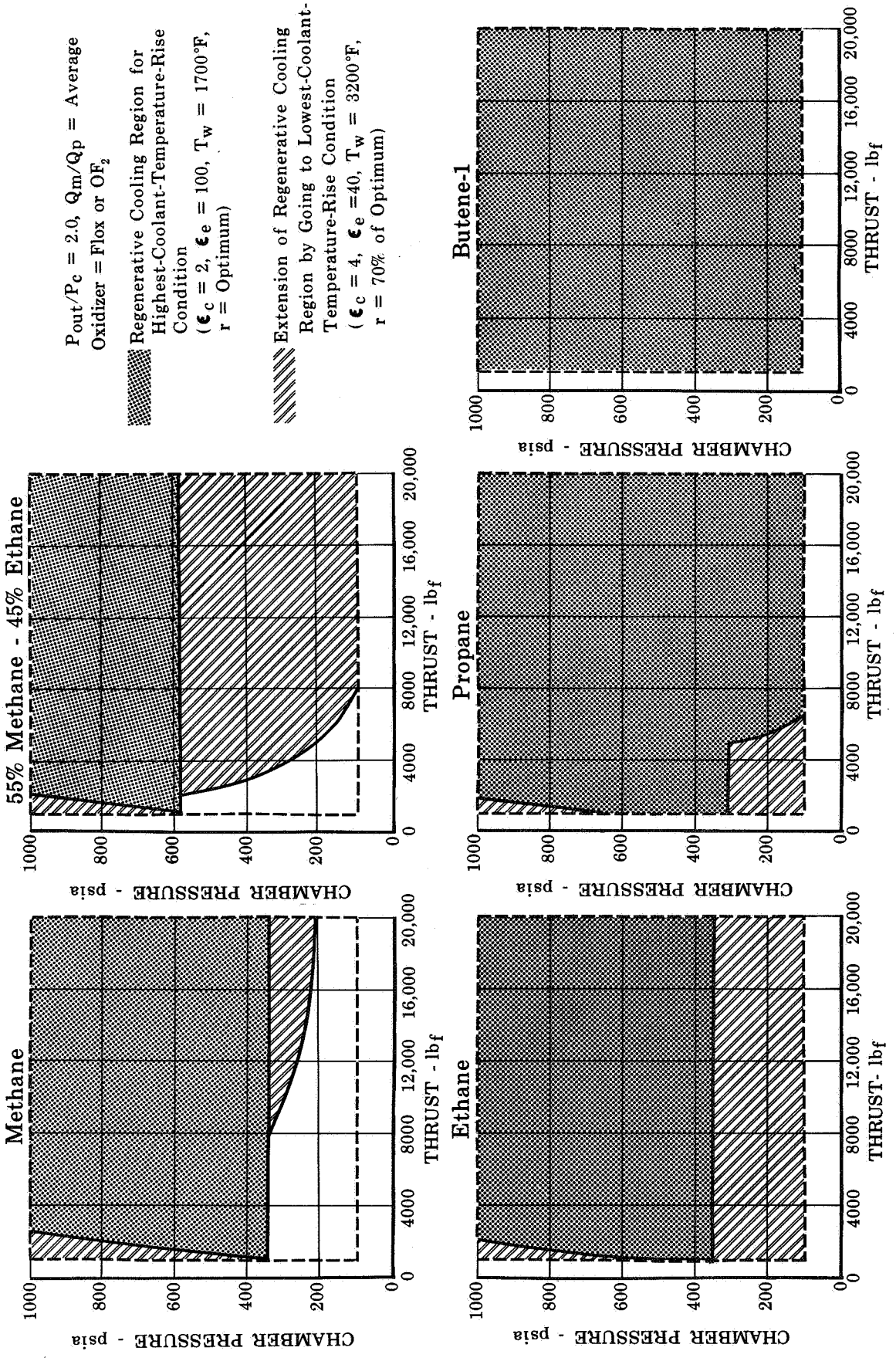


Figure 32. Feasibility Study Regenerative Cooling Limits: P_{out}/P_c = 2.0, Q_m/Q_p = Average FD 23283A

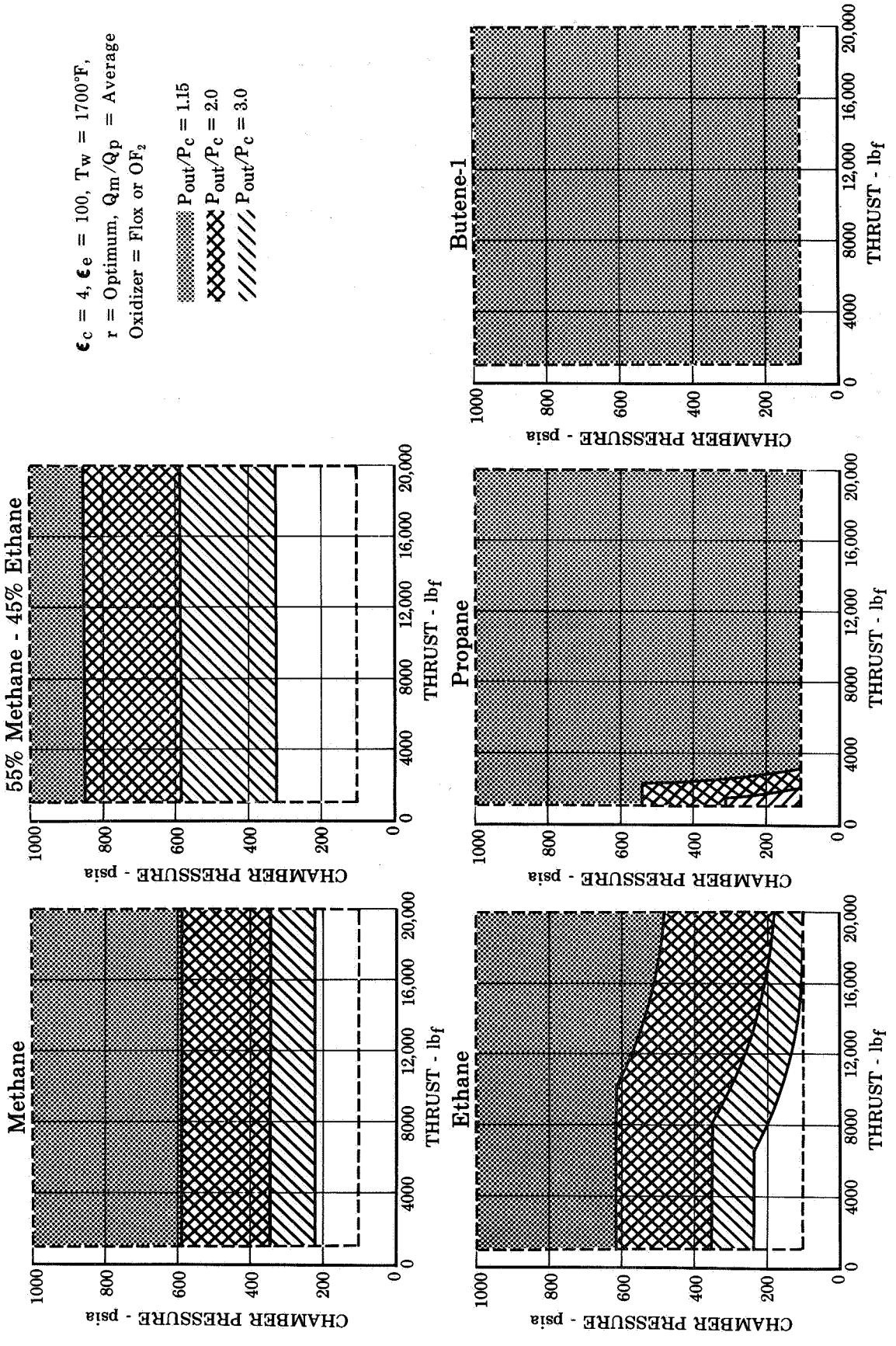


Figure 33. Feasibility Study - Regenerative Cooling Limits: ϵ_c = 4, ϵ_e = 100, T_w = 1700°F, FD 23284A
r = Optimum, Q_m/Q_p = Average

The basic limits presented in figure 33 were premised upon use of a coolant jacket discharge pressure/chamber pressure ratio of 2.0, as were all the limits discussed previously. This ratio is of importance when practical applications are considered, since it is affected by the type of engine cycle selected. The P_{out}/P_c ratios in the range of 2.0 to 3.0 are appropriate for expander cycle engines, whereas values from 1.15 to 1.65 are most typical for pressure-fed or gas generator cycle engines. Limits determined for P_{out}/P_c ratios of 1.15, 2.0 and 3.0 are also included in the illustration. There is no noticeable effect of P_{out}/P_c ratio on upper chamber pressure limits within the ground rules for the feasibility study, but there is a substantial effect on the lower pressure cooling limits, where higher pressures suppress boiling, which was the limiting criterion.

SECTION V
DETAILED HEAT TRANSFER STUDY

A. APPROACH

1. General

To evaluate feasibility, the heat absorption capacities of the fuels were compared to the total heat inputs to thrust chambers on a gross overall basis for a relatively large number of fuels, thrust levels, chamber pressures, etc. However, because heat flux varies significantly along the axis of the rocket thrust chamber, local conditions must be considered in a more detailed screening to determine practical regenerative cooling limits. This more extensive examination was the objective of the detailed heat transfer study.

Consideration of local conditions requires that actual coolant passage design data be generated, which involves a significant analytical effort. It is therefore impractical to attempt a study over the same wide ranges of variables that were treated in the feasibility effort. Initial contract requirements were to make calculations to determine practical limits for regenerative cooling within the chamber pressure range of from 100 to 1000 psia for two oxidizer/fuel combinations at each of three thrust levels, 1000, 5000, and 20,000 lb, considering three wall temperature limits (and associated materials) in each instance. The base case for each combination was for optimum mixture ratio and an expansion ratio of 100. Mixture ratio was to be varied down to 70% optimum and expansion ratio down to 40 to determine whether limits could be extended.

The thrust chamber wall temperature limits specified were (1) 1700°F for stainless steel, (2) 2100°F for a metal such as Haynes 25, and (3) 3200°F for a wall with a heat barrier coating. Fuel and oxidizer combinations selected by the NASA-LeRC project manager for the various thrust levels were

1000 lb_f Thrust	5000 lb_f Thrust	20,000 lb_f Thrust
Flox/Methane	Flox/Methane	Flox/Methane
OF_2/Butene-1	OF_2/55% Methane - 45% Ethane	OF_2/Propane

To assure that the greatest value would be realized for the effort expended in the detailed heat transfer study, results were reviewed as work progressed so that emphasis could be shifted to permit investigation in areas that showed promise. In implementing this approach, it became necessary to eliminate some of the cases in the cooling limit investigation so that other studies could be accomplished within the planned effort. In final form, the study consisted of three parts:

1. Cooling limit determination
2. Investigation of influence of assumed parameters
3. Investigation of off-design operation for a fixed design.

The cooling limit determination met the requirements originally outlined, but with changes in the number of materials considered at each thrust level and, most notably, the addition of nickel as a thrust chamber material. The investigation of the influence of various parameters was accomplished to evaluate the effects on results of the various assumptions that were necessary to permit determination of limits. Limits for a fixed design were investigated to evaluate the possibility of off-design operation of thrust chambers designed for 8000-lb thrust at 500-psia chamber pressure; three different oxidizer/fuel combinations were considered. Results obtained in the three different phases of the study are presented in Paragraph B. Assumptions, cooling limit criteria, and analytical procedures are discussed in the following subparagraphs.

2. Assumptions

The important variables for the detailed heat transfer study were defined by contract requirements; however, several additional assumptions were necessary for the calculations. The most important of these were as follows:

1. Thermal Skin thrust chamber construction was assumed for all cases. A description of this concept for thrust chamber design is presented in Appendix A. The Thermal Skin approach offers advantages over more conventional tubular designs in several respects. Thermal Skin thrust chambers can be fabricated at low cost and in a much shorter time, which is important to later hardware portions of the program. More basic to the extension of regenerative cooling to high chamber pressures, however, is the latitude

provided in the design of coolant passage geometry. For example, for the flox/methane propellant combination at 5000-lb thrust, the maximum chamber pressure cooling limit is increased from approximately 230 to over 1000 psia by using Thermal Skin rather than accepting the coolant passage geometry limits imposed if tubular wall thrust chambers were employed (see Appendix A).

2. The base material for chambers with thermal barrier coatings operating at 3200°F was Haynes 25 alloy. The allowable interface temperature, therefore, was 2100°F.

3. The chamber contraction ratio (ϵ_c) was 4. Selection of this value was based on injector considerations, which indicated that for the chamber pressure range of primary interest (500 to 1000 psia), contraction ratios of at least 4 will be required to keep the injector element thrust size in a range conducive to high performance.

4. The chamber cooling jacket inlet pressure/chamber pressure ratio (P_{in}/P_c) was taken to be 3 for flox/methane and OF_2/55% methane - 45% ethane. This value is representative of the P_{in}/P_c level in an expander cycle for jacket pressure drops consistent with limits discussed later. With the OF_2/butene-1 and OF_2/propane propellant combinations, a gas generator cycle would have to be used and therefore the P_{in}/P_c ratio was assumed to be 1.65.

5. The chamber characteristic length was assumed to be 30 inches. This value was specified in contract requirements; furthermore, it probably reflects approximately the required L^* for high combustion performance with the flox/light hydrocarbon fuels.

6. The heat reduction factor due to carbon deposition on the chamber walls (Q_m/Q_p) is equal to the average value established for the respective fuels based on previous combustion tests.

7. The heat flux profile in the chamber was assumed to be that predicted by the Bartz short form equation; only the level was adjusted by the Q_m/Q_p ratio. With the Bartz profile, the peak heat flux occurs at the throat, and therefore the coolant passage design is more critical at the throat station than at other axial locations. Coolant passages were sized so that the hot-side wall temperature at the throat was equal to the maximum permissible design value. On either side of the throat region, the number of coolant slots was held constant and the passages were changed to suit the chamber geometry until widths reached dimensions that produced excessive bending stresses (i.e., equal to the stress that causes a 0.2% yield). At such points, coolant passages were split and the number of passages was doubled. Subsequent splits were also made as dictated by stress considerations. The design approach used was necessary to

systematize calculation procedures for the relatively large number of chambers studied. However, it resulted in some regions of the chamber being overcooled as indicated by the fact that the combustion-side wall temperatures were below the design level. It is possible to optimize the passages so that wall temperature is held constant throughout the chamber permitting a reduction in coolant velocities and hence extension of regenerative cooling as limited by jacket coolant pressure drop considerations. However, the optimization procedure is a lengthy iterative process that is impractical to apply in a generalized study such as this. To provide an indication of the gains that can be achieved through optimization, the necessary iterations were accomplished, using the Bartz profile for a selected case. Results are discussed in Paragraph B3b.

The values assumed for the parameters discussed in the foregoing items 3 through 6, as well as the extent to which coolant passage geometry is optimized, can affect the limit values obtained. However, the only practical approach for the cooling limit investigation was to maintain constant values for all cases so that comparable results would be obtained. To provide the reader with an indication of the importance of the assumptions on the results obtained, assumed values were varied for specific cases. The effects of the variations on limit results are presented in Paragraph B3a.

3. Cooling Limit Criteria

Chamber pressure regenerative cooling limits were established based on considerations of the following criteria:

1. Upper limit heat flux for nucleate boiling (transition to film boiling)
2. Thermal decomposition of the coolant due to high coolant-side wall temperatures
3. Allowable operating temperature for engine structural components
4. Feasibility of fabricating the required coolant passage dimensions
5. Pressure drop through the coolant passages.

Each of these criteria is treated in greater detail in the following discussion. The first three criteria correspond to those used in the feasibility study. In the detailed study, the first two criteria, (i.e., boiling and fuel thermal decomposition) could be treated more precisely because variations in heat flux and coolant conditions (temperature and pressure) along the flow path in the chamber wall were considered. The third criterion, which is related to the structural temperature operating limits, applies only to the outlet coolant bulk temperature, and thus was treated in the same manner in both parts of the study. The last two criteria are related to the coolant passage design and thus apply only to the detailed study.

The first and fifth criteria were of greatest importance in the detailed heat transfer study. It was found that the boiling criterion set limits at subcritical pressures whereas the coolant pressure drop set the cooling limits for supercritical coolant pressures.

a. Transition to Film Boiling

For subcritical coolant pressures, transition to film boiling occurs when the upper limit heat flux for nucleate boiling is exceeded. Because of the high wall temperatures that accompany the transition from nucleate to film boiling, it was assumed that this mode of heat transfer could not be tolerated in the coolant passages at any chamber location.

Only the coolant outlet state was known in the feasibility study, and thus limits were established by ensuring that the coolant outlet temperature was lower than the corresponding saturation temperature at a given subcritical coolant pressure. This approach thus assured that bulk boiling would not be encountered. In the detailed study the same comparison was made, but in addition, local heat flux values were compared to upper limit heat fluxes for nucleate boiling. This comparison produced a second subcritical cooling limit.

b. Thermal Decomposition Temperature

In the detailed heat transfer study as in the feasibility study, the incipient decomposition temperature (T_{id}) was used to set an upper coolant temperature level (see Appendix C). In the detailed study however, the

limit was placed on local coolant film temperature rather than on the outlet coolant bulk temperature. The limiting film temperatures were

Fuel	Limiting Film Temperature, °R
Methane	1865
55% Methane - 45% Ethane	1715
Propane	1320
Butene-1	1160

c. Structural Temperature Limit

The structural temperature limit was assumed to be 1760°R and, as in the feasibility study, the coolant bulk temperature at the outlet of the heat exchanger was limited to temperatures less than 1760°R.

d. Coolant Passage Fabrication

As discussed in subparagraph 2, Assumptions, Thermal Skin thrust chamber construction was assumed because of the latitude it provides in the design of coolant passages. Although the feasibility of Thermal Skin thrust chambers has been demonstrated (see Appendix A), design and fabrication limits have not been fully investigated. Later tasks in the program require fabrication of Thermal Skin thrust chambers and to assure that study results would be applicable to the hardware effort, it was decided not to base results upon limits that can be achieved with future development of techniques, but rather to assume coolant passage dimensions consistent with demonstrated state-of-the-art engraving practice.

Minimum dimensions for the width (w), web thickness (s), and wall thickness (δ) (see figure 34) were set, based on past experience, to be 0.012, 0.015, and 0.025 inch. The maximum permissible passage depth/width ratio (ℓ/w) was assumed to be 1.33. This depth/width ratio is about the current limit for single-pass etching of nickel and stainless steel without significant side-etch effects that would cause higher tolerances on passage width. As additional engraving experience is gained, the permissible depth/width ratio will undoubtedly increase.

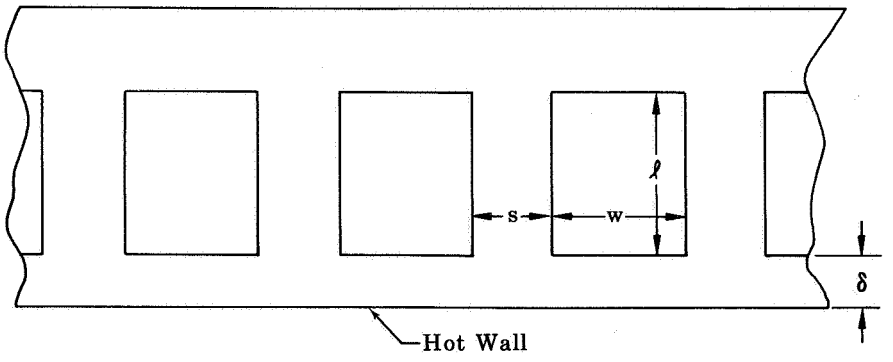


Figure 34. Thermal Skin$_{TM}$ Passage Dimensions FD 23344

Coolant passage roughness was assumed to be 100 microinches, based on measurements in coolant passages of stainless steel and nickel Thermal Skin plates that were previously fabricated.

In addition (and not related to engraving) the coolant passage width (w) was assumed to be equal to the web thickness (s) throughout the chamber, based on a two-dimensional analysis (see Appendix E) that indicated that these proportions maximize the fin efficiency of the web.

e. Coolant Pressure Drop

The cooling jacket pressure drop limits as specified by the contract were that, at chamber pressures up to 200 psia, the limiting pressure drop was 100 psia. Over 200 psia, the limiting pressure drop was equal to half the chamber pressure.

4. Analysis

This subparagraph contains a brief description of the computer programs and procedures used in determining the chamber pressure limits. A detailed discussion of the assumptions and equations used in the analysis is presented in Appendix E.

The determination of each regenerative cooling chamber pressure limit required that a unique chamber be designed and analyzed for a specified set of conditions. Two computer programs were used in the analysis.

The first program, for the IBM 1130 computer, was used to size the thrust chamber and to obtain preliminary estimates of coolant passage dimensions at the throat and at the injector stations for different coolant flow directions so that a preferred coolant direction could be selected.

The second program, for the IBM 360 computer, was used to analyze the complete thrust chamber cooling jacket. Important outputs from the 360 computer program included final values for coolant passage geometry (size and number of coolant slots), coolant conditions and properties, heat flux, and wall temperature at several stations along the chamber. The analysis involves a stepwise integration and simultaneous solution of the continuity, momentum, energy, and state equations along the coolant flow path. The program accounts for (1) coolant passage roughness effects on the coolant film coefficient (through the use of the methods given in Appendix E), (2) coolant property variations with temperature,* and (3) the effect of wall thermal conduction in the web between coolant passages.

Parallel and counterflow coolant directions were evaluated using the 1130 computer program. The passage sizes obtained for the counterflow configuration are also valid for a pass-and-a-half coolant configuration because in this simplified analysis the wall temperature is assumed to be constant and thus the heat pickup in the nozzle portion of the chamber (and hence the coolant temperature at the throat station) would be the same for both flow configurations.

*The coolant thermodynamic transport properties for methane, 55% methane - 45% ethane, propane, and butene-1 that were used in the analysis are presented in graphic form and discussed in detail in Appendix F.

Typical results obtained are shown in figures 35 through 37 for 1000, 5000 and 20,000 lb thrust. Note that the passage sizes shown in these figures are only approximate (and therefore preliminary) because they were obtained by assuming the coolant pressure level at the throat and injector stations. However the indicated trends of passage size variation with chamber pressure and flow direction are correct, and these approximate sizes were used to select the coolant flow direction for subsequent analysis with the 360 computer program. The counterflow configuration was the obvious choice for the 5000- and 20,000-lb thrust levels because it provided larger coolant passages than for parallel flow. At the 1000-lb thrust level, the preferred coolant flow direction is not as obvious; counterflow however does provide larger coolant passages at the injector station for most chamber pressures and larger passage sizes in the throat region at chamber pressures above 400 psia for a 1700°F wall temperature, which is of most interest. Based on these results, counterflow cooling was used exclusively in establishing regenerative cooling limits.

After the coolant flow direction had been selected and the thrust chamber sized using the 1130 program, the chamber pressure cooling limits at supercritical coolant pressure were determined by a two-step iteration procedure based on calculations made using the 360 computer program. The first iteration established coolant passage geometry and coolant pressure drop. For several assumed chamber pressure levels, calculations of pressure drop and wall temperature were made for several coolant passage designs (passage size and number). The design that provided the desired wall temperature at the throat was then determined from a plot similar to that shown in figure 38. Each passage design was checked for manufacturing feasibility and stress level before it was accepted.

In the second iteration, the chamber pressure that could be used for the particular wall temperature without violating one of the other cooling limit criteria was established. At supercritical coolant pressures the coolant jacket pressure drop was the limiting criterion and therefore, in establishing an upper limit for regenerative cooling, the second iteration involved the determination of the chamber pressure at which the cooling jacket pressure drop was equal to the limit ($1/2\ P_c$) as shown in figure 39.

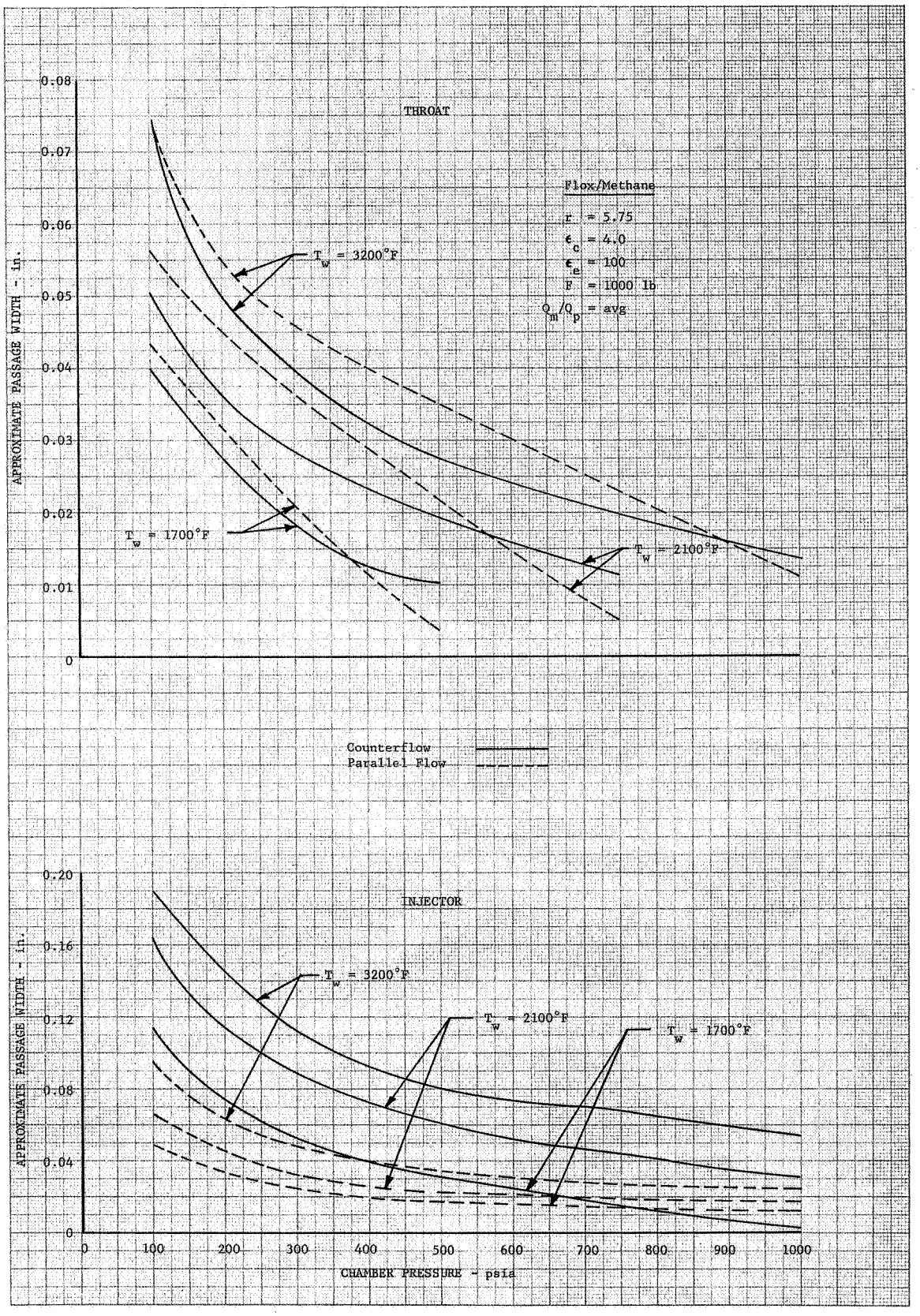


Figure 35. Variation in Coolant Passage Width at Throat and Injector: Flox/Methane, 1000-lb Thrust

DF 62622

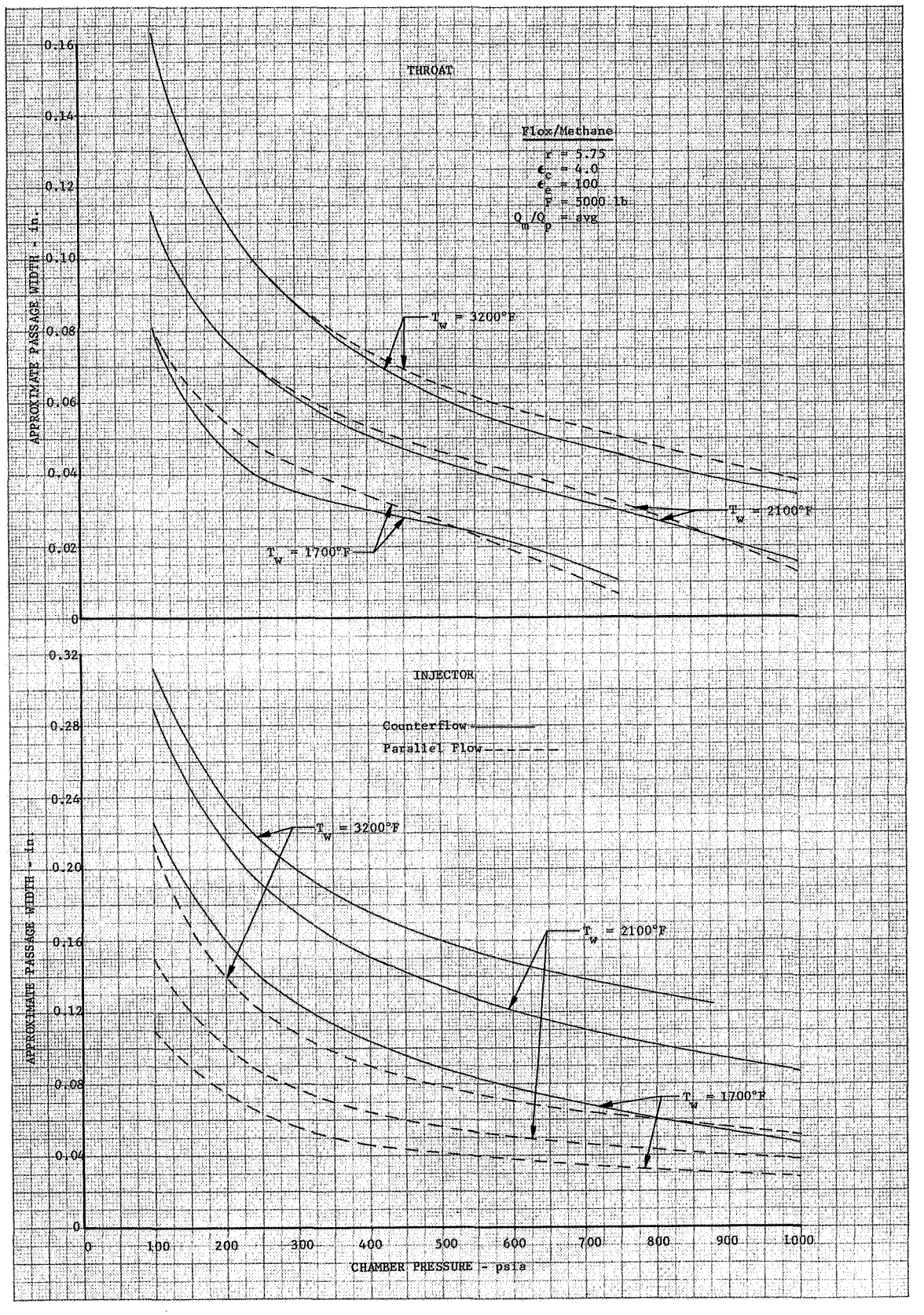


Figure 36. Variation in Coolant Passage Width at Throat and Injector: Flox/Methane, 5000-lb Thrust

DF 62623

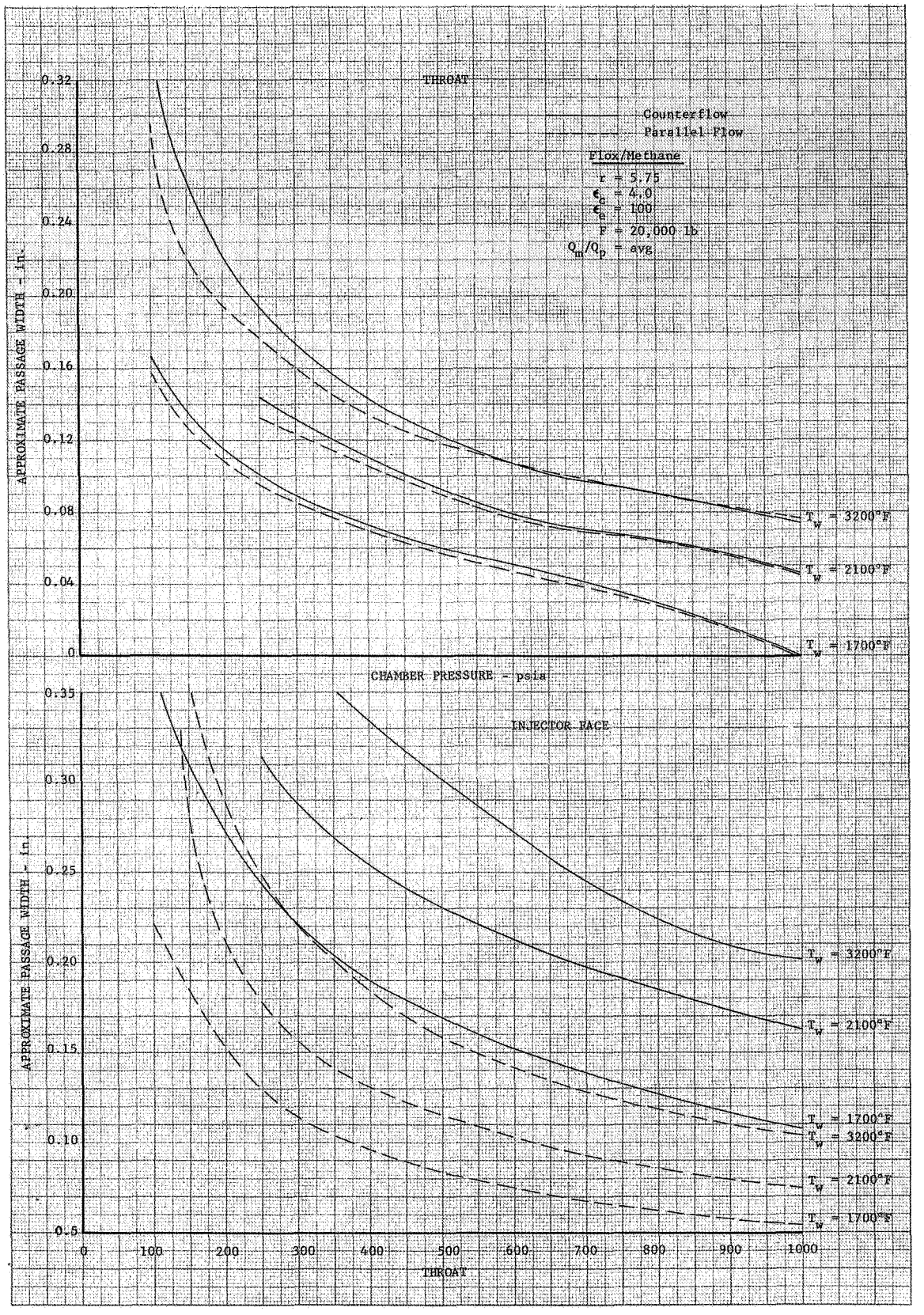


Figure 37. Variation in Coolant Passage Width at Throat and Injector: Flox/Methane, 20,000-lb Thrust

DF 60147

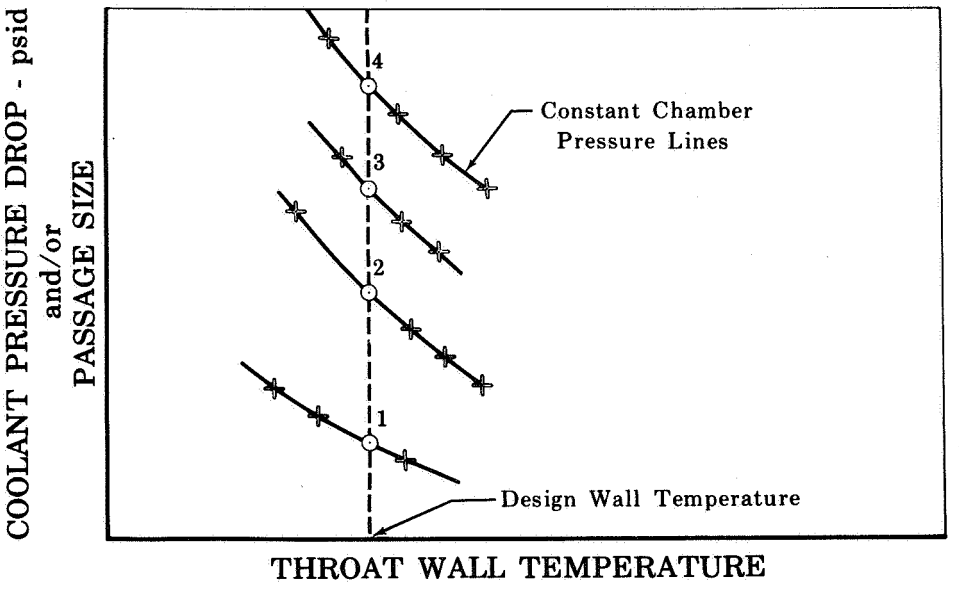


Figure 38. Coolant Passage Geometry and Pressure Drop Iteration FD 23345

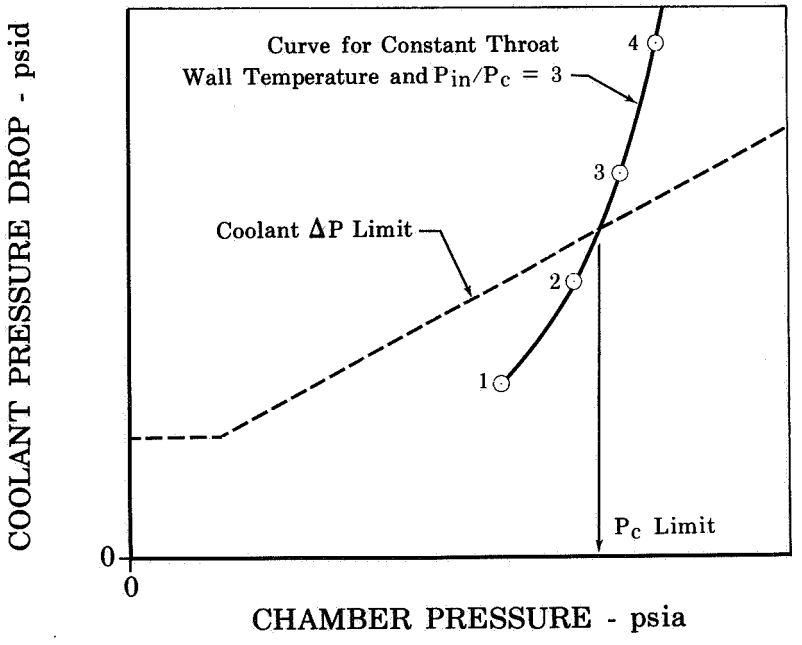


Figure 39. Procedure Used to Determine Chamber Pressure Limit for Supercritical Coolant Pressures FD 23346

Lower chamber pressure limits for regenerative cooling were determined by applying the transition-to-film-boiling criteria. These lower chamber pressure limits were determined either by bulk boiling considerations or by comparing local heat flux values in the chamber to the upper limit heat flux for nucleate boiling.

B. REGENERATIVE COOLING CHAMBER PRESSURE LIMITS

1. Scope

In the detailed heat transfer study, regenerative cooling limits were investigated at thrust levels of 1000, 5000, and 20,000 lb. Both upper and lower chamber pressure regenerative cooling limits for a given thrust level were determined so that practical regenerative cooling regions could be identified. Investigations of influences of assumptions on limits and of effects of off-design operation were also accomplished; however, because primary interest in the hardware portion of the program is in high operating chamber pressures, the investigations were limited to upper limit conditions. Upper chamber pressure limits for regenerative cooling are discussed in subparagraph 2, assumptions and off-design operation are treated in subparagraphs 3 and 4, respectively, and lower chamber pressure limits are included in subparagraph 5.

2. Upper Chamber Pressure Limits

a. General

In establishing the upper regenerative cooling limits at a given thrust level and for a given propellant combination, the cooling limit was first established for optimum mixture ratio and an expansion ratio of 100. Then, in an attempt to extend the regenerative cooling limits to higher chamber pressures, calculations were made for decreases in expansion ratio to 40 and decreases in mixture ratio to 70% optimum.

Table IX summarizes the upper regenerative cooling chamber pressure limits for the various propellants, thrust levels, chamber materials (with corresponding wall temperatures), expansion ratios, and mixture ratios considered. Results for each propellant combination will be presented graphically and treated individually in the following discussion. To summarize briefly, no cooling limits were found below 1000 psia (the maximum chamber pressure level considered in the study) for OF_2/butene-1

Table IX. Summary of Regenerative Cooling Chamber Pressure Limits (Q_m/Q_p = avg)

Thrust Level			1000 lb						5000 lb						20,000 lb					
Propellant			Flox/Methane			OF_2/Butene-1			Flox/Methane			OF_2/55% Methane-45% Ethane			Flox/Methane			OF_2/Propane		
Expansion Ratio			40	60	100	40	60	100	40	60	100	40	60	100	40	60	100	40	60	100
1700°F Nickel 200	% Optimum r	100	825	776	731	> 1000	>1000	> 1000	> 1000	>1000	989	> 1000	>1000	> 1000	> 1000	>1000	> 1000	> 1000	>1000	>1000
		90	838			> 1000			> 1000			> 1000			> 1000			> 1000		
		70	968			> 1000			> 1000			> 1000			> 1000			> 1000		
1700°F 347 Stainless Steel	% Optimum r	100			293				415	375	350	896	944	944			355			
		90							452			903								
		70							522			798								
2100°F Haynes 25	% Optimum r	100	645	625	595	>1000	>1000	>1000	830	780	730	> 1000	>1000	> 1000	825	775	736	> 1000	>1000	>1000
		90	655			>1000			860			> 1000			840			> 1000		
		70	750			>1000			884			> 1000			855			> 1000		

Notes: a. All chamber pressure limits (in psia) for Q_m/Q_p = avg, ϵ_c = 4; P_{in}/P_c = 3.0 for flox/methane and OF_2/55% Methane-45% Ethane; P_{in}/P_c = 1.65 for OF_2 Butene-1, OF_2 Propane.

b. L^* = 30 inch

at the 1000-lb thrust level or for OF_2/propane at the 20,000-lb thrust level. At the 5000-lb thrust level, cooling can be accomplished at chamber pressures above 1000 psia with OF_2/55% methane - 45% ethane for all thrust chamber materials except 347 stainless steel.

In contrast to the other propellant combinations, which were selected for evaluation at only one thrust level, flox/methane was investigated at all three thrust levels. Cooling limits for flox/methane were generally lower than those indicated for the other propellants at all thrust levels. There are two primary reasons for these results. First, and most important, heat loads were higher for flox/methane because the Q_m/Q_p value assumed was higher than for other propellants. Second, methane is less dense than the other fuels and therefore higher velocities (and hence higher pressure drops) are required to generate equivalent heat transfer coefficients.

Important cooling passage dimensions and conditions at the upper chamber pressure cooling limit for the cases studied are presented in table X. For cases where there was no limit below 1000 psia, conditions are given for that maximum chamber pressure level. Coolant pressure drop was the limiting criterion for all cases where the regenerative cooling limit was less than 1000 psia.

Examination of the values given for various parameters in table X will show that assumed limits have not been exceeded. Throat coolant passage dimensions (which are minimum dimensions for the thrust chamber jacket) are greater than the minimum values of 0.015-in. depth by 0.012-in. width. Coolant outlet temperatures are below the 1760°R set by structural considerations, and maximum film temperatures are below the levels set for incipient thermal decomposition.

Table X. Cooling Jacket Parameters For Cooling Limits

Table V-1. Cooling Jacket Parameters For Cooling Limits

Thrust Level lb_f	Propellant	Mixture Ratio, r	ϵ_e	P_c psia	Q_m/Q_p	P_{in}/P_c	Wall Material	Max. Wall Temp, °F	Number of Throat Slots	Slot Width at Throat in.	Slot Height at Throat in.	Web Thickness at Throat in.	Hot Wall Thickness in.	Throat Dia., in.	Thrust Chamber Length L/D*	Max. Film Temp., °R	ΔP psi	Outlet Bulk Temp. °R	Max. Velocity ft/sec
1000	Flox/CH_4	5.75	100	731	0.765	3.0	Ni 200	1692	96	0.0164	0.0219	0.0164	0.025	0.956	11.145	1821	362.5	1663	488.9
1000	Flox/CH_4	5.75	60	776	0.765	3.0	Ni 200	1685	97	0.0160	0.0213	0.0160	0.025	0.937	17.755	1780	386.3	1633	485.5
1000	Flox/CH_4	5.75	40	825	0.765	3.0	Ni 200	1697	97	0.0156	0.0208	0.0156	0.025	0.915	15.843	1787	408.9	1629	483.7
1000	Flox/CH_4	5.16	40	838	0.765	3.0	Ni 200	1705	93	0.0162	0.0217	0.0162	0.025	0.912	15.871	1716	421.0	1548	486.9
1000	Flox/CH_4	4.02	40	968	0.765	3.0	Ni 200	1689	83	0.0172	0.0228	0.0172	0.025	0.855	16.417	1527	492.5	1348	479.1
1000	Flox/CH_4	5.75	100	293	0.765	3.0	St. Steel	1696	117	0.0208	0.0278	0.0208	0.025	1.503	18.290	1337	147.3	1332	622.2
1000	Flox/CH_4	5.75	100	595	0.765	3.0	Haynes 25	2098	101	0.0172	0.0230	0.0172	0.025	1.058	20.386	1697	294.7	1523	470.9
1000	Flox/CH_4	5.75	60	625	0.765	3.0	Haynes 25	2115	102	0.0168	0.0224	0.0168	0.025	1.043	16.942	1691	309.8	1499	469.3
1000	Flox/CH_4	5.75	40	645	0.765	3.0	Haynes 25	2103	104	0.0163	0.0218	0.0163	0.025	1.034	14.903	1646	326.9	1472	470.2
1000	Flox/CH_4	5.16	40	655	0.765	3.0	Haynes 25	2105	100	0.0170	0.0226	0.0170	0.025	1.031	14.925	1584	330.3	1382	468.2
1000	Flox/CH_4	4.02	40	750	0.765	3.0	Haynes 25	2182	87	0.0184	0.0246	0.0184	0.025	0.971	15.372	1452	371.0	1229	453.8
5000	Flox/CH_4	5.75	100	989	0.765	3.0	Ni 200	1698	118	0.0250	0.0334	0.0250	0.025	1.831	17.394	1336	487.8	1121	424.1
5000	Flox/CH_4	5.75	100	350	0.765	3.0	St. Steel	1666	134	0.0367	0.0489	0.0367	0.025	3.078	15.736	1177	166.1	929	388.5
5000	Flox/CH_4	5.75	60	375	0.765	3.0	St. Steel	1663	139	0.0345	0.0460	0.0345	0.025	3.002	12.248	1145	189.6	901	394.4
5000	Flox/CH_4	5.75	40	415	0.765	3.0	St. Steel	1681	140	0.0328	0.0438	0.0328	0.025	2.876	10.257	1136	203.5	883	385.5
5000	Flox/CH_4	5.16	40	452	0.765	3.0	St. Steel	1691	136	0.0326	0.0434	0.0326	0.025	2.771	10.356	1100	226.8	830	385.5
5000	Flox/CH_4	4.02	40	522	0.765	3.0	St. Steel	1658	126	0.0330	0.0440	0.0330	0.025	2.600	10.534	974	258.3	690	359.4
5000	Flox/CH_4	5.75	100	730	0.765	3.0	Haynes 25	2087	128	0.0269	0.0358	0.0269	0.025	2.140	16.805	1255	366.6	1003	403.4
5000	Flox/CH_4	5.75	60	780	0.765	3.0	Haynes 25	2092	131	0.0257	0.0342	0.0257	0.025	2.090	13.338	1213	392.0	964	395.8
5000	Flox/CH_4	5.75	40	830	0.765	3.0	Haynes 25	2118	133	0.0247	0.0329	0.0247	0.025	2.041	11.324	1187	411.3	929	384.7
5000	Flox/CH_4	5.16	40	860	0.765	3.0	Haynes 25	2127	131	0.0247	0.0330	0.0247	0.025	2.014	11.374	1127	423.4	858	380.9
5000	Flox/CH_4	4.02	40	884	0.765	3.0	Haynes 25	2109	119	0.0271	0.0361	0.0271	0.025	2.001	11.397	1007	448.1	721	356.4
20,000	Flox/CH_4	5.75	100	350	0.765	3.0	St. Steel	1654	159	0.0613	0.0818	0.0613	0.0270	6.156	14.518	989	177.1	692	378.8
20,000	Flox/CH_4	5.75	100	736	0.765	3.0	Haynes 25	2134	157	0.0433	0.0577	0.0433	0.0315	4.262	15.059	1009	369.2	707	333.0
20,000	Flox/CH_4	5.75	60	775	0.765	3.0	Haynes 25	2100	162	0.0415	0.0554	0.0415	0.0305	4.222	11.526	968	386.9	661	314.1
20,000	Flox/CH_4	5.75	40	825	0.765	3.0	Haynes 25	2103	168	0.0388	0.0518	0.0388	0.0295	4.094	9.250	932	415.7	630	303.3
20,000	Flox/CH_4	5.16	40	840	0.765	3.0	Haynes 25	2100	167	0.0389	0.0518	0.0389	0.0290	4.075	9.490	891	426.8	589	299.7
20,000	Flox/CH_4	4.02	40	855	0.765	3.0	Haynes 25	2092	149	0.0435	0.0580	0.0435	0.0290	4.069	9.492	824	432.4	515	263.0
5000	Flox/$55\%CH_4 - 45\%C_2H_6$	5.47	100	944	0.645	3.0	St. Steel	1705	161	0.0186	0.0248	0.0186	0.0290	1.860	17.331	1005	471.5	825	329.8
5000	Flox/$55\%CH_4 - 45\%C_2H_6$	5.47	60	944	0.645	3.0	St. Steel	1704	166	0.0182	0.0243	0.0182	0.0290	1.878	13.743	959	472.2	789	319.3
5000	Flox/$55\%CH_4 - 45\%C_2H_6$	5.47	40	896	0.645	3.0	St. Steel	1703	173	0.0181	0.0241	0.0181	0.0290	1.945	11.505	916	450.4	751	310.2
5000	Flox/$55\%CH_4 - 45\%C_2H_6$	3.83	40	900	0.645	3.0	St. Steel	1705	165	0.0193	0.0258	0.0193	0.0290	1.982	11.432	755	442.9	566	226.9
20,000	OF_2/Propane	4.74	100	1000	0.420	1.65	Nickel 200	706	100	0.0577	0.0770	0.0577	0.0250	3.627	15.367	778	62.0	553	78.1
20,000	OF_2/Propane	4.74	100	1000	0.420	1.65	Haynes 25	1531	100	0.0486	0.0649	0.0486	0.0450	3.627	15.367	787	77.0	532	89.2
1000	OF_2/Butene-1	3.86	100	1000	0.255	1.65	Ni 200	1564	30	0.0455	0.0607	0.0455	0.0250	0.819	21.451	1061	10.0	735	20.4
1000	OF_2/Butene-1	3.86	100	1000	0.255	1.65	Haynes 25	1994	30	0.0455	0.0607	0.0455	0.0250	0.819	21.451	1098	4.0	708	20.2
1000	OF_2/Butene-1	3.06	60	1000	0.255	1.65	Haynes 25	2023	30	0.0458	0.0612	0.0458	0.0250	0.827	18.821	1095	3.1	693	19.9
1000	OF_2/Butene-1	2.70	40	1000	0.255	1.65	Haynes 25	2012	30	0.0463	0.0625	0.0463	0.0250	0.839	16.589	1064	3.3	659	21.0

The results presented in tables IX and X show that thrust chamber material selection can have an effect on cooling limits that is equal to or greater than that of wall temperature. Figure 40 presents the regenerative cooling chamber pressure limits for nickel 200, Haynes 25, and 347 stainless steel plotted as functions of thrust for flox/methane at the optimum mixture ratio (5.75) and an expansion ratio of 100 to 1. Increasing the permissible wall temperature from 1700 to 2100°F by using Haynes 25 rather than 347 stainless steel provides an increase in the chamber pressure regenerative cooling limits by 300 to 400 psi. However, by substituting nickel for the stainless steel and maintaining the 1700°F wall temperature limit, the increase in limits is from 400 to 800 psi. The reason for the dramatic increase with nickel is the high conductivity of the material. The effect is peculiar to the Thermal Skin design (at least as contrasted to a tubular chamber) because of the contribution of the webs between passages to the heat transferred to the coolant.

The comparison of the various thrust chamber materials with flox/methane propellants was made early in the study and, as a result, 347 stainless steel was dropped from further consideration as the material for 1700°F wall temperature.

At the 5000-lb thrust level, Haynes 25 with a thermal barrier coating (in addition to nickel 200, Haynes 25, and 347 stainless steel) was evaluated for use with flox/methane and with OF_2/55% methane - 45% ethane. It was found that the thermal barrier coating permitted cooling at chamber pressures above 1000 psia with both propellant combinations because of the heat transfer reduction resulting from the reduced value of $(T_{aw} - T_w)$ realized from the high permissible operating wall temperature (3200°F). Based upon the very high limit found for the thermal barrier coating, and the reason therefor, it appeared that similar results would be obtained at other thrust levels. It was therefore believed that the effort required for rigorous calculation might well be applied to the investigation of other effects, and further treatment of thermal barrier chambers was eliminated in the basic limit investigation. However, a thermal barrier coating was evaluated for OF_2/Butene-1 at 1000-lb thrust but with $Q_m/Q_p = 1$; (see Paragraph B2d following).

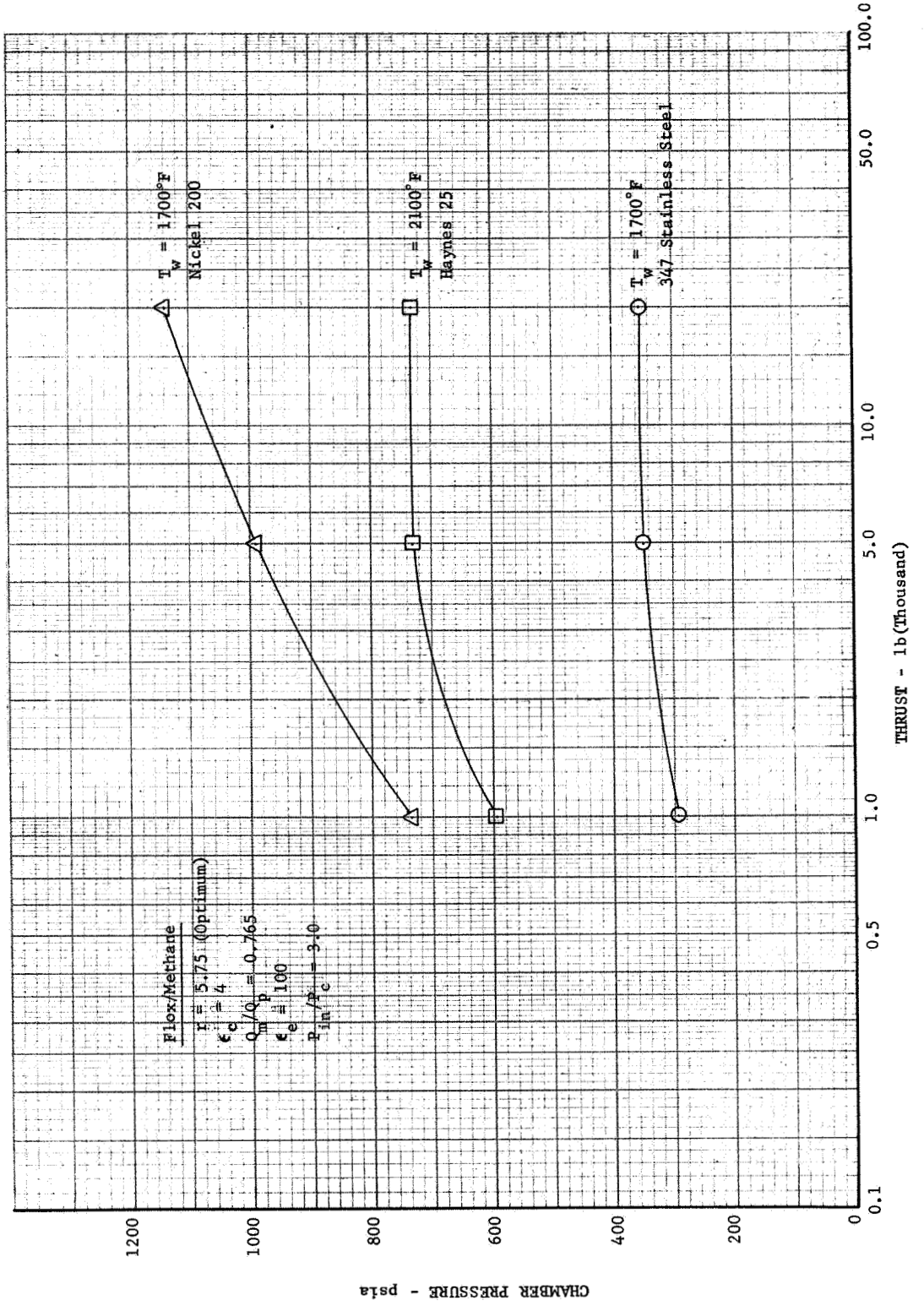


Figure 40. Variation of Regenerative Cooling Chamber Pressure Limits With Thrust: Flox/Methane DF 59065

b. Cooling Limits for Flox/Methane

Flox/methane was the only propellant combination evaluated at all three thrust levels. Figures 41 through 43 present cooling limit curves for the propellants at levels of 1000, 5000, and 20,000 lb, respectively. Figure 40 shows the variation of the regenerative cooling limits with thrust level.

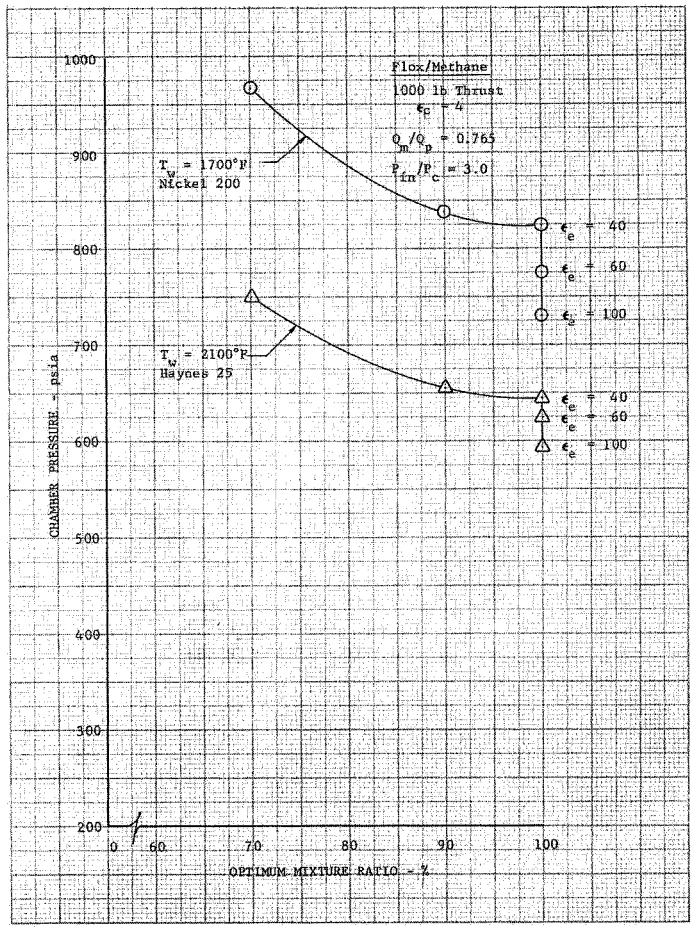


Figure 41. Regenerative Cooling Chamber Pressure Limits: Flox/Methane 1000-lb Thrust

DF 59063

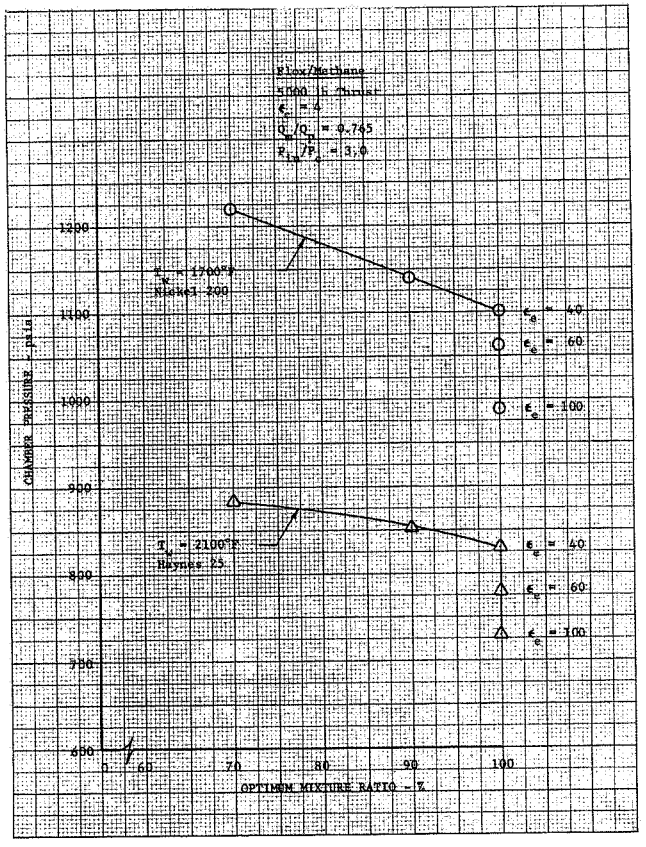


Figure 42. Regenerative Cooling Chamber Pressure Limits: Flox/Methane, 5000-lb Thrust

DF 59062

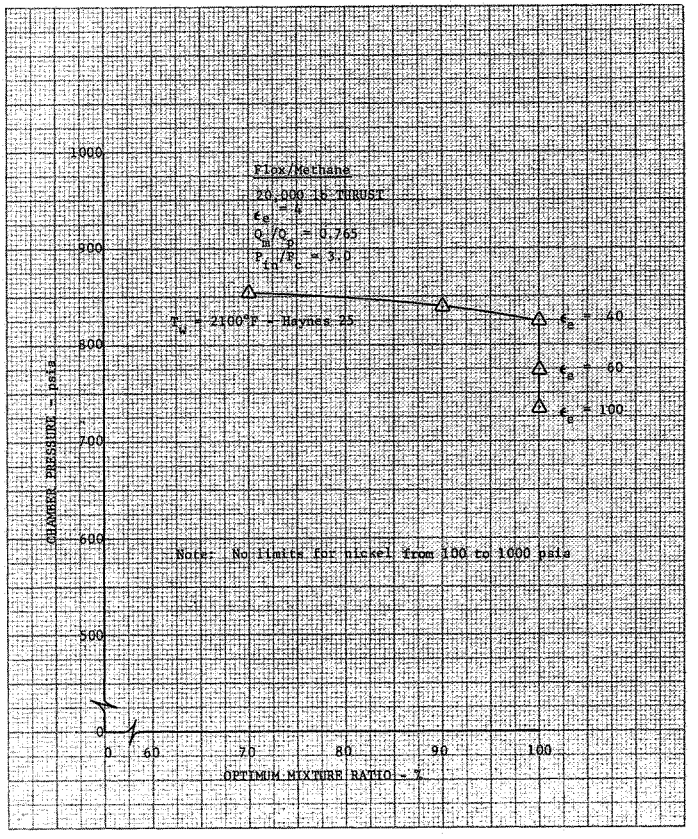


Figure 43. Regenerative Cooling Chamber Pressure Limits: Flox/Methane, 20,000-lb Thrust

DF 59064

It was found that cooling limits increased with increasing thrust level and with decreasing mixture ratio and expansion ratio. This trend is related to the variation of methane coolant temperature in the high heat flux portions of the chamber (i.e., at the throat and in the combustion chamber) with thrust, expansion ratio, and mixture ratio. As the coolant temperature increases, a higher velocity and hence a higher pressure drop are required because the wall-to-bulk temperature difference as well as the coolant density are reduced. The coolant temperature level increases as (1) mixture ratio increases, causing the cooling flow rate to decrease, and (2) expansion ratio decreases, causing the heat transfer in the nozzle to decrease. The coolant temperature increases as thrust decreases because heat transfer does not drop off as rapidly with decreasing thrust as does the coolant flow rate.

Figure 44 illustrates the magnitude of the throat heat fluxes at the upper chamber pressure limits for regenerative cooling. This figure shows the throat heat flux levels for flox/methane. Values for other propellants are tabulated in table X.

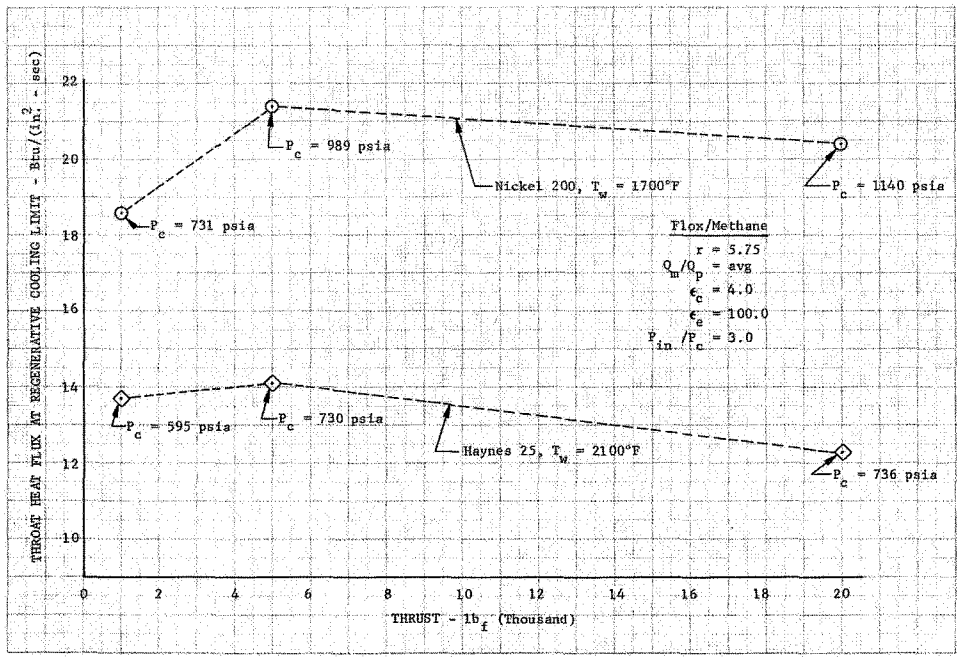


Figure 44. Throat Heat Flux at the Upper Chamber Pressure Limit for Regenerative Cooling DF 62626

c. Cooling Limits for OF_2/55% Methane - 45% Ethane

Figure 45 presents the cooling limit curve for OF_2/55% methane - 45% ethane for 347 stainless steel chambers (limits for both nickel 200 and Haynes 25 are above 1000 psia chamber pressure). The trends of this curve are different from those noted for flox/methane. For flox/methane, the chamber pressure limits increased as both expansion ratio and mixture ratio were decreased (as might be expected). The cooling limits for OF_2/55% methane - 45% ethane decrease with decreases in expansion ratio and mixture ratio.

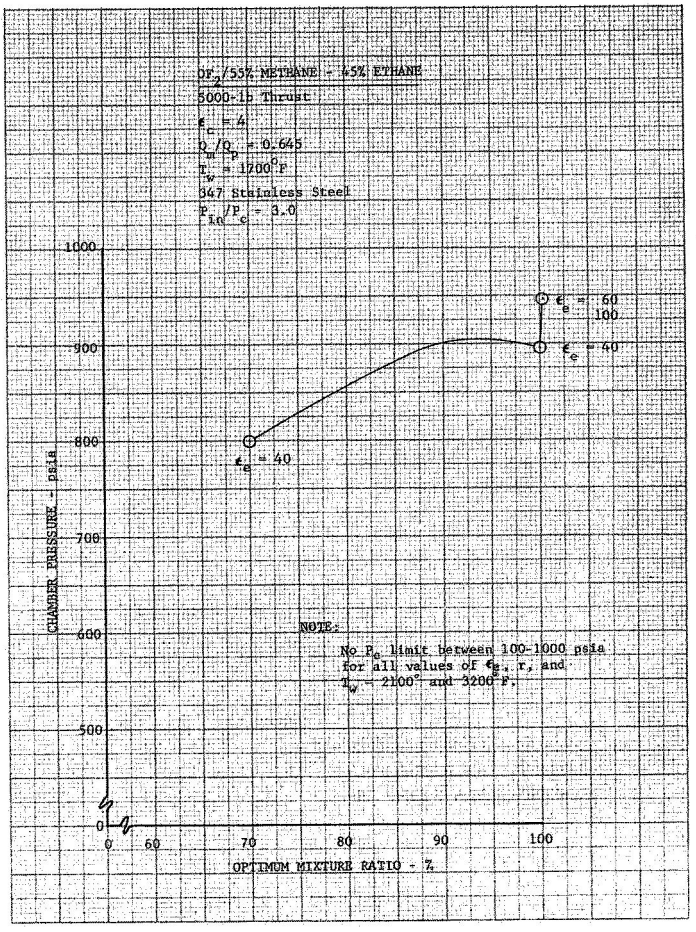


Figure 45. Regenerative Cooling Chamber Pressure Limits: OF_2/55% Methane-45% Ethane, 5000-lb Thrust

DF 59347

The decrease in cooling limits with a decreased expansion ratio is an effect caused by the relationship between heat pickup in the nozzle section and the coolant statepoint at the throat station of the cooling jacket. In contrast to methane, the 55% methane - 45% ethane coolant reaches the throat station in the compressed liquid state. Since there is less heat pickup in the nozzle at an expansion ratio of 40 than at either 60 or 100, the coolant statepoint at the throat station is closer to the dome region where variations in density with temperature are fairly large. As a result, at $\epsilon_e = 40$ there is more variation in coolant density from the film to the bulk condition and the term ρ_f/ρ_b in the coolant heat transfer coefficient equation is reduced. Therefore a higher velocity (hence higher pressure drop) is required to cool at $\epsilon_e = 40$ than at higher expansion ratios.

The different trends in the cooling limit curves for flox/methane and OF_2/55% methane - 45% ethane with changes in mixture ratio are related to differences in the variation of the combustion-side heat transfer coefficient with mixture ratio. Figure 46 compares curves of throat heat flux versus mixture ratio for the two propellant combinations. Note that although there is a slight peak in the flox/methane heat flux curve, it is relatively flat with mixture ratio. However, because of variations in combustion-side film properties for OF_2/55% methane - 45% ethane, the heat flux increases with decreasing mixture ratio.

d. Cooling Limits for OF_2/Butene-1

The results obtained with OF_2/butene-1 at 1000-lb thrust and with a Haynes 25 chamber are shown in figure 47. The upper set of curves (a) shows that if the chamber is designed for a 2100°F wall temperature (using the minimum wall thickness based on fabrication and stress considerations), the film temperature would be above the tolerable level for thermal decomposition (1160°R). By designing for a lower wall temperature, or by increasing the wall thickness, the butene-1 film temperature can be maintained below 1160°R, and the chamber can be cooled to a chamber pressure above 1000 psia without exceeding the cooling jacket pressure drop criterion. The required wall temperatures for maintaining the film temperature at 1160°R are given by the middle set of curves (b). The lower curve (c) shows the wall thickness required to maintain 1160°R film temperature if 2100°F wall temperature is used.

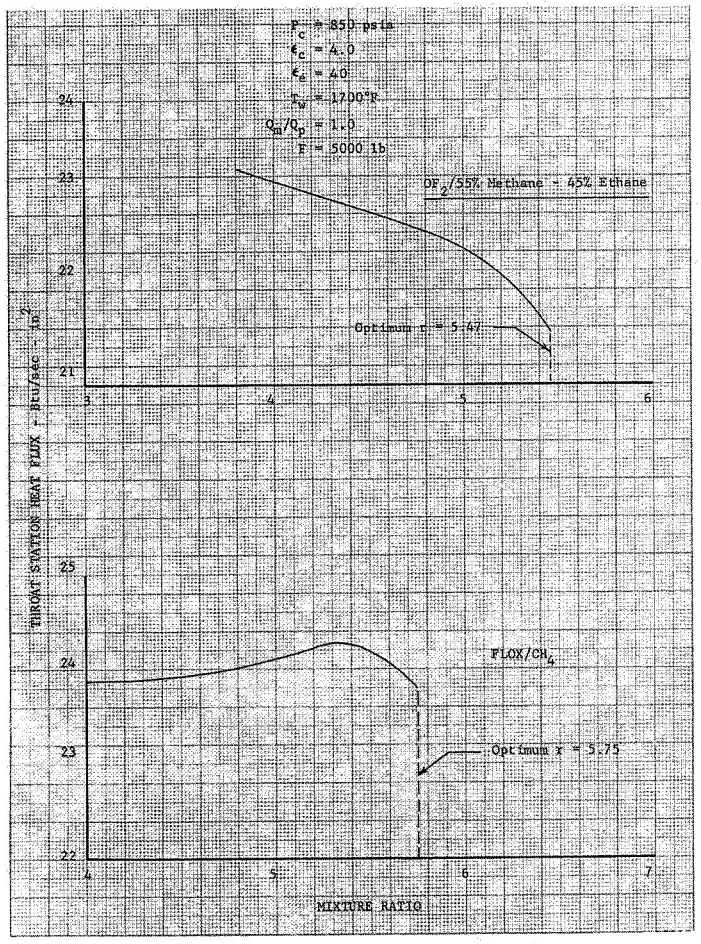


Figure 46. Throat Station Heat Flux Comparison

DF 60149

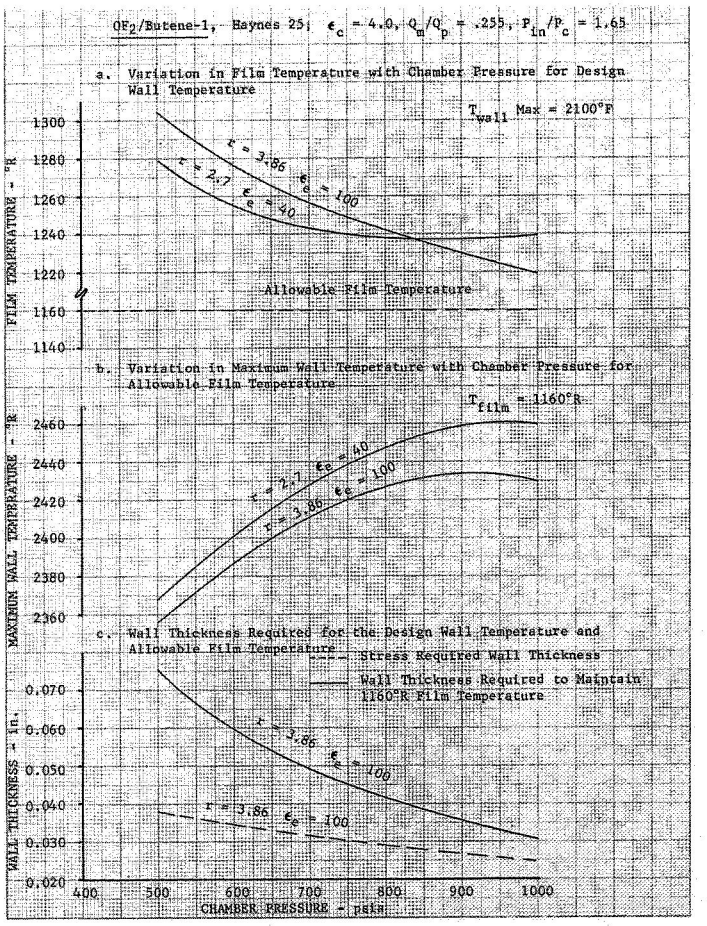


Figure 47. Regenerative Cooling Study Results for 1000-lb Thrust, OF_2/Butene-1 Thrust Chamber

DF 59068

A Haynes 25 chamber with a thermal barrier coating was analyzed for use with OF_2/butene-1 propellants at 1000-lb thrust for $Q_m/Q_p = 1$ (no heat reduction due to carbon deposition on the chamber walls). The results are summarized in figure 48, which presents coolant pressure drop, coolant film temperature, and wall temperature at the interface between the coating and the Haynes 25 base material as functions of chamber pressure. At this set of conditions, the coolant pressure drop would have to be extremely high and above the allowable limit of 1/2 of chamber pressure to keep (1) the interface wall temperature below its allowable value of 2560°R and (2) the butene-1 film temperature to an acceptable level (1160°R). Note in figure 48 that the interface wall temperature and film temperature values are acceptable only at 500 psia chamber pressure. However, at this chamber pressure the coolant pressure drop would be over 1000 psia, and the pressure drop curve is vertical, indicating that the coolant passages are choked.

Even if the film temperature requirement were to be relaxed on the assumption that the limit was conservative, the coolant pressure drop required to maintain the wall interface temperature at an acceptable value would still be above the allowable level of 1/2 chamber pressure. Therefore regenerative cooling at these conditions does not appear feasible.

3. Influence of Assumptions

As explained in paragraph A2, it was necessary to assume values for a number of important parameters so that the foregoing regenerative cooling limits could be determined. It was also necessary to assume a systematic variation of coolant passage geometry, rather than to optimize the passages for each case. To assess the effect of the assumptions on chamber pressure limits, ranges of values for the assumed parameters were evaluated for selected cases and a coolant passage optimization was completed for one thrust chamber design.

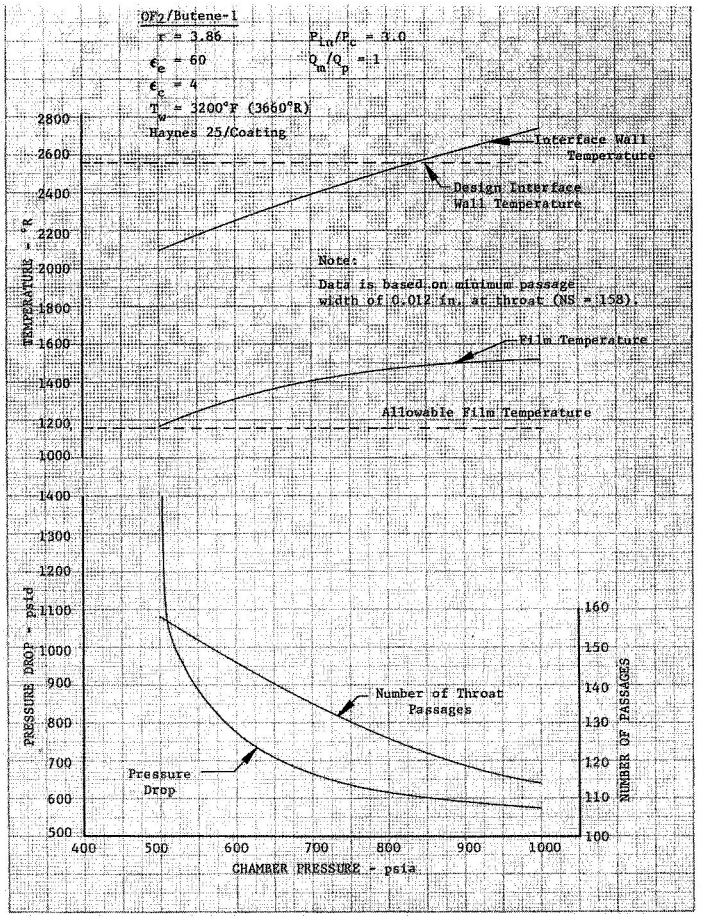


Figure 48. Regenerative Cooling Study Results for a 1000-lb Thrust, OF_2/Butene-1, Thermal Barrier Coated Chamber DF 59341

a. Parametric Study

Typical results of parametric evaluations of Q_m/Q_p, ϵ_c, and P_{in}/P_c are presented in figures 49 through 51. Figure 49 shows the effect of Q_m/Q_p on the regenerative cooling chamber pressure limit for flox/methane. The so-called average value for flox/methane is 0.765. The selection of this value for primary consideration was based on previous experimental results. Note that the allowable chamber pressure cooling limit decreases significantly with increases in Q_m/Q_p from the average value to 1.0.

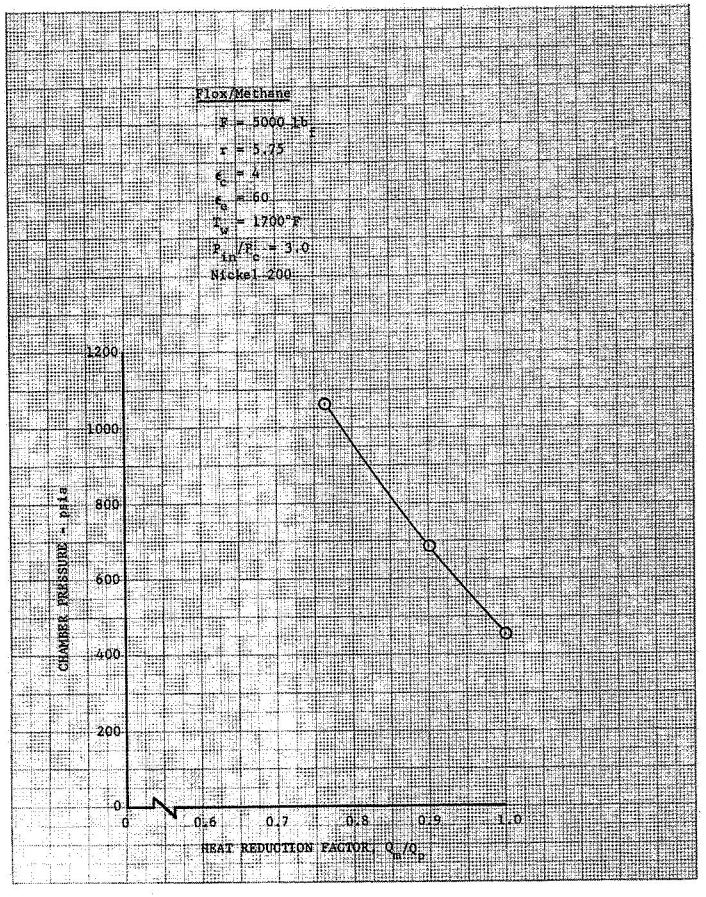


Figure 49. Effect of Heat Reduction Factor on Regenerative Cooling Chamber Pressure Limits

DF 59541

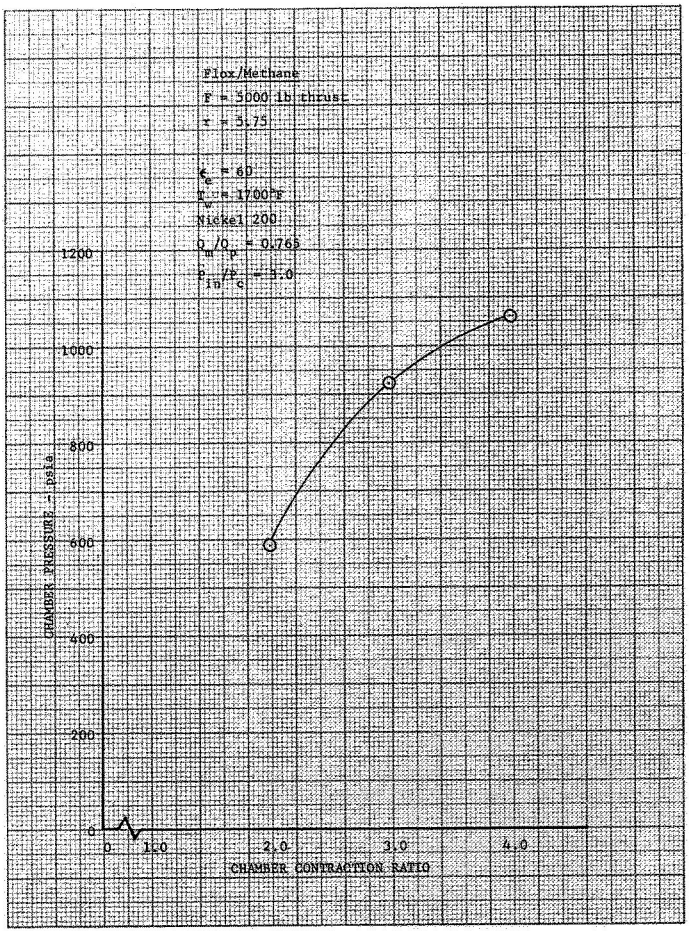


Figure 50. Effect of Chamber Contraction Ratio on Regenerative Cooling Chamber Pressure Limits

DF 59067

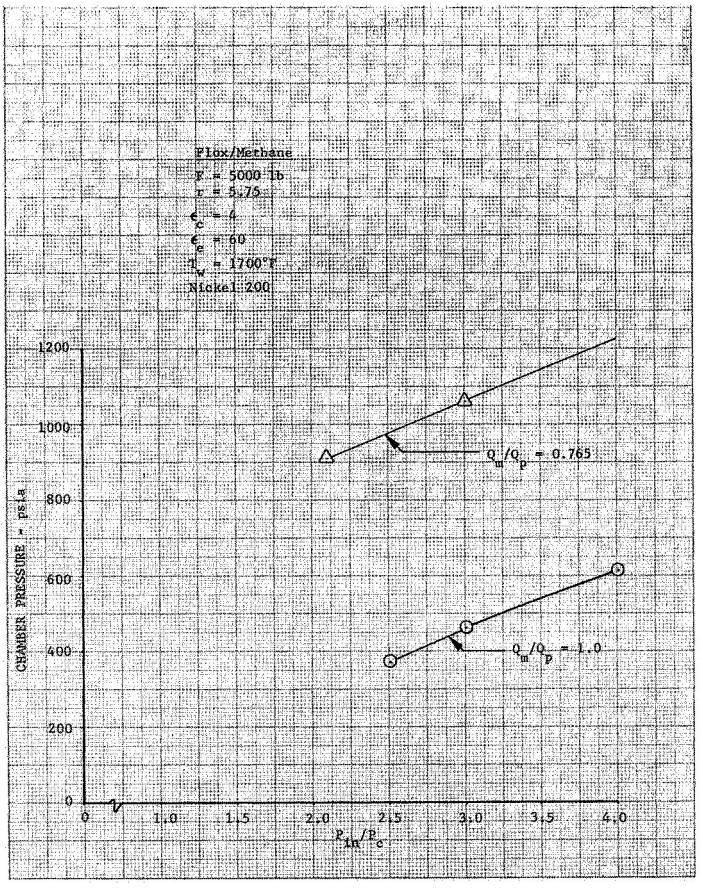


Figure 51. Effect of Cycle Considerations (P_{in}/P_c) on Regenerative Cooling Chamber Pressure Limits

DF 59344

The effect of chamber contraction ratio on regenerative cooling chamber pressure limit is shown in figure 50 for flox/methane at the 5000-lb thrust level. The chamber pressure cooling limit decreases with decreasing contraction ratio because the higher velocities associated with smaller chambers produce higher heat fluxes.

The effects of changes in the cooling jacket inlet pressure-to-chamber pressure ratio are shown in figure 51. The cooling limits decrease as this pressure ratio decreases. This results from the reduction in coolant density with the reduction in cooling jacket pressure level. Reduced density necessitates a higher coolant velocity and thus a higher coolant pressure drop to cool the chamber wall at a given heat flux level.

The variation of the cooling limits with combustion chamber characteristic length is illustrated in figure 52. Note that limits can be increased by decreasing L*.

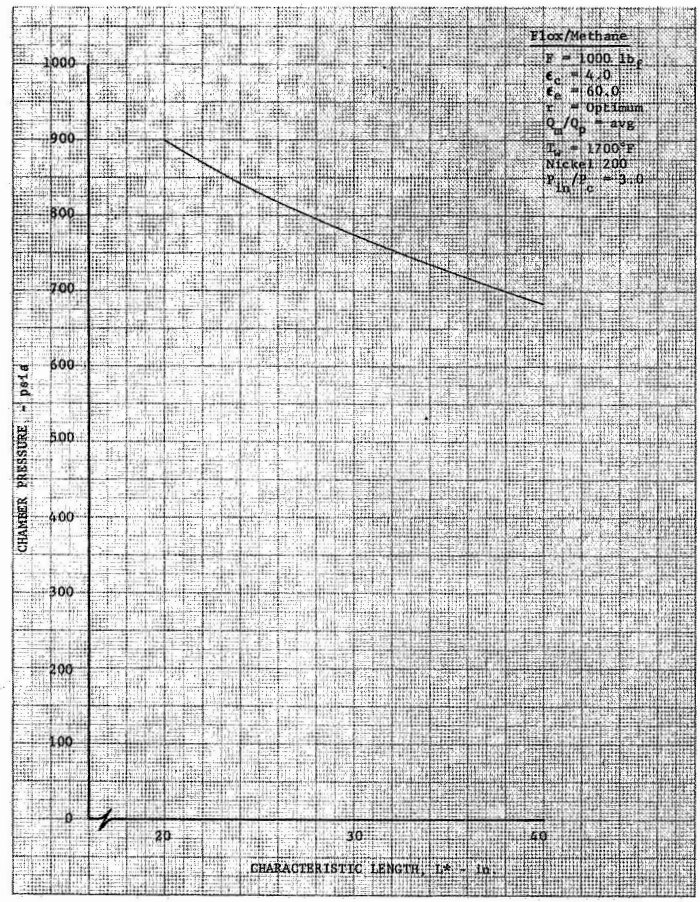


Figure 52. Effect of L* on Regenerative Cooling Chamber Pressure Limits DF 60148

b. Coolant Passage Optimization

(1) Contract Studies

As explained in Paragraph A2, coolant passages were sized so that the combustion-side wall temperature was equal to the maximum permissible design value at the throat station. On either side of the throat, passage widths were permitted to increase (while maintaining the width equal to the web thickness) as required to suit chamber geometry until stress considerations dictated branching. With the consequent area schedule, wall temperatures were reduced in the combustion chamber and nozzle region.

Figure 53 shows a typical plot of wall temperature versus chamber position. The wall temperature is equal to the design value only at the throat and therefore the rest of the chamber is overcooled. In the overcooled areas, the coolant film coefficients and hence coolant velocities are higher than required. If the coolant passage widths are increased in the overcooled areas so that the wall temperature is increased, coolant velocities and hence coolant pressure drop can be reduced.

The coolant pressure drop will be minimized when the coolant passages are optimized so that the wall temperature is equal to the design value throughout the chamber. However, because most of the coolant pressure drop occurs in the high heat flux regions of the chamber, optimization of the coolant passages in the combustion chamber and in the throat area provides the most significant reduction in coolant pressure drop. In the high expansion ratio portion of the nozzle where the heat fluxes are low, the coolant pressure drop is also low and thus passage optimization does not have a significant effect on the overall coolant pressure drop.

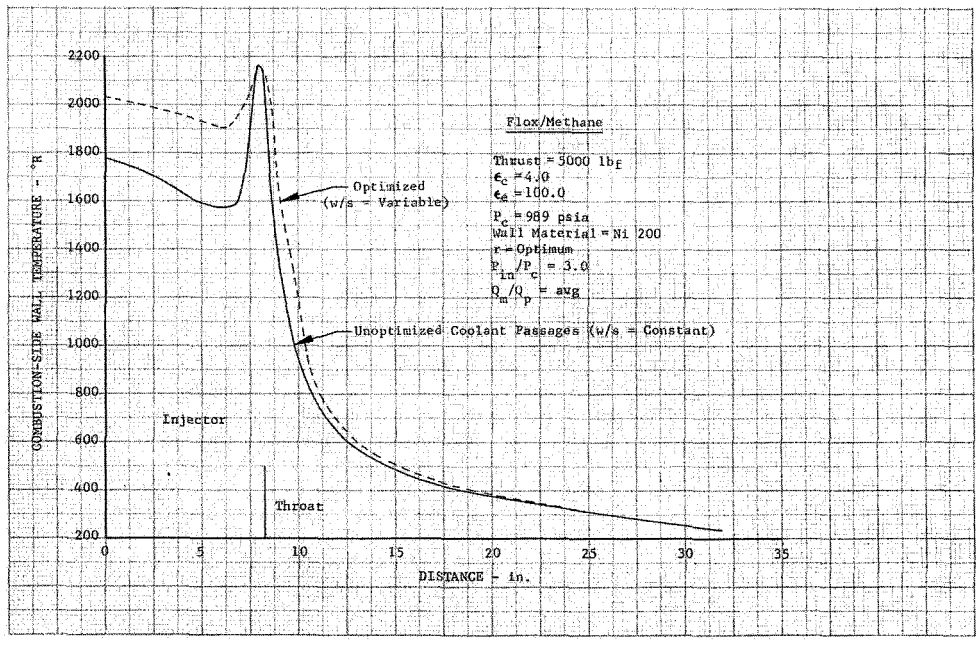


Figure 53. Variation of Combustion-Side Wall Temperature With Chamber Location DF 60448

Since the coolant pressure drop criterion set the regenerative cooling limits just presented, coolant passage optimization can be expected to permit the extension of regenerative cooling to higher chamber pressures. The optimization procedure is an iterative one requiring the completion of successive thrust chamber design calculations with adjustment of inputs between calculations. It is therefore a much more unwieldy procedure than would be practicable to use in a study of this nature. The omission, however, serves to make the results conservative.

To determine how conservative the limits determined might be, optimization studies for a 5000-lb thrust flox/methane chamber were completed. In this optimization, the coolant passage widths were increased to the maximum permissible value, which was dictated by either stresses or the assumed minimum land width of 0.015-in. The resulting wall temperature profile is shown in figure 53. A comparison of the coolant pressure drops for optimized and unoptimized passages is shown in figure 54.

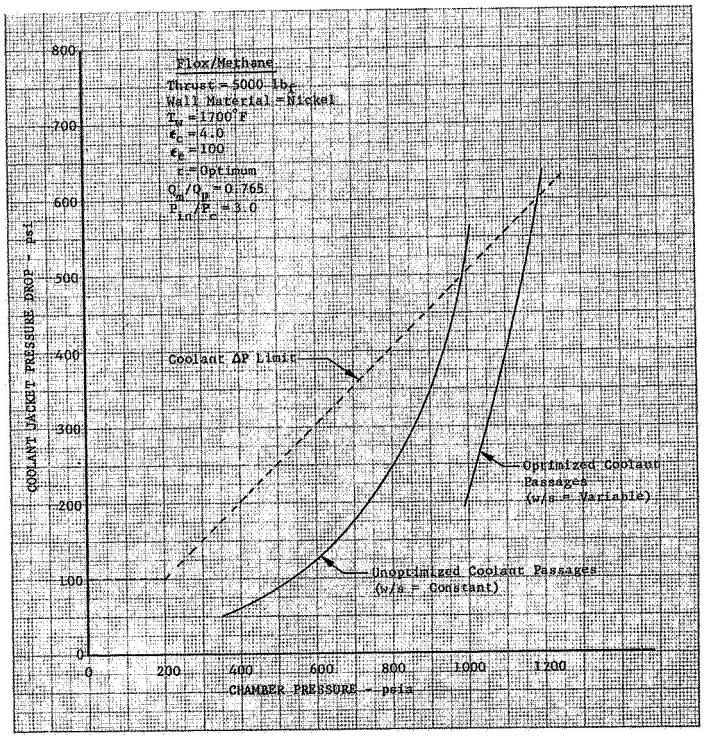


Figure 54. Coolant Passage Pressure Drop Comparison for Optimized and Unoptimized Coolant Passage Configurations

DF 60449

Note from figure 54 that the cooling limits would be 1190 psia for the optimized chamber rather than the quoted value of 989 psia for the unoptimized chamber. Further optimization is permissible by going to a variable depth passage, and hence the cooling limit could be increased still further as discussed in the following subparagraph.

(2) Independent Thermal Skin Studies

In continuing efforts to extend the applicability of the Thermal Skin thrust chamber design, we have initiated studies independent of the Contract NAS3-11190 effort to investigate the effects of the limitations imposed by current fabrication technology. Results obtained to date in these studies are summarized in figure 55.

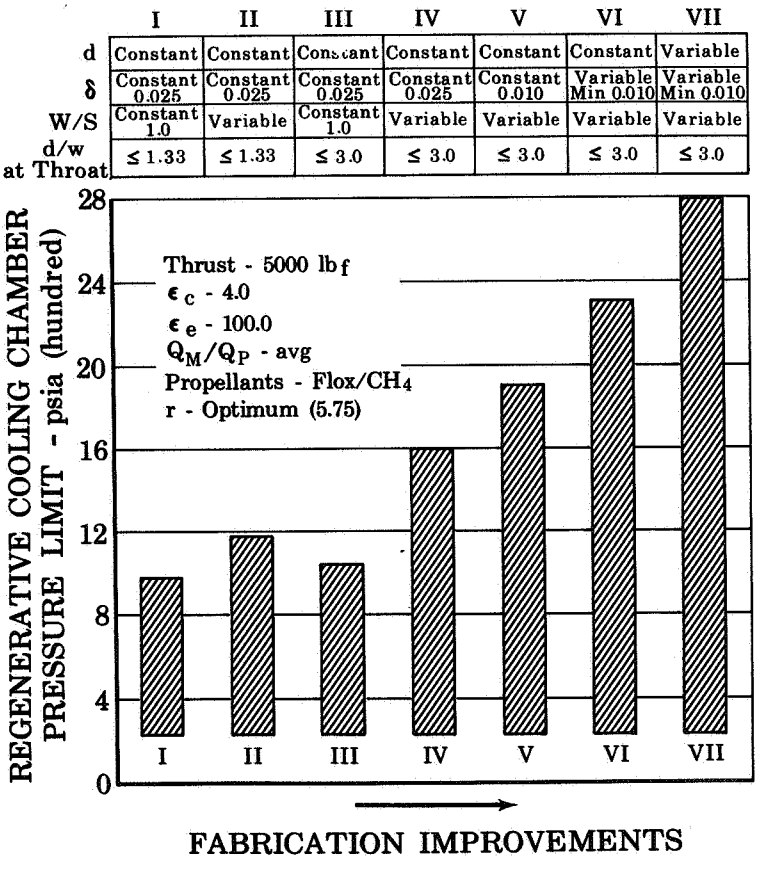


Figure 55. Increased Chamber Pressure With Fabrication Improvements FD 24575A

This illustration presents chamber pressure regenerative cooling limits (as set by the coolant pressure drop limitation of 50% P_c) for flox/methane, nickel thrust chambers at the 5000-lb thrust level for the optimum mixture ratio (5.75) and a contraction ratio, an expansion

ratio, and a Q_m/Q_p of 4, 100, and 0.765, respectively. The bars represent cooling limits determined when the assumptions relating to coolant passage depth (ℓ), hot wall thickness (δ), depth/width ratio (ℓ/w), and width/web thickness (w/s) are changed from those used in defining the cooling limits under Contract NAS3-11190. The first bar shows the cooling limit determined under the contract and, thus is considered the base case. Note that this limit is for constant depth coolant passages, a constant wall thickness of 0.025 in., a maximum ℓ/w ratio of 1.33, and a constant w/s ratio of 1.0. The second bar shows the limit for the optimized case studied under the contract, in which coolant passage widths in the combustion chamber and throat region were increased to bring the wall temperature closer to the design limit of 1700°F. This moderate coolant passage optimization increased the cooling limit to 1190 psia. The other cases (III through VII) show the levels that can be achieved with improvements in fabrication technology. The assumptions for which these limits were obtained are given below.

- Bar III shows the effect of increasing the coolant passage maximum depth/width ratio from 1.33 to 3.0. Note that, for this case, the w/s ratio was maintained equal to one throughout the chamber. By comparing the limit obtained with bar I, the effect of increasing the maximum ℓ/w ratio is seen to be approximately 50 psi.

- Bar IV shows the combined effect of coolant passage optimization and deeper coolant slots. Comparing this limit to the base case (bar I) an increase of approximately 600 psi is apparent.

- Bar V shows the effect of decreasing the hot-side wall thickness from 0.025 to 0.010 in. This wall thickness reduction has the effect of increasing the chamber pressure cooling limits by approximately 300 psi, as can be seen by comparing bars IV and V. The combined effect of increasing the coolant passage depth, coolant passage optimization (variable w/s), and thinner walls is to increase the cooling limit from 990 to 1900 psia.

- Bar VI shows the coolant limit that can be obtained by varying hot wall thickness. At the throat station the wall thickness would be 0.010 in.; in the combustion chamber a thicker wall would be used.
- Bar VII illustrates the advantage of using variable depth passages. Comparing this limit to the base case, an increase of from 990 to 2800 psia in the cooling limits can be realized.

The advantages of the foregoing chamber coolant passage configurations at a chamber pressure level of 1000 psia are shown in figures 56 and 57. Figure 56 compares the wall temperature profiles that are obtained with the various assumptions. It is interesting to note that only by going to variable depth passages and variable hot wall thickness can a nearly constant wall temperature profile be achieved in the combustion chamber. Furthermore, for this case the nozzle portion of the chamber is still overcooled.

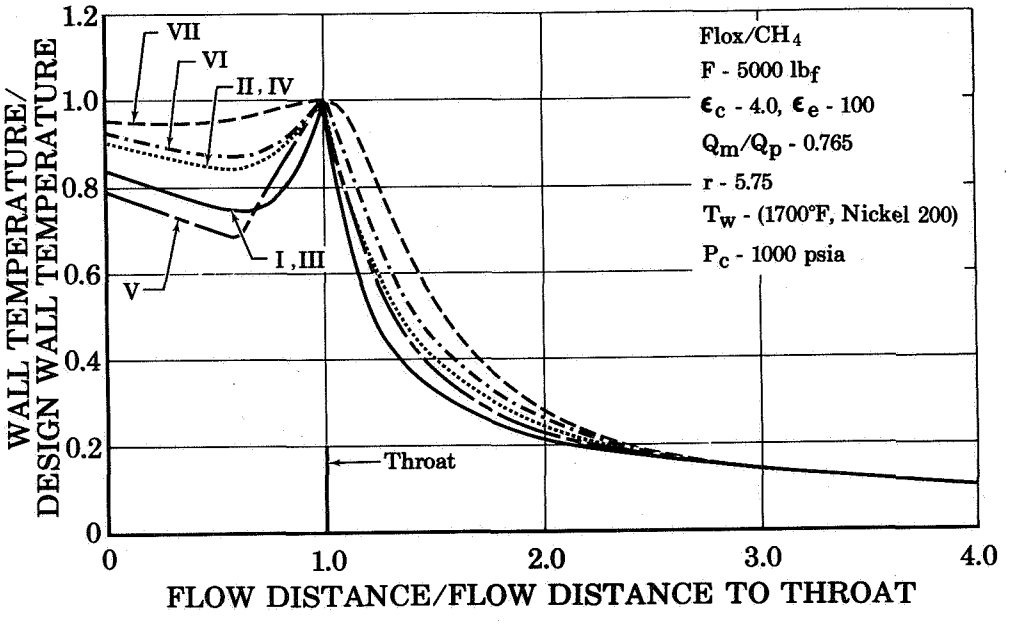


Figure 56. Wall Temperature Profile for Various Thermal Skin Channel Designs

FD 24646A

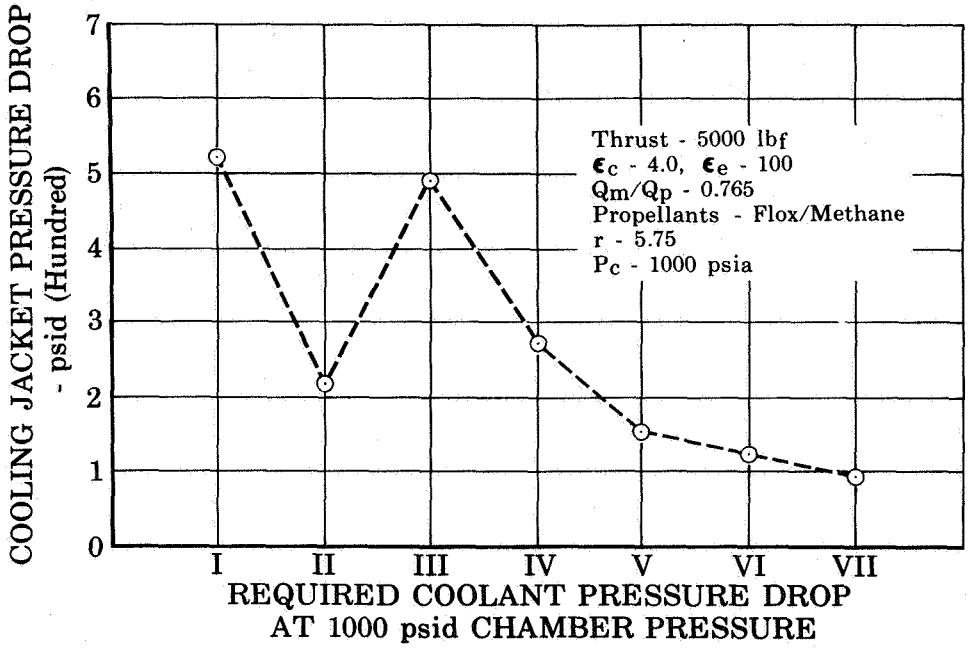


Figure 57. Required Coolant Pressure Drop at P_c = 1000 psia FD 24644A

Coolant jacket pressure drops at 1000-psia chamber pressure are shown in figure 57 for each of the configurations. The coolant jacket ΔP decreases significantly as the wall temperature approaches the design value throughout the chamber. However, although startling gains in maximum chamber pressure occur as more complex structural configurations are incorporated, (see figure 55), figure 57 shows the jacket pressure drop achieved for a 1000-psia chamber pressure engine does not decrease in proportion. The pressure loss for coolant passage optimization, increased passage depth, and reduced wall thickness (Case V) is not much greater than that which can be achieved when all restraints are neglected (Case VII).

4. Off-Design Operation

At the request of the NASA Program Manager, detailed heat transfer studies of off-design operation were made at the 8000-lb thrust level using flox/methane, OF_2/55% methane - 45% ethane, and OF_2/propane propellants. The 8000-lb thrust chambers were designed for operation at a 500-psia chamber pressure level with a throat wall temperature of 1700°F

for $Q_m/Q_p = 1.0$ (i.e., for no heat reduction due to carbon deposition on the chamber walls). The effects of reducing Q_m/Q_p to the average values and of varying chamber pressure from the design point were then assessed. The thrust chamber material was nickel in all cases. Results obtained are presented in figures 58 through 63.

Note that

1. At the design point, the cooling jacket pressure drop is highest with methane, but still within the 1/2 chamber pressure limit.
2. The coolant pressure drop, throat wall temperature, and the coolant exit temperature are lower for average values of Q_m/Q_p than for $Q_m/Q_p = 1.0$.
3. For either value of Q_m/Q_p (average or 1.0) and for all three propellant combinations, the coolant pressure drops and wall temperatures increase, and coolant exit temperatures decrease with increasing chamber pressure.

Based on these indications, it can be concluded that the thrust chamber cooling jacket should be designed for the highest chamber pressure level in the operating range.

5. Lower Regenerative Cooling Limits Set By Boiling Consideration

In the preceding paragraphs, attention was devoted entirely to the upper chamber pressure limits for regenerative cooling. The lowest chamber pressure at which regenerative cooling can be employed without risking transition into the film boiling region was also determined. In establishing the lower cooling limits, the two conditions under which film boiling can occur, bulk boiling and high heat fluxes, were considered (see Appendix E). For bulk boiling, the saturation state defines the maximum allowable coolant condition and therefore the approach taken was the same as that followed in the feasibility study. For instances in which bulk boiling was not a problem, heat flux levels were compared to the upper limit heat flux for nucleate boiling to check for subcooled film boiling.

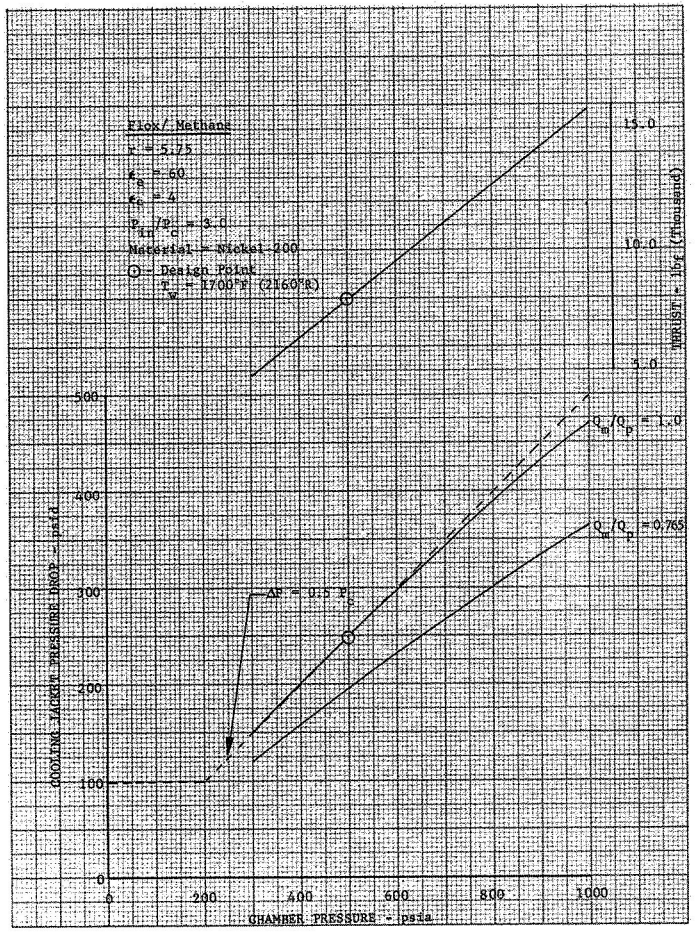


Figure 58. Variation in Thrust and Cooling Jacket Pressure Drop With Chamber Pressure for a Fixed Thrust Chamber Configuration: Flox/Methane

DF 59060

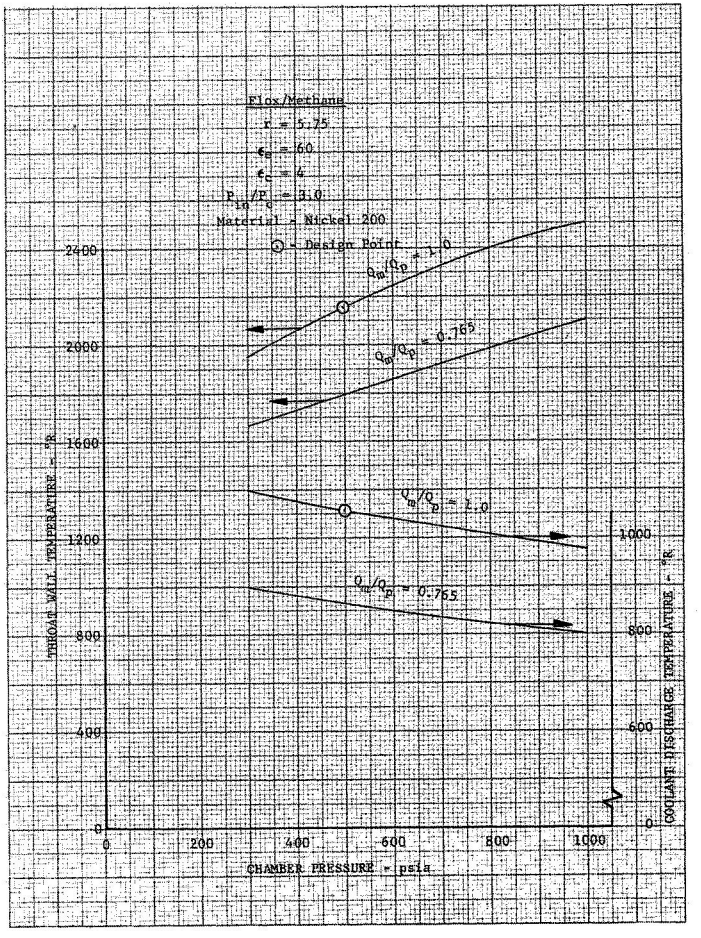


Figure 59. Variation in Throat Wall and Coolant Discharge Temperatures With Chamber Pressure for a Fixed Thrust Chamber Configuration: Flox/Methane

DF 59061

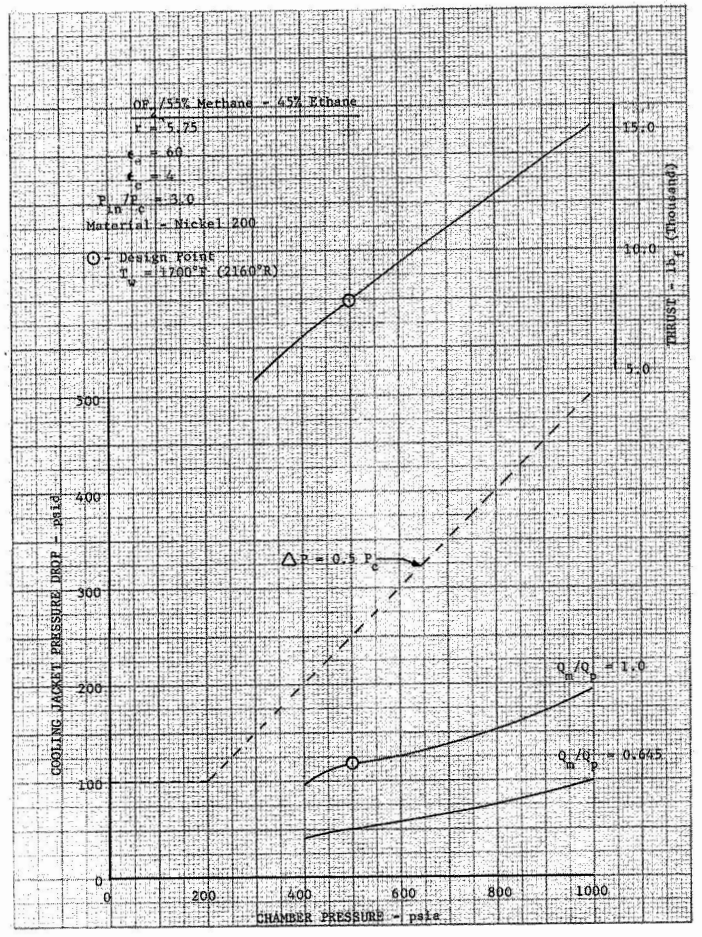


Figure 60. Variation in Thrust and Cooling Jacket Pressure Drop With Chamber Pressure for a Fixed Thrust Chamber Configuration: OF_2/55% Methane - 45% Ethane

DF 59022

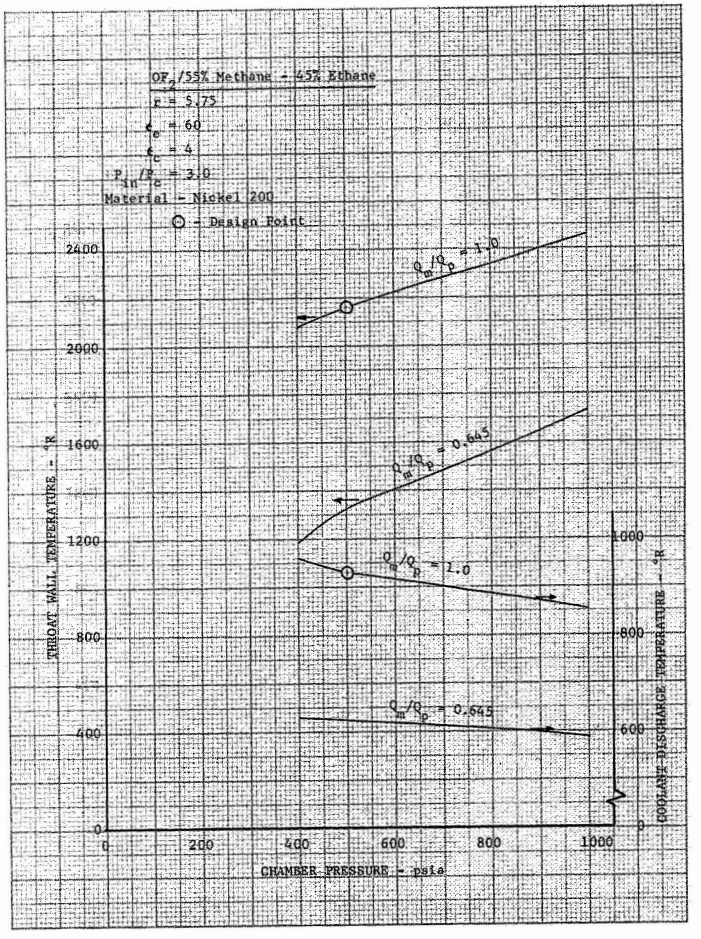


Figure 61. Variation in Throat Wall and Coolant Discharge Temperatures With Chamber Pressure for a Fixed Thrust Chamber Configuration: OF_2/55% Methane - 45% Ethane

DF 59059

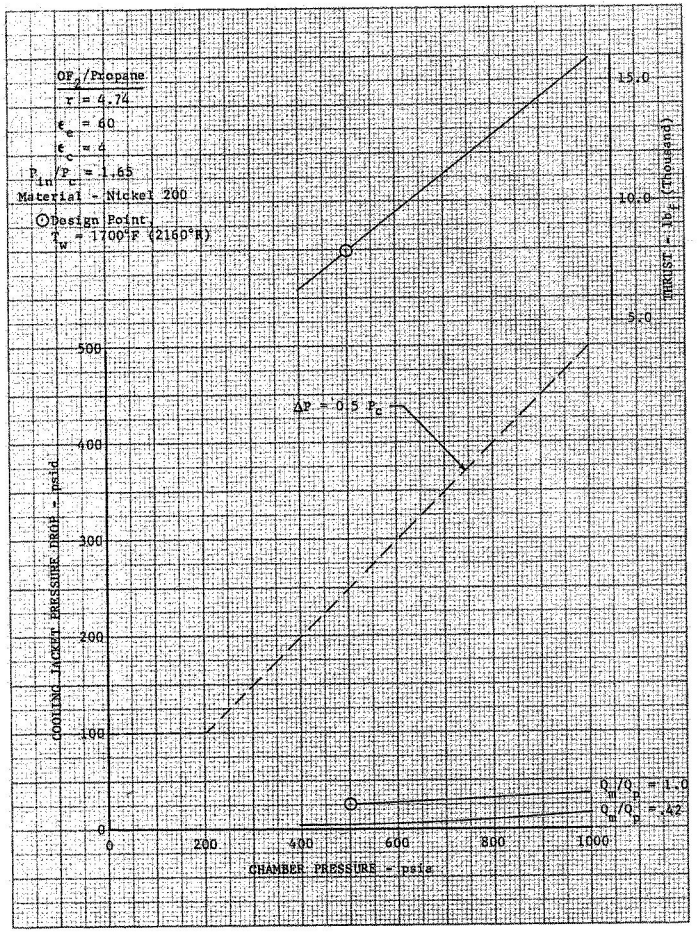


Figure 62. Variation in Thrust and Cooling Jacket Pressure Drop With Chamber Pressure for a Fixed Thrust Chamber Configuration: OF_2/Propane

DF 59343

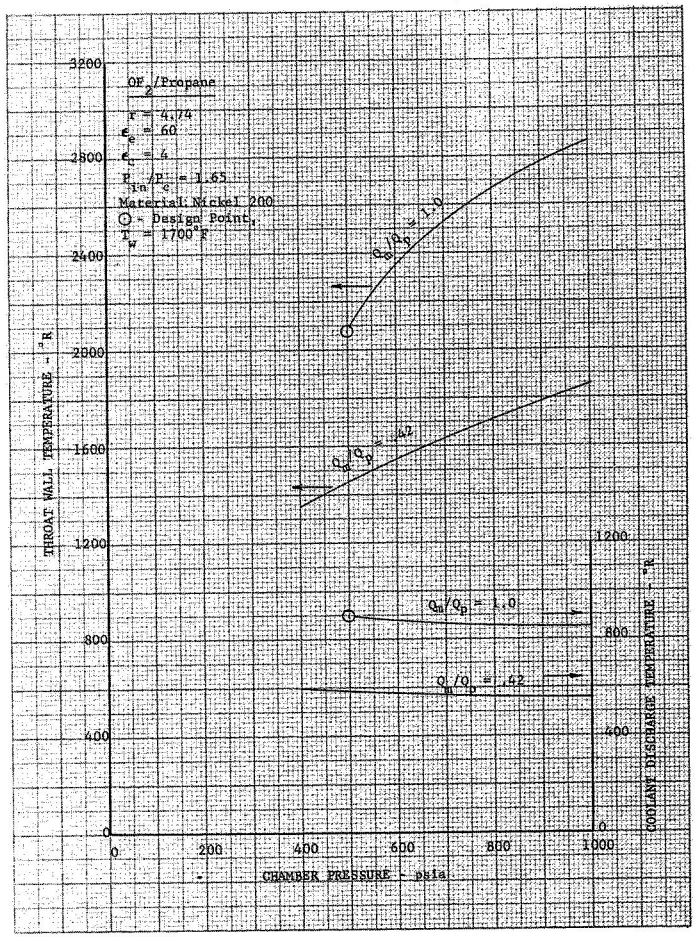


Figure 63. Variation in Throat Wall and Coolant Discharge Temperatures With Chamber Pressure for a Fixed Thrust Chamber Configuration: OF_2/ Propane

DF 59342

The lower chamber pressure cooling limits set by the bulk boiling consideration are presented in table XI. Both methane and the methane-ethane blend have low liquid phase heat capacities and thus can not be used as subcritical coolants without operating in the bulk boiling regime. Consequently, the lower chamber pressure limits for flox/methane and OF_2/55% methane - 45% ethane were established by the lowest chamber pressure that has a supercritical coolant pressure at the heat exchanger exit.

Propane and butene-1 have large liquid phase heat capacities and thus can be used as subcritical coolants at chamber pressures down to 100 psia without reaching the saturation state and hence the bulk boiling limit. However, the application of these fuels is also restricted by subcooled film boiling. As chamber pressure is increased above 100 psia, the heat flux at the throat increases until, at some level, the upper limit heat flux for nucleate boiling is exceeded. Under this condition, even though the overall enthalpy rise is low, high local heat fluxes in the chamber prohibit the use of regenerative cooling until the pressure in the coolant jacket reaches a supercritical level.

Figures 64 and 65 show the chamber pressures at which subcooled film boiling will occur with OF_2/butene-1 at 1000-lb thrust and OF_2/propane at 20,000-lb thrust respectively. In both figures, curves defining the variation in throat heat flux with chamber pressure are compared with curves for the upper limit heat flux for nucleate boiling. The upper limit heat flux values are computed by equations developed by Pratt & Whitney Aircraft given in Appendix E.

Figures 64 and 65 show that subcooled film boiling would not occur until chamber pressures of approximately 260 psia for butene-1 or 140 psia for propane were reached. Therefore, these two fuels can be used as subcritical coolants from these respective chamber pressure levels to below 100 psia. Because they can also be used as supercritical coolants at high chamber pressures, they have two regions of applicability, one for subcritical pressures and one for supercritical pressures. These regions are illustrated and discussed further in the following summary.

Table XI. Summary of Low Chamber Pressure Cooling Limits Set by Bulk Boiling Considerations (Q_m/Q_p = avg)

Thrust Level			1000 lb						5000 lb						20,000 lb					
Propellant			Flox/Methane			OF_2/Butene-1			Flox/Methane			OF_2/55% Methane-45% Ethane			Flox/Methane			OF_2/Propane		
Expansion Ratio			40	60	100	40	60	100	40	60	100	40	60	100	40	60	100	40	60	100
1700°F Nickel 200	% Optimum r	100	233	233	233	<100	<100	<100	233	233	233	330	330	330	233	233	233	<100	<100	<100
		90	233			<100			233			330			233			<100		
		70	233			<100			233			330			233			<100		
1700°F 347 Stainless Steel	% Optimum r	100			249				244	248	253	330	330	330			251			
		90							231			330								
		70							234			330								
2100°F Haynes 25	% Optimum r	100	233	233	233	<100	<100	<100	231	231	241	330	330	330	233	233	231	<100	<100	<100
		90	233			<100			229			330			233			<100		
		70	233			<100			229			295			233			<100		

Notes: a. All chamber pressure limits (in psia) for Q_m/Q_p = avg; ϵ_c = 4; P_{in}/P_c = 3.0 for flox/methane and OF_2/55% Methane-45% Ethane; P_{in}/P_c = 1.65 for OF_2/Butene-1, OF_2 Propane.

b. L^* = 30 inch

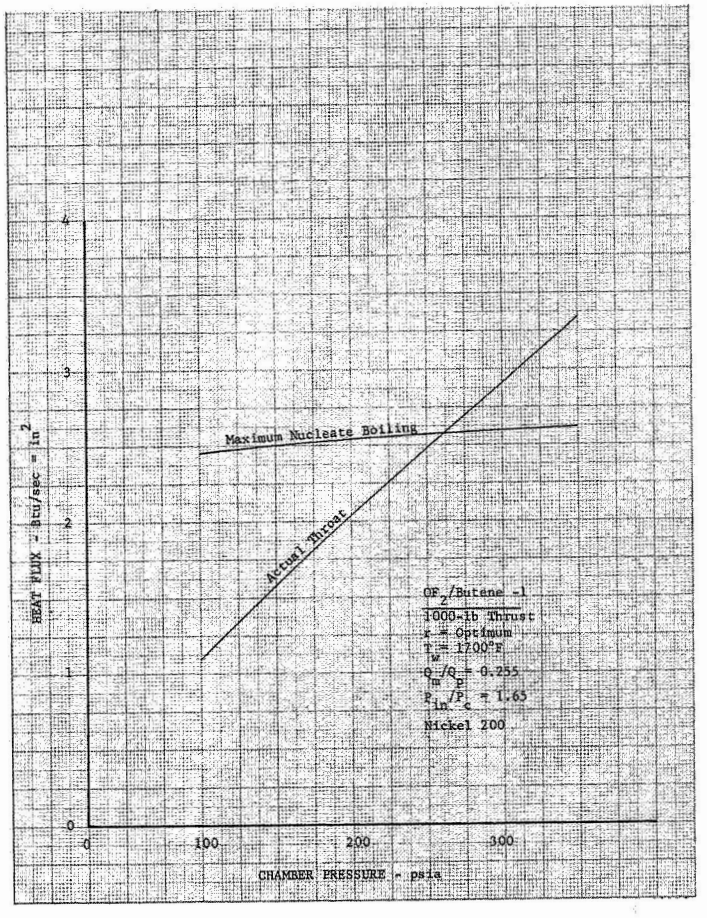


Figure 64. Comparison of Actual Throat and Maximum Nucleate Boiling Heat Fluxes: OF_2/Butene-1

DF 60150

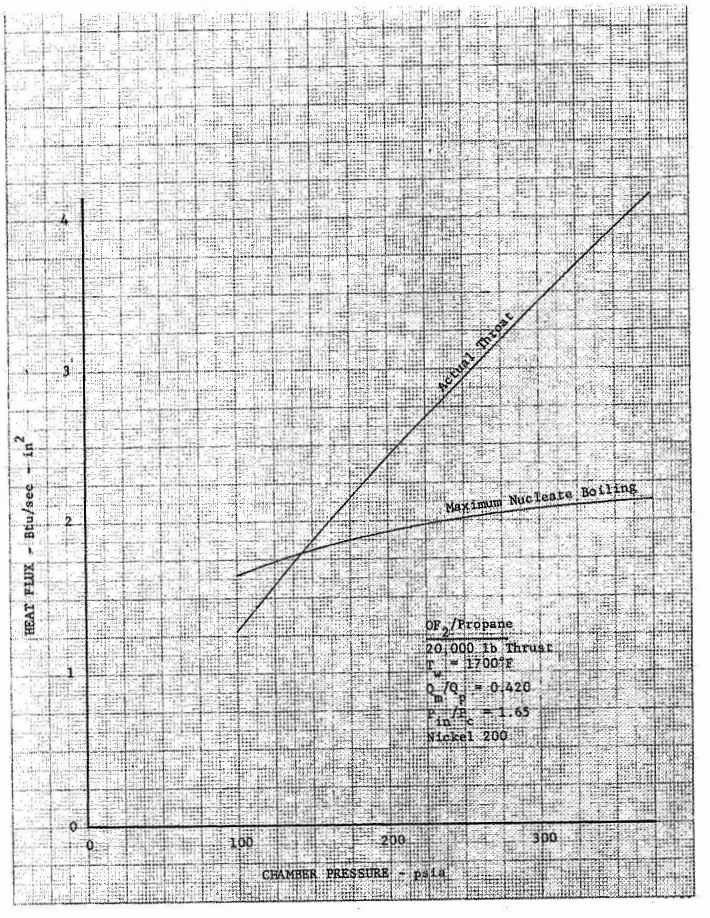


Figure 65. Comparison of Actual Throat and Maximum Nucleate Boiling Heat Fluxes: OF_2/Propane

DF 60151

C. SUMMARY OF RESULTS

Figures 66 through 70 summarize the results obtained in the detailed heat transfer study. The first three of these figures illustrate the regions (on chamber pressure - nozzle expansion ratio maps) in which regenerative cooling can be used at the 1000, 5000, and 20,000-lb thrust levels. The regions are for the following conditions: contraction ratio of 4, optimum mixture ratios, nickel 200 thrust chamber material, maximum wall temperature equal to 1700°F, and average values for the Q_m/Q_p factor. The cooling jacket inlet pressure/chamber pressure ratio was selected for the respective propellant combinations based on engine cycle considerations.

The cooling regions for flox/methane and the OF_2/55% methane - 45% ethane blend are continuous. Throughout the regions shown for these two propellants, the fuel coolant would be at supercritical pressures. For OF_2/butene-1 and OF_2/propane, two cooling regions, one for supercritical and the other for subcritical coolant pressures, are shown. The supercritical and subcritical regions are separated by areas in which subcooled film boiling is anticipated and therefore in which regenerative cooling is not practicable.

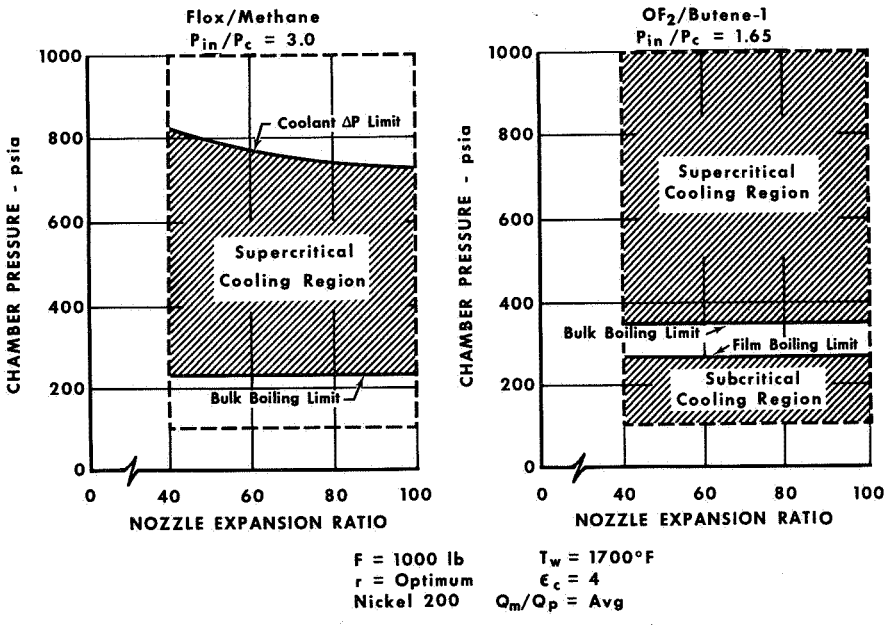


Figure 66. Regenerative Cooling Limits at 1000-lb Thrust for Flox/Methane and OF_2/Butene-1 GS 7329

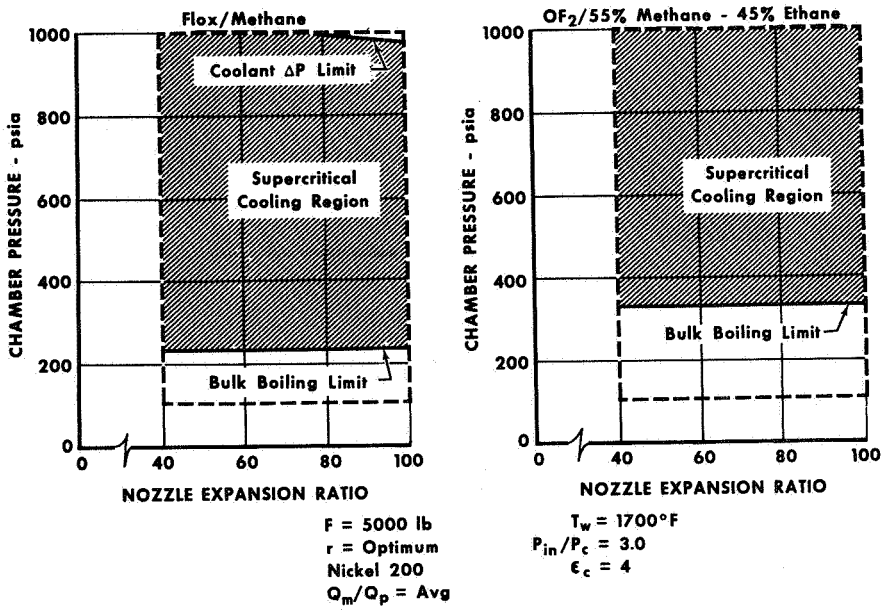


Figure 67. Regenerative Cooling Limits at 5000-lb Thrust for Flox/Methane and OF_2/55% Methane - 45% Ethane GS 7333

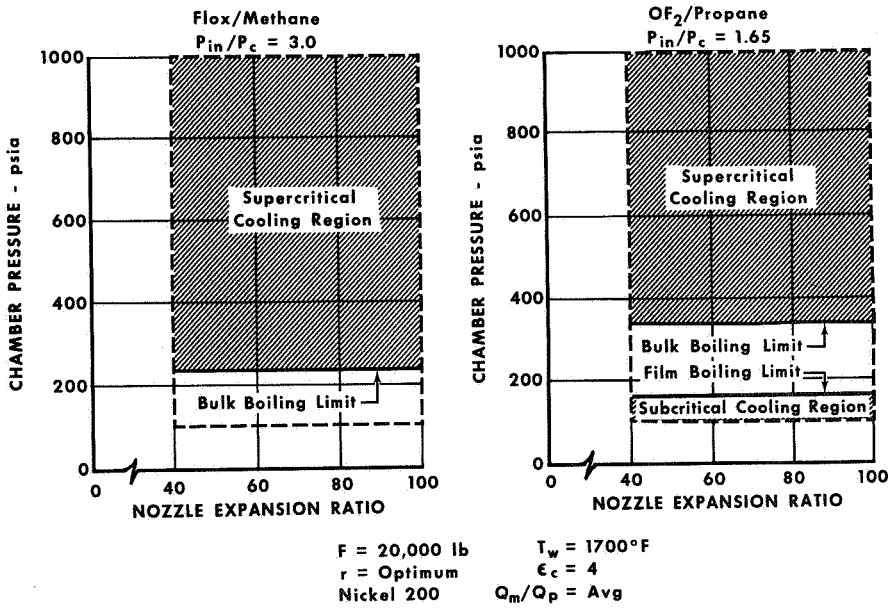


Figure 68. Regenerative Cooling Limits at 20,000-lb Thrust for Flox/Methane and OF_2/Propane GS 7334

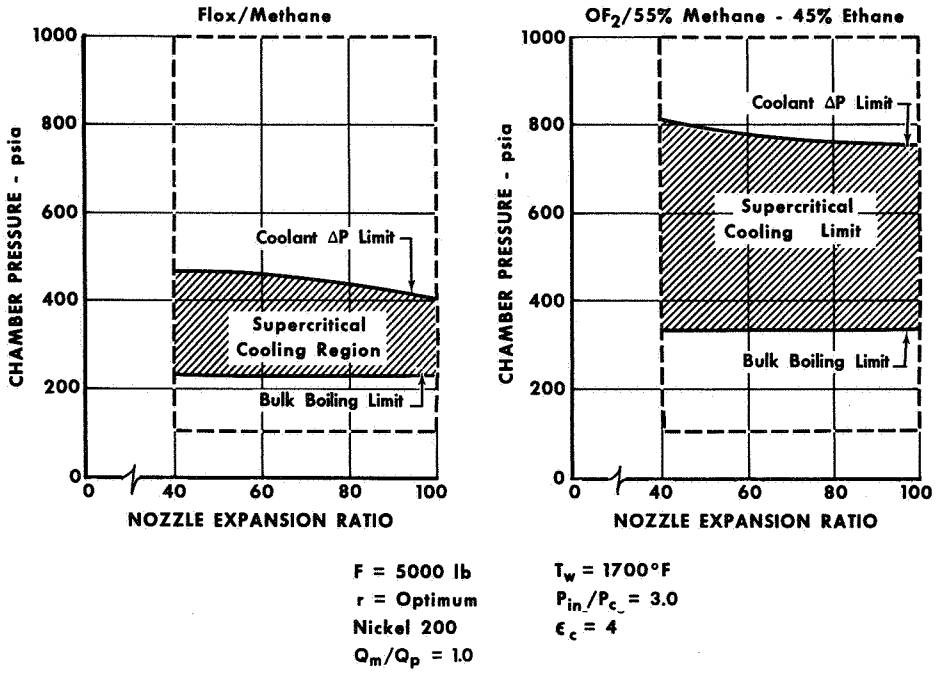


Figure 69. Regenerative Cooling Limits for Q_m/Q_p = 1, Flox/Methane and OF_2/55% Methane-45% Ethane GS 7335

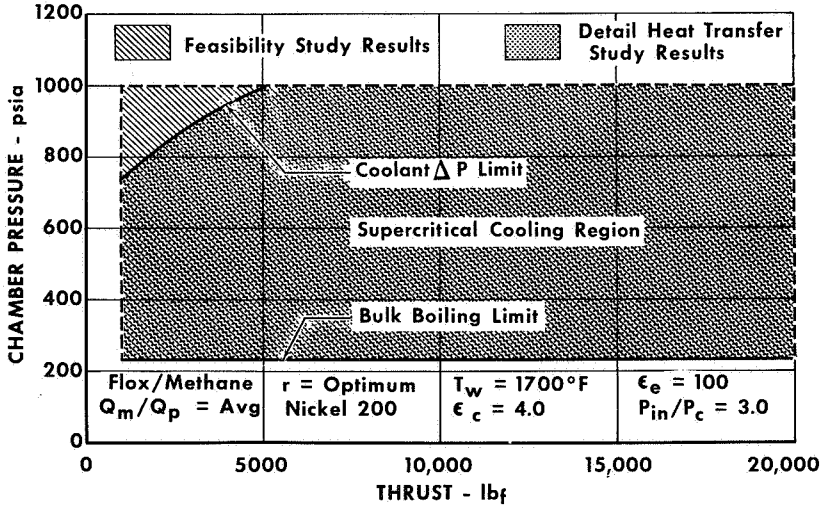


Figure 70. Permissible Regenerative Cooling Region for Flox/Methane GS 7033A

Figure 69 illustrates the cooling regions for flox/methane and OF_2/55% methane - 45% ethane for the case of no heat reduction (i.e., for Q_m/Q_p = 1). By comparing this figure with figure 67, the effect of the Q_m/Q_p factor can be realized.

The last figure (figure 70) shows the applicable regenerative cooling region for flox/methane (which was evaluated at all thrust levels) on a chamber pressure - thrust map. This is the same type map that was obtained in the feasibility study. By comparing figure 70 with the corresponding map obtained for flox/methane in the feasibility study (figure 33), it can be seen that limits associated with local heat flux conditions and coolant passage designs (namely the coolant jacket pressure drop limitation of 1/2 chamber pressure) restrict regenerative cooling to a smaller area than that indicated when only high coolant temperature limits determined using coolant heat capacities are considered.

PRECEDING PAGE BLANK NOT FILMED.

SECTION VI
ENGINE CYCLE STUDIES

A. INTRODUCTION

To provide performance information that would supplement heat transfer studies for propellant evaluation, engine cycle studies were accomplished concurrently with the detailed heat transfer investigation. The effort was concentrated on a comparison of high chamber pressure turbo-expander and gas generator engine cycles at the 5000-lb_f thrust (which was considered a likely level for subsequent hardware design). The propellant combinations flox/methane, OF_2/55% methane - 45% ethane, OF_2/propane and OF_2/methane were considered in the studies; butene-1 was not treated, since it is more appropriate for low chamber pressure, pressure-fed applications.

B. TURBO-EXPANDER CYCLE

Turbo-expander engine cycles rely upon the energy absorbed by the coolant, which is the turbine working fluid to power the turbopumps (figure 71). Thus engine operating limits are dependent upon fuel properties and thrust chamber heat transfer. Heat transfer and cycle studies indicated that energy absorbed is adequate to power the turbine when methane and the 55% methane - 45% ethane blend are used. The properties of the other fuels considered in the detailed heat transfer studies, butene-1 and propane, do not suit them for application to the expander system. Expander cycle studies were therefore confined to methane and the methane-ethane blend.

Figure 72 shows the variation in turbo-expander cycle chamber pressure limits with Q_m/Q_p ratio at the 5000-lb_f thrust level for flox/methane, OF_2/methane, and OF_2/55% methane - 45% ethane. The limits assumed the use of nickel thrust chambers. Both coolant jacket pressure drop and temperature rise were varied with chamber pressure and Q_m/Q_p as required for jacket cooling. The limits given were generated assuming high-speed partial-admission turbines with efficiency levels of 70%.

Note in figure 72 that the OF_2/methane limits exceed those of the flox/methane propellant combination for Q_m/Q_p levels greater than 0.864, whereas for lesser Q_m/Q_p values the reverse is true. The interrelationships between jacket coolant flow rate, pressure drop, and temperature rise are responsible for this characteristic.

The attainable operating chamber pressures for OF_2/55% methane - 45% ethane are the lowest of the three considered propellant combinations. These low attainable chamber pressure limits are direct results of the low amounts of energy absorbed by the coolant or working fluid (approximately 76% of that absorbed in the flox/methane cycle). The reduced energy available at the jacket discharge results in a reduction in available turbine work and hence the lower limits.

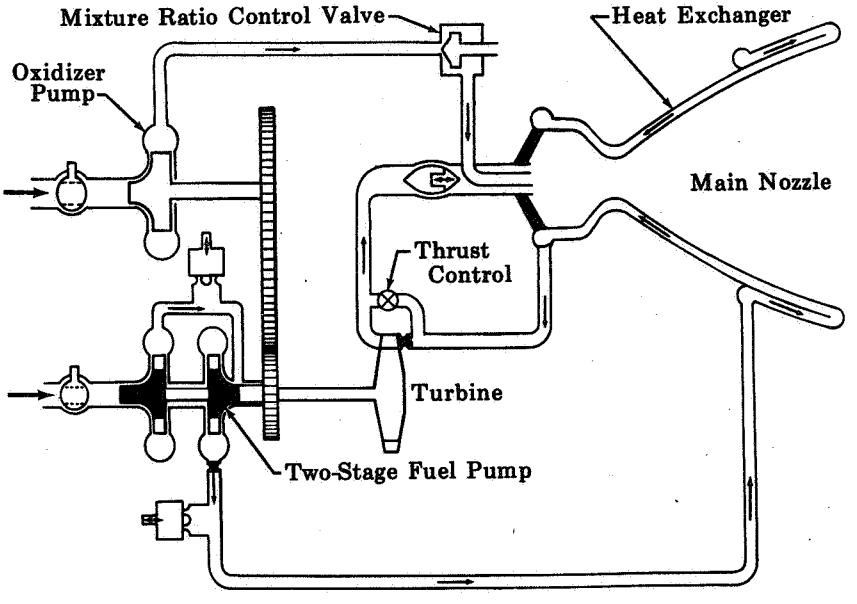


Figure 71. Turbo-Expander Schematic FD 12811D

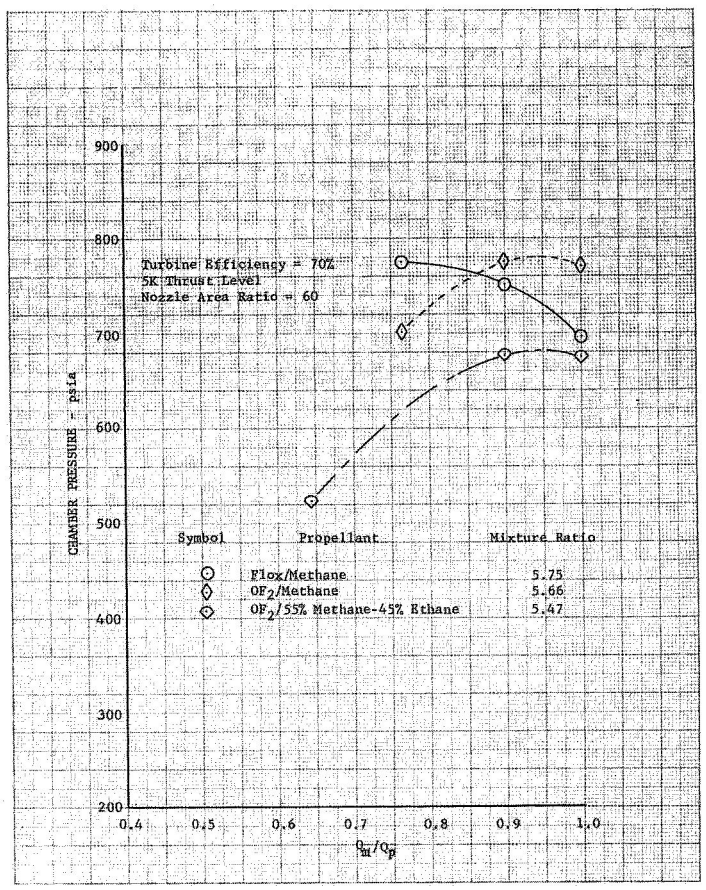


Figure 72. Effect of Heat Transfer On Expander Cycle Limit

DF 60434

C. GAS GENERATOR CYCLE

The chamber pressure limits for the gas generator cycle are affected by thrust chamber heat transfer only to a small extent. However, the cycle is subject to specific impulse losses that result from the diversion of small quantities of oxidizer and fuel to the gas generator for turbine power (figure 73). The extent of these losses for the flox/methane, OF_2/methane, OF_2/55% methane - 45% ethane, and the OF_2/propane propellant combinations, for a thrust level of 5000 lb_f is shown in figure 74 for average Q_m/Q_p ratios and in figure 75 for $Q_m/Q_p = 1.0$. The losses were minimized by assuming that the turbine exhaust gases were expanded through a nozzle having an expansion ratio of 60 to provide useful thrust. As for the expander cycle, nickel thrust chambers were assumed.

Gas generator cycle specific impulse losses increase with increasing levels of chamber pressure because of increased pump head rise and horsepower requirements; this increase is reflected in greater turbine flow requirements. Also the losses increase as Q_m/Q_p increases from the average value to 1.0 because higher coolant jacket pressure drops and hence higher pump discharge pressures are required with $Q_m/Q_p = 1.0$.

Note from figures 74 and 75 that the specific impulse loss is generally less with the more dense fuels. This is the result of lower required jacket coolant pressure drops with these fuels and hence lower pump head rise and turbine work requirements. The notable exception to this is the OF_2/55% methane - 45% ethane propellant combination which, for chamber pressures less than about 650 psia, demonstrates loss values greater than those for the methane propellant combinations. This exception is caused by the high critical pressure of the methane-ethane blend. To avoid the bulk boiling heat transfer regime, the jacket coolant discharge pressure was maintained above critical. The 55% methane - 45% ethane blend has a high critical pressure of 976 psia. Consequently, the attempt to hold the injector inlet pressure at 115% of chamber pressure and circumvent the bulk boiling heat transfer regime failed at all chamber pressures less than 845 psia. Elimination of boiling required that the jacket coolant discharge pressure be maintained at 976 psia for all chamber pressure values below 845 psia level. This requirement resulted in high pump head rise and horsepower requirements and hence increased specific impulse losses.

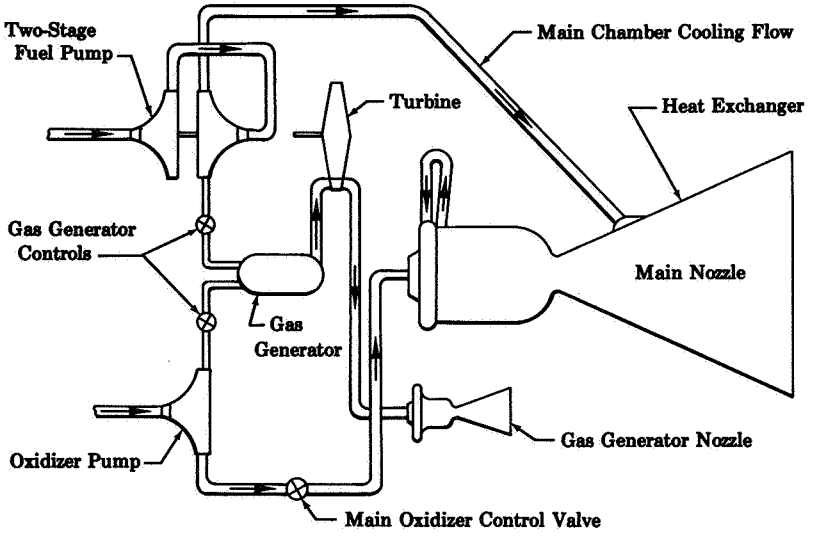


Figure 73. Gas Generator Schematic FD 23485

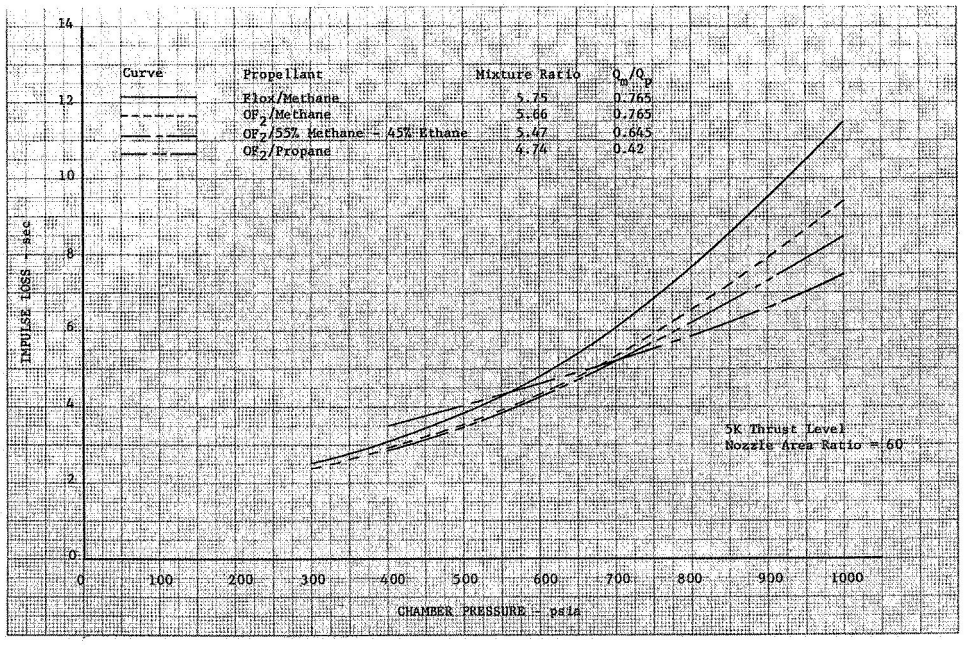


Figure 74. Variation in Impulse Loss With Chamber Pressure for Gas Generator Cycles at Average Q_m/Q_p DF 60435

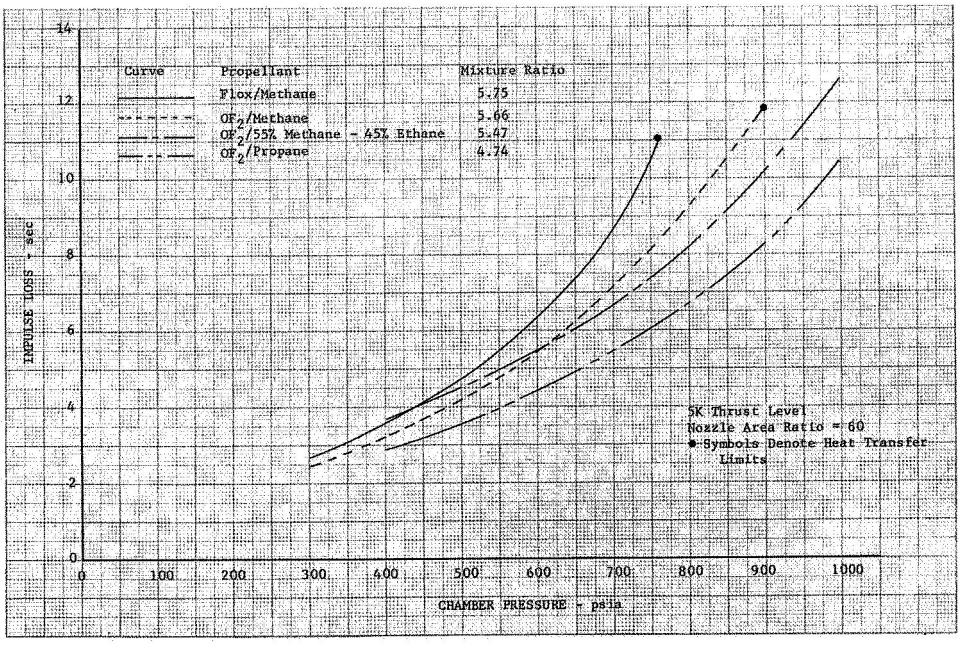


Figure 75. Variation in Impulse Loss With Chamber Pressure for Gas Generator Cycles at $Q_m/Q_p = 1.0$ DF 60436

For methane and propane, with critical pressures of 673 psia and 619 psia, respectively, fuel injector inlet pressures were held to 115% of chamber pressure as long as these values exceeded the critical pressure. As a result, pump head, turbine work, and hence impulse loss values were minimized.

D. PERFORMANCE COMPARISON

Figures 76 and 77 compare ideal performance* for both the expander and gas generator cycles at a 5000-lb_f thrust level for average and 1.0 Q_m/Q_p ratios, respectively. Regardless of the chamber pressure or Q_m/Q_p ratio levels considered, heat transfer and cycle limits notwithstanding, the flox/methane expander cycle provides the highest value of ideal vacuum specific impulse. It is therefore considered that, unless the desire to press for chamber pressure levels greater than approximately 700 psia exceeds the benefits of high delivered performance, the flox/methane turbo-expander cycle represents the most favorable engine configuration. Furthermore, if the thrust chamber cooling jacket coolant passage configuration were optimized (see Section V, Paragraph B3a) so that the wall temperature were constant throughout the chamber, the cooling jacket pressure drop would be reduced and operation at chamber pressures higher than 700 psia could be accomplished with flox/methane.

* Ideal performance is defined as the performance level for $\eta_c^* = 100\%$ and $\eta_{CF} = 100\%$. Therefore, ideal expander cycle performance is equal to theoretical, and ideal gas generator cycle performance is equal to theoretical less the impulse loss resulting from propellant use in the gas generator.

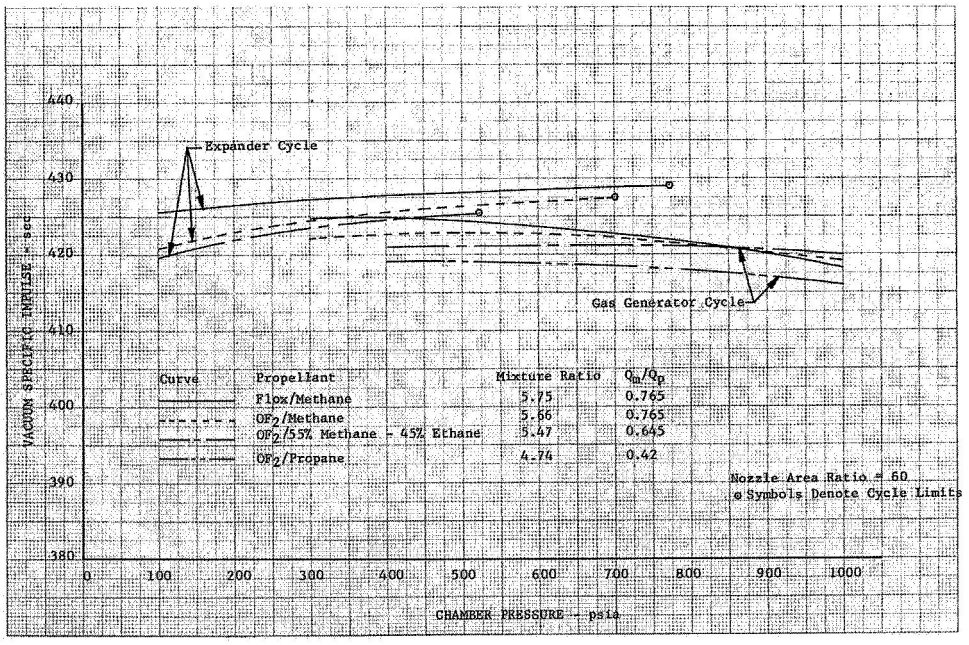


Figure 76. Theoretical Performance Comparison of 5K Thrust Level Expander and Gas Generator Cycles at Average Q_m/Q_p DF 60437

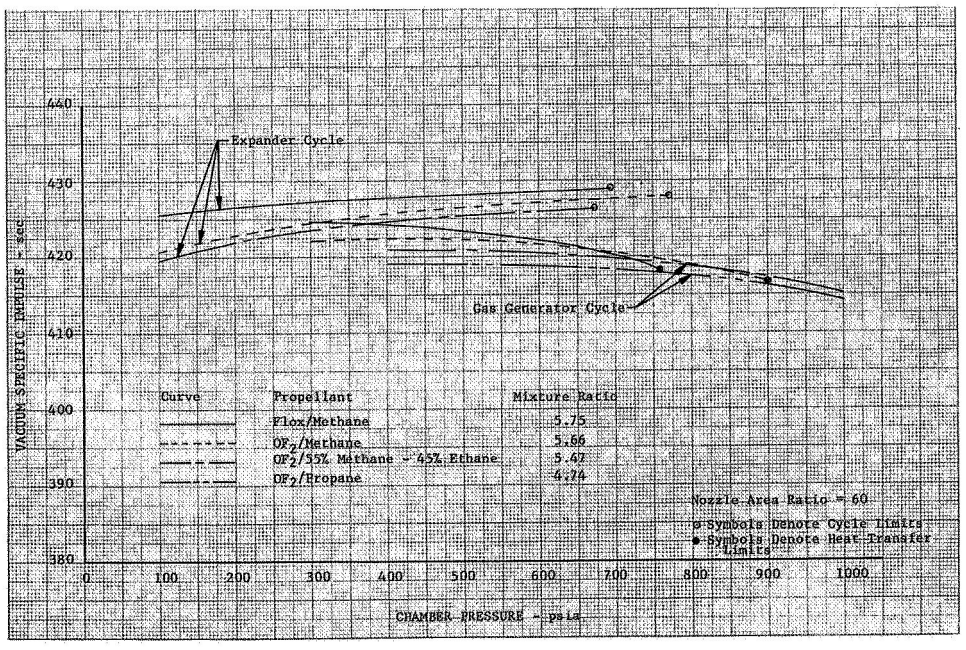


Figure 77. Theoretical Performance Comparison of 5K Thrust Level Expander and Gas Generator Cycles at Q_m/Q_p = 1.0 DF 60438

SECTION VII
REFERENCES

1. "Investigation of Light Hydrocarbon Fuels With Flox Mixtures as Liquid Rocket Propellants - Final Report," PWA FR-1443, Contract NAS3-4195, NASA CR-54445, 1 September 1965.

2. "Investigation of Light Hydrocarbon Fuels With Fluorine-Oxygen Mixtures as Liquid Rocket Propellants - Final Report," PWA FR-2227, NASA CR-72147, Contract NAS3-6296, 15 September 1967.

APPENDIX A
THERMAL SKIN$_{TM}$ CHAMBERS

A new approach for fabrication of regeneratively cooled rocket engine thrust chambers, called Thermal Skin, has been developed and demonstrated at Pratt & Whitney Aircraft's Florida Research and Development Center. The Thermal Skin concept features a bonded sandwich construction of plates (with preformed internal cooling passages), which are formed into thrust chamber contours. The coolant passages in the Thermal Skin plates are engraved by a photochemical milling process that is controllable and rapid, and requires no special tooling other than a photographic master.

To demonstrate the feasibility of the Thermal Skin concept, two subscale rocket thrust chambers (1,000-lb thrust at 300 psia chamber pressure) were fabricated from nickel for tests with fluorine/hydrogen propellants. Figure A-1 illustrates the fabrication steps. After the coolant passages were sized, an engraving master was made and then used for engraving the passages into the nickel plates. The engraved plates were then brazed together, formed to the desired contour, trimmed and placed on a welding fixture so they could be seam-welded together. After the welding operation, the coolant inlet and exit manifolds were added to complete the chamber construction. A completed thrust chamber is shown in figure A-1.

Seven tests were made with the Thermal Skin chambers at chamber pressures from 300 to 820 psia using fluorine/hydrogen propellants at mixture ratios from 8 to 13.3. The chambers were cooled with gaseous hydrogen. The total accumulated firing time was 145 seconds. A photograph taken during one of the test firings is shown in figure A-2. A post-test chamber photograph is shown in figure A-3. The throat heat flux for the 820-psia chamber pressure test has been calculated to be 32 Btu/in^2-sec, which compares to calculated values of 13 and 17 Btu/in^2-sec for the RL10 and J2 engines, respectively.

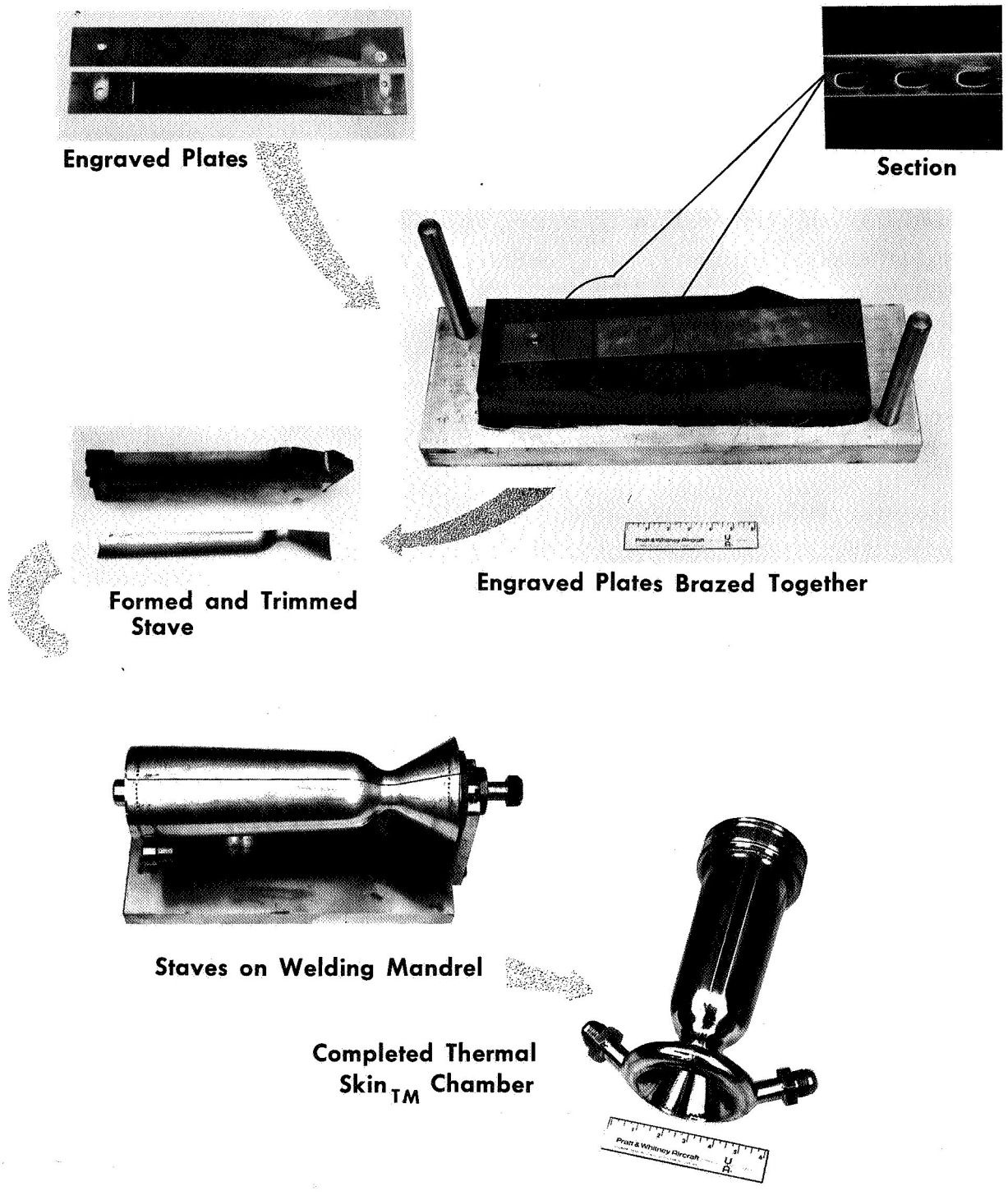


Figure A-1. Thermal Skin$_{TM}$ Thrust Chamber Fabrication GS 7035A

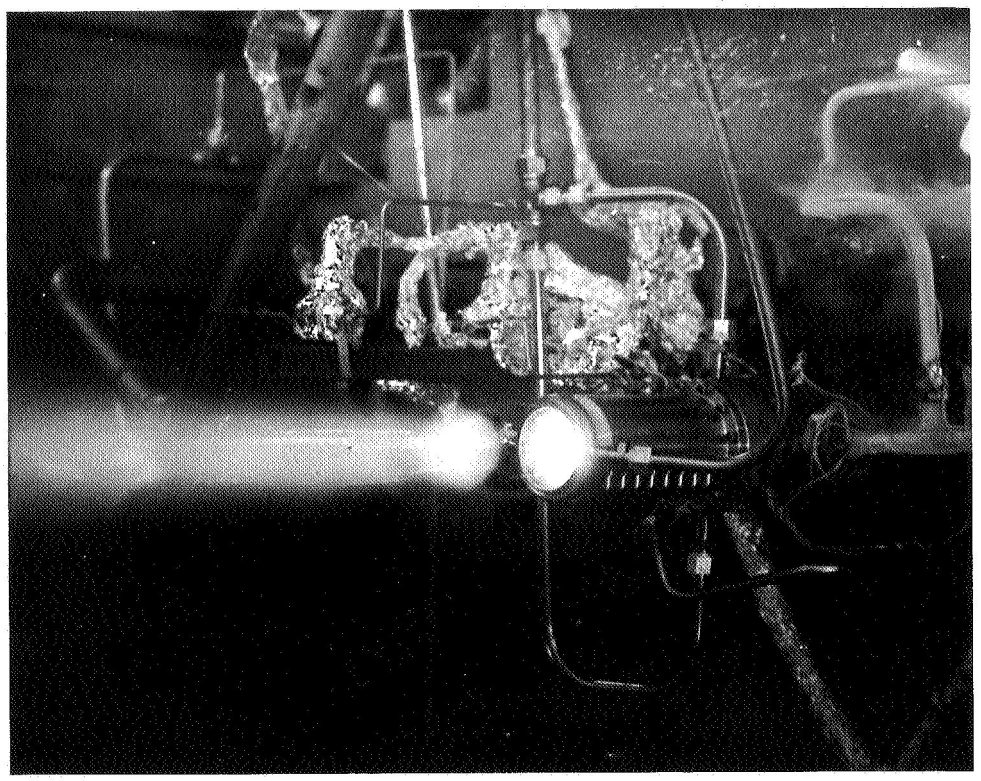


Figure A-2. Photograph of 1K Engine During Hot Firing Test FE 64950

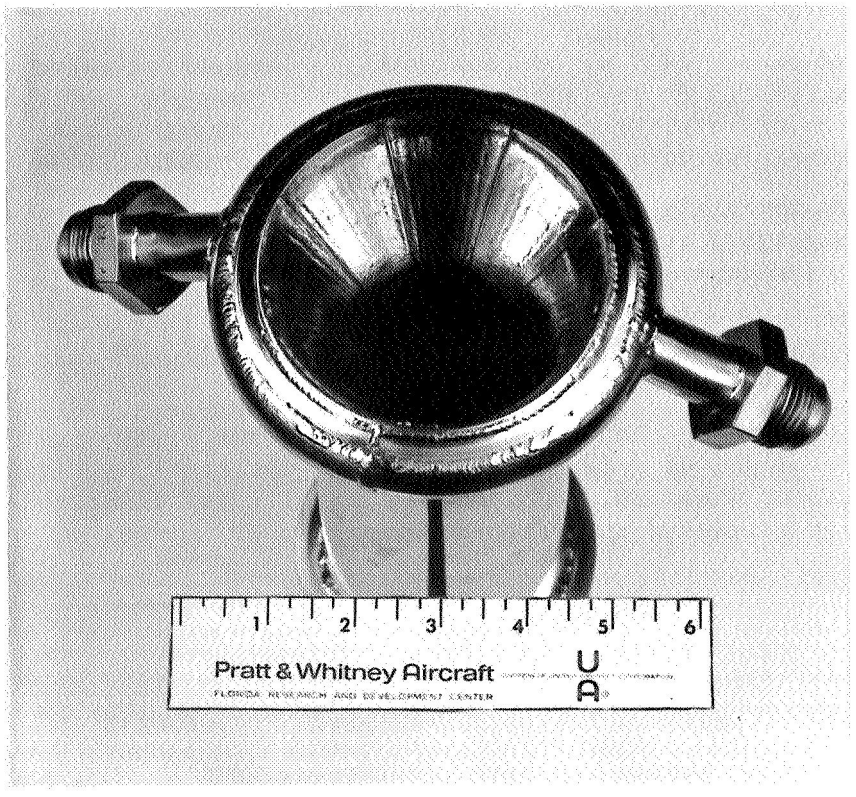


Figure A-3. Thermal Skin$_{TM}$ Chamber Assembly FE 62698

Based on the subscale Thermal Skin chamber demonstration program and design studies for other applications, the following advantages have become apparent for Thermal Skin thrust chambers:

1. The coolant passage flow area can be varied along the length of the chamber to permit close matching of the coolant heat transfer coefficient with local heat fluxes. This feature can be used to minimize the coolant pressure drop.
2. Internal branching of the coolant slots can be readily achieved to minimize stresses in the large-diameter portions of the thrust chamber.
3. The thickness of the metal web separating the coolant passages can be sized to provide internal heat conduction within the Thermal Skin wall so that the webs are effective cooling fins. The degree to which the fin effect can be used depends on the wall heat flux, thermal conductivity of the wall material, passage spacing and height, and wall thickness. By judicious choice of dimensional parameters, it is possible to make the effective area for heat rejection to the coolant greater than the area of absorption from the combustion gases. This feature improves the cooling capability of the wall for a given coolant pressure drop or, conversely, minimizes the required coolant pressure drop for a given heat load.
4. The smooth wall in contact with the combustion gases, as contrasted to the surface provided by tubular construction, reduces total heat flow to the coolant by minimizing the chamber surface area for a given chamber diameter.
5. The materials used for the various layers can be selected to provide the best combination of thermal and structural performance.
6. Thrust chamber fabrication is simplified; this results in reduced costs and shorter lead time for Thermal Skin chambers than for tubular wall chambers.
7. Thermal Skin chambers can be designed for lightweight units. The weight of a flox/methane 10,000-lb thrust, 500-psia chamber pressure, 60 expansion ratio thrust chamber has been estimated to be approximately 85 lb.

The advantage of Thermal Skin construction over tubular wall construction for application in the 1000 to 20,000-lb thrust range with flox/methane propellants has been evaluated. Figure A-4 shows the estimated cooling limits for both tubular-wall and thermal skin thrust chambers. The chamber pressure cooling limit curve for Thermal Skin chambers

reflect the limits obtained in the detailed heat transfer study. They were set by the coolant jacket pressure drop criterion of 1/2 chamber pressure. The cooling limits given for tubular wall chambers were obtained using the smallest ID double-tapered tubes currently available. The cooling limit for tubular chambers are set by stress and wall temperature considerations. The advantage of Thermal Skin is apparent. The cooling limits are increased by approximately 200 to 800 psi depending on thrust level.

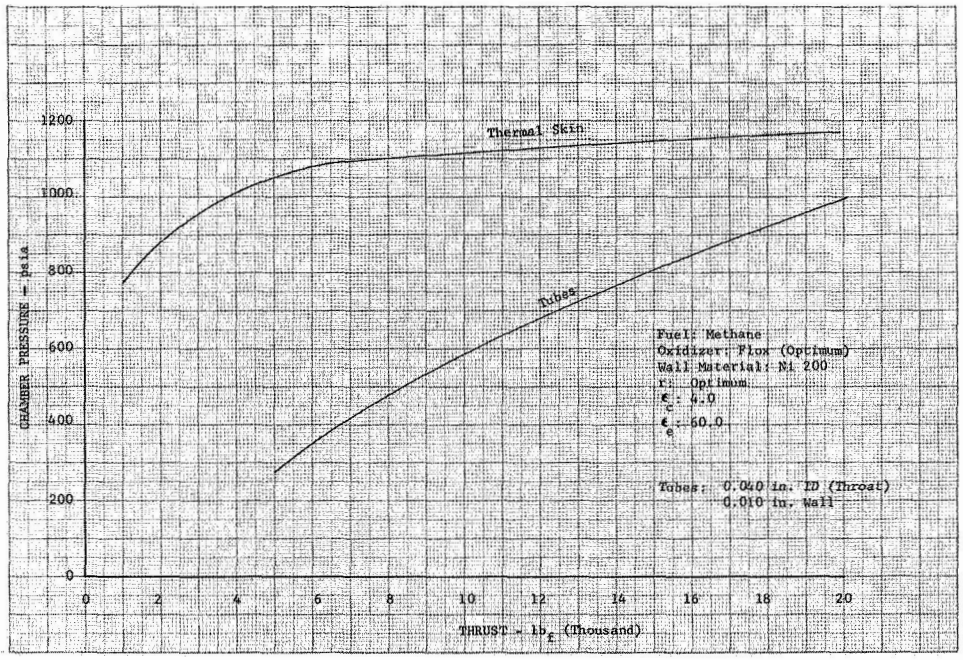


Figure A-4. Comparison of Chamber Pressure vs Thrust for Thermal Skin™ and Tubular Chambers DF 60235

APPENDIX B
HEAT TRANSFER REDUCTION DUE TO CARBON DEPOSITION ON CHAMBER WALLS

1. DISCUSSION

With the flox/LPG propellants, as with any combination using hydrocarbon fuels, carbonaceous material is deposited on thrust chamber walls during combustion. Experience has shown that the thickness of the deposited layer varies throughout the chamber and nozzle, with the greatest thickness being observed in the combustion zone and throat entrance, where gas velocities are lowest and the opportunity for free carbon formation is greatest. Downstream of the throat, where high Mach numbers prevail and combustion is essentially complete, lesser deposits are encountered.

The effect of a carbon layer is to reduce heat flux in the same manner as a thermal barrier coating. Schematic representations of coated and uncoated walls are compared in figure B-1. The local heat flux can be written for both the uncoated and coated walls as:

$$q = h_g \left(T_{aw} - T_w\right) \tag{B-1}$$

$$q_{co} = \left(\frac{1}{\frac{1}{h_g} + \frac{t_{co}}{k_{co}}}\right)\left(T_{aw} - T_w\right) \tag{B-2}$$

where:

q = heat flux to uncoated walls

q_{co} = heat flux to wall with coating

t_{co} = thickness of coating

k_{co} = thermal conductivity of coating

h_g = heat transfer coefficient between the combustion gases and the chamber wall

T_{aw} = adiabatic wall temperature of the combustion gases

T_w = chamber wall temperature on the combustion gas side

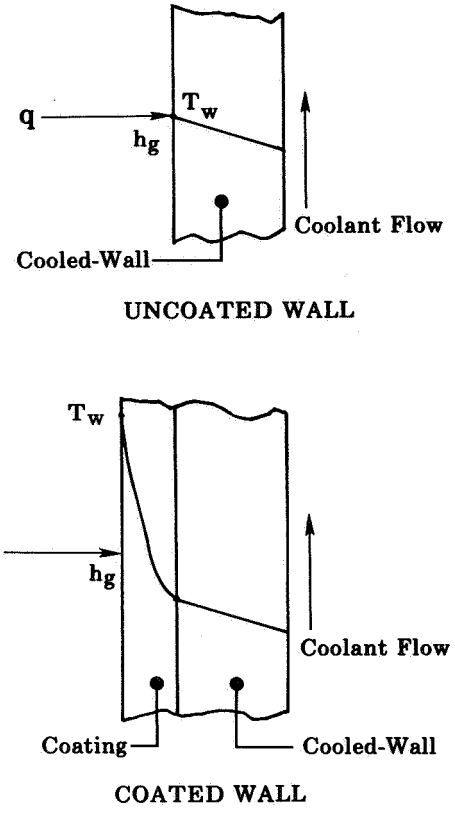


Figure B-1. Schematic Diagram Showing Temperature Distribution Through Coated and Uncoated Heated Walls FD 21635A

The ratio of the heat fluxes for a coated and uncoated wall for a given value of wall metal temperature T_w can be determined by dividing equation B-2 by equation B-1.

$$\frac{q_{co}}{q} = \frac{1}{1 + \frac{h_g t_{co}}{k_{co}}} \qquad \text{(B-3)}$$

As the quantity $h_g t_{co}/k_{co}$ and thus as the coating thickness is increased, the effectiveness of the coating in reducing heat flux is also increased.

The equilibrium thickness of the carbon layer is dependent on the amount of free carbon and on surface shear stresses induced by velocity gradients in the boundary layer. It is determined by a balance of the deposition and erosion rates at the surface. Deposition of solid particles increases with the amount of free carbon in the combustion gases, whereas erosion rate increases with velocity gradient.

The factors influencing formation and erosion of carbon coatings do not lend themselves to analysis, and therefore it is not possible to predict coating thicknesses theoretically. In addition, there is a wide variation in the thermal conductivity of various forms of carbon (from 0.2 Btu/hr-ft-°R for Acheson 2301 to 215 Btu/hr-ft-°R for pyrolytic carbon). Therefore, the exact characteristics of the carbonaceous material that would have to be known to use the relations for insulating coatings cannot readily be obtained, so an alternative approach was taken in the study.

The procedure used to account for accumulation of carbon on thrust chamber walls was the adjustment of the gas-side film coefficient. Data obtained in testing under Contracts NAS3-4195 and NAS3-6296 (References 1 and 2) show that both injector configuration and fuel hydrogen/carbon ratio affect heat transfer. These effects are illustrated in figure B-2, which presents the ratio of measured-to-predicted heat transfer (Q_m/Q_p) as a function of fuel hydrogen/carbon ratio for both liquid/liquid and liquid oxidizer/gaseous fuel injectors. Although this figure was originally derived using data obtained in short sea level chambers, the limits presented also encompass the data obtained for full-length altitude chambers. In the study, the average-value curve was used primarily. The effect of changes in Q_m/Q_p from the average value to 1.0 (no reduction in heat transfer) was also evaluated.

2. APPENDIX B REFERENCES

1. "Final Report, Investigation of Light Hydrocarbon Fuels With Flox Mixtures as Liquid Rocket Propellants," Contract NAS3-4195, NASA CR-54445, PWA FR-1443, September 1965.
2. "Final Report, Investigation of Light Hydrocarbon Fuels With Fluorine-Oxygen Mixtures as Liquid Rocket Propellants," Contract NAS3-6296, NASA CR-72147, PWA FR-2227, 15 September 1967.

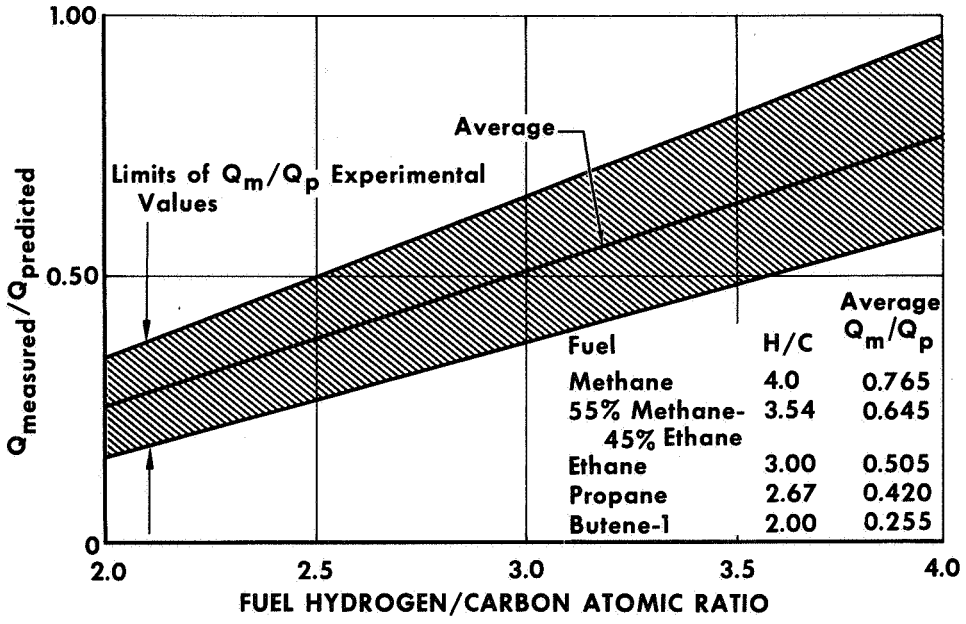


Figure B-2. Effect of Fuel Hydrogen-To-Carbon Ratio on Total Engine Heat Transfer GS 7015B

APPENDIX C
THERMAL DECOMPOSITION OF FUELS

1. DISCUSSION

In the thrust chamber coolant passages, it is desirable to keep the hydrocarbon coolant temperature at a low level so that carbon formation, which can result in the plugging and fouling of the passages, is not excessive. For the regenerative cooling analysis, the incipient thermal decomposition temperature (T_{ID}) was used, which is based upon a 1% decomposition rate per hour, as the upper coolant temperature limit (Reference 1).* Reasons for using the incipient thermal decomposition temperature concept as a limit in the study are as follows:

1. If thermal decomposition of the fuel does not occur, carbon will not form and passage fouling will not be a problem
2. Establishment of the concept is based upon experimental data for the hydrocarbons of interest
3. The concept is easy to apply because the limiting temperature becomes a function only of the hydrocarbon fuel.

Although the physical situation existing in the rocket engine coolant passage is not exactly the same as that which existed in the experimental apparatus used to obtain the data given in the references for this method, the relative values for T_{ID} for the various fuels are believed to be valid.

The procedure for calculating T_{ID} for a general reaction (component A $\xrightarrow{K}$ Products) is straight-forward and may be found in sources such as Reference 2. The equations used in calculating T_{ID} are reviewed in this Appendix and require that the following assumptions be made.

1. Gas phase reaction
2. Isothermal process
3. Isobaric process
4. Classic collision theory
5. Irreversible reaction
6. Reaction in first order with respect to Component A.

*References used in this Appendix are presented in Paragraph 2.

The following basic equations apply.

$$\frac{d\,C_A}{dt} = K\,C_A \qquad \text{(C-1)}$$

$$-\int_{C_{Ao}}^{C_A} \frac{d\,C_A}{C_A} = K \int_o^t dt \qquad \text{(C-2)}$$

where:

$$K = K' \exp(-\Delta E/RT) \qquad \text{(C-3)}$$

C_A = concentration of A at time t
C_{A_o} = initial concentration of A
ΔE = activation energy
K = specific rate constant
K' = frequency factor
R = gas constant

Equation (C-3) is often referred to as the Arrhenius Equation. Integration of equation (C-2) and substitution of equation (C-3) for K yields the following equation.

$$\ln\left(C_{Ao} / C_A\right) = K't \exp\left(-\Delta E/RT\right) \qquad \text{(C-4)}$$

The concentration of A at any time may be expressed in terms of the original concentration and the degree of completion of the reaction, i.e.

$$C_A = C_{Ao}\,(1-x_A) \qquad \text{(C-5)}$$

Substituting (C-5) into (C-4) and solving for T yields

$$T = \frac{-\Delta E/R}{\ln\left[-\ln\left(1-x_A\right)\right] - \ln\left(K't\right)} \qquad \text{(C-6)}$$

The value T_{ID} is calculated by substituting t = 3600 sec and x_A = 0.01 (one percent by weight decomposition per hour). Table C-1 lists the activation energy, frequency factor, thermal decomposition temperature, and references for the experimental data for the hydrocarbon fuels of interest.

Table C-1. Thermal Decomposition Temperature for the Hydrocarbon Fuels of Interest

FUEL	ΔE, Kcal/gm-mole	K', sec^{-1}	T, °R	REFERENCE
Methane	91.0	4.5×10^{13}	1865	3
Ethane	70.2	1.535×10^{14}	1715	3
55% Methane-45% Ethane	84.8	7.77×10^{13}	1400	*
Propane	67.1	2.58×10^{14}	1320	4
Butene-1	45.0	5.0×10^{9}	1160	5

* Values for ΔE and K' obtained by molar-averaging values for methane and ethane.

After establishing temperatures at which incipient thermal decomposition would occur for the fuels of interest, it was still necessary to determine which coolant-side temperature should be limited by the T_{ID} level. In the feasibility study, since coolant passage design was not considered, the computed bulk temperature at the cooling jacket outlet was used. In the detailed heat transfer study, where the cooling system was analyzed and therefore coolant temperature variations along the thrust chamber were computed, the film temperature was limited by the T_{ID} levels. Use of bulk temperature would give optimistic results since there are regions near the wall that are at higher temperatures. Conversely, use of wall temperature would give pessimistic results because only a microscopically thin layer of fluid approaches the wall temperature. Thus, the film temperature, defined as the average of the bulk and wall temperatures, is considered to be the best choice.

Pratt & Whitney Aircraft tested propane in electrically heated tubes to determine the effects of coke formation (due to fuel thermal decomposition) on the heat transfer characteristics (Reference 6). For two-hour test periods, results showed that heat transfer coefficients were reproducible and no deposits were formed. For testing periods of approximately nine hours, heat transfer coefficients were reduced up to 48% and carbonaceous deposits were formed in the inlet section of the tubes where film boiling and accompanying high wall temperatures (approximately 2100°R) were present. However, the midsection of the tubes were still

completely free of deposits. Examination of the test data revealed that the average wall and film temperatures in the midsection were approximately 1470° and 1300°R, respectively, for the test period. Although these test results were obtained with only one of the fuels of interest, they do indicate that the coke deposition should not be a problem in rocket engines as long as film temperatures are not excessively high.

2. APPENDIX C REFERENCES

1. "Evaluation of Hydrocarbon Materials as Vaporizing Fuels," Final Report, ASD-TR-62-254, August 1962.
2. Daniels, F. and R. A. Alberty, "Physical Chemistry," John Wiley & Sons Co., New York, 1956.
3. Kozlov, G. I. and V. G. Knorre, "Single-Pulse Shock Tube Studies on Kinetics of the Thermal Decomposition of Methane," Combustion and Flame, Vol. 6, No. 4, March 1961.
4. Laidler, K. J., N. H. Sagert, and Wojciechowski, "Kinetics and Mechanisms of the Thermal Decomposition of Propane," Dept. of Chemistry, Univ. of Ottawa, Canada.
5. Kerr, J. A., R. Spencer, A. F. Trotman - Dickenson, "The Pyrolysis of 1-Butene and the Resonance Energy of the Allyl Radical," J. Chem. Soc. 1965, 6652-4 (Eng).
6. "Final Report for Study of Turbojet Main Burners for Use With Contaminated Fuel," PWA FR-1254, Prepared Under Navy, Bureau of Naval Weapons, Contract NOw 63-0489-d, 5 March 1965.

APPENDIX D
FEASIBILITY STUDY - METHOD OF ANALYSIS

1. GENERAL

In the feasibility study, regenerative cooling limits for the hydrocarbon fuels were evaluated on the basis of the heat capacity of the fuels and the integrated or total heat transfer to the thrust chamber. For supercritical pressures, the feasibility of regenerative cooling was determined by comparing the computed fuel coolant temperature at the exit of the cooling jacket to limits set either by fuel thermal decomposition or by the allowable structural temperature limit. At subcritical pressures, bulk boiling was the limiting criterion and thus the saturated liquid state was the limiting cooling jacket exit condition. The method of analysis followed in the feasibility study is described in this Appendix.

2. CALCULATION OF THRUST CHAMBER HEAT TRANSFER

The total heat transfer to the thrust chamber was calculated by performing the following integration using an IBM 360 computer program.

$$Q = \left(\frac{Q_m}{Q_p}\right)\int_0^{A_s} h_g (T_{aw} - T_w)\, dA_s \qquad \text{(D-1)}$$

The combustion-side heat transfer coefficient, h_g, was computed using the simplified Bartz equation (Reference 1).* This equation was selected because it can be readily applied and also because (as shown in figure D-1) it agrees closely with the more rigorous boundary layer solutions by Sibulkin (Reference 2) and Elliott (Reference 3). In addition, with the hydrocarbon fuels carbon deposition on the chamber walls has a significant effect on heat transfer, and based on currently available data (see Appendix B), is best handled by reducing the film coefficients by the factor Q_m/Q_p. The amount of carbon formation, and therefore the Q_m/Q_p factor for a given fuel is related to injector design and consequently the unknowns

*References for this Appendix are given in Paragraph 6.

in Q_m/Q_p are believed to override completely any slight error introduced by using the simplified Bartz equation.

The form of the Bartz equation used is

$$h_g = 0.026 \frac{k_f}{D}\left(\frac{\dot{w}_p}{A}\frac{D}{\mu_f}\frac{\rho_f}{\rho_b}\right)^{0.8}\left(Pr_f\right)^{0.4} \qquad \text{(D-2)}$$

In this equation the transport properties are evaluated at a film temperature, T_f, which is the arithmetic average of the static gas temperature and the wall temperature.

The adiabatic wall temperature, T_{aw}, was calculated from the equation

$$T_{aw} = \left(T_o - T_s\right)\mathcal{R} + T_s \qquad \text{(D-3)}$$

where

$$T_o = T_c'\sqrt{\eta_c^*}$$

$$\mathcal{R} = \sqrt[3]{Pr_b}$$

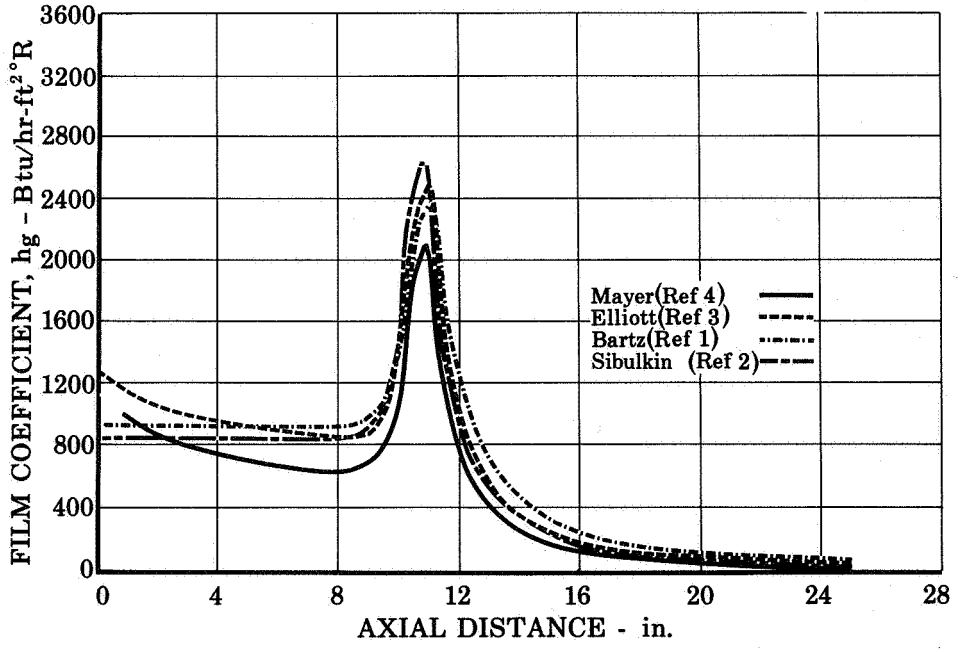


Figure D-1. Comparison of Combustion Gas Heat Transfer Prediction Methods FD 21672A

By use of one-dimensional isentropic gas dynamic equations, the static temperature and pressure can be expressed as functions of area ratio. Thus, by knowledge of the following items, which are inputs to the IBM 360 computer program, equation D-1 can be integrated.

1. Propellant flow rate
2. Total temperature
3. Combustion gas transport properties as functions of temperature
4. Nozzle throat diameter
5. Specific heat ratio of the gases
6. Contraction ratio and characteristic length of the combustion chamber
7. Untruncated design area ratio and length of the nozzle.

The propellant flow rate and throat diameter are computed using the equations

$$\dot{w}_p = \frac{F}{I'_{vac}\ \eta_c^*\ C_s} \tag{D-4}$$

$$D^* = \left[\frac{4\ C^{*\prime}\ \eta_c^*\ \dot{w}_p}{\pi P_c g}\right]^{1/2} \tag{D-5}$$

In these equations, the theoretical performance parameters, I'_{vac} and c*', as well as the combustion temperature, T'_c, and the ratio of specific heats for the combustion gases, γ, are determined by propellant theoretical performance calculations for shifting equilibrium conditions. Theoretical performance values were computed for all five fuels specified with both flox (using the optimum fluorine concentration for each fuel) and OF_2 oxidizers. The heat of formation used for OF_2 was the new NBS value of +5.86 Kcal/mole for the gas at 298°K. This provides a reference enthalpy value of 65.2 Btu/lb_m at the OF_2 normal boiling point. Performance curves for the propellants are presented in Appendix G.

Transport properties of the combustion gases for all the oxidizer/fuel combinations of interest were generated as functions of mixture ratio and temperature. The c* efficiency was assumed to be 96% and the nozzle

aerodynamic efficiency, C_s, was taken to be 97%. Because of the difficulty of assigning a value for kinetic losses (accepted prediction procedures have not agreed with experimental results as described in Reference 5), these were neglected.

The geometry of the subsonic portion of the thrust chamber was computed assuming a generalized contour (figure D-2) which is dependent upon input values of characteristic length, contraction ratio, and throat diameter. The geometry of the supersonic nozzle was computed using the method of characteristics for input values of untruncated nozzle area ratio and nozzle length.

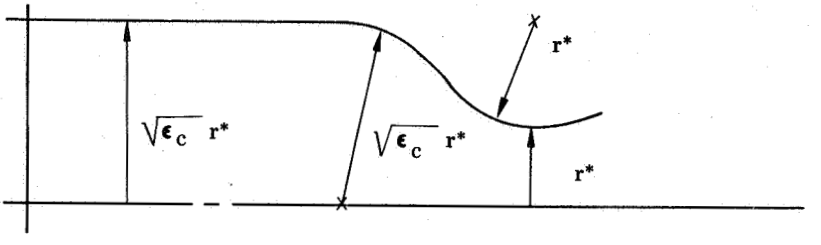


Figure D-2. Chamber Contour FD 23470

3. GENERATION OF BASIC PARAMETRIC CURVES

The heat transfer to the thrust chamber was determined using the computer program described in the previous paragraph for approximately 72 cases. A "case" is defined by the fuel and oxidizer combination, mixture ratio, contraction ratio, expansion ratio, wall temperature, chamber pressure, and thrust level. For each of the cases considered the coolant enthalpy rise was calculated by dividing the integrated heat transfer value by the coolant flow rate. With data from these few cases, it is possible to calculate the enthalpy rise and therefore to determine

temperature rise and coolant state (gas,liquid,or two-phase) for all combinations of the variables and propellants considered in the feasibility study. These calculations are possible because the relative effects on thrust chamber heat transfer of most of the variables considered are independent of changes in the other variables. For example, the percentage increase in heat transfer between two thrust levels is independent of the wall temperature. Figure D-3 shows the variation of the total heat transferred to the thrust chamber as a function of thrust for wall temperatures of 1700 and 2100°F. The percentage increase in heat transfer between 1000 and 20,000-lb thrust is 638.6% at T_w = 1700°F and 631.6% at T_w = 2100°F. It can thus be concluded that the effect of a change in thrust on heat transfer is essentially independent of the value of wall temperature. Similarly, it can be shown that the ratio of total heat transfer values at any thrust level is essentially independent of the fuel, the oxidizer, and the mixture ratio. This leaves only contraction ratio, expansion ratio, and chamber pressure as parameters that influence the Δ heat transfer - Δ thrust relationship.

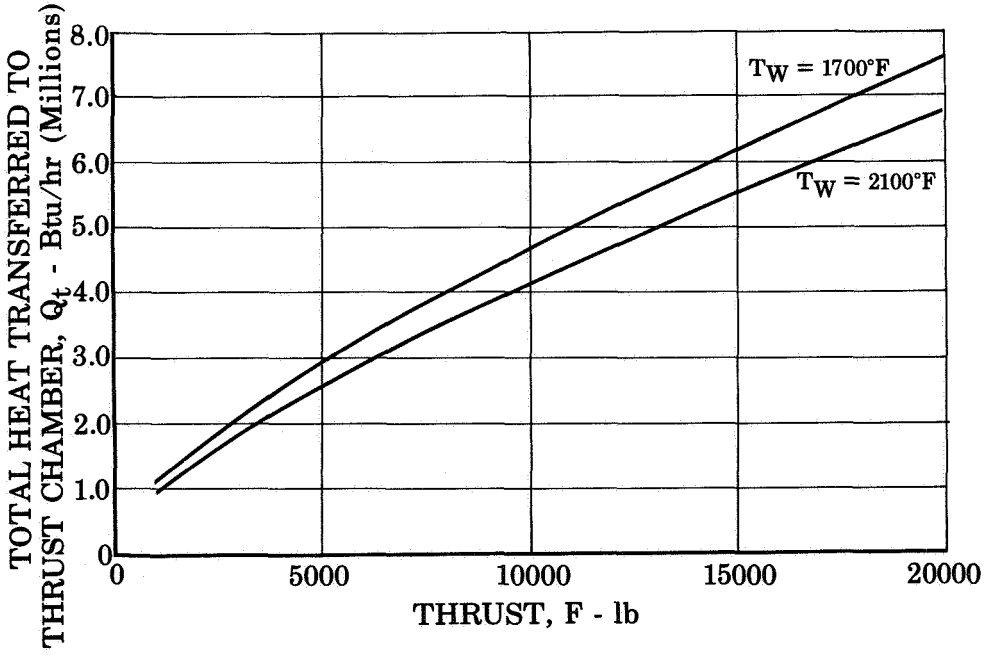


Figure D-3. Variation in Thrust Chamber Total Heat Transferred With Thrust Level

FD 21632

Relationships between variables similar to those just discussed for thrust level can be shown for each of the eight primary variables that were evaluated in the study. In table D-1, the eight variables for the cooling feasibility analysis are listed; each is shown in turn in the first column as the primary variable. The variables that have significant effects on the percentage change in heat transfer and those that have negligible effects for incremental changes of the particular primary variable are listed in the second and third columns, respectively.

Table D-1. Variables to be Considered in Cooling Feasibility Analysis

Primary Variable	Variable With Significant Effects	Variable With Negligible Effects
F	ϵ_c, ϵ_e, P_c	Fuel, Oxidizer, r, T_w
P_c	T_w	Fuel, Oxidizer, F, r, ϵ_c, ϵ_e
ϵ_c	ϵ_e, F, P_c	Fuel, Oxidizer, r, T_w
ϵ_e	ϵ_c, F, P_c	Fuel, Oxidizer, r, T_w
T_w	P_c	Fuel, Oxidizer, r, ϵ_c, ϵ_e
Fuel	Oxidizer, r	F, P_c, ϵ_c, ϵ_e, T_w
Oxidizer	Fuel, r	F, P_c, ϵ_c, ϵ_e, T_w
r	Oxidizer, Fuel	F, P_c, ϵ_c, ϵ_e, T_w

From table D-1 the primary and influencing variables (columns 1 and 2) can be classified into groups based upon their interrelationships as follows:

Group A	Group B	Group C
Fuel, Oxidizer, r	P_c, T_w	F, P_c, ϵ_c, ϵ_e

Examination of the relationships of the variables in Group C permits a further simplification. Since the simplified Bartz equation does not give a boundary layer solution, the contraction ratio, ϵ_c, affects heat transfer only in the combustion chamber, whereas the expansion ratio, ϵ_e, affects heat transfer primarily in the nozzle portion of the thrust chamber.

Combustion chamber heat transfer dependency on expansion ratio is caused by changes in specific impulse with expansion ratio. Changes in specific impulse affect throat diameter (see equations D-4 and D-5) and thus combustion chamber surface area. However, specific impulse changes only approximately 3% as expansion ratio is increased from 40 to 100; therefore, the dependency of combustion chamber heat transfer on expansion ratio is quite small.

The effect of chamber pressure on the heat transfer - thrust relationship as related to the chamber geometry terms ϵ_c and ϵ_e results almost entirely from relative changes in chamber surface area and nozzle surface area as the throat diameter varies. Since the chamber characteristic length, L*, was held constant at 30 inches in the study, the chamber surface area is proportional to the throat diameter at any contraction ratio, whereas the nozzle surface area for a given expansion ratio and contour is proportional to the square of the throat diameter. By estimating the nozzle and combustion chamber heat transfer rates separately for the variables in groups B and C above, the variables of interest can thus now be grouped as shown in table D-2.

Table D-2. Parameter Groups

Group 1	Group 2	Group 3	Group 4
Fuel, Oxidizer, r	P_c, T_w	F, ϵ_e	F, ϵ_c

With this grouping, it is possible to summarize in only six curves all heat transfer data necessary to determine the coolant enthalpy rise required for all combinations of the variables of interest. Figures D-4 through D-9 show the basic parametric curves.

The significance of these curves as well as their development can be explained by the use of partial derivatives. The fuel coolant enthalpy rise for cooling the thrust chamber is a function of the eight variables involved in the study, i.e.,

$$\Delta H = f(\text{fuel, oxidizer, r, } P_c, T_w, F, \epsilon_c, \epsilon_e) \qquad \text{(D-6)}$$

In the study a base enthalpy rise (ΔH_o) was established for flox/methane at its optimum mixture ratio (5.75), 5000-lb thrust, 250-psia chamber pressure, contraction ratio of 3, an expansion ratio of 60 and a wall temperature of 2100°R. The change in fuel enthalpy rise from this preselected base point, in terms of the variables of interest, is given as follows:

$$\Delta(\Delta H) = \left(H_{fuel} - H_{CH_4}\right) + \left(H_{ox} - H_{flox}\right) + \left(\frac{\partial H}{\partial r}\right)\Delta r + \left(\frac{\partial H}{\partial P_c}\right)\Delta P_c + \left(\frac{\partial H}{\partial T_w}\right)\Delta T_w + \left(\frac{\partial H}{\partial F}\right)\Delta F + \left(\frac{\partial H}{\partial \epsilon_c}\right)\Delta\epsilon_c + \left(\frac{\partial H}{\partial \epsilon_e}\right)\Delta\epsilon_e \qquad \text{(D-7)}$$

The symbol ($H_{fuel} - H_{CH_4}$) refers to a change in fuel (coolant) enthalpy rise due to a change in fuel type from a base fuel (methane) with all remaining variables held constant. Similarly, the symbol ($H_{ox} - H_{flox}$) refers to a change in fuel (coolant) enthalpy rise due to a change in oxidizer type from the base oxidizer (flox) with all remaining variables held constant. As previously stated, the chamber and nozzle heat loads can be separated; therefore

$$\frac{\partial H}{\partial F}\Delta F = \left(\frac{\partial H_c}{\partial F}\right)\Delta F + \left(\frac{\partial H_e}{\partial F}\right)\Delta F \qquad \text{(D-8)}$$

$$\frac{\partial H}{\partial T_w}\Delta T_w = \left(\frac{\partial H_c}{\partial T_w}\right)\Delta T_w + \left(\frac{\partial H_e}{\partial T_w}\right)\Delta T_w \qquad \text{(D-9)}$$

$$\frac{\partial H}{\partial \epsilon_c}\Delta\epsilon_c = \left(\frac{\partial H_c}{\partial \epsilon_c}\right)\Delta\epsilon_c + \cancel{\left(\frac{\partial H_e}{\partial \epsilon_c}\right)}^{\,0}\Delta\epsilon_c \qquad \text{(D-10)}$$

$$\frac{\partial H}{\partial \epsilon_e}\Delta\epsilon_e = \cancel{\left(\frac{\partial H_c}{\partial \epsilon_e}\right)}^{\,0}\Delta\epsilon_e + \left(\frac{\partial H_e}{\partial \epsilon_e}\right)\Delta\epsilon_e \qquad \text{(D-11)}$$

$$\frac{\partial H}{\partial P_c}\Delta P_c = \left(\frac{\partial H_c}{\partial P_c}\right)\Delta P_c + \left(\frac{\partial H_e}{\partial P_c}\right)\Delta P_c \qquad \text{(D-12)}$$

The effects of fuel type and mixture ratio on thrust chamber heat transfer cannot be prorated among the chamber and nozzle sections since these variables are assumed to exert equal influence at all locations. Substituting equations D-8 through D-12 into equation D-7 yields the following relation for total change in fuel enthalpy rise.

$$\Delta(\Delta H) = (H_{fuel} - H_{CH_4}) + (H_{ox} - H_{flox}) + \left(\frac{\partial H}{\partial r}\right)\Delta r + \left(\frac{\partial H_c}{\partial P_c}\right)\Delta P_c + \left(\frac{\partial H_e}{\partial P_c}\right)\Delta P_c + \left(\frac{\partial H_c}{\partial T_w}\right)\Delta T_w + \left(\frac{\partial H_e}{\partial T_w}\right)\Delta T_w + \left(\frac{\partial H_c}{\partial F}\right)\Delta F + \left(\frac{\partial H_c}{\partial \epsilon_c}\right)\Delta \epsilon_c + \left(\frac{\partial H_e}{\partial \epsilon_e}\right)\Delta \epsilon_e + \left(\frac{\partial H_e}{\partial F}\right)\Delta F \qquad \text{(D-13)}$$

It is now possible to arrange the partial differentials according to their relationships. Based on the groupings given in table D-2, the variables that affect the respective partial differentials and those that do not can be identified as shown in table D-3. Based on the relationships indicated in table D-3, the six parametric curves were formulated. The partial differentials are identified with the curves as described in the following paragraphs.

The fuel enthalpy rises in the chamber and nozzle can be obtained from the variables contained in Groups 3 and 4 of table D-2 by separating the following terms

$$\Delta H_c' = \Delta H_{co} + \left(\frac{\partial H_c}{\partial F}\right)\Delta F + \left(\frac{\partial H_c}{\partial \epsilon_c}\right)\Delta \epsilon_c \qquad \text{(D-14)}$$

$$\Delta H_e' = \Delta H_{eo} + \left(\frac{\partial H_e}{\partial F}\right)\Delta F + \left(\frac{\partial H_e}{\partial \epsilon_e}\right)\Delta \epsilon_e \qquad \text{(D-15)}$$

from equation D-13. The quantities ΔH_{co} and ΔH_{eo} bias the fuel enthalpy rises to the base case values. Figure D-4 provides the coolant enthalpy rise ($\Delta H_c'$) for the combustion chamber region upstream of the throat as a function of thrust and contraction ratio for flox/methane at a mixture ratio of 5.75, a chamber pressure of 250 psia, and a wall temperature of 2100°F. Figure D-5 presents $\Delta H_e'$ for the expansion nozzle for the same conditions.

Table D-3. Variables That Affect Partial Differentials

Group	Partial Differentials	Variables Affecting Partial Differentials	Variables Not Affecting Partial Differentials
1	$(H_{fuel} - H_{CH_4})$, $(H_{ox} - H_{flox})$, $\frac{\partial H}{\partial r}$	fuel, oxidizer, r	P_c, F, T_w, ϵ_c, ϵ_e
2	$\frac{\partial H_c}{\partial P_c}$, $\frac{\partial H_e}{\partial P_c}$, $\frac{\partial H_c}{\partial T_w}$, $\frac{\partial H_e}{\partial T_w}$	P_c, T_w	fuel, oxidizer, r, F, ϵ_c, ϵ_e
3	$\frac{\partial H_e}{\partial F}$, $\frac{\partial H_e}{\partial \epsilon_e}$	F, ϵ_e	fuel, oxidizer r, P_c, T_w, ϵ_c
4	$\frac{\partial H_c}{\partial F}$, $\frac{\partial H_c}{\partial \epsilon_c}$	F, ϵ_c	fuel, oxidizer, r, P_c, T_w, ϵ_e

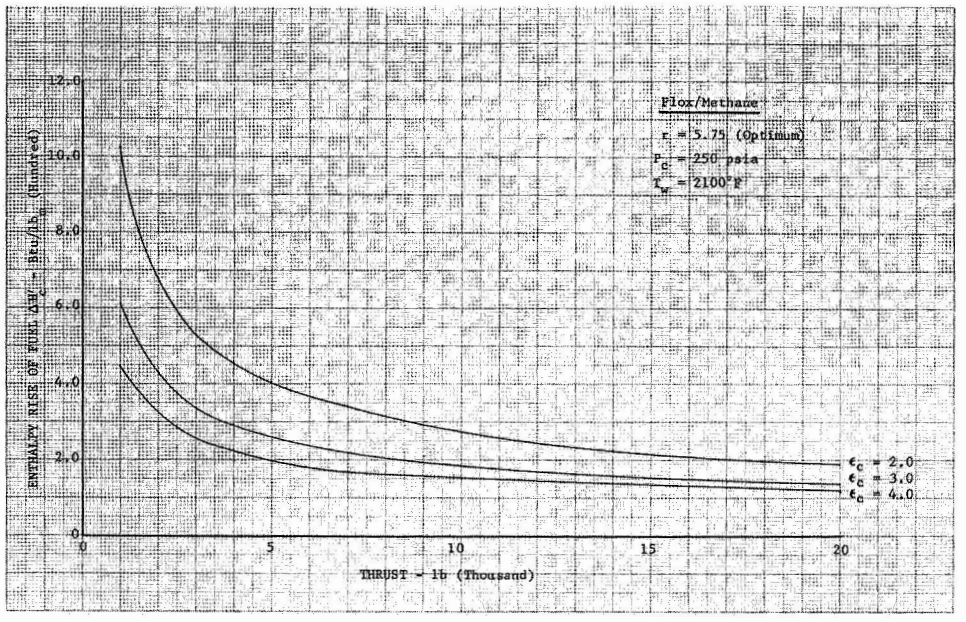


Figure D-4. Variation in Combustion Chamber Fuel Enthalpy Rise With Thrust Level and Chamber Contraction Ratio DF 58062

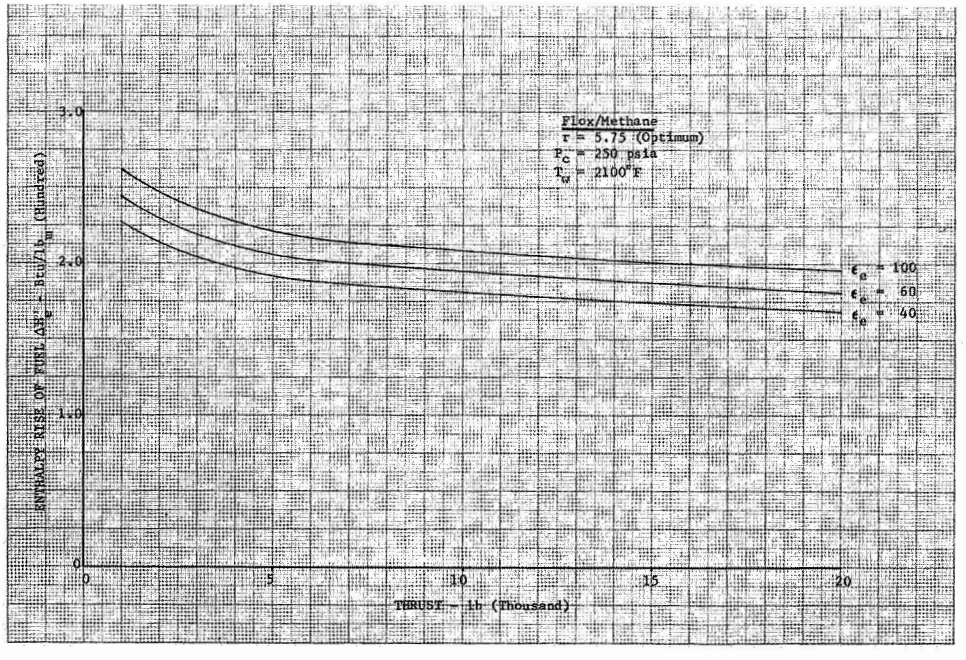


Figure D-5. Variation in Nozzle Fuel Enthalpy Rise With Thrust Level and Nozzle Expansion Ratio DF 58063

Adjustments to the chamber and nozzle enthalpy rise for variations in wall temperature and chamber pressure from base values can be made by defining a ratio or adjustment factor defined by equations D-16 and D-17. Equation D-16 is obtained by separating the variables given in Group 2 from equation D-13.

$$\Delta H_c/\Delta H'_c = \left[\Delta H'_c + \left(\frac{\partial H_c}{\partial P_c}\right)\Delta P_c + \left(\frac{\partial H_c}{\partial T_w}\right)\Delta T_w\right]\frac{1}{\Delta H'_c}$$

$$= 1 + \left(\frac{\partial H_c}{\partial P_c}\right)\frac{\Delta P_c}{\Delta H'_c} + \left(\frac{\partial H_c}{\partial T_w}\right)\frac{\Delta T_w}{\Delta H'_c} \qquad \text{(D-16)}$$

Equation D-17 is obtained in a similar manner as equation D-16.

$$\Delta H_e/\Delta H'_e = \left[\Delta H'_e + \left(\frac{\partial H_e}{\partial P_c}\right)\Delta P_c + \left(\frac{\partial H_e}{\partial T_w}\right)\Delta T_w\right]\frac{1}{\Delta H'_e}$$

$$= 1 + \left(\frac{\partial H_e}{\partial P_c}\right)\frac{\Delta P_c}{\Delta H'_e} + \left(\frac{\partial H_e}{\partial T_w}\right)\frac{\Delta T_w}{\Delta H'_e} \qquad \text{(D-17)}$$

Figure D-6 is a plot of the correction to chamber heat flux for variations in chamber pressure and wall temperature. While figure D-6 is based on calculations for a particular propellant combination, mixture ratio, thrust, and contraction, it is equally valid for other propellants, mixture ratios, thrust, and contraction ratios because these are parameters that have negligible effects on the Δ heat transfer - Δ chamber pressure and the Δ heat transfer - Δ wall temperature relationships. Figure D-7 provides a chamber pressure and wall temperature correction for the nozzle similar to that of figure D-6 for the combustion chamber.

The enthalpy rise for the entire thrust chamber is the sum of the corrected chamber and nozzle enthalpy rises. Therefore, equation D-18 represents the enthalpy rise for all variables except changes in fuel type, oxidizer type, and mixture ratio.

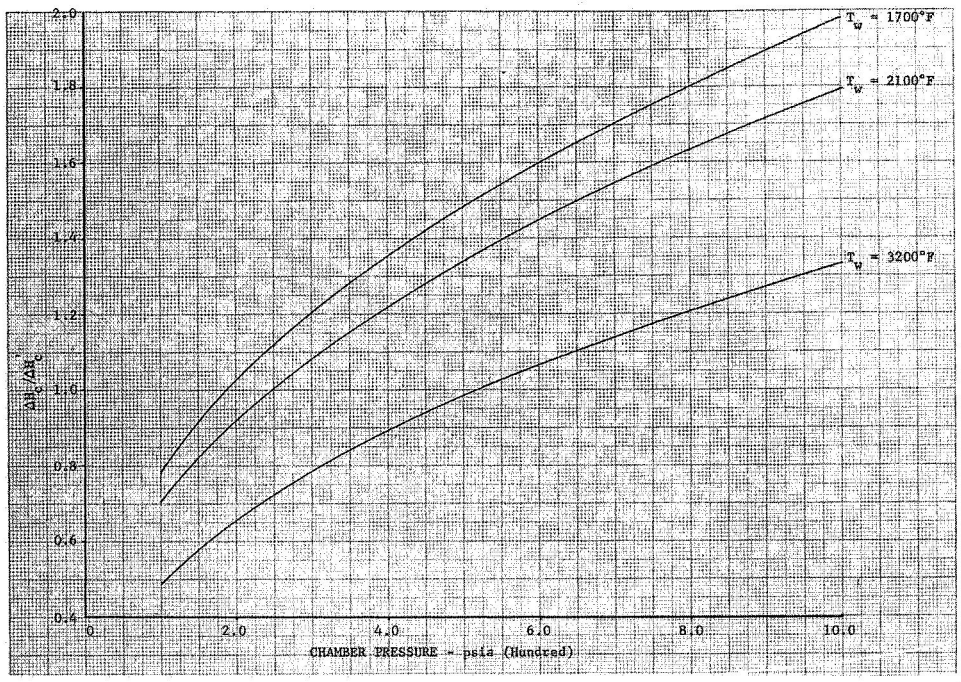


Figure D-6. Variation of Wall Temperature Correction Factor With Chamber Pressure for Chamber Fuel Enthalpy Rise

DF 58064

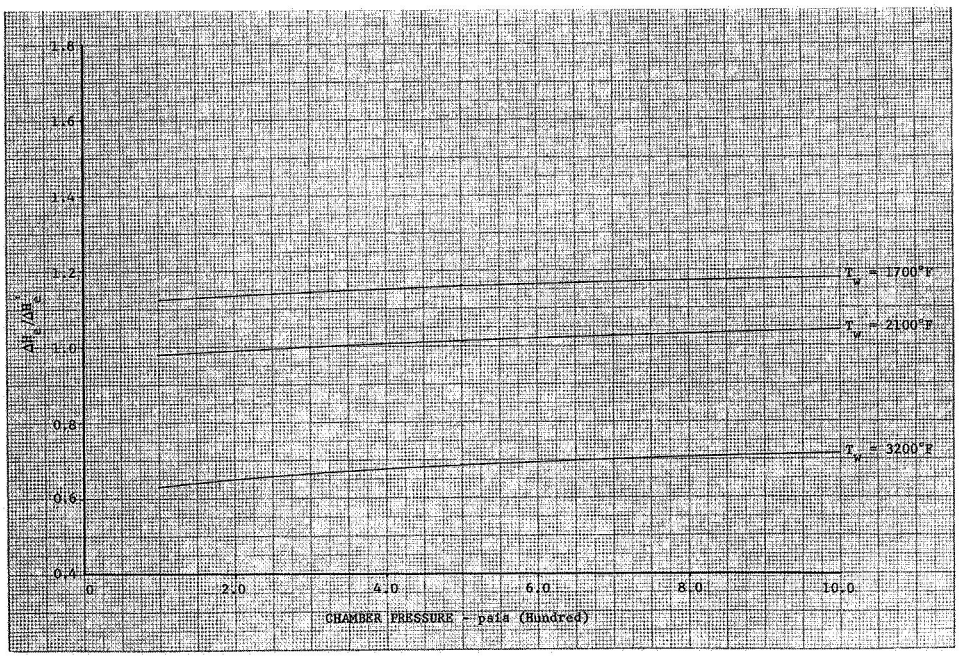


Figure D-7. Variation of Wall Temperature Correction Factor With Pressure for Nozzle Fuel Enthalpy Rise

DF 58065

$$\Delta H' = \Delta H'_c \left(\Delta H_c / \Delta H'_c\right) + \Delta H'_e \left(\Delta H_e / \Delta H'_e\right)$$

$$= \Delta H_{co} + \left(\frac{\partial H_c}{\partial F}\right)\Delta F + \left(\frac{\partial H_c}{\partial \epsilon_c}\right)\Delta \epsilon_c +$$

$$\left(\frac{\partial H_c}{\partial P_c}\right)\Delta P_c + \left(\frac{\partial H_c}{\partial T_w}\right)\Delta T_w + \Delta H_{eo} +$$

$$\left(\frac{\partial H_e}{\partial F}\right)\Delta F + \left(\frac{\partial H_e}{\partial \epsilon_e}\right)\Delta \epsilon_e + \left(\frac{\partial H_e}{\partial P_c}\right)\Delta P_c + \left(\frac{\partial H_e}{\partial T_w}\right)\Delta T_w$$

The above equation can be simplified with the aid of the identities given by equations D-8 through D-12.

$$\Delta H' = \Delta H_o + \left(\frac{\partial H}{\partial P_c}\right)\Delta P_c + \left(\frac{\partial H}{\partial T_w}\right)\Delta T_w +$$

$$\left(\frac{\partial H}{\partial F}\right)\Delta F + \left(\frac{\partial H}{\partial \epsilon_c}\right)\Delta \epsilon_c + \left(\frac{\partial H}{\partial \epsilon_e}\right)\Delta \epsilon_e \qquad \text{(D-18)}$$

where

$$\Delta H_o = \Delta H_{co} + \Delta H_{eo}$$

The correction for fuel type, oxidizer type, and mixture ratio is given in equation D-19 and is obtained by separating these variables from equation D-13.

$$\Delta H/\Delta H' = \left[\Delta H' + \left(H_{fuel} - H_{CH_4}\right) + \left(H_{ox} - H_{flox}\right) + \left(\frac{\partial H}{\partial r}\right)\Delta r\right]\frac{1}{\Delta H'}$$

$$= \left[1 + \left(H_{fuel} - H_{CH_4}\right)\frac{1}{\Delta H'} + \left(H_{ox} - H_{flox}\right)\frac{1}{\Delta H'} + \left(\frac{\partial H}{\partial r}\right)\frac{\Delta r}{\Delta H'}\right] \qquad \text{(D-19)}$$

Since the correction factor $\Delta H/\Delta H'$ is a function of three variables, and because only two oxidizers are considered, two curves for $\Delta H/\Delta H'$ are presented, one for each oxidizer. Figure D-8 is used to adjust the enthalpy rise ($\Delta H'$) for other mixture ratios or other fuels; the curves for each fuel are based on the optimum flox concentration for that particular compound or blend.

If OF_2 rather than flox is used as the oxidizer, figure D-9 is used rather than figure D-8. In both figures D-8 and D-9, the appropriate average value for Q_m/Q_p for each of the fuels has been used.

Finally, the enthalpy rise of the fuel for a specified set of variables and desired fuel and oxidizer can be obtained by multiplying equation D-18 by equation D-19.

$$\Delta H = \Delta H' \ (\Delta H/\Delta H')$$

$$= \Delta H_o + (H_{fuel} - H_{CH_4}) + (H_{ox} - H_{flox}) + \left(\frac{\partial H}{\partial r}\right)\Delta r +$$

$$\left(\frac{\partial H}{\partial P_c}\right)\Delta P_c + \left(\frac{\partial H}{\partial T_w}\right)\Delta T_w + \left(\frac{\partial H}{\partial F}\right)\Delta F +$$

$$\left(\frac{\partial H}{\partial \epsilon_c}\right)\Delta \epsilon_c + \left(\frac{\partial H}{\partial \epsilon_e}\right)\Delta \epsilon_e \qquad \text{(D-20)}$$

Equation D-20 is identical to equation D-7 since $\Delta H - \Delta H_o = \Delta(\Delta H)$.

Given the coolant ΔH, the coolant state and outlet temperature may be determined from a temperature-enthalpy chart for the fuel of interest.

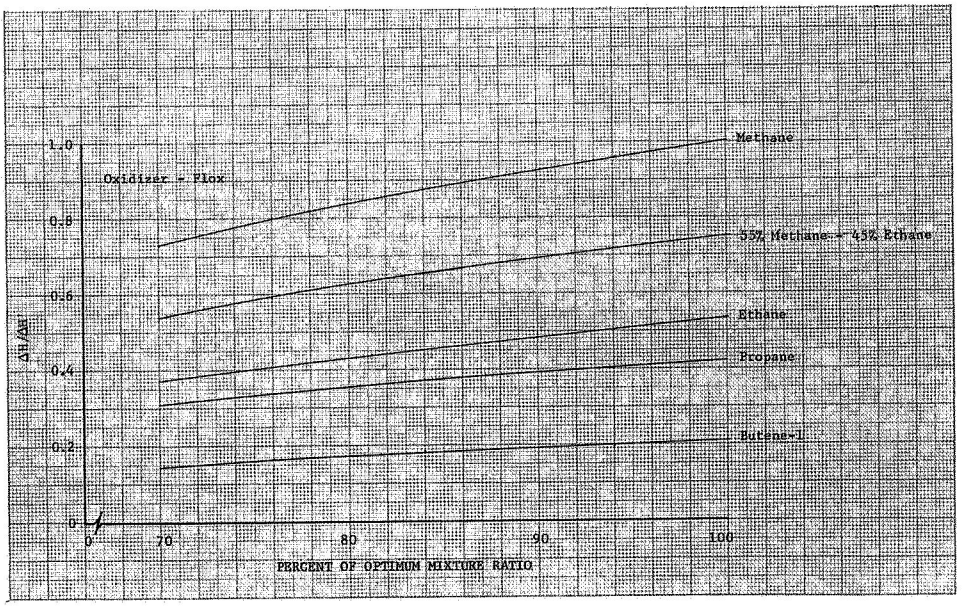


Figure D-8. Variation of Fuel Type Correction Factor With Propellant Mixture Ratio for Fuel Enthalpy Rise

DF 58066

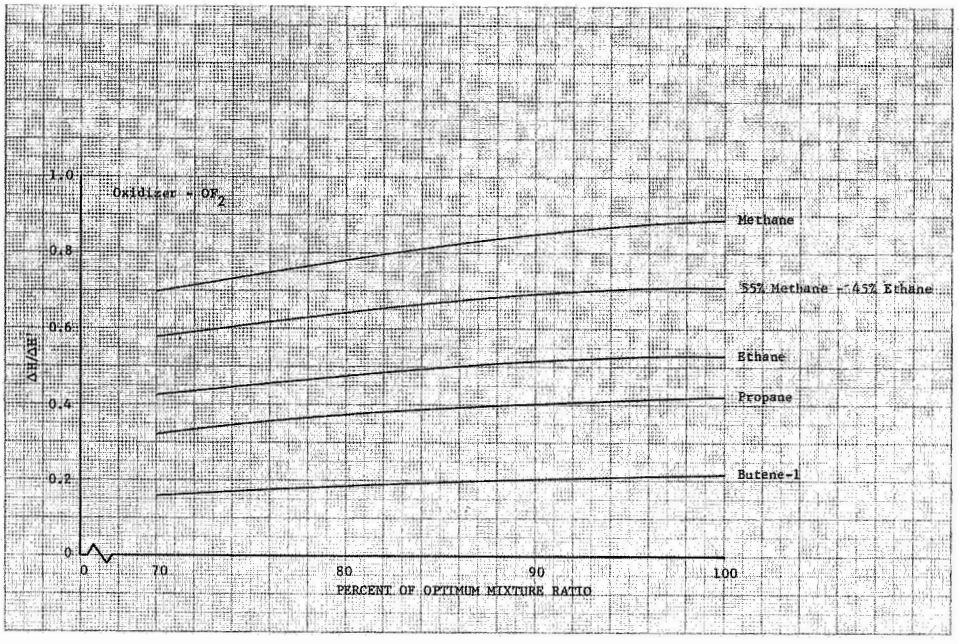


Figure D-9. Variation of Fuel Type Correction Factor With Propellant Mixture Ratio for Fuel Enthalpy Rise DF 58067

4. METHOD ACCURACY

To demonstrate the accuracy of the method used in the feasibility study, the cases shown in table D-4 were evaluated using the basic curves and then compared to values obtained by the IBM 360 computer program referred to in Paragraph 2 of this Appendix. Note that the differences obtained by the two methods and hence the errors introduced by using the parametric curves are quite small.

Table D-4. Cases Evaluated Using Basic Curves and Compared to IBM 360 Computer Values

Fuel	Oxidizer	Mixture Ratio	Contraction Ratio	Expansion Ratio	Wall Temperature, °F	Thrust, lb	Chamber Pressure, psia	Fuel Enthalpy Based on Parametric Curves Btu/lb_m	Computed Fuel Enthalpy Btu/lb_m	Error, %
Methane	Flox	4.0	2.0	100	1700	5000	850	581	592	1.33
Propane	OF_2	3.79	2.0	100	1700	4157	100	222.9	221	0.86
Butene-1	OF_2	2.7	4.0	40	3200	1000	1000	114.27	113.26	1.29

5. ANALYSIS

To facilitate obtaining numerical results, the six basic curves shown in figures D-4 through D-9 were stored in an IBM 1130 computer program. Upon the specification of the eight variables, the program was able to compute the coolant (fuel) enthalpy rise. Also, by specifying the desired coolant enthalpy rise and seven of the eight variables, the program has the capability to solve for the remaining variable.

6. APPENDIX D REFERENCES

1. Bartz, D.R., "A Simple Equation for Rapid Estimation of Rocket Nozzle Convective Heat Transfer Coefficients," Jet Propulsion, 27, (49), 1957.

2. Sibulkin, M., "Heat Transfer to an Incompressible Turbulent Boundary Layer and Estimation of Heat Transfer Coefficients at Supersonic Nozzle Throats," Journal of Aeronautical Sciences, pp. 162-176, February 1956.

3. Elliott, D.G., D.R. Bartz, S. Silver, "Calculation of Turbulent Boundary Layer Growth and Heat Transfer in Axi-symmetric Nozzles," Jet Propulsion Laboratory, February 1963.

4. Mayer, E., "Analysis of Convective Heat Transfer in Rocket Nozzles," ARS Journal, pp. 911-916, July 1961.

5. "Final Report, Investigation of Light Hydrocarbon Fuels with Fluorine-Oxygen Mixtures as Liquid Rocket Propellants," Contract NAS3-6296, NASA CR-72147 (PWA FR-2227), 15 September 1967.

APPENDIX E
DETAILED HEAT TRANSFER STUDY - METHOD OF ANALYSIS

1. GENERAL

Two computer programs were used for the determination of regenerative cooling chamber pressure limits in the detailed heat transfer study. The first program, for an IBM 1130 computer, performed a preliminary design analysis to establish thrust chamber geometry and to provide a first approximation of coolant passage sizes for counter and parallel coolant flows. The preliminary passage sizing information was used to select the preferred coolant flow direction. The second program, for an IBM 360 computer, performed a detailed Thermal Skin heat transfer analysis. This program provided a stepwise solution for determination of the fluid state and wall temperature at points along the coolant passage.

The two computer programs, used in series, permitted the determination of regenerative cooling limits. Upper chamber pressure limits (with the fuels at supercritical pressures in the passages) were generally set by coolant pressure drop limitations; lower chamber pressure limits (at subcritical pressures) were determined by analysis for bulk or film boiling.

This Appendix contains a description of the computer programs and the boiling analysis used in the detailed heat transfer study.

2. PRELIMINARY DESIGN ANALYSIS (1130 COMPUTER PROGRAM)

The 1130 computer program performed the following operations:

1. Combustion chamber sizing
2. Coolant passage sizing at the throat and injector locations
3. Stress analysis.

The equations used in these operations are discussed in the following subparagraphs.

a. Combustion Chamber Sizing

The combustion chamber was sized for a specified set of conditions defined by values for (1) thrust, (2) chamber pressure, (3) expansion ratio, (4) contraction ratio, (5) mixture ratio, and (6) an oxidizer/fuel propellant combination. The propellant flow rate and fuel coolant

flow rate were determined from the familiar equations,

$$\dot{w}_p = F/(I'_{vac}\ \eta_c{}^*C_s) \tag{E-1}$$

$$\dot{w}_f = \dot{w}_p/(1 + r) \tag{E-2}$$

where I'_{vac} is the theoretical specific impulse for shifting equilibrium and the c* efficiency and nozzle efficiency values were assumed to be 96% and 97.5% respectively (kinetic losses were not considered). The required throat area, throat radius, and chamber length were determined using the relations,

$$A^* = (c^{*\prime}\eta_c{}^*\dot{w}_p)/P_c g_c \tag{E-3}$$

$$R^* = \sqrt{A^*/\pi} \tag{E-4}$$

$$R_c = \sqrt{\epsilon_c}\ (R^*) \tag{E-5}$$

$$V = L^*A^* \tag{E-6}$$

$$L = V/\bar{A} \tag{E-7}$$

where

$$\bar{A} = \int_0^L \pi R^2 dL$$

b. Coolant Passage Sizing

Coolant passages were sized by determining the coolant-side film coefficient required to maintain the desired hot-side wall temperature, and then computing the dimensions necessary to produce the coefficient. The heat input at any given station was determined as

$$q = (Q_m/Q_p)h_g(T_{aw} - T_w) \tag{E-8}$$

where

$$Taw = \frac{T_o\ \left(\eta_c^*\right)^2\left(1 + \frac{\gamma - 1}{2}\mathscr{R}M^2\right)}{\left(1 + \frac{\gamma - 1}{2}M^2\right)} \tag{E-9}$$

$$\mathscr{R} = \left[Pr_f\right]^{1/3} \tag{E-10}$$

The combustion-side heat transfer coefficient, h_g, was computed using the Bartz short form equation (see Appendix D). Average values for heat reduction due to carbon deposition, Q_m/Q_p, were employed (see Appendix B).

The coolant-side coefficient is defined as:

$$h_c = q/(T_{wc} - T_b) \tag{E-11}$$

where

$$T_{wc} = T_w - \frac{q\delta}{K_w} \tag{E-12}$$

The wall thickness δ, and other pertinent cooling passage dimensions are defined in figure E-1. Wall temperature (T_w) was specified, as was the corresponding material, which in turn defined the wall thermal conductivity, K_w.

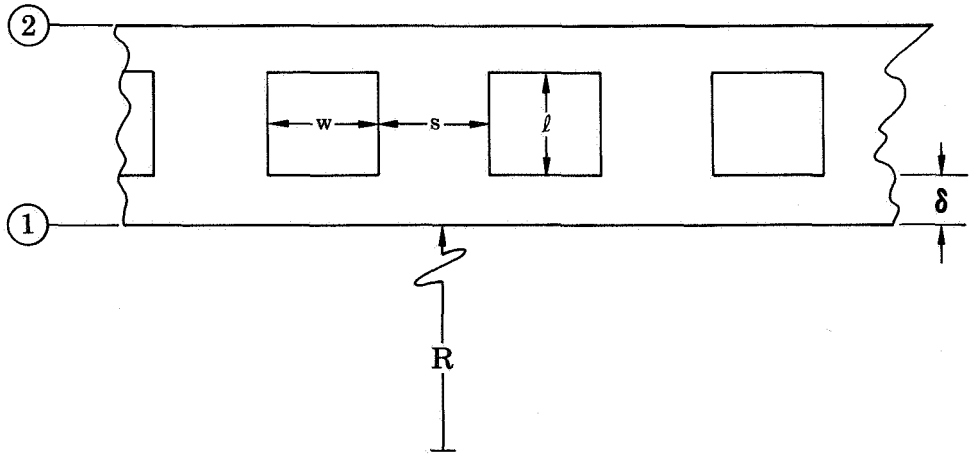


Figure E-1. Cross Section of Thermal Skin$_{TM}$ Wall Showing Symbols Used FD 23455

The purpose of the IBM 1130 computer calculation was to permit selection of the coolant flow direction for which passage dimensions were largest. For this purpose, it was necessary only to evaluate locations where minimum dimensions would be expected. These locations were at the throat and at the injector station. The throat is the region of highest theoretical heat fluxes; the injector station is of

concern primarily because of the parallel coolant flow case. While heat fluxes near the injector are not as high as at the throat, they are significant and with parallel flow the coolant is at its maximum density at that station, and hence small passages are required to achieve high coefficients. Parametric curves generated in the feasibility study (see Appendix D), which considered combustion chamber and nozzle heat transfer separately, were used to estimate coolant bulk temperature (T_b) at the throat and injector stations for use in the calculations.

The Dittus-Boelter equation for heating of a fluid with fully developed turbulent flow

$$h_c = \frac{0.023K_f}{D_h} (Re_b)^{0.8}\left(\frac{\rho_f}{\rho_b}\right)^{0.8} (Pr_f)^{0.4} \qquad \text{(E-13)}$$

was used to establish coolant passage dimensions required to achieve the required coefficient.

By expressing coolant passage dimensions by identities based on ratios that were held constant for the study*

$$\ell = w/(w/\ell) = w/1.33 \qquad \text{(E-14)}$$

$$s = w/(w/s) = w/1.0 \qquad \text{(E-15)}$$

and noting that, therefore, the number of slots for a given chamber radius and wall thickness is a unique function of the slot width

$$N_s = \frac{2\pi(R+\delta)}{w} \frac{(w/s)}{w/s+1} = \frac{\pi(R+\delta)}{w} \qquad \text{(E-16)}$$

the Reynolds number in equation (E-13) can be expressed in terms of total flow and total coolant flow area, and then the terms can be rearranged to permit solution for slot width directly as

$$w = \frac{(1.01)K_f(w/\ell+1)}{h_c} (Pr_f)^{0.4} \left[\frac{\dot{w}_f(\rho_f/\rho_b)}{\pi\mu_f(R+\delta)} \frac{(w/\ell)}{(w/\ell+1)} \frac{(w/s+1)}{w/s}\right]^{0.8} \qquad \text{(E-17)}$$

*w/ℓ was held constant at 1.33 based on current state-of-the-art engraving practice, and w/s was assumed to be 1.0, which was a value shown to produce maximum fin efficiencies in previous studies.

When the minimum passage width for a given case was established at one of the two locations analyzed, the depth (which was assumed constant along the coolant passage for ease of engraving) was fixed. The width at the other station was then determined, using equation (E-17), assuming the same number of passages. Subsequent stress analysis showed that branching was not necessary in the combustion chamber regions; the coolant passage widths at the injector station were not sufficient to necessitate splitting of the passages even at the highest thrust level (20,000 lb). In the studies made, the minimum required dimensions always occurred at the throat station.

c. Wall Stress Calculation

Independently of the heat transfer calculations, Thermal Skin chamber wall thicknesses (δ) at the throat and chamber stations were determined based on stress calculations. The stresses of concern were the bending and shear stresses in the inner, or chamber wall, the braze tensile strength, and the thermal stresses. In all calculations, coolant passages were assumed to have square corners. Since past experience has shown that rounded corners are obtained in etched coolant passages, this assumption yields conservative results.

The allowable wall thickness based upon bending stress was determined from a fixed-end uniform load beam analysis with bending about the fixed ends:

$$\delta_b = \sqrt{Pw^2/2\,\sigma y} \qquad \text{(E-18)}$$

The allowable wall thickness based upon the inner wall yielding in shear is

$$\delta_s = Pw/2\sigma y \qquad \text{(E-19)}$$

The allowable passage space required to prevent tensile failure of the braze joint is determined as follows:

$$S_T = Pw/\sigma_T \qquad \text{(E-20)}$$

The allowable wall thickness based on thermal stress consideration was based on the difference in expansion at the outer radius (location 2 on figure E-1) as compared to that at the inner radius (location 1 on figure E-1).

$$\delta_{TH} = \frac{(\alpha R\Delta T)_1 - (\alpha R\Delta T)_2}{\left[\left(\frac{R_1}{\delta_1 E_1}\right) + \left(\frac{R_2}{\delta_2 E_2}\right)\right] \sigma y} \qquad \text{(E-21)}$$

The thermal stress is caused by the differences in expansion at the outer and inner radii. The temperature differences ΔT_1 and ΔT_2 are the differences in temperatures between ambient and the respective wall temperatures and E_1 and E_2 are the corresponding moduli of elasticity at these locations. In these equations, the coolant pressure (P) for counterflow was based on an assumed pressure loss of half the allowable at the throat station and of the total allowable at the injector station. For parallel flow, the pressure at the injector was assumed to be the inlet pressure and half the allowable pressure loss was assumed at the throat station. The 0.2% yield strength was evaluated at the mean of the outside wall temperature (T_w) and the coolant side wall temperature (T_{wc}). The allowable braze stress was based upon the tensile strength of the braze evaluated at the coolant bulk temperature.

If the wall thicknesses determined from the stress calculations of equations E-18 through E-21 were greater than those assumed for the heat transfer calculations, a greater wall thickness was assumed and the heat transfer calculations were repeated until the wall thickness required for strength was less than that used in the heat transfer calculations for passage width.

3. THERMAL SKIN HEAT TRANSFER ANALYSIS (IBM 360 PROGRAM)

a. General

A detailed Thermal Skin heat transfer analysis was performed using an IBM 360 computer program. The analysis consisted of a stepwise solution of the continuity, energy, momentum, and state equations for determination of the coolant conditions and wall temperature at stations along the coolant passages. The IBM 360 computer was used in conjunction with the IBM 1130 computer. For a specified set of conditions (i.e., for values of thrust, chamber pressure, expansion ratio, contraction ratio, mixture ratio, and an oxidizer/fuel propellant combination) computed values (from the IBM 1130 program) of the following parameters were input to the

IBM 360 program: (1) throat diameter, (2) fuel flow rate, (3) the wall thickness, which is held constant throughout the chamber, and (4) number of coolant slots at throat location. By specifying the number of coolant slots at the throat and the wall thickness, the coolant passage geometry was completely defined because: (1) the slot spacing dimension (s) was equal to the slot width at all stations throughout the thrust chamber for best fin efficiency (see subparagraph b) and (2) the coolant passage depth was also maintained constant; the depth was equal to 1.33 times the throat-station passage width.

The number of slots was held constant in the combustion chamber because stress analysis using the IBM 1130 program indicated that the injector-station passage widths were not large enough at any thrust level and chamber pressures up to 1000 psia to require branching. However, coolant passage branching was employed in the nozzle portion of the chamber; a conservative approach was taken by splitting the passages at stations where the width equaled the injector-station coolant passage width.

For a given set of conditions, iterations were made on the number of coolant slots using the IBM 360 computer program until the combustion-side wall temperature at the throat location was equal to the maximum allowable value for the particular material being considered. Once the number of coolant slots had been determined, the coolant pressure drop, maximum film temperatures, etc. were compared to allowable values to establish regenerative cooling limits. A final stress analysis for the passage geometry was made after limits had been established.

The following paragraphs contain the assumptions and important equations used in the IBM 360 heat transfer computer program.

b. Assumptions

The following general assumptions were made in the analysis.

1. The coolant flow is both steady and one-dimensional.
2. Conduction heat transfer within the coolant is negligible.
3. Heating of the coolant due to viscous dissipation is negligible.
4. Radiation is negligible with respect to forced convection heat transfer in the coolant passages.
5. Entrance effects on coolant heat transfer coefficients are negligible.

6. The combustion-side heat transfer coefficient (h_g) and adiabatic wall temperature (T_{aw}) are independent of the cooling process and can be evaluated independently. The Bartz short-form equation was used for calculating h_g, and T_{aw} was calculated using one-dimensional isentropic equations as in the feasibility study.
7. Two-dimensional heat transfer effects within the Thermal Skin wall are adequately represented by a fin analysis.

Assumptions 1 through 6 are self-explanatory but some comment is required to clarify assumption 7. Conduction between passages contributes significantly to heat transfer in Thermal Skin thrust chambers. To evaluate this effect, two-dimensional conduction calculations are generally used; however, these are unwieldy and time-consuming. To determine whether a more adaptable calculation could be used, combustion- and coolant-side wall temperatures as predicted by (1) two-dimensional and (2) one-dimensional plus fin effect analyses were compared. For the comparison, the throat wall temperatures for a flox/methane, 5000-lb thrust, 350-psia chamber pressure engine with nickel walls were evaluated. The two-dimensional results indicated combustion- and coolant-side wall temperatures of 1721 and 1459°R, whereas the one-dimensional plus fin effects gave 1776 and 1500°R, respectively. The agreement between the methods is considered to be adequate and typical, and thus forms the basis for assumption 7.

c. Equations

Figure E-2 shows an elemental section of a coolant flow passage in the direction of flow. The calculation of the coolant-side heat transfer coefficient is based upon knowledge of the wall temperature, thus requiring an iterative solution of the heat transfer through the chamber wall.

The iterative technique employed may be summarized in words as follows. Assuming that all quantities and their gradients are known at station j-1, the bulk temperature, static pressure, and heat flux are estimated at station j. The gas-side and coolant-side wall temperatures are then calculated. The coolant-side heat transfer coefficient can now be evaluated and the fluid bulk temperature at station j is estimated by making calculations across the wall. Comparison is made of the bulk temperatures calculated from the enthalpy rise of the coolant stream from j-1 to j and the value calculated across the wall at j (see following sketch).

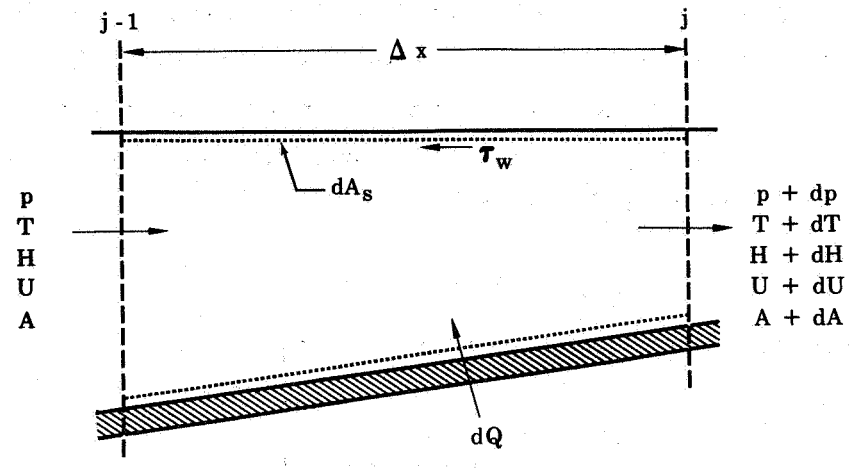
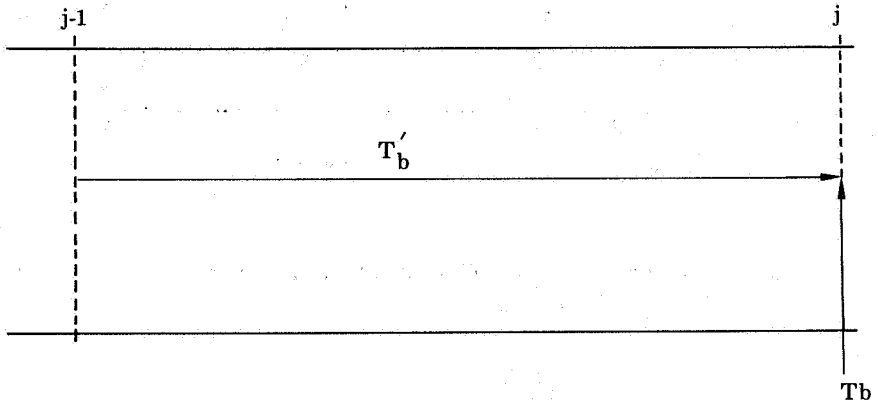


Figure E-2. Elemental Section of Coolant Flow Passage FD 23456



FD 23457

If $(T_b' - T_b)$ is not within a specified tolerance, the iterative calculations are repeated until convergence is made. Iterations for pressure drop are also made.

The combustion-side wall temperature is calculated by equation (E-22).

$$T_w = T_{aw} - \frac{q}{(Q_m/Q_p)\ h_g} \qquad \text{(E-22)}$$

The combustion gas heat transfer coefficient (h_g) and the adiabatic wall temperature (T_{aw}) are known quantities and are independently calculated as discussed in Appendix D. One-dimensional calculations are made to determine the coolant side wall temperature as given by equation (E-23).

$$T_{wc} = T_w - \frac{q\,\delta}{k_w} \qquad \text{(E-23)}$$

The thermal conductivity is evaluated at the average wall temperature. Bulk temperature calculations at station j are made by considering heat transfer from the periphery of the slot. Two-dimensional effects are approximated by assuming that the web material acts as a stub fin with a base temperature of T_{wc}. Figure E-3 shows the equivalent fin geometry in terms of the symbols of figure E-1.

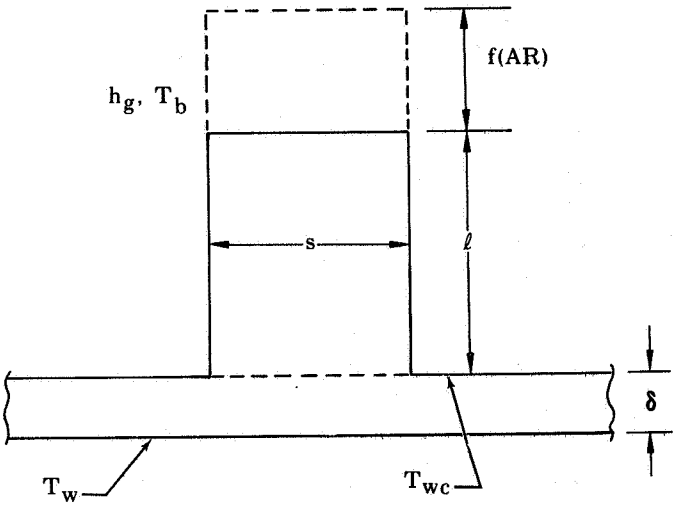


Figure E-3. Equivalent Fin Geometry for Thermal $Skin_{TM}$ Passage FD 23458

$$T_b = T_{wc} - \frac{q}{\eta_{fin}\, h_c}\left(\frac{PB}{PS}\right) \qquad \text{(E-24)}$$

where,

$$\eta_{fin} = \left[\tanh\,(m)\right]\left(\frac{1}{m}\right)$$

$$m = \left[\ell + w(AR)\right]\sqrt{2h_c/k_w S}$$

$$PS = \left[2\ell + (1 + AR)w\right]N_s$$

$$PB = 2\pi(R + \delta)$$

The term AR is used to control the amount of periphery that transfers heat. Based upon two-dimensional studies, best results were obtained for AR = 0, which corresponds to heat transfer from all coolant passage walls except the back wall.

The coolant heat transfer coefficient that was used in the analysis is based upon work reported in Reference 1*, which was developed to account for surface roughness effects on heat transfer.

$$h_c = St\left(\frac{T_b}{T_{wc}}\right)^{0.55} C_{pb}\left(\frac{\dot{w}_f}{N_s A}\right) \qquad \text{(E-25)}$$

where

$$St = \frac{f/2}{0.92 + \sqrt{f/2}\left[5.5(\epsilon^*)^{0.2}(P_{rb})^{0.44} - A(\epsilon^*)\right]} \qquad \text{(E-26)}$$

$$\epsilon^* = R_{e_b}\sqrt{f/2}(\epsilon/D_h) \qquad \text{(E-27)}$$

$$A(\epsilon^*) = \sqrt{2/f} + 2.5\ \ln(2\epsilon/D_h) + 3.75 \qquad \text{(E-28)}$$

The term ϵ in equations E-27 and E-28 is the passage surface roughness (100 μ - inches was used in the detailed heat transfer study). The isothermal friction factor was obtained by performing iterative calculations for the function shown in figure E-4. The dimensionless terms ϵ^* and $A(\epsilon^*)$ are used to correlate the friction factor data normally presented on a Moody Diagram.

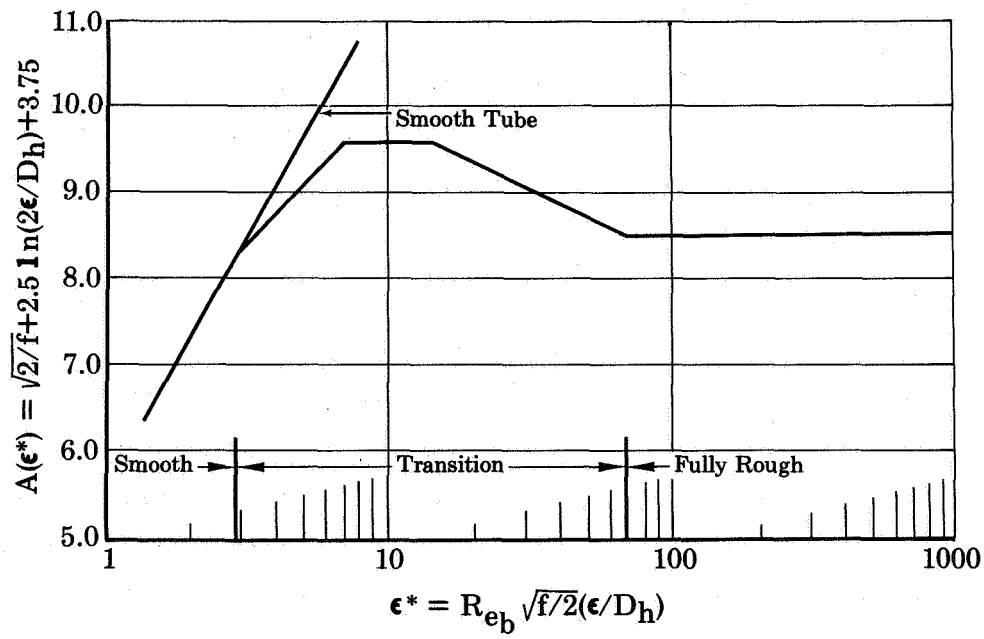


Figure E-4. Friction Similarity Function for Close-Packed Sand Grain Roughness FD 23459

*References for this Appendix are given in Paragraph 5.

The coolant temperature, pressure and state was determined by simultaneously integrating the continuity, energy, momentum, and thermodynamic state equations. The equation of state is given in terms of the BWR equation as described in Appendix F. Since the flow is steady, the use of a constant mass flow rate in the calculations satisfies the continuity equation. With the aid of figure E-2, the energy and momentum equations can be written as follows.

$$H_j = H_{j-1} + \frac{dQ}{\dot{w}_f} + \left(\frac{dp}{dx}\right)\frac{\Delta x}{\bar{\rho} J} \qquad \text{(E-29)}$$

$$\frac{dp}{dx} = \frac{4\bar{f}_h}{\bar{D}_h}\,(\overline{VH}) - \frac{\dot{w}_f(U_j - U_{j-1})}{g_c \bar{A}\,\Delta x} \qquad \text{(E-30)}$$

where

$$\overline{VH} = \left(\frac{\dot{w}_f}{\bar{A}}\right)^2 \frac{1}{2g_c\bar{\rho}}$$

The bars over the symbols in equations E-29 and E-30 refer to average values over the increment of length Δx. The pressure is determined by equation E-31.

$$p_j = p_{j-1} + \left(\frac{dp}{dx}\right)\Delta x \qquad \text{(E-31)}$$

The friction factor (f_h) represents the isothermal friction factor corrected for heat transfer as given by equation E-32 and based on work reported in Reference 2.

$$f_h = f\left(\frac{\mu_w}{\mu_b}\right)^{10 f\sqrt{\rho_w/\rho_b}} \qquad \text{(E-32)}$$

Sudden expansions and contractions in flow area are treated by incompressible flow equations and are lumped at the upstream station (j-1). Once the pressure and enthalpy are known at a station j, the bulk temperature is determined from enthalpy-pressure-temperature data. The thermodynamic and transport properties are an integral part of the analysis and are discussed separately in Appendix F.

4. BOILING ANALYSIS

At the upper chamber pressure limits for regenerative cooling, the fuels were at supercritical pressure in the coolant passages. It was found that the maximum allowable coolant pressure drop established limits in almost all cases, and these were determined using a relatively straightforward graphic solution as described in Section V.

At the lower chamber pressure limits, the fuels are at subcritical pressures and thus three different heat transfer processes are possible in rocket thrust chambers: forced convection, forced convection nucleate boiling, or forced convection film boiling. If the first process occurs, the wall in contact with the coolant will be at a temperature less than the local saturation temperature. As the wall temperature is increased to approximately the saturation temperature, boiling will occur. Existence of the boiling mode can be determined by comparing the heat flux to the upper-limit heat flux for nucleate boiling. For heat fluxes greater than this upper-limit value, film boiling will occur. Film boiling will also occur, regardless of the heat flux level, when the bulk temperature reaches the saturation level and there is bulk boiling, or net vapor generation, that causes the amount of available liquid to be insufficient to wet the wall. The transition to film boiling is accompanied by a large increase in wall temperature and therefore the conditions that produce it set the low chamber pressure cooling limits.

For bulk boiling the saturation state defines the maximum allowable coolant condition and therefore the approach taken was the same as that followed in the feasibility study. Lower pressure limits were at the lowest chamber pressures that would allow the fuel to remain at a supercritical pressure in the jacket until the critical temperature was exceeded. The limits were therefore largely dependent upon the liquid phase heat capacities of the individual fuels.

In the study, when it was found that critical temperatures were exceeded, it was assumed that the lower chamber pressure cooling limit occurred when the jacket outlet pressure was just equal to the critical pressure. This point was established by comparing the predicted coolant pressure drop with the limiting pressure drop for which supercritical

pressures were maintained in the jacket. Solutions were obtained graphically, as illustrated in figure E-5. The predicted jacket pressure drops in the illustration are the levels required to maintain the assumed wall temperature limit. The boiling limit line represents the condition at which jacket discharge pressure equals critical pressure. Jacket inlet pressures were assumed for the various fuels based on the type of engine cycle for which they were appropriate, gas generator or expander.

Note that curves such as those of figure E-5 were also used to establish the upper cooling limit. The upper limit corresponds to the chamber pressure at which the predicted-coolant-pressure-drop curve intersects the line reflecting the allowable cooling jacket pressure drop limit.

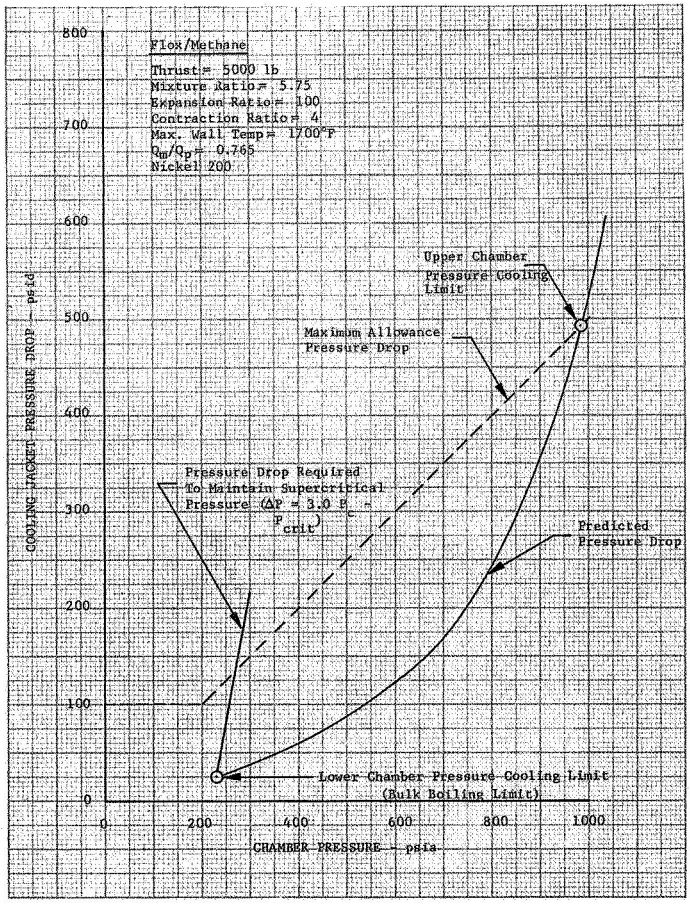


Figure E-5. Graphical Determination of Chamber Pressure Corresponding to Critical Jacket Outlet Pressure DF 60252

Fuels with large liquid phase heat capacities can be used as coolants at subcritical pressures without the occurrence of bulk boiling. However, if local heat fluxes in the chamber are sufficiently high, subcooled film boiling could occur. To check for this possibility, the upper-limit heat fluxes were determined from Reference 3 using the following equation:

$$q_{max} = \left[a + b\,(T_{sat} - T_b)U^c\right]\left[d + eP\right] \qquad \text{(E-33)}$$

where

T_{sat} = fuel saturation temperature
T_b = fuel bulk temperature
U = bulk velocity
P = fuel pressure

In equation E-33, a, b, c, d, and e are experimentally determined constants for each fuel. For butene-1 and propane, which have large liquid phase heat capacities, these values are as follows:

Fuel	a	b	c	d	e
Propane	0.3227	9.43×10^{-4}	0.5	1.0376	-2.51×10^{-4}
Butene-1	0.2736	7.43×10^{-4}	0.6	1.0619	-4.11×10^{-4}

The following values were assumed for the terms T_{sat}, T_b, U, and P.

	T_{sat}	T_b, °R	U, ft/sec	P
Propane	f(P)	400	70	1.65 P_c
Butene-1	f(P)	350	45	1.65 P_c

The coolant velocities (U) were selected as being nominal values used for the respective fuels at low chamber pressures. The throat bulk temperatures (T_b) were computed at a chamber pressure of 250 psia; a constant value was used because the coolant enthalpy rise in the nozzle of the thrust chamber is not a strong function of chamber pressure. The coolant pressure was assumed to be 1.65 times chamber pressure. This is considered to be the maximum probable since with both of these propellant combinations (OF_2/Butene-1 and OF_2/propane) either a gas generator or a pressure-fed engine cycle would be used. For these two cycles, the maximum inlet

coolant-to-chamber pressure ratio would be approximately 1.65. Furthermore, since the coolant jacket pressure drop will be low in the nozzle, it was neglected and the throat coolant pressure was assumed to be 1.65 times chamber pressure.

5. APPENDIX E REFERENCES

1. Dipprey, Duane F. and Rolf H. Sabersky, "Heat and Momentum Transfer in Smooth and Rough Tubes at Various Prandtl Numbers," CIT, JPL Report No. 32-269, 6 June 1962.

2. Maurer, G. W. and B. W. Le Tourneau, "Friction Factors for Fully Developed Turbulent Flow in Ducts With and Without Heat Transfer," ASME Paper No. 63-WA-98.

3. Glickstein, M.R., and R.H. Whitesides, (Pratt & Whitney Aircraft), "Forced Convection Nucleate and Film Boiling of Several Aliphatic Hydrocarbons," ASME Paper No. 67-HT-7.

APPENDIX F
FUEL THERMODYNAMIC AND TRANSPORT PROPERTIES

1. GENERAL

This Appendix presents the correlations and methods used in the preparation of the computer programs to calculate thermodynamic and transport properties of the hydrocarbon fuels considered in the study. Figures F-1 through F-16 at the end of this appendix present the variation of vapor pressure, density, viscosity, and thermal conductivity as functions of temperature and pressure for methane, 55% methane - 45% ethane, propane, and butene-1. Enthalpy - temperature diagrams for these fuels and for ethane are presented in Section IV.

Because of the importance of specific heat in heat transfer calculations, equations are given for each fuel; however, this property is not presented in curve form.

The properties have been evaluated for both liquid and gas regions for the pressure and temperature ranges given in table F-1. The minimum temperatures in table F-1 correspond to 10°R above the freezing points of the fuels.

The Benedict-Webb-Rubin (BWR) equation of state (References 1, 2, and 3)* is used to predict density, enthalpy, and specific heat of the hydrocarbon fuels in the gas and liquid regions except where otherwise noted. The BWR equation gives pressure as a function of temperature and density:**

$$P = RT\rho + (B_oRT - A_o - C_o/T^2)\rho^2 + (bRT - a)\rho^3 + a\alpha\rho^6 + \frac{c\rho^3}{T^2}\left[(1 + \gamma\rho^2)e^{-\gamma\rho^2}\right] \quad \text{(F-1)}$$

The BWR constants (A_o, B_o, C_o, a, b, c, α, and γ) for methane, ethane, propane, and butene-1 are given in table F-2. For a given temperature and pressure, the corresponding density is solved by the Newton-Raphson iteration procedure. Since six solutions are possible for the BWR equation, the correct solution is obtained by providing a suitable first guess dependent upon the particular phase (gas or liquid) being considered. For a gas phase, the perfect gas law provides a first estimate, whereas for a liquid phase the hydrocarbon liquid density at the normal boiling point provides a good first estimate. A vapor pressure curve fitted by a polynomial equation is used to determine the phase for a given pressure and temperature.

---

* References for this Appendix are given in paragraph 7.
** Symbols are defined separately for this Appendix in paragraph 6.

Table F-1. Fuel Property Pressure and Temperature Range

Fuel	Temperature, °R min	Temperature, °R max	Pressure, psia min	Pressure, psia max
Methane	173	2100	14.7	3000
55% Methane - 45% Ethane	143	2100	14.7	3000
Propane	164.3	2100	14.7	3000
Butene-1	168.4	2100	14.7	3000

Table F-2. Benedict-Webb-Rubin-Constants for Hydrocarbons (Metric Units)

Hydrocarbon	Methane	Ethane	Propane	Butene-1
Molecular Wt	16.031	30.047	44.062	56.11
B_o	0.0426000	0.0627724	0.0973130	0.116025
A_o	1.85500	4.15556	6.87225	9.060
$C_o \times 10^{-6}$	0.0225700	0.179592	0.508256	0.927280
b	0.00338004	0.0111220	0.0225000	0.0348156
a	0.0494000	0.345160	0.947700	1.682
$c \times 10^{-6}$	0.00254500	0.0327670	0.129000	0.274920
$\alpha \times 10^{-3}$	0.124359	0.243389	0.607175	0.910889
$\gamma \times 10^{-2}$	0.600000	1.18000	2.2000	0.0295945
P	← Pressure, atm →			
R	← Gas constant, 0.08207 liter atm/gm-mole °K →			
T	← Temperature, °K →			
ρ	← Density, gm-mole/liter →			
Reference	2	2	2	4

Transport properties (viscosity and thermal conductivity) for both gas and liquid phases are determined from residual correlations. Since there are differences in the methods for calculating thermodynamic and transport properties of the hydrocarbon fuels, each fuel will be discussed separately.

Most of the published data available on the hydrocarbons of interest are expressed in cgs units. To avoid conversion of the data into English units, computer calculations are made using cgs units. Conversion factors are then used to obtain final answers in English units. Equations included in the following paragraphs are expressed in cgs units and the Kelvin temperature scale except for the enthalpy-temperature equations (Btu/lb_m and °R) and where otherwise noted. The methods used to calculate the properties of the fuels are discussed in the following paragraphs.

2. METHANE

a. Density

Below the normal boiling point the density of liquid methane is represented by equation F-2.

$$\rho = 36.3 - 0.0872\ T \qquad \text{(F-2)}$$

Due to the incompressibility of the liquid in this region the atmospheric densities are considered applicable to all pressures. Densities above the normal boiling point are calculated by using BWR equation of state (equation F-1) for both liquid and gas.

b. Enthalpy

The saturated liquid enthalpy for methane from 173 to 300°R was determined from a polynomial curve fit (equation F-3) of the data given in References 5 and 6.

$$H_s = 60.80066 + 69.0458T_n + 3.191946T_n^2 - 4.895118T_n^3 + 5.780765T_n^4 + 4.577758T_n^5 \qquad \text{(F-3)}$$

where

$$T_n = 0.01369863T - 3.383562 \text{ and T is in °R}$$

Compressed liquid and gas enthalpies were calculated from equation F-4 as functions of pressure and temperature. Equation F-4 is derived from the BWR equation in Reference 2.

$$H = H^{o} + \left[(B_o RT - 2A_o - 4C_o/T^2)\rho + (2bRT - 3a)\rho^2/2 + 6/5\ a\alpha\rho^5 + \frac{c\rho^2}{T^2}\left(\frac{3}{\gamma\rho^2}(1 - e^{-\gamma\rho^2}) - \frac{e^{-\gamma\rho^2}}{2} + \gamma\rho^2 e^{-\gamma\rho^2}\right)\right]\frac{43.5573}{M} \qquad \text{(F-4)}$$

The zero pressure enthalpy (H°) used in equation F-4 is also given in References 5 and 6 and fitted with a polynomial curve (equations F-5a and F-5b).

For $201°R < T \leq 1460°R$,

$$H^\circ = 586.2009 + 412.6456T_n + 98.2059T_n^2 + 14.84894T_n^3 - 17.16396T_n^4 \qquad \text{(F-5a)}$$

where

$$T_n = 0.001587301T - 1.31746$$

For $1460°R < T \leq 2100°F$

$$H^\circ = 1093 + 0.9276\ (T - 1460) \qquad \text{(F-5b)}$$

where

T is in °R

c. Specific Heat

Liquid methane specific heats from 173 to 300°R are obtained by the numerical differentiation of the polynomial curve representing the enthalpy-temperature relationship (equation F-3). The specific heats in the remaining regions (liquid above 300°R, vapor, and gas) are calculated from equation F-6, which was derived by taking the partial derivative of equation F-4 with respect to temperature at a constant pressure to obtain

$$C_p = C_p^{\,o} + \frac{\partial}{\partial T}\left[(B_o RT - 2A_o - 4C_o/T^2)\rho + (2bRT - 3a)\rho^2/2 + 6a\alpha\rho^5/5 + c\rho^2/T^2\left(\frac{3}{\gamma\rho^2}(1 - e^{-\gamma\rho^2}) - \frac{e^{-\gamma\rho^2}}{2} + \gamma\rho^2 e^{-\gamma\rho^2}\right)\right]_p \qquad \text{(F-6)}$$

The terms enclosed in brackets are evaluated at two temperatures bracketing the given temperature but at the same pressure. The temperature dependence of C_p° is given in Reference 7 for the hydrocarbons of interest.

For methane, Cp° is:

$$Cp^\circ = 4.75 + 1.2 \times 10^{-2}(T) + 0.303 \times 10^{-5}(T)^2 - 2.63 \times 10^{-9}(T)^3 \qquad \text{(F-6a)}$$

d. Viscosity

The viscosities for methane in both the gas and liquid states are correlated by plotting the logarithm of residual viscosity ($\mu - \mu^*$) versus ln density. Residual viscosity is the difference between the actual viscosity (μ) at any temperature and pressure and the viscosity at the same temperature and one atmosphere pressure (μ^*). Actual viscosity (μ) was obtained from published experimental data and (μ^*) is calculated using the Hirschfelder equation (References 8 and 9):

$$\mu^* = 266.93 \times 10^{-5} \frac{\sqrt{MT}}{\sigma^2 \Omega} \qquad \text{(F-7)}$$

The collision integral (Ω) is curve fitted as a function of the parameter, kT/ϵ. A detailed description of the collison integral Ω is contained in Reference 10. The following is the curve fit of ($\mu - \mu^*$) as a function of $\ln\rho$.

If $\rho \leq 1.3012$

$$\ln(\mu - \mu^*) \times 10^{-3} = 0.907 \ln\rho - 0.1103 \qquad \text{(F-8)}$$

If $21.9999 \geq \rho > 1.3012$

$$D = 0.70704403 \ln\rho - 1.1855030$$

$$\ln(\mu - \mu^*) \times 10^{-3} = 0.041137695 D^8 + 0.067203522 D^7 + 0.091308594 D^6 + 0.043525696 D^5 + 0.024414062 D^4 + 0.19119263 D^3 + 0.31362915 D^2 + 1.5425178 D + 1.4961678 \qquad \text{(F-9)}$$

If $28.4005 \geq \rho > 21.9999$

$$D = 7.83224885 \ln\rho - 25.210553$$

$$\ln (\mu - \mu^*) \times 10^3 = 0.10251741 D^3 + 0.25265281 D^2 + 0.69327272 D + 4.3542343 \quad \text{(F-10)}$$

If $\rho > 28.4005$

$$\ln (\mu - \mu^*) \times 10^{-3} = 5.40267730 \quad \text{(F-11)}$$

and

$$\mu = (\mu - \mu^*) + \mu^*$$

e. Thermal Conductivity

The thermal conductivity of methane is calculated by using a residual thermal conductivity correlation. The logarithm of residual thermal conductivity (K - K*) is plotted vs $\ln\rho$ and curve fitted with a polynomial that gives (K - K*) as a function of ρ.

If $\rho \leq 15.0001$

$$D = 0.73853875 \ln\rho - 1.0$$

$$\ln (K - K^*) \times 10^{-5} = -0.39219666 D^9 - 0.13617802 D^8 + 0.84539795 D^7 + 0.27536392 D^6 - 0.55462646 D^5 - 0.1265192 D^4 + 0.14646912 D^3 + 0.020587206 D^2 + 1.8664937 D + 0.61243562 \quad \text{(F-12)}$$

If $15.0001 < \rho \leq 23.0009$

$$D = 4.6789756 \ln\rho - 13.6709$$

$$\ln (K - K^*) \times 10^{-5} = 0.033517431 D^2 + 0.41812401 D + 2.9495558 \quad \text{(F-13)}$$

If $23.0009 < \rho$

$$D = 10.167236 \ln\rho - 32.879309$$

$$\ln (K - K^*) \times 10^{-5} = -0.0075839148 D^3 + 0.0043566285 D^2 + 0.25289536 D + 3.6421521 \quad \text{(F-14)}$$

For temperatures above the critical point, K* is given by equation F-15 from Reference 11.

$$\frac{K^*\lambda}{C_p^*} \times 10^6 = (14.52 T - 5.14)^{2/3} \quad \text{(F-15)}$$

Below the critical point K* is found by using the equation F-16

$$\frac{K^*\lambda}{C_p^*} = 0.455 \times 10^{-5} T_r \qquad \text{(F-16)}$$

and

$$K = (K - K^*) + K^* \qquad \text{(F-17)}$$

3. METHANE - ETHANE BLEND

a. Density

Saturated liquid densities from 143°R to the critical point for the 55% methane - 45% ethane blend are determined from a polynomial curve fit (equation F-18) of data from the Institute of Gas Technology. Below the bubble point at 1 atm, the fluid is considered to be incompressible. Liquid densities for 2000 and 3000 psia from the bubble point at 1 atm to the critical temperature are given by equations F-19 and F-20.

For saturated liquid

$$T_n = 0.0009661835\ T - 2.381642$$
$$\rho = \exp\ (3.406605 - 0.1599578\ T_n - 0.05128347\ T_n^2) \qquad \text{(F-18)}$$

For P = 2000 psia

$$T_n = 0.008888889\ T - 2.813333$$
$$\rho = \exp\ (3.289638 - 0.2392909\ T_n - 0.06437952\ T_n^2) \qquad \text{(F-19)}$$

For P = 3000 psia

$$T_n = 0.008888889\ T - 2.813333$$
$$\rho = \exp\ (3.304783 - 0.1898683\ T_n - 0.03577048\ T_n^2 - 0.01757840\ T_n^3) \qquad \text{(F-20)}$$

where

ρ is in lb_m/ft^3

and

T is in °R.

Intermediate densities are calculated by a linear interpolation with respect to pressure between equations F-18, F-19, and F-20. All other densities are calculated using the BWR equation (equation F-1). The constants for the BWR equation pertaining to mixtures are defined as functions of the individual consituents (methane and ethane).

$$Bo = \sum_i x_i B_{oi}$$

$$Ao = \left[\sum_i (x_i A_{oi}^{1/2}) \right]^2$$

$$Co = \left[\sum_i (x_i C_{oi}^{1/2}) \right]^2$$

$$b = \left[\sum_i (x_i b_i^{1/3}) \right]^3$$

$$a = \left[\sum_i (x_i a_i^{1/3}) \right]^3$$

$$c = \left[\sum_i (x_i c_i^{1/3}) \right]^3$$

$$\alpha = \left[\sum_i (x_i \alpha_i^{1/3}) \right]^3$$

$$\gamma = \left[\sum_i (x_i \gamma_i^{1/2}) \right]^2$$

b. Enthalpy

Since no experimental enthalpy data were available for the 55% methane - 45% ethane blend, a method was developed to estimate an enthalpy-temperature diagram. This method requires two basic assumptions, which are as follows:

1. The total enthalpy of the blend was the sum of the individual component enthalpies (no heat of mixing)
2. The introduction of the ethane into the methane had no effect upon the heat of vaporization of methane for a given ΔT from the critical temperature.

The only effect of the ethane introduction was to shift the methane critical temperature to the critical temperature of the blend. A similar effect was assumed for the ethane.

The first assumption allows the estimation of the superheated and low-pressure vapor regions of the diagram. Since the critical temperature and pressure were known from Reference 12, the second assumption makes it possible to calculate the enthalpy of the saturated liquid by superimposing the domes of each component so that the critical temperature of each component occurred at the blend critical temperature. Then, by using the properly weighted average of each component, the latent heat of vaporization was computed as a function of ΔT from the critical temperature. This calculation yields the enthalpy of the saturated liquid since both the enthalpy of the saturated vapor and the latent heat of vaporization are known as functions of temperature. The tie lines shown on the

methane-ethane blend enthalpy diagram (figure F-8) are also from Reference 12 by virtue of the bubble point and dew-point lines presented for the mixture. The resulting enthalpy diagram was represented by a bivariant table for computerized calculations.

c. Specific Heat

The procedure used to calculate specific heat for the methane-ethane blend consists of determining the enthalpy change (ΔH) for an incremental temperature change ($\Delta T = 1°R$) at constant pressure and using the relationship $Cp \approx (\Delta H/\Delta T)$. Enthalpies at any state are calculated using the procedure outlined in paragraph 3b.

d. Viscosity

Viscosities for the blend in both the liquid and gas regions can be determined from a plot of residual viscosity. The equation used to calculate the viscosity of the blend at one atmosphere is determined by using Wilke's equation (F-21) given in Reference 13.

$$\mu^* = \frac{\mu_m}{\left[1.0 + \frac{X_e}{X_m}\phi_{me}\right]} + \frac{\mu_e}{\left[1.0 + \frac{X_m}{X_e}\phi_{em}\right]} \qquad \text{(F-21)}$$

where

$$\phi_{me} = \frac{\left[1.0 + \left(\frac{\mu_m}{\mu_e}\right)^{1/2}\left(\frac{M_e}{M_m}\right)^{1/4}\right]^2}{\left[2\sqrt{2}\left(1.0 + \frac{M_m}{M_e}\right)^{1/2}\right]}$$

$$\phi_{em} = \frac{\left[1.0 + \left(\frac{\mu_e}{\mu_m}\right)^{1/2}\left(\frac{M_m}{M_e}\right)^{1/4}\right]^2}{\left[2\sqrt{2}\left(1.0 + \frac{M_e}{M_m}\right)^{1/2}\right]}$$

The subscripts m and e refer to methane and ethane. The equations for the curve fit of $(\mu - \mu^*)$ vs ρ are as follows:

If $\rho < 0.5$

$$D = 1.242670 \ln\rho + 1.861353$$

$$\mu - \mu^* = \exp(-16.35109 + 0.8283588\ D) \qquad \text{(F-22)}$$

If $0.5 \leq \rho < 14.0$

$$D = 0.6002035 \ln\rho - 0.5839707$$

$$\mu - \mu^* = \exp(-13.71449 + 1.864589\ D + 0.1261698\ D^2 + 0.1215274\ D^3 + 0.06594565\ D^4) \qquad \text{(F-23)}$$

If $\rho \geq 14.0$

$$D = 2.182713 \ln\rho - 6.760303$$

$$\mu - \mu^* = \exp(-10.52535 + 1.336846\ D + 0.4254688\ D^2 - 0.04043832\ D^3 + 0.5200037\ D^4 + 1.473565\ D^5 - 0.6350878\ D^6 - 2.141313\ D^7 + 0.3761332\ D^8 + 1.065608\ D^9) \qquad \text{(F-24)}$$

and

$$\mu = (\mu - \mu^*) + \mu^* \qquad \text{(F-25)}$$

where

ρ is in lb_m/ft^3

and

μ is in $lb_m/ft\text{-}sec$

e. Thermal Conductivity

Thermal conductivity of the methane-ethane blend is calculated from a residual correlation. Equation F-26 (Reference 13) is used to calculate the thermal conductivity of the blend at one atmosphere:

$$K^* = 0.5\ (K_{sm} + K_{rm}) \qquad \text{(F-26)}$$

where

$$K_{sm} = \sum_i X_i K_i$$

$$\frac{1}{K_{rm}} = \sum_i \frac{X_i}{K_i}$$

The equations for $(K - K^*)$ are:

If $\rho \leq 0.55$

$$D = 1.661167 \ln\rho + 1.993107$$

$$(K - K^*) = \exp(-8.516916 + 0.6907582\ D) \qquad \text{(F-27)}$$

If $0.55 < \rho \leq 13.06$

$$D = 0.6314347 \ln\rho - 0.6225051$$

$$(K - K^*) = \exp(-5.980042 + 1.911614\ D + 0.1098717\ D^2 + 0.04439277\ D^3) \quad \text{(F-28)}$$

If $\rho > 13.06$

$$D = 2.028821 \ln\rho - 6.213164$$

$$(K - K^*) = \exp(-3.11672 + 0.8741091\ D + 0.1057057\ D^2 + 0.1029658\ D^3 + 0.06155806\ D^4 - 0.01462934\ D^5) \quad \text{(F-29)}$$

and

$$K = (K - K^*) + K^* \quad \text{(F-30)}$$

where

K is in Btu/hr-ft-°R

and

ρ is in lb_m/ft^3

4. PROPANE

a. Density

Below the normal boiling point, the density of propane is calculated by the equation

$$\rho = (0.8261 - 0.001096\ T)\ 22.65 \quad \text{(F-31)}$$

At all temperatures above the normal boiling point, density is calculated using the method used for methane.

b. Enthalpy

The saturated liquid enthalpy of propane from 164.3 to 595°R was determined from a polynomial curve fit (equation F-32) of the data given in References 5 and 6.

$$H_s = 137.7276 + 139.5612\ T_n + 23.57331\ T_n^2 - 27.42277\ T_n^3 - 220.2665\ T_n^4 + 144.8025\ T_n^5 + 765.2504\ T_n^6 - 199.8298\ T_n^7 + 983.2995\ T_n^8 + 106.3663\ T_n^8 + 440.5010\ T_n^{10}. \quad \text{(F-32)}$$

where

$$T_n = 0.003990423\ T - 1.658419$$

and

T is in °R

Because of the incompressibility of propane in the liquid phase at the pressures of interest, equation F-32 is also used to calculate compressed liquid enthalpies. The enthalpies for the remaining state points are calculated as a function of pressure and temperature by using equation F-4. The zero pressure enthalpy (H°) used in equation F-4 is given by equations F-33 and F-34.

For $414°R < T \leq 1700°R$

$$H^\circ = 654.6950 + 457.1841 \times T_n + 112.8528 \times T_n^2 - 48.01331 \times T_n^3 + 36.88433 \times T_n^4 \ . \qquad \text{(F-33)}$$

where

$$T_n = 0.001557996\ T - 1.648593$$

and for

$1700°R < T \leq 2100°R$

$$H^\circ = 1134.0 + 0.5056\ (T - 1700) \qquad \text{(F-34)}$$

where

T is in °R

c. Specific Heat

Below the normal boiling point a constant liquid specific heat for propane of 23.5 cal/gm-mole-°K is used. Above the normal boiling point, specific heat is calculated using the method used for methane.

d. Viscosity

Viscosity of propane is determined in the same manner as methane. The equation used to calculate viscosity at 1 atm is as follows:

$$\mu^* = 266.93 \times 10^{-5} \frac{\sqrt{MT}}{\sigma^2 \Omega} \qquad \text{(F-35)}$$

Equations for the curve fit of $(\mu - \mu^*)$ vs ρ are as follows:

If $\rho \leq 0.5005$

$$\mu = \mu^*$$

If $-0.5005 < \rho \leq 21.9780$

$$D = 0.52851475 \ln\rho - 0.63313$$

$$\ln(\mu - \mu^*) \times 10^{-6} = 0.2245\,D^7 + 0.1647\,D^6 - 0.292385\,D^5 - 0.131162\,D^4 + 0.243959\,D^3 + 0.139996\,D^2 + 2.865838\,D + 7.11 \quad \text{(F-36)}$$

If $21.9780 < \rho \leq 32.9991$

$$D = 4.9326 \ln\rho - 16.24159$$

$$\ln(\mu - \mu^*) \times 10^{-6} = 0.041159\,D^4 + 0.05796\,D^3 + 0.074249\,D^2 + 0.6491676\,D + 10.917767 \quad \text{(F-37)}$$

If $\rho \geq 32.9991$

$$D = 6.03009 \ln\rho - 22.0423$$

$$\ln(\mu - \mu^*) \times 10^{-6} = 0.97673\,D^6 + 1.29143\,D^5 - 0.27377\,D^4 - 0.33330\,D^3 + 0.704704\,D^2 + 1.44707\,D + 12.63167 \quad \text{(F-38)}$$

and

$$\mu = (\mu - \mu^*) + \mu^* \quad \text{(F-39)}$$

e. Thermal Conductivity

Thermal conductivity of propane is calculated using the same type correlation that was used to calculate methane thermal conductivity. The equation used to determine K* is:

$$\frac{K^*\lambda}{C_p^*} \times 10^6 = (14.52\,T_r - 5.14)^{2/3} \quad \text{(F-40)}$$

The curve fit equations for (K - K*) versus density are as follows:

If $\rho < 7.2727$

$$(K - K^*) = 0.02075\rho^{1.145} \quad \text{(F-41)}$$

If $\rho \geq 7.2727$

$$(K - K^*) = 0.92\rho^{1.926} \quad \text{(F-42)}$$

and

$$K = (K - K^*) + K^* \quad \text{(F-43)}$$

5. BUTENE-1

a. Density

Below the normal boiling point, density is calculated by a polynomial curve fit of data given in References 5, 14, and 15:

$$T_n = 0.005839416\ T - 1.919708$$

$$\rho = \exp\ (3.808464 - 0.1261802\ T_n - 0.1021148\ T_n^2 - 0.009013067\ T_n^3 + 0.06139752\ T_n^4) \qquad \text{(F-44)}$$

where:

T is in °R

and

ρ is in lb_m/ft^3

For all temperatures above the normal boiling point, density is calculated using the method used for methane.

b. Enthalpy

Saturated liquid enthalpy for butene-1 from 168.4 to 650°R was determined from a polynomial curve fit (equation F-45) of the data given in references 5 and 6.

$$H_s = 146.3458 + 155.787\ T_n + 1.046343\ T_n^2 + 53.6013\ T_n^3 + 150.8771\ T_n^4 - 141.8474\ T_n^5 - 317.8708\ T_n^6 + 144.538\ T_n^7 + 203.0093\ T_n^8 \qquad \text{(F-45)}$$

where

$$T_n = 0.0034602\ T - 1.588235$$

and

T is in °R

Because of the incompressibility of butene-1 in the liquid phase at the pressures of interest, equation F-45 is also used to calculate compressed liquid enthalpies. The enthalpies for the remaining state points are calculated as functions of pressure and temperature by using equation F-4. The zero pressure enthalpy (H°) used in equation F-4 is given by equations F-46 and F-47.

For $480°R < T \leq 1760°R$

$$H° = 555.146 + 467.6889\ T_n + 126.2882\ T_n^2 - 21.8505\ T_n^3 + 22.51021\ T_n^4 - 11.0125\ T_n^5 - 14.4352\ T_n^6 - 10.49382\ T_n^7 \qquad \text{(F-46)}$$

where

$$T_n = 0.00125\ T - 1.2$$

and for

$$1760°R < T \leq 2100°R$$

$$H° = 1125 + 0.84326\ (T - 1760) \qquad \text{(F-47)}$$

and

T is in °R

c. Specific Heat

The procedure used to calculate specific heat for butene-1 consists of determining the enthalpy change (ΔH) for an incremental temperature change ($\Delta T = 1°R$) at constant pressure and using the relationship $C_p \approx \Delta H/\Delta T$. Enthalpies for any state are calculated using the procedure outlined in paragraph 5b.

d. Viscosity

The viscosity of saturated liquid butene-1 from 168.4 to 480.73°R (normal boiling point) is given by a polynomial curve fit of the data presented in Reference 14.

$$D = 0.01503759\ T - 3.511278$$

$$\mu = \exp\ (-6.558496 - 1.469023\ D + 0.5461106\ D^2 - 0.2365479\ D^3 + 0.1746158\ D^4 - 0.08284349\ D^5 \qquad \text{(F-48)}$$

where

T is in °R

and

μ is in $lb_m/ft\text{-}sec$

The viscosities of both gas and liquid butene-1 above the normal boiling point are determined from a residual viscosity correlation. The viscosity at one atmosphere (μ^*) is calculated using the Flynn and Thodos equation (Reference 16):

If $T_r \leq 1.5$

$$\mu^*\xi = 34.0 \times 10^{-5} (T_r)^{0.94} \quad \text{(F-49)}$$

If $T_r > 1.5$

$$\mu^*\xi = 17.78 \times 10^{-5} (4.58\ T_r - 1.67)^{5/8} \quad \text{(F-50)}$$

The residual viscosity of butene-1 is given by:

If $\rho \leq 3.44$

$$D = 0.02055273\ \ln\rho - 1.5139229$$

$$\mu - \mu^* = \exp(-16.72008 + 1.700598\ D) \quad \text{(F-51)}$$

If $3.44 < \rho \leq 17.0$

$$D = 1.251766\ \ln\rho - 2.546521$$

$$\mu - \mu^* = \exp(-12.77754 + 1.714417\ D - 0.5131499\ D^2) \quad \text{(F-52)}$$

If $\rho > 17.0$

$$D = 2.408628\ \ln\rho - 7.824157$$

$$\mu - \mu^* = \exp(-10.48283 + 1.047840\ D + 0.2850519\ D^2 + 0.08635191\ D^3) \quad \text{(F-53)}$$

and

$$\mu = (\mu - \mu^*) + \mu^*$$

where

ρ is in lb_m/ft^3

T is in °R

and

μ is in $lb_m/ft\text{-}sec$

e. Thermal Conductivity

The thermal conductivity of saturated liquid butene-1 from 168.4°R to the normal boiling point is given in Reference 17. The thermal conductivity of butene-1 above the normal boiling point is given by a residual thermal conductivity correlation. The thermal conductivity at 1 atm is calculated using the equation used for propane. The residual viscosity is determined by using the correlation presented in Reference 18.

If $\rho_r < 0.5$

$$(K - K^*)\lambda\ Z_c^5 = 14.0\ (e^{0.535\rho_r} - 1.0) \times 10^{-8} \quad \text{(F-54)}$$

If $0.5 \leq \rho_r < 2.0$

$$(K - K^*)\lambda\ Z_c^5 = 13.10\ (e^{0.67\rho_r} - 1.069) \times 10^{-8} \quad \text{(F-55)}$$

If $2.0 \leq \rho_r < 2.80$

$$(K - K^*)\lambda Z_c^5 = 2.976 \left(e^{1.155\rho_r} + 2.016\right) \times 10^{-8} \qquad \text{(F-56)}$$

and

$$K = (K - K^*) + K^* \qquad \text{(F-57)}$$

6. APPENDIX F NOMENCLATURE

Symbol	Description	Units
C_p	Specific heat at constant pressure	cal/gm-mole °K
C_p^o	Specific heat at zero pressure	cal/gm-mole °K
C_p^*	Specific heat at one atmosphere	cal/gm-mole °K
D	f (ρ) for evaluation of residual transport properties	
H	Enthalpy	Btu/lb_m
H^o	Enthalpy at zero pressure	Btu/lb_m
H_s	Enthalpy of saturated liquid	Btu/lb_m
k	Boltzmann constant	
K	Thermal conductivity	cal/cm sec °K
K*	Thermal conductivity at one atmosphere	cal/cm sec °K
M	Molecular weight	
P	Pressure	psia
P_c	Critical pressure	atm
P_s	Saturation pressure	psia
R	Gas constant, 0.0807	liter atm/gm-mole °K
T	Temperature	°K
T_n	Normalized temperature for calculating enthalpy and density	°K
T_c	Critical temperature	°K
T_r	Reduced temperature, T/T_c	
W_f	Weight fraction	
X	Mole fraction	
ρ	Density	gm-mole/liter
ρ_s	Density of saturated liquid	
ρ_r	Reduced density, ρ/ρ_c	

Symbol	Description	Units
λ	Characteristic constant, $T_c^{1/6} M^{1/2} / P_c^{2/3}$	
ξ	Characteristic constant, $T_c^{1/6} / M^{1/2} P_c^{2/3}$	
μ	Viscosity	centipoise
μ^*	Viscosity at one atmosphere	centipoise
ϵ	Leonard Jones constant	
σ	Effective collision diameter for molecules	Angstrom units
Ω	Collision integral	

7. APPENDIX F REFERENCES

1. Benedict, M., G. B. Webb, L. C. Rubin, "An Empirical Equation for Thermodynamic Properties of Light Hydrocarbons and Their Mixtures," Journal of Chemical Physics, Vol. 8, April 1940.

2. Benedict, M., G. B. Webb, L. C. Rubin, "An Empirical Equation for Thermodynamic Properties of Light Hydrocarbon and Their Mixtures," Chemical Engr. Progress, Vol. 47, No. 8, August 1951.

3. Opfell, J. B., W. G. Schlinger, and B. H. Sage, "Benedict Equation of State," Industrial and Engineering Chemistry, Vol. 46, No. 6, June 1954.

4. Canjar, L. N., R. F. Smith, E. Volianitis, J. F. Galluzzo, and M. Cabarcos, "Correlation of Constants in the Benedict-Webb-Rubin Equation of State," Industrial and Engineering Chemistry, Vol. 47, No. 5, May 1955.

5. Maxwell, J. B., Data Book on Hydrocarbons, D. Van Nostrand Company, Inc., New York, 1950.

6. Din, F. (Ed.) Thermodynamic Functions of Gases, Butterworths, London, 1961.

7. Hougen, O. A., K. M. Watson, R. A. Ragatz, Chemical Process Principles, Part II, Thermodynamics, 2nd Ed., Wiley, New York, 1959.

8. Hirschfelder, J. O., C. F. Curtis, R. B. Bird, Molecular Theory of Gases, Wiley, New York, 1954.

9. Bird, R. B., J. D. Hirschfelder, and C. F. Curtiss, "Theoretical Calculation of the Equation of State and Transport Properties of Gases and Liquids," Transactions of the A.S.M.E., Oct. 1954.

10. Chapman, S., and T. G. Cowling, The Mathematical Theory of Non-Uniform Gases, Cambridge University Press, 1939.

11. Drazoslav, M., G. Thodos, "The Thermal Conductivity of Hydrocarbon Gases at Normal Pressure", American Institute of Chemical Engineers Journal, Vol. 7, No. 2, June 1961.

12. Ellington, R. T., B. E. Eakin, J. D. Parent, O. T. Bloomer, "Vapor-Liquid Phase Equilibria in the Binary System of Methane, Ethane and Nitrogen," Institute of Gas Technology, Chicago, Ill. Pub. in Thermodynamic and Transport Properties of Gases, Liquids and Solids, A.S.M.E., McGraw-Hill Inc., New York, 1959.

13. Reid, R. C. and T. K. Sherwood, Properties of Gases and Liquids, McGraw-Hill, Inc, 1958.

14. American Petroleum Institute Project 44, Selected Values of Physical & Thermodynamic Properties of Hydrocarbons and Related Derivatives, (Elsevier Publishing Co., Inc.) New York, 1950.

15. Gas Data Book, The Matheson Company, Inc., New York, 1966.

16. L. I. Steil and G. Thodos, "The Prediction of Transport Properties of Pure Gaseous and Liquid Substances, Progress in International Research on Thermodynamic and Transport Properties," ASME, Academic Press, New York, 1962.

17. R. H. Gallant, "Physical Properties of Hydrocarbons - Part 9 - Thermal Conductivity of C_1 to C_4 Hydrocarbons," Hydrocarbon Processing, Vol. 45, No. 12, Dec. 1966.

18. Steil, L. J. and G. Thodos, "The Thermal Conductivity of Nonpolar Substances in the Dense Gaseous and Liquid Regions," A. J. Ch. E. Journal, Vol. 10, No. 1, Jan. 1964.

8. BIBLIOGRAPHY

1. "Investigation of Light Hydrocarbon Fuels with Flox Mixtures as Liquid Rocket Propellants," Quarterly Progress Report No. 1, Contract NAS3-4195, Pratt & Whitney Aircraft Report FR-1107, Nov. 1964.

2. Butler, J. N. and R. S. Brokaw, "Thermal Conductivity of Gas Mixtures in Chemical Equilibrium," Journal of Chemical Physics 26, 1636-1639 (1956).

3. Brokaw, R. S., "Thermal Conductivity of Gas Mixtures in Chemical Equilibrium," Journal of Chemical Physics 32, 1005-1006, 1960.

4. Weber, J. H., "Thermodynamic Properties of 1-Butene," A.I.CH.E. Journal, Vol. 1, No. 2, June 1955.

5. Kozicki, W. R., R. F. Cuffel, and B. H. Lage, "Latent Heat of Vaporization of 1-Butene," Journal of Chemical and Engineering Data, Vol. 7, No. 2, April 1962.

6. Kobe, K. A. and E. G. Long, "Thermochemistry for the Petrochemical Industry, Part III - Monoolefinic Hydrocarbons, C_2, C_4," Petroleum Refiner, Vol. 28, No. 3, March 1949.

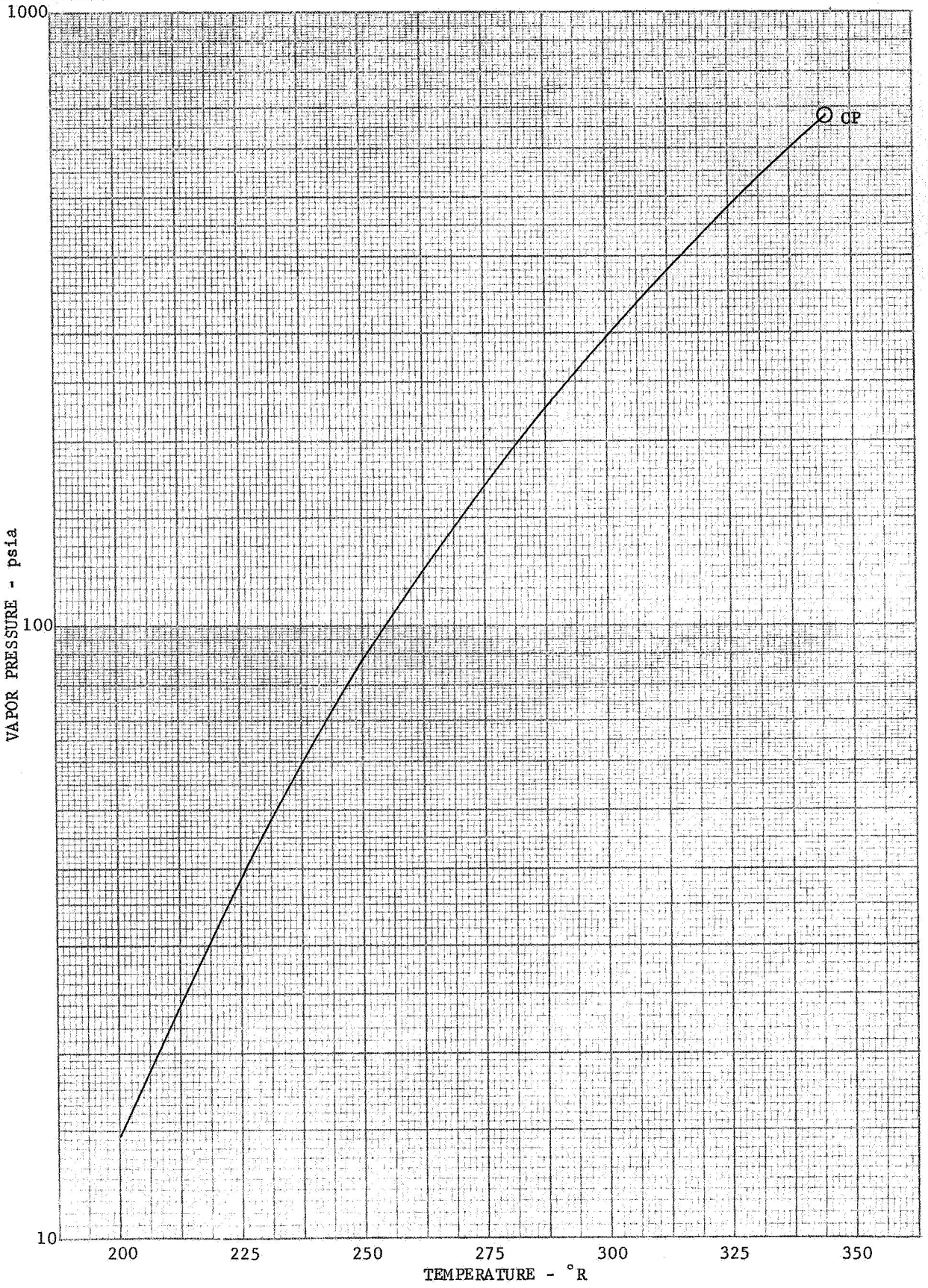


Figure F-1. Vapor Pressure of Methane DF 60368

DF 60369

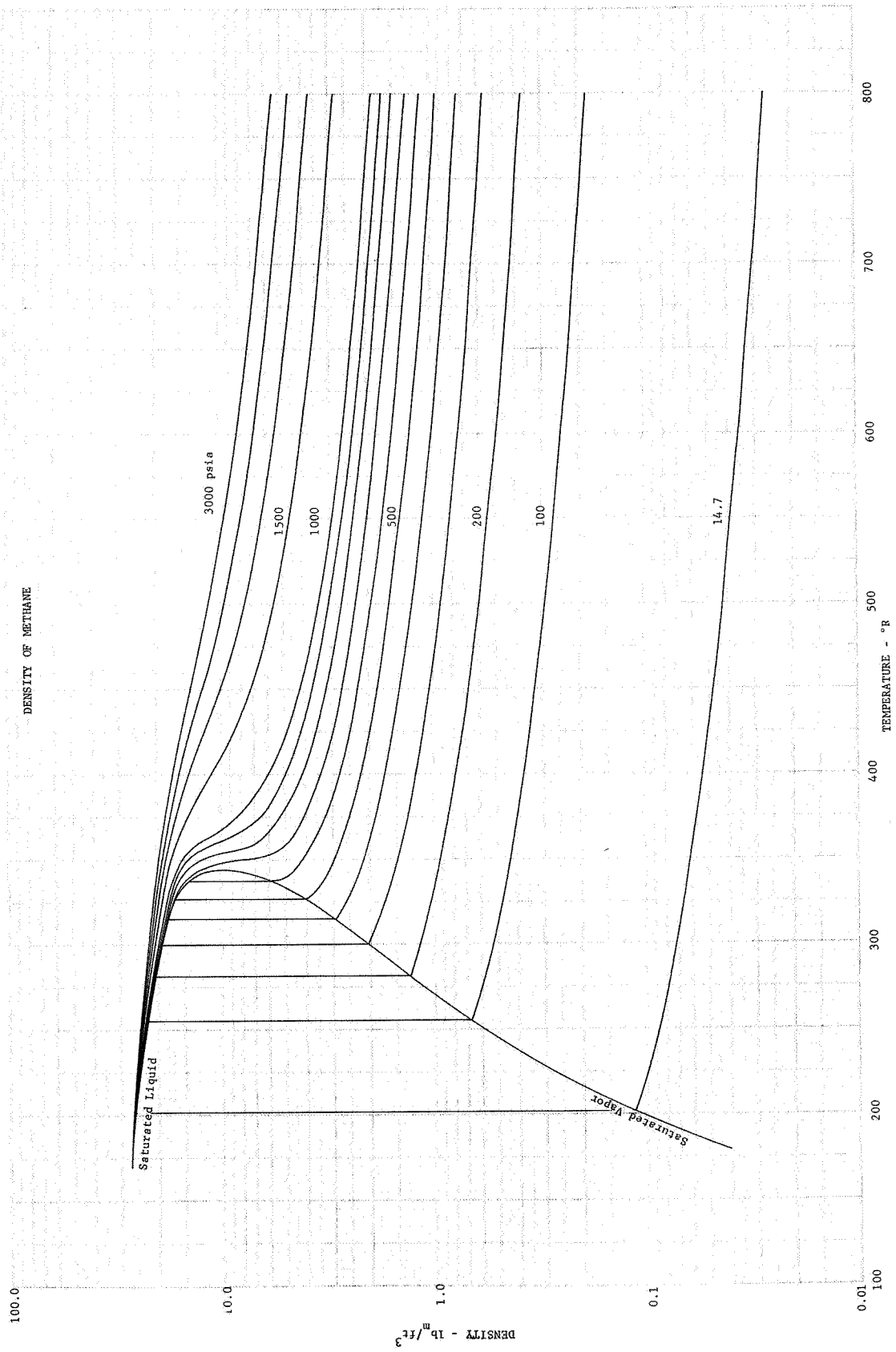
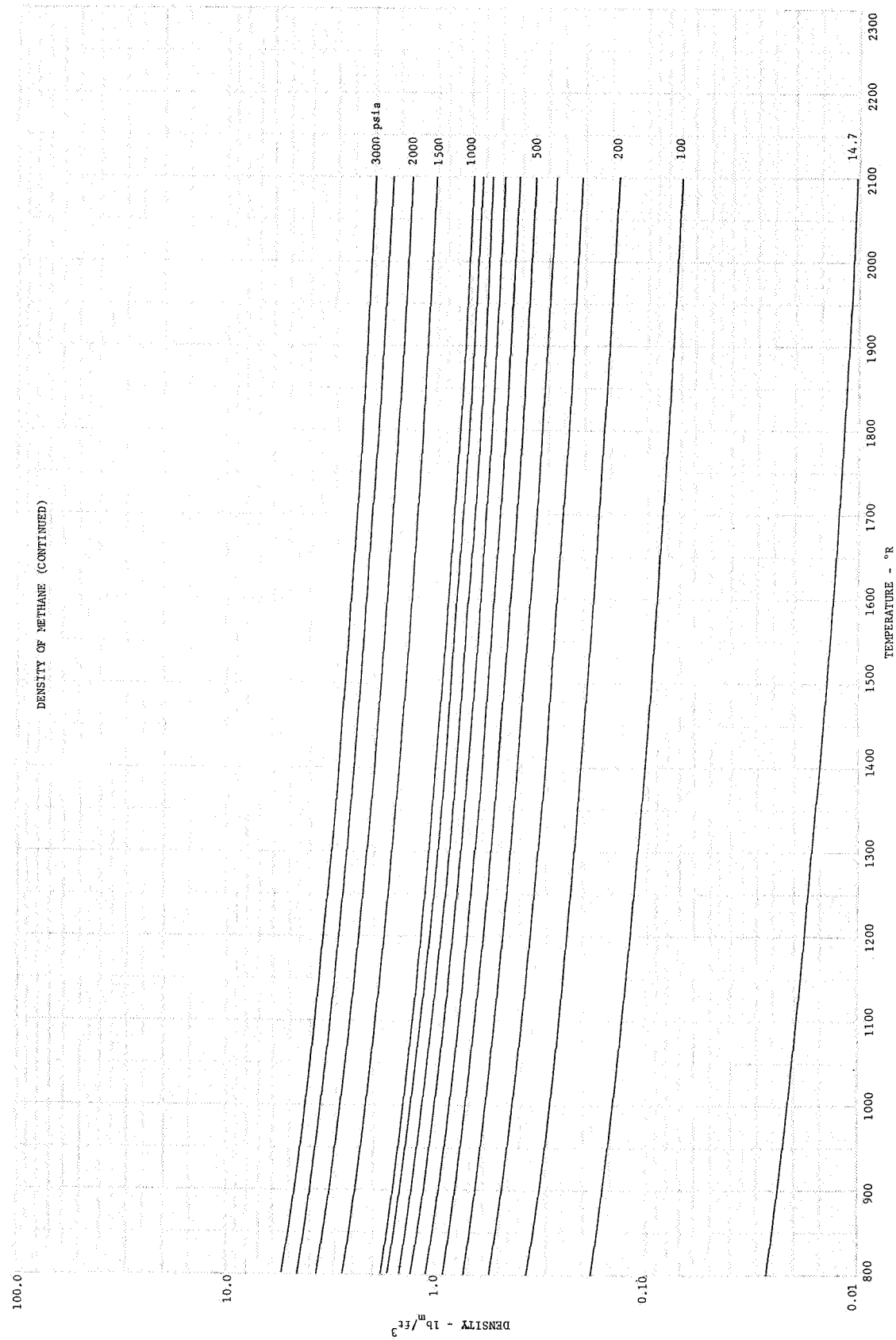


Figure F-2a. Density of Methane, Sheet 1



DF 60370

Figure F-2b. Density of Methane, Sheet 2

DF 60371

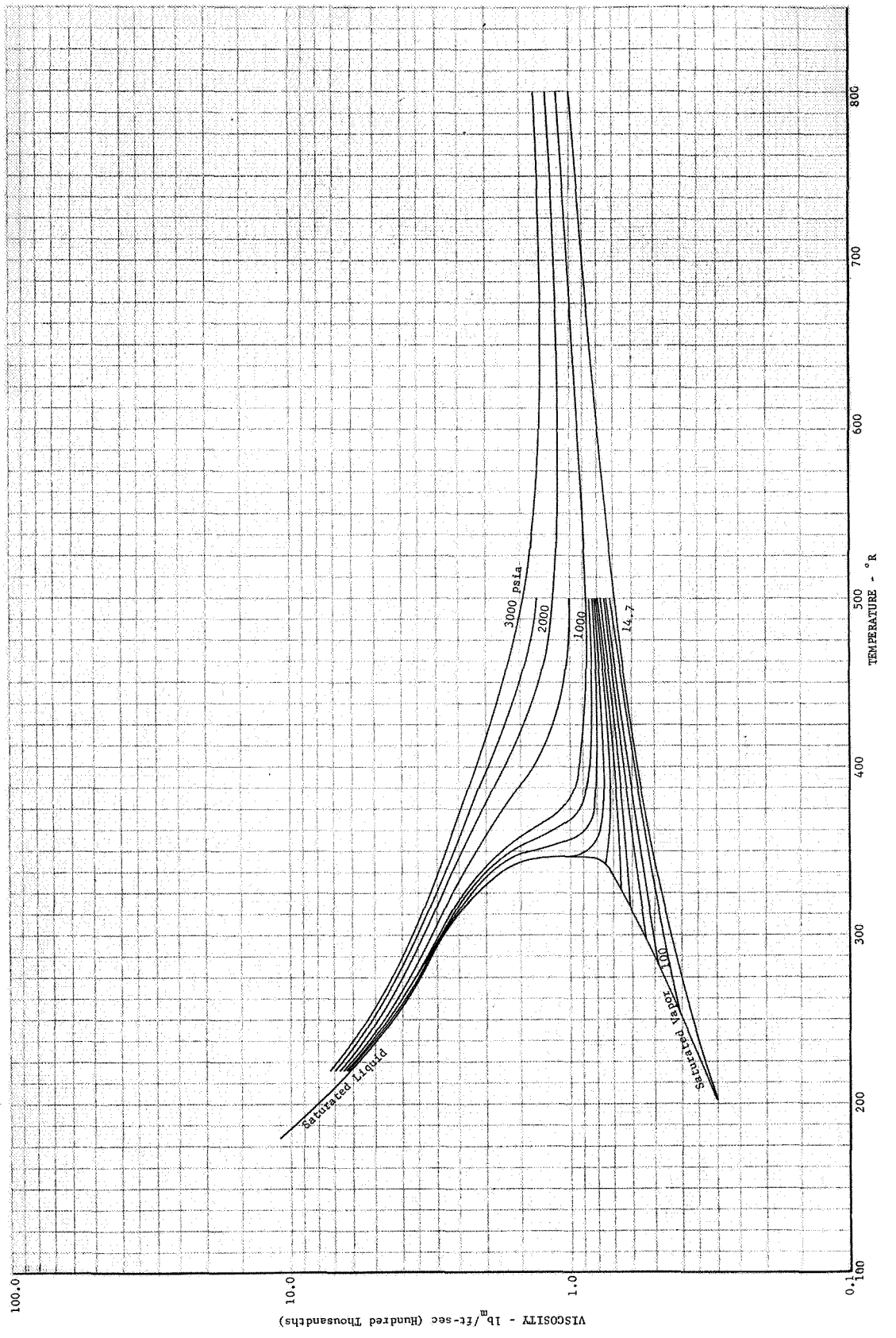
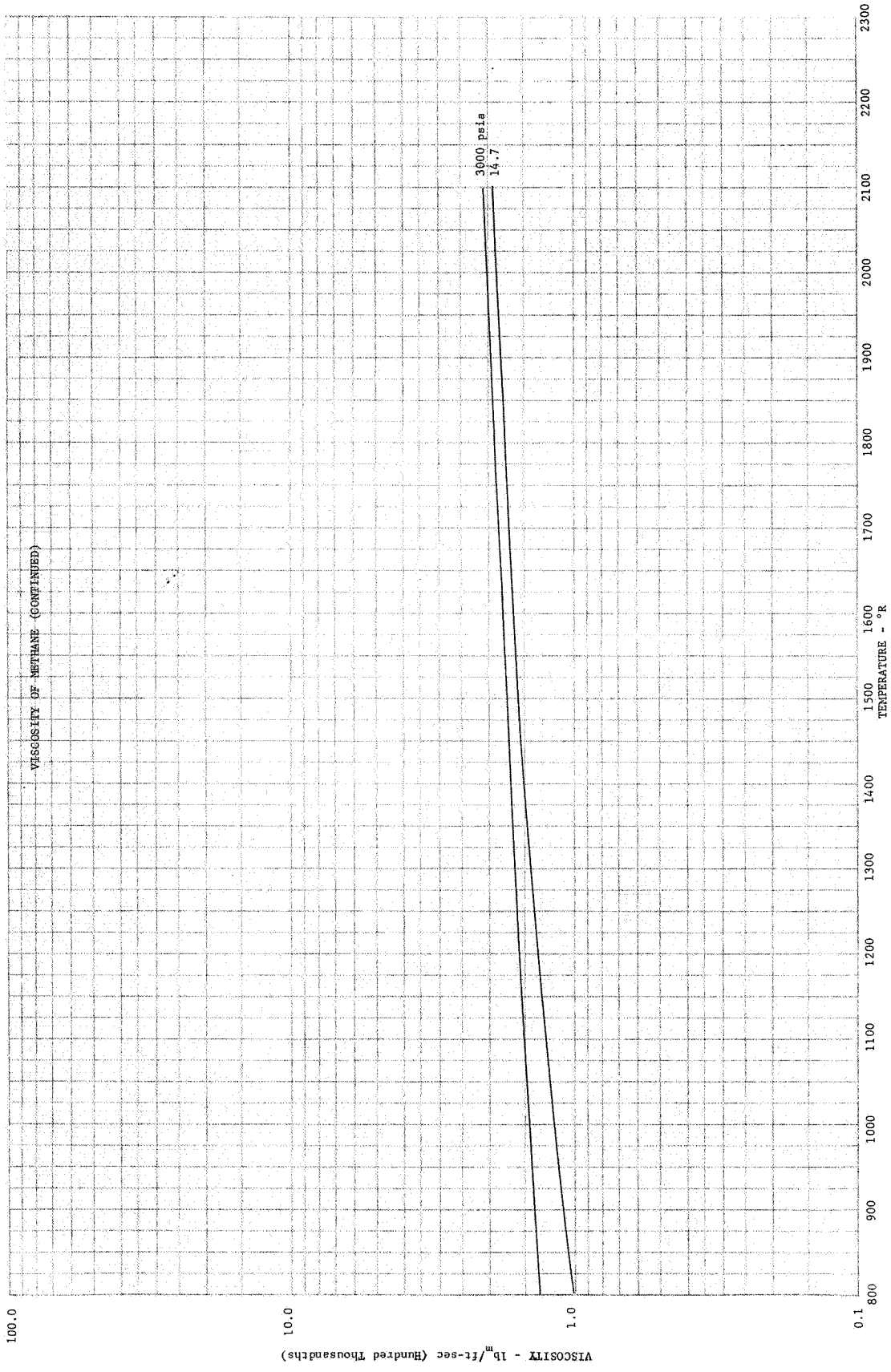


Figure F-3a. Viscosity of Methane, Sheet 1



DF 60372

Figure F-3b. Viscosity of Methane, Sheet 2

DF 60373

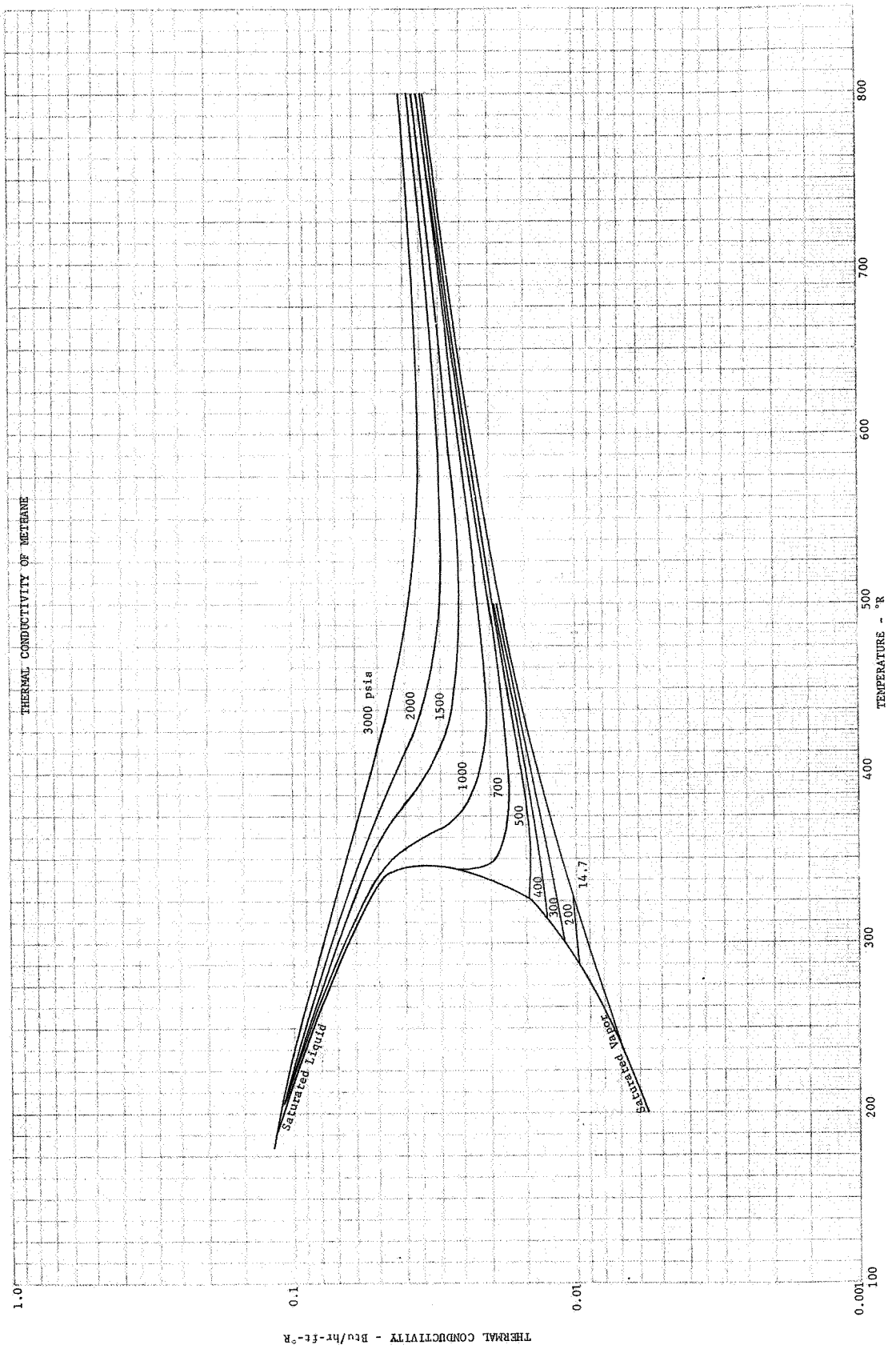
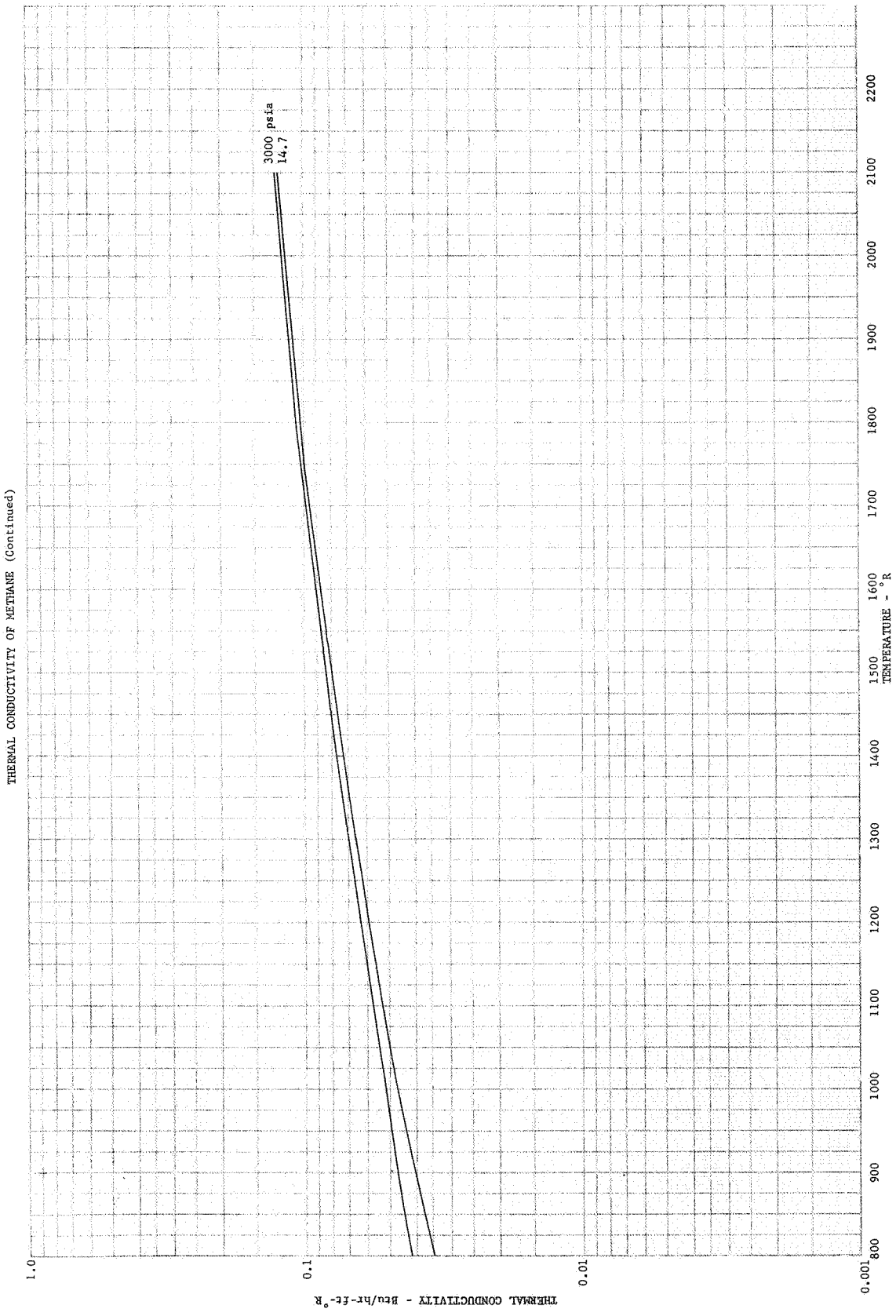


Figure F-4a. Thermal Conductivity of Methane, Sheet 1



DF 60374

Figure F-4b. Thermal Conductivity of Methane, Sheet 2

DF 60375

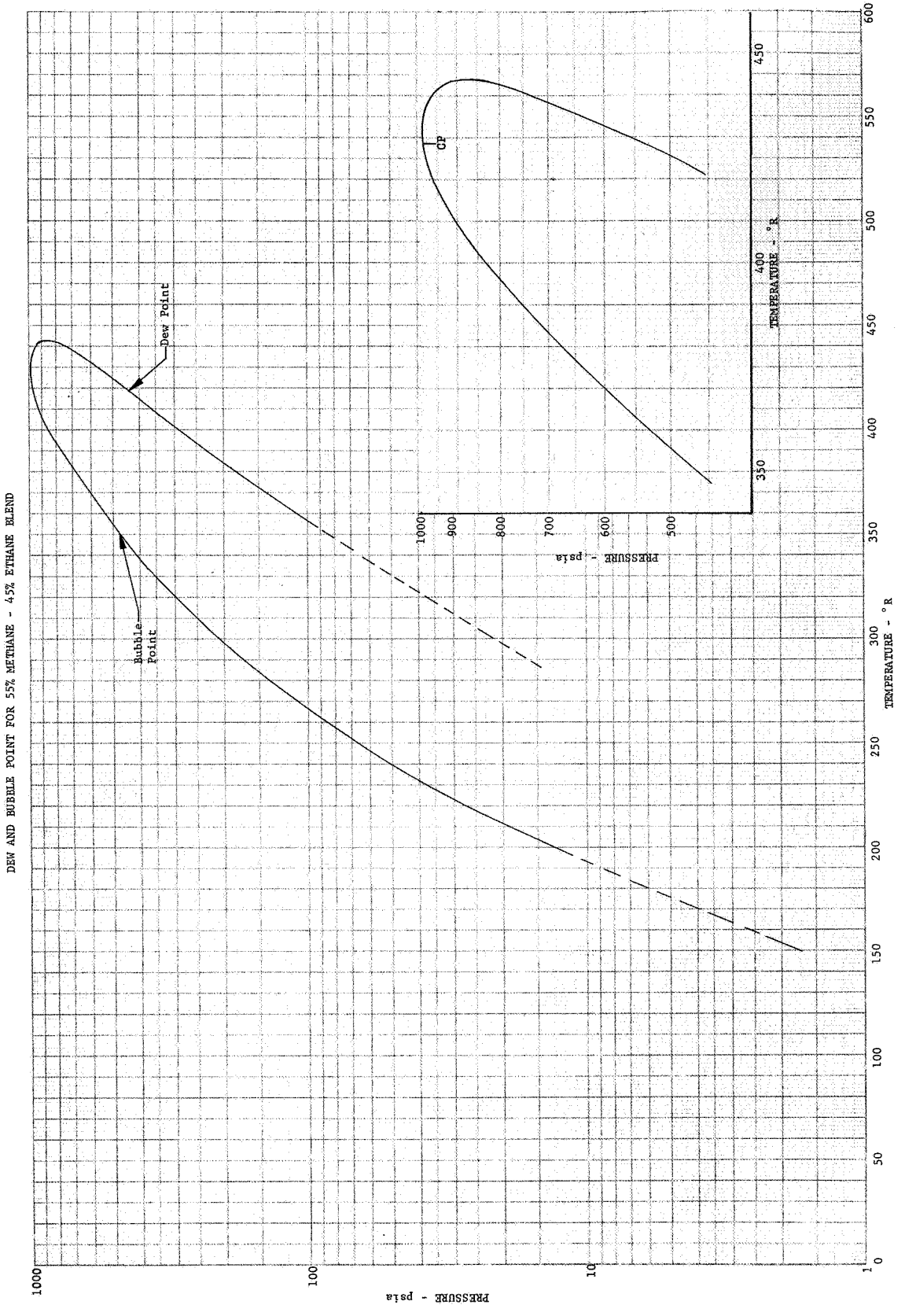
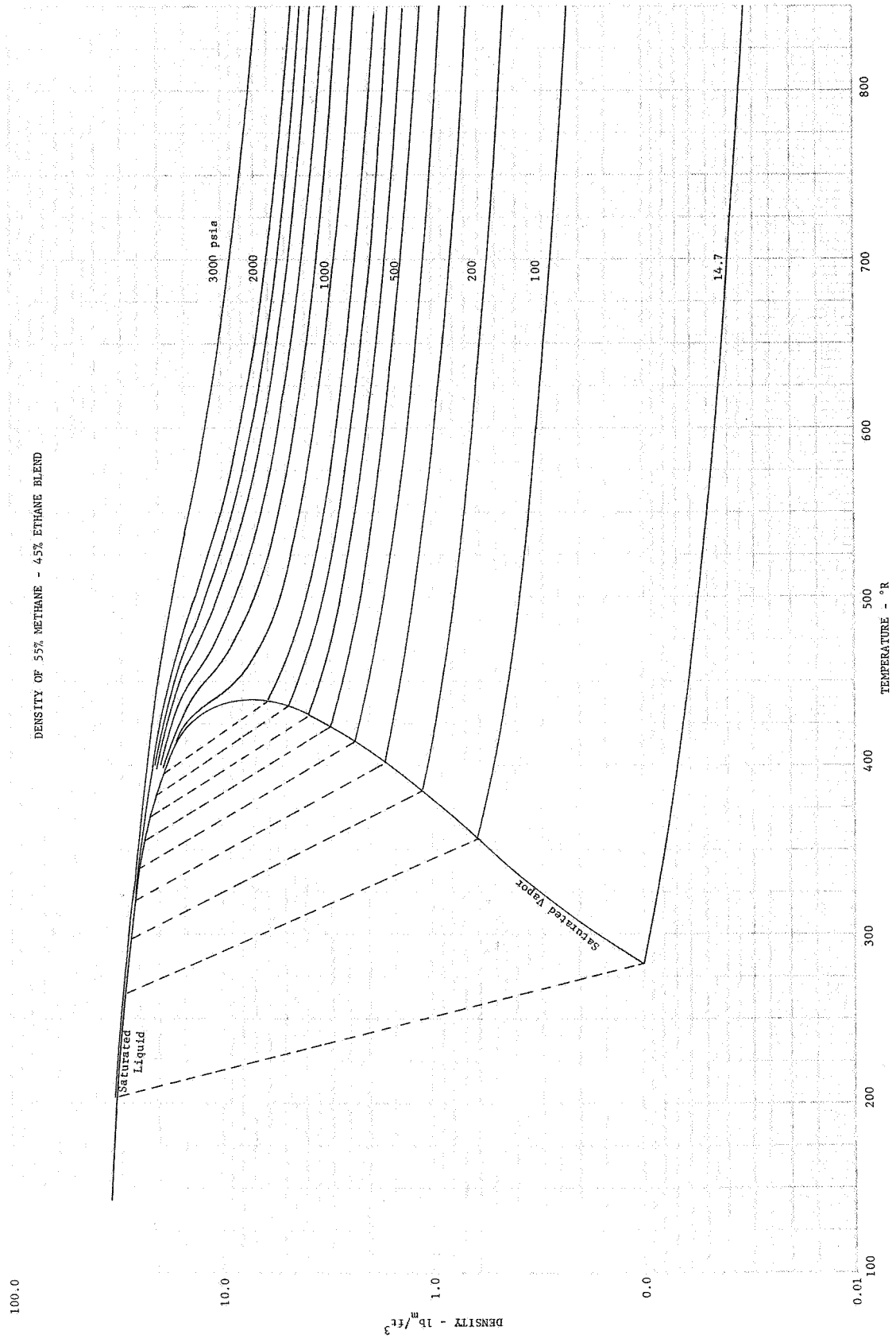
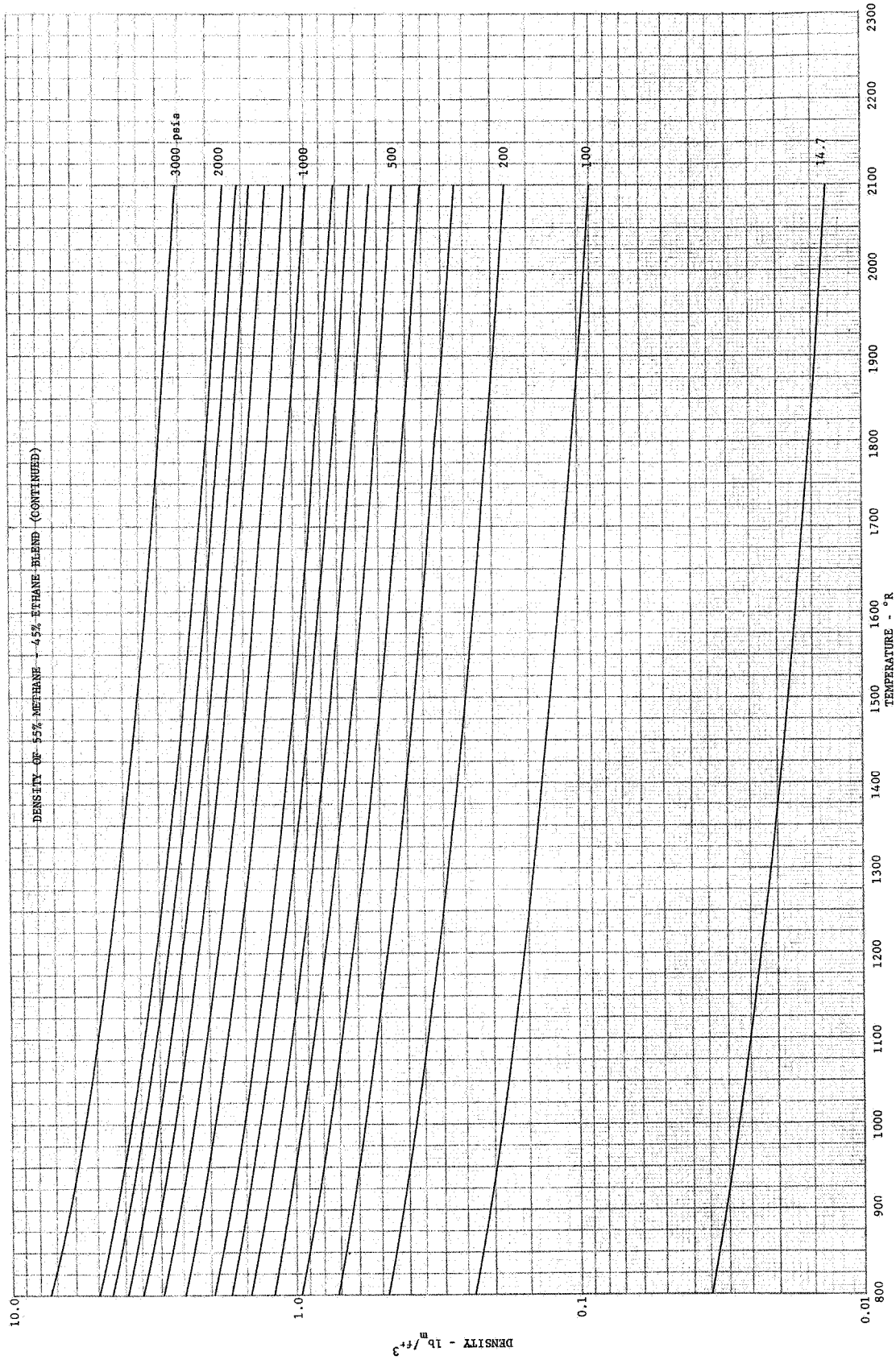


Figure F-5. Dew and Bubble Point for 55% Methane - 45% Ethane



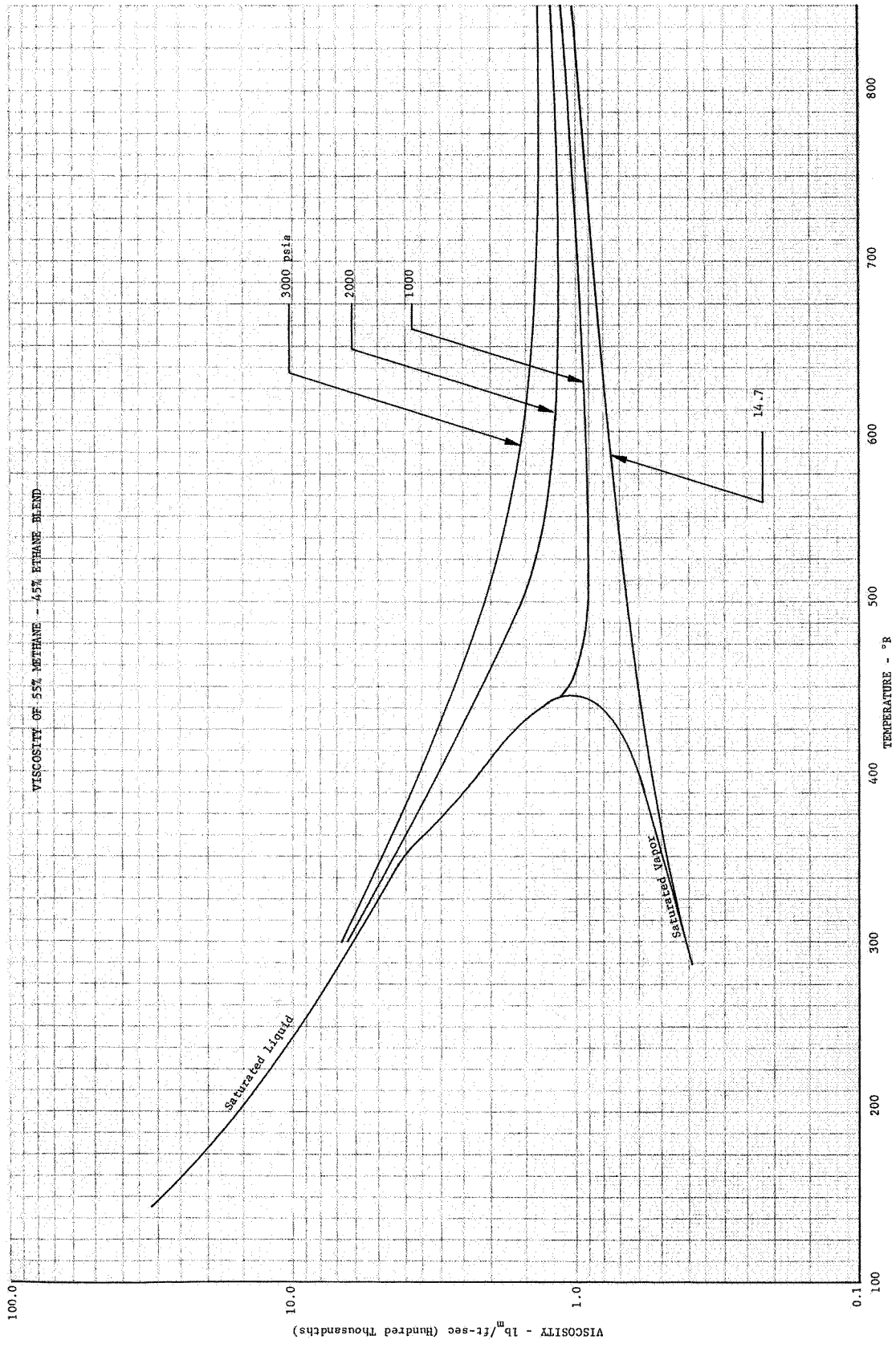
DF 60376

Figure F-6a. Density of 55% Methane - 45% Ethane Blend, Sheet 1



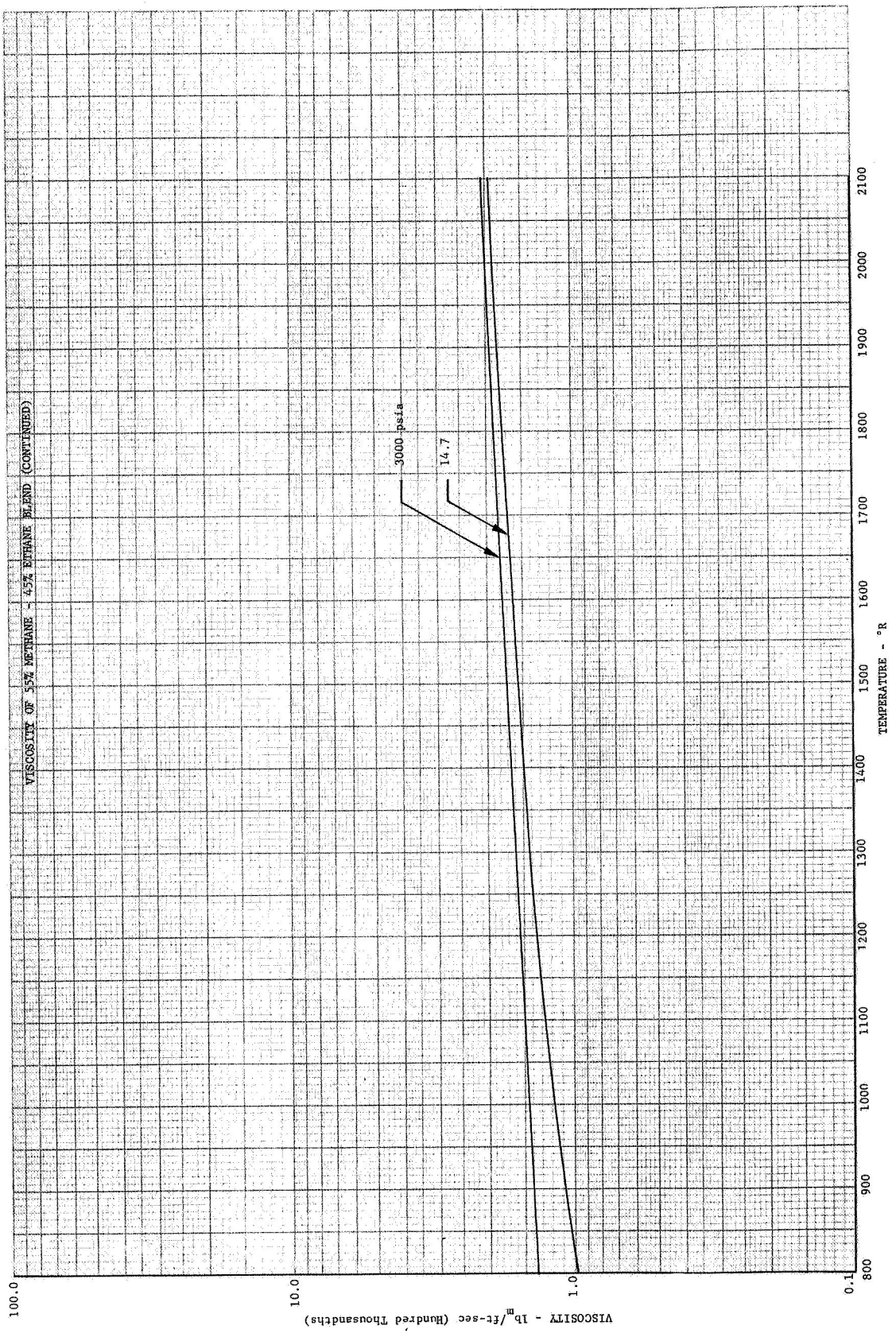
DF 60377

Figure F-6b. Density of 55% Methane - 45% Ethane Blend, Sheet 2



DF 60378

Figure F-7a. Viscosity of 55% Methane - 45% Ethane Blend, Sheet 1



DF 60379

Figure F-7b. Viscosity of 55% Methane - 45% Ethane Blend, Sheet 2

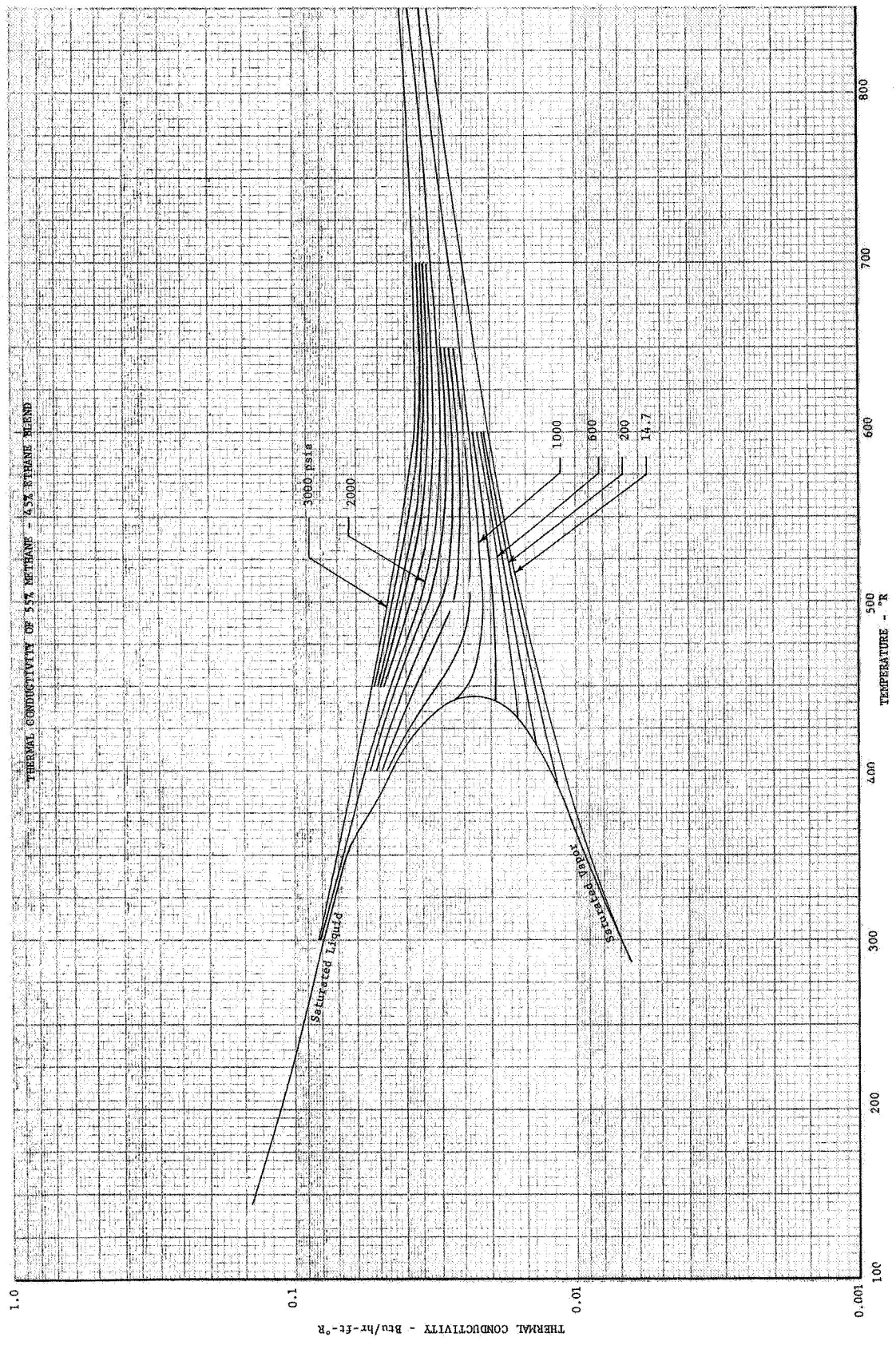
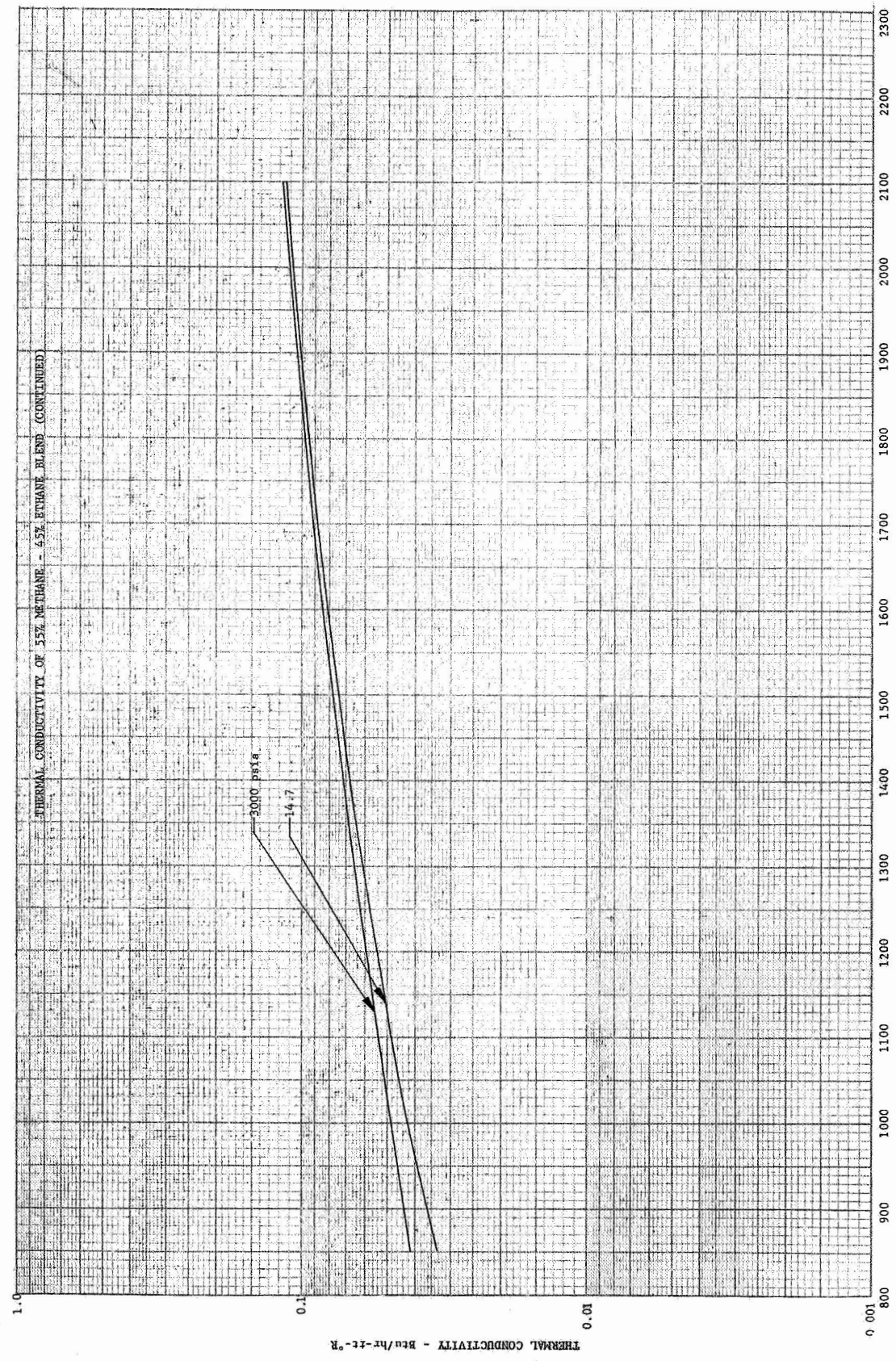


Figure F-8a. Thermal Conductivity of 55% Methane - 45% Ethane Blend, Sheet 1

DF 60380



DF 60381

Figure F-8b. Thermal Conductivity of 55% Methane - 45% Ethane Blend, Sheet 2

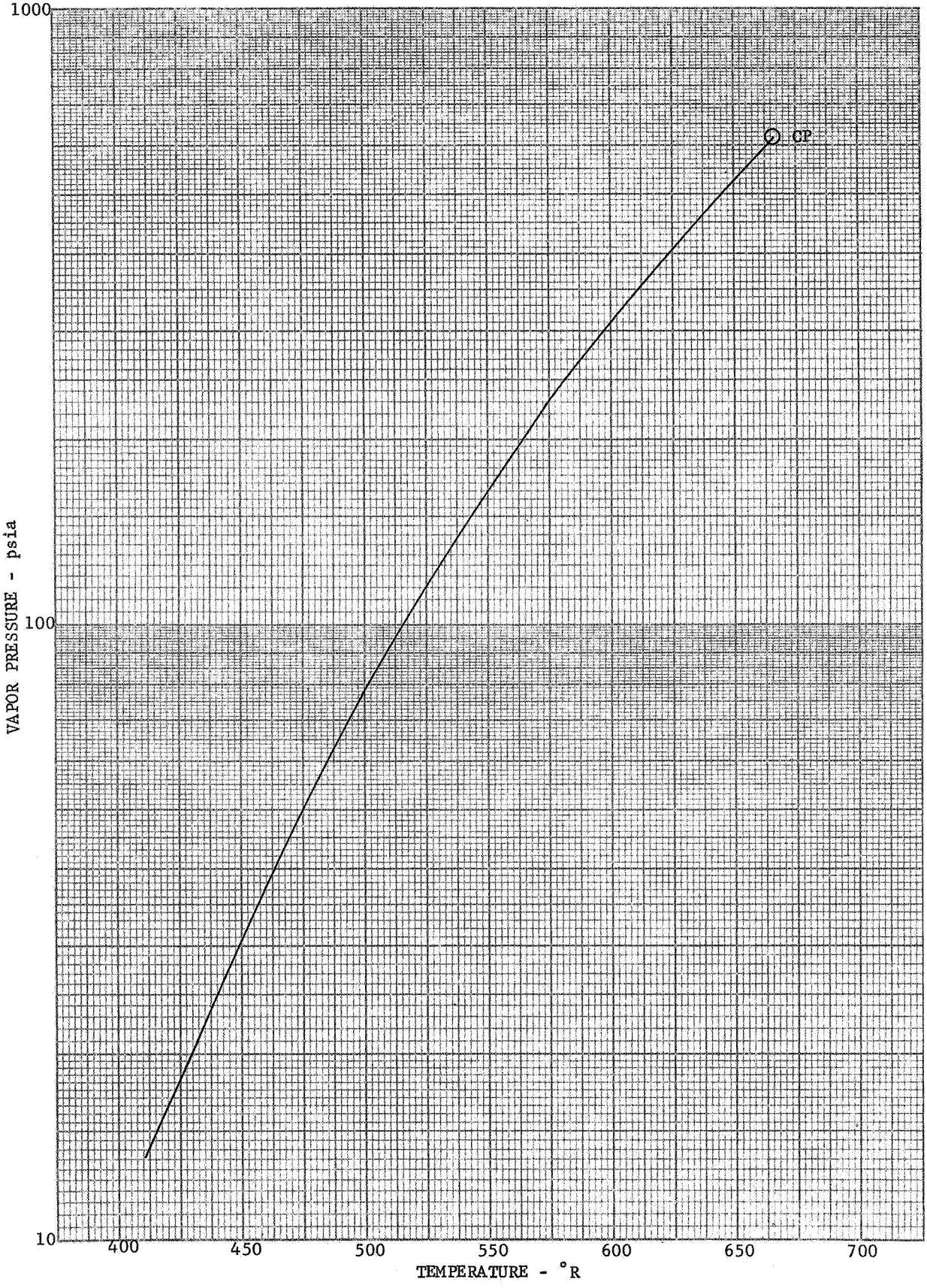


Figure F-9. Vapor Pressure of Propane DF 60382

DF 60383

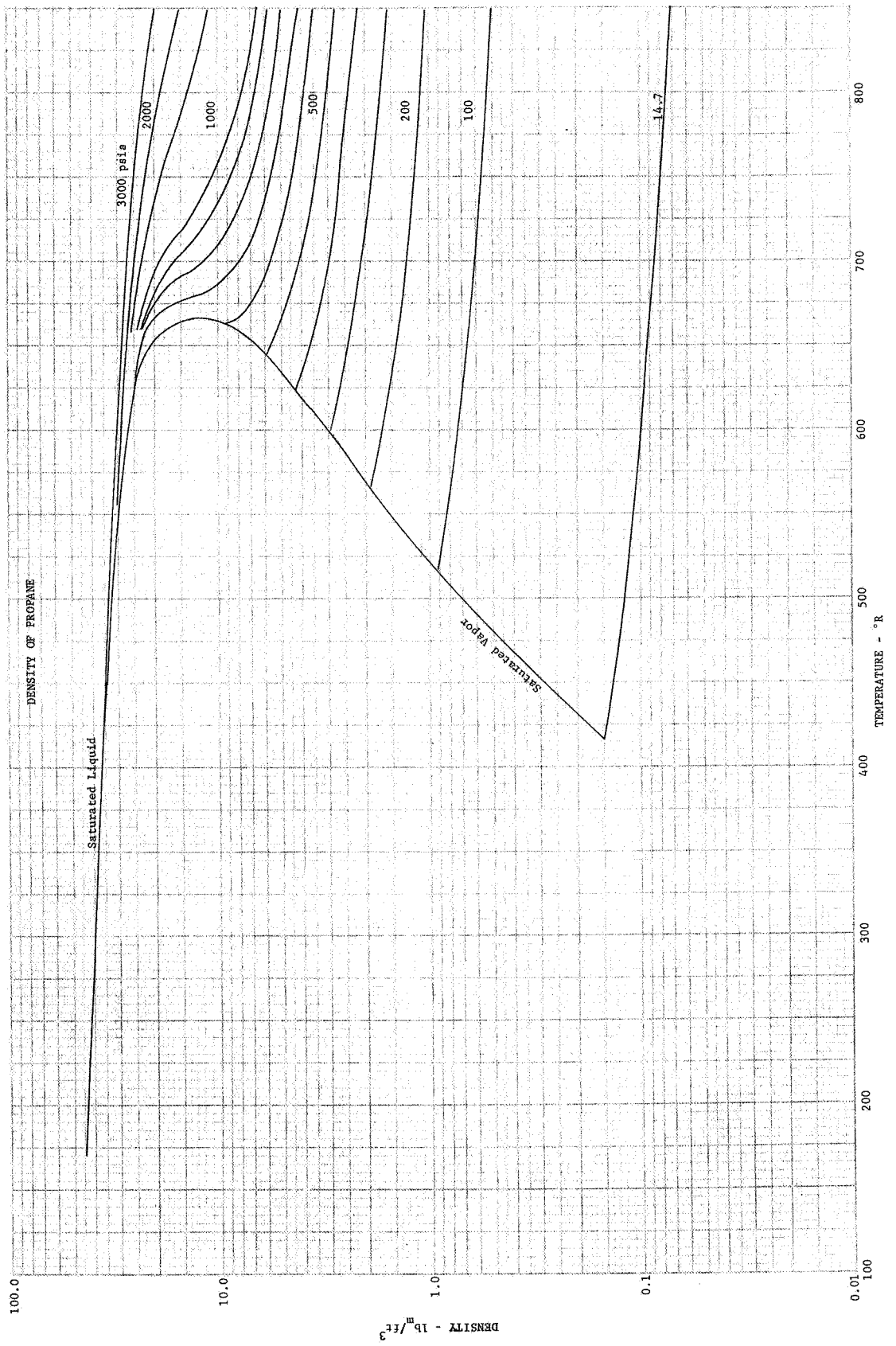
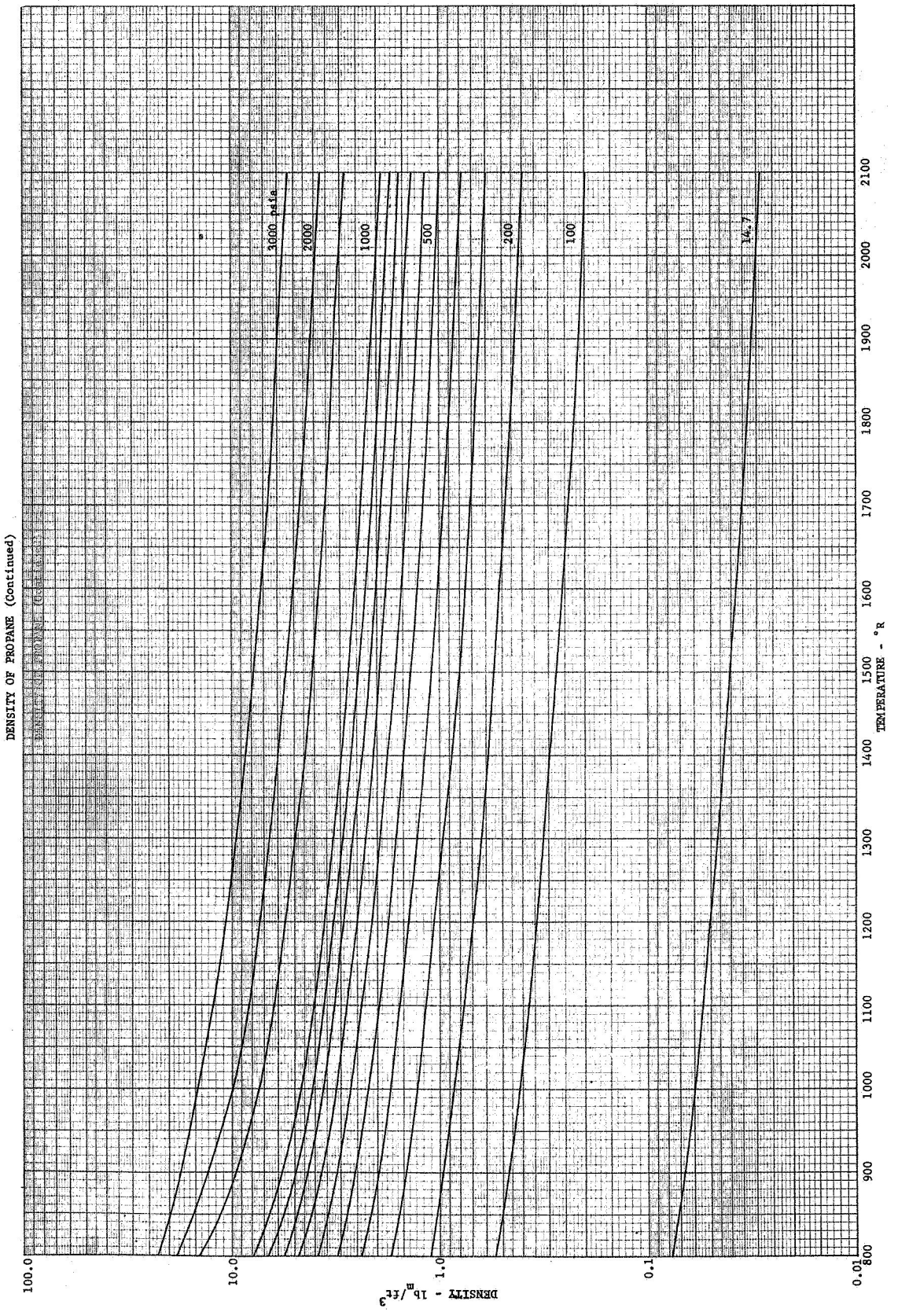
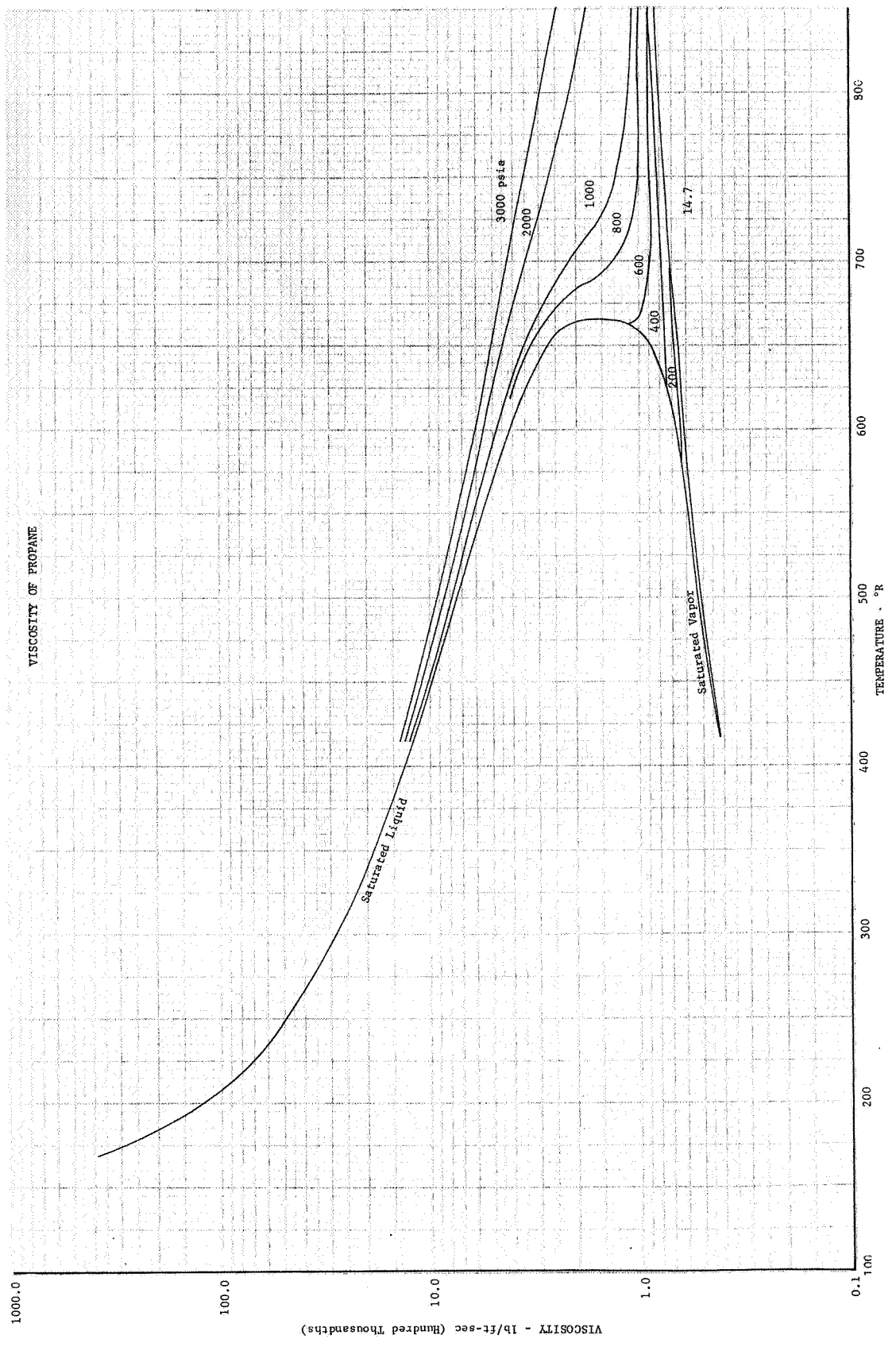


Figure F-10a. Density of Propane, Sheet 1



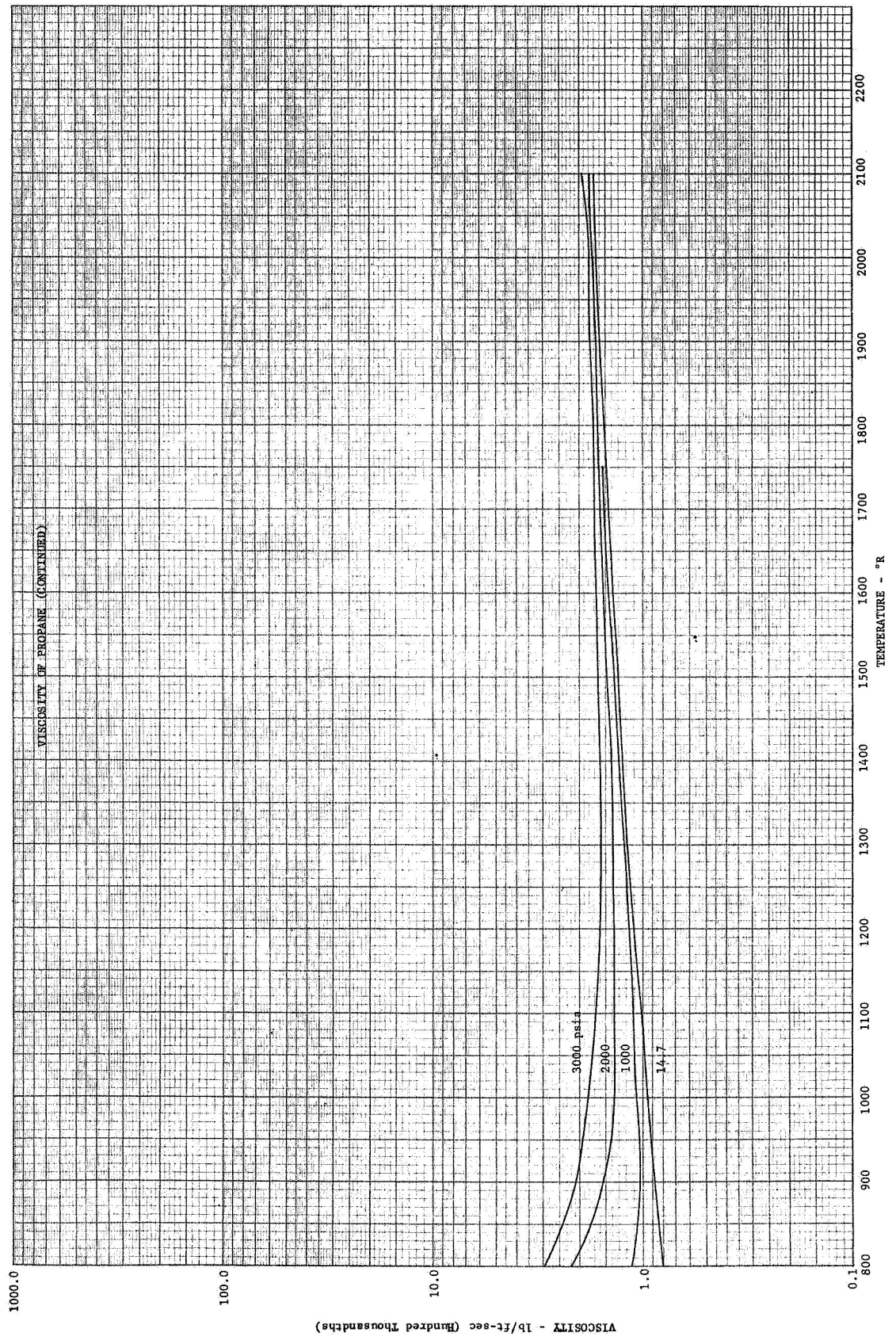
DF 60384

Figure F-10b. Density of Propane, Sheet 2



DF 60385

Figure F-11a. Viscosity of Propane, Sheet 1



DF 60386

Figure F-11b. Viscosity of Propane, Sheet 2

DF 60387

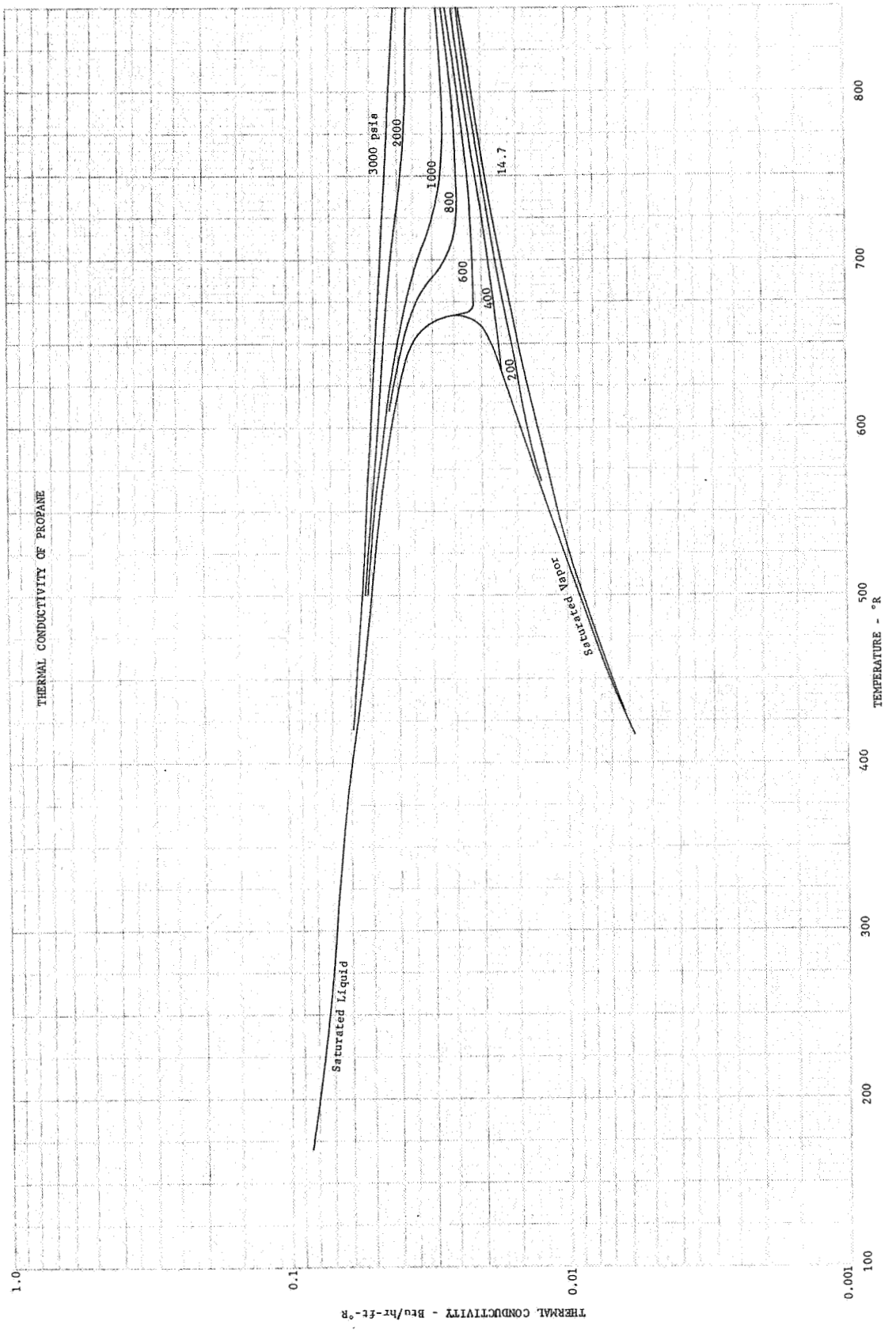
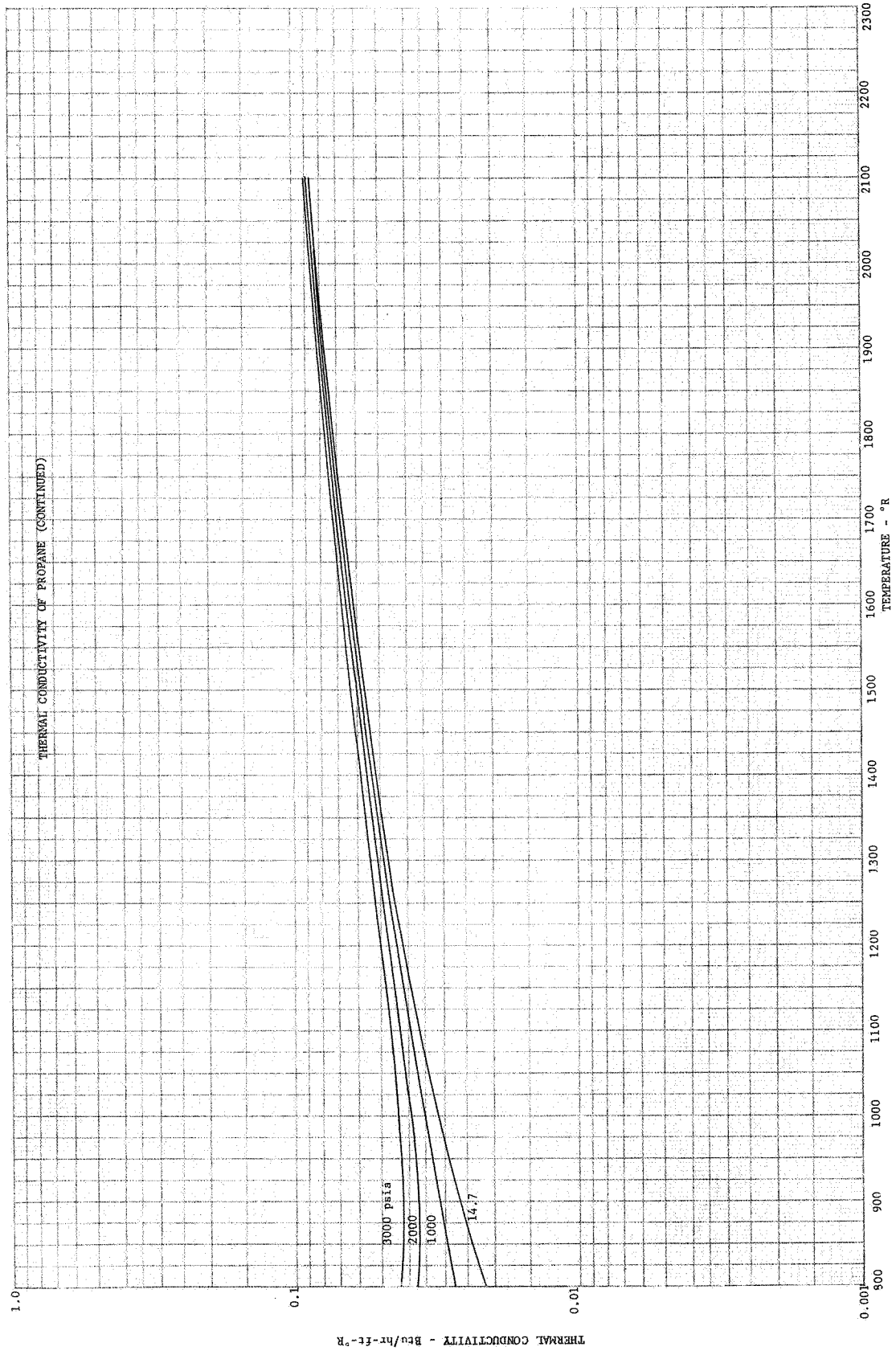


Figure F-12a. Thermal Conductivity of Propane, Sheet 1



DF 60388

Figure F-12b. Thermal Conductivity of Propane, Sheet 2

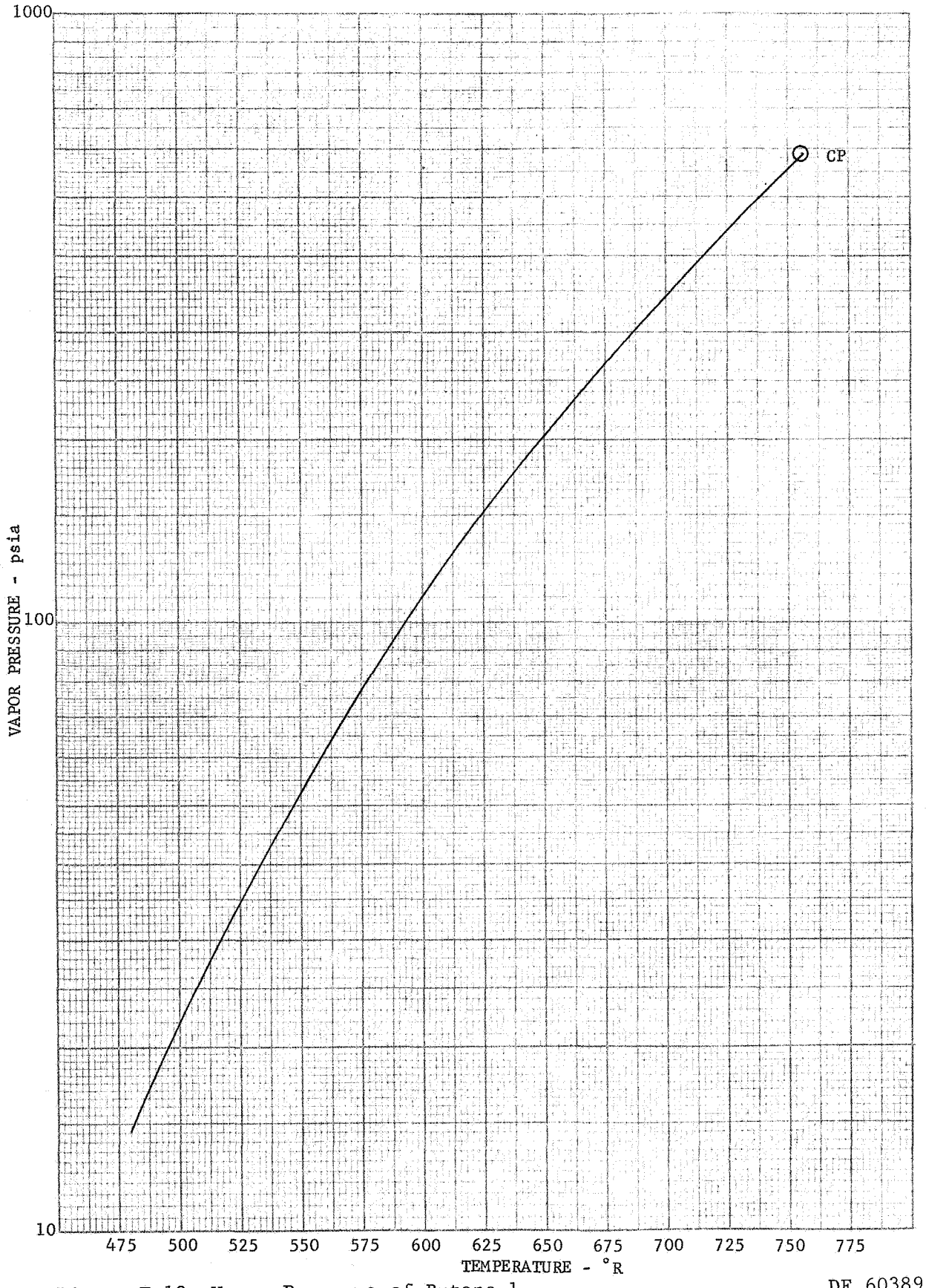
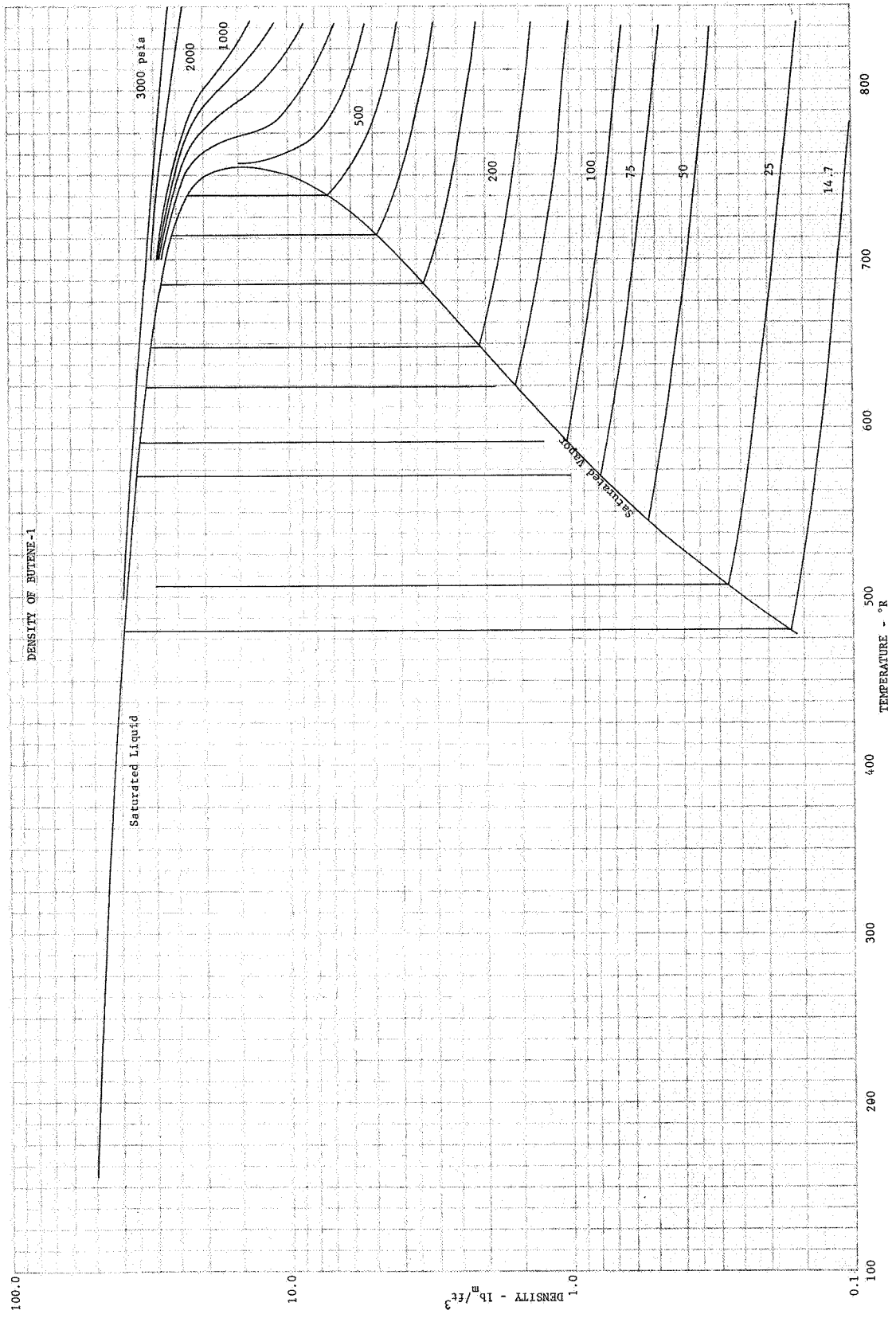


Figure F-13. Vapor Pressure of Butene-1

DF 60389



DF 60390

Figure F-14a. Density of Butene-1, Sheet 1

DF 60391

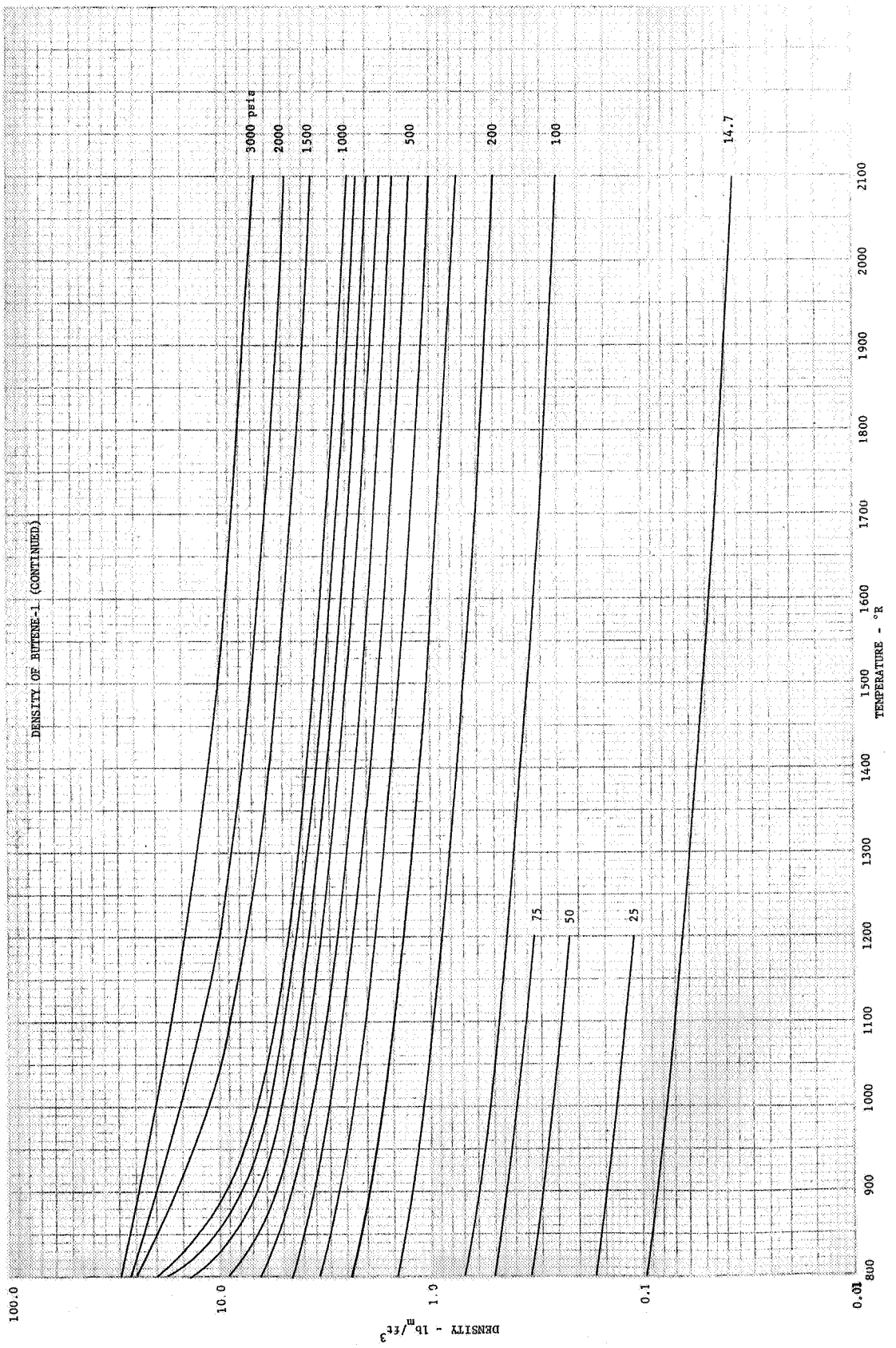
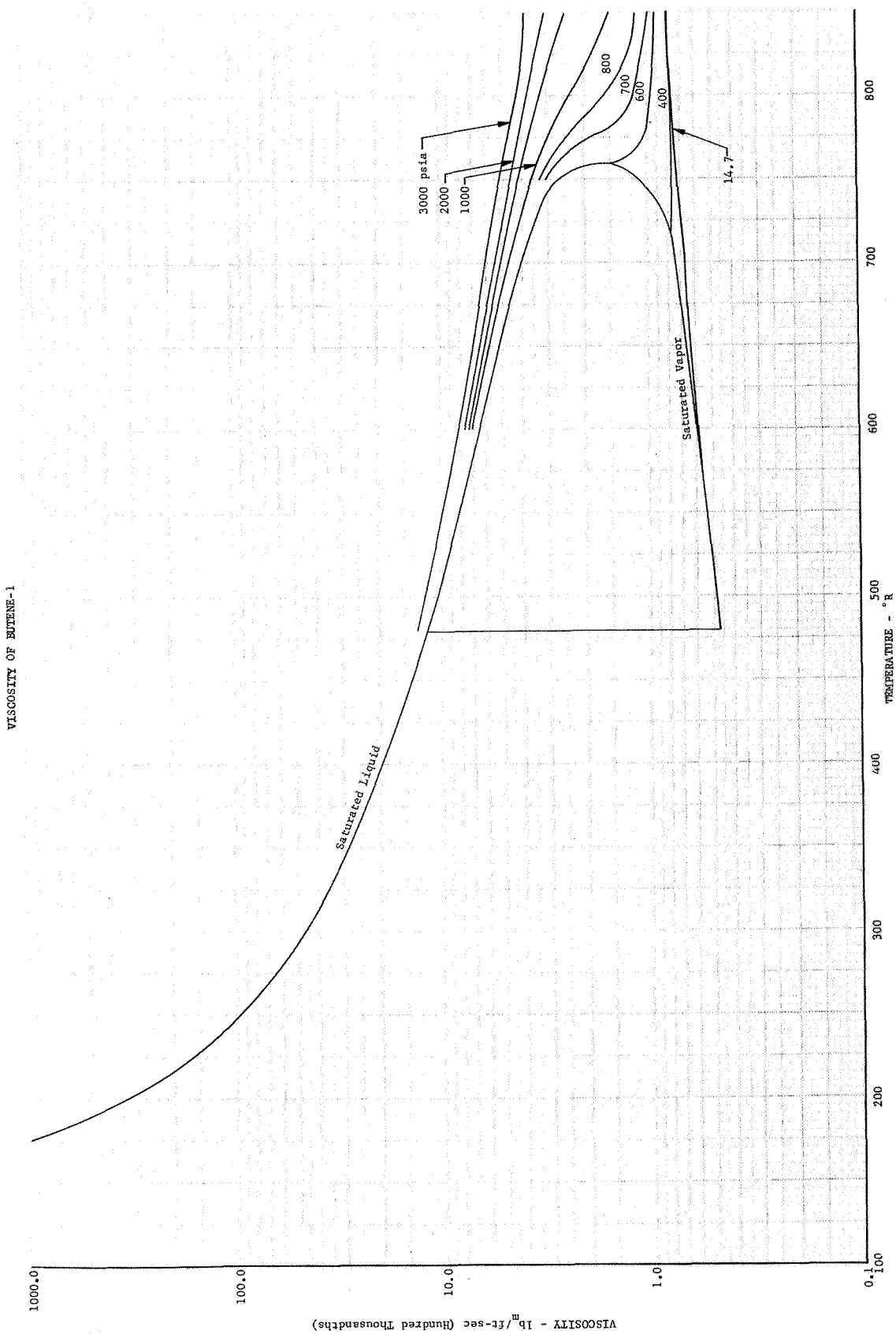


Figure F-14b. Density of Butene-1, Sheet 2



DF 60392

Figure F-15a. Viscosity of Butene-1, Sheet 1

DF 60393

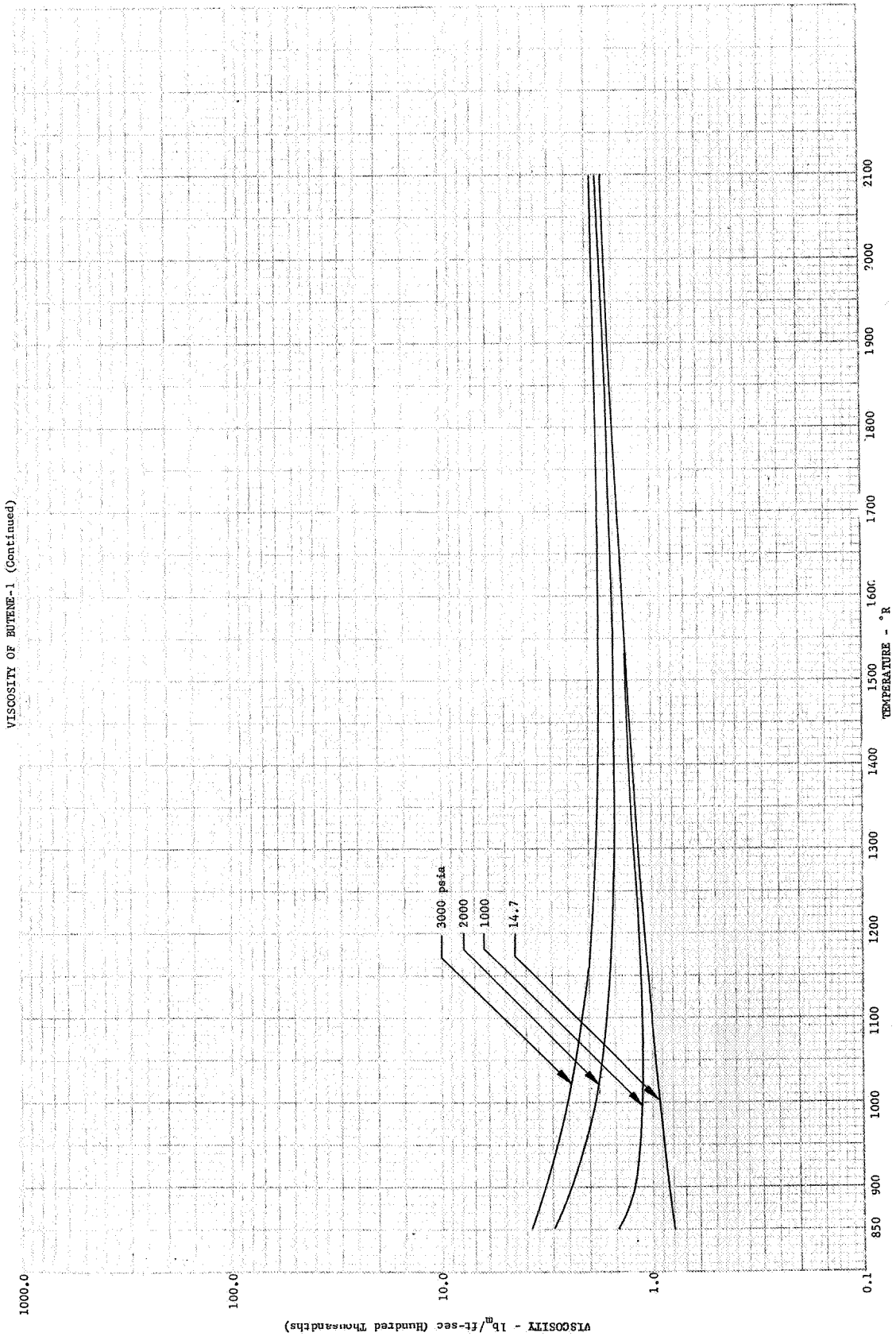
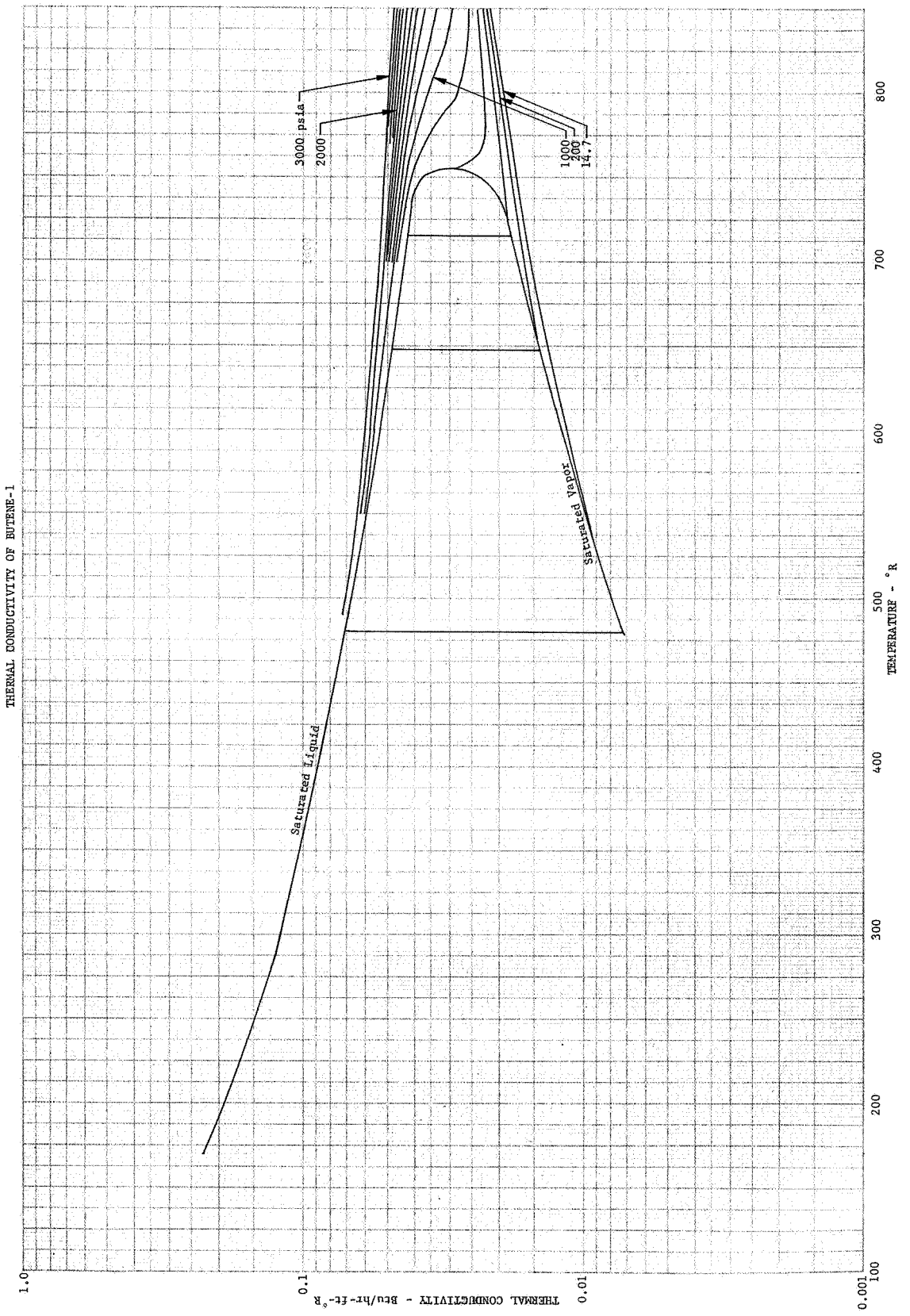
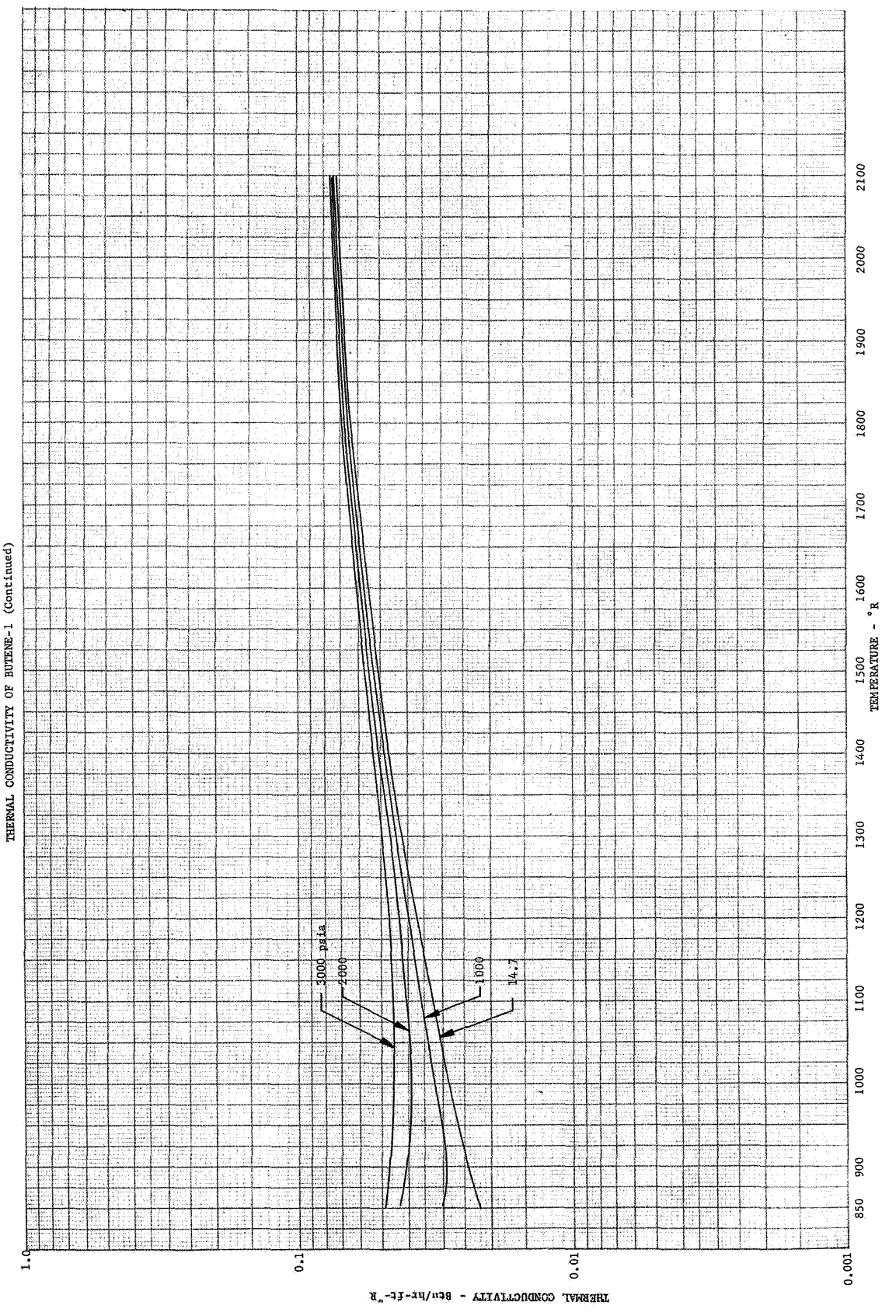


Figure F-15b. Viscosity of Butene-1, Sheet 2



DF 60394

Figure F-16a. Thermal Conductivity of Butene-1, Sheet 1



DF 60395

Figure F-16b. Thermal Conductivity of Butene-1, Sheet 2

APPENDIX G
THEORETICAL PERFORMANCE CURVES

Figures G-1 through G-10 present theoretical shifting equilibrium performance data for the five fuels (methane, 55% methane - 45% ethane, ethane, propane, and butene-1) with optimum flox mixtures and OF_2. All data were computed for fuel temperatures 10°R above normal freezing points. The values used for F_2 and OF_2 enthalpies were -145.8 and +65 Btu/lb, respectively, which correspond to the enthalpies of the oxidizers at their normal boiling points. The OF_2 enthalpy value reflects the latest heat of formation value of +5.86K cal/mole, based on NBS determination, for the gas at 298°K.

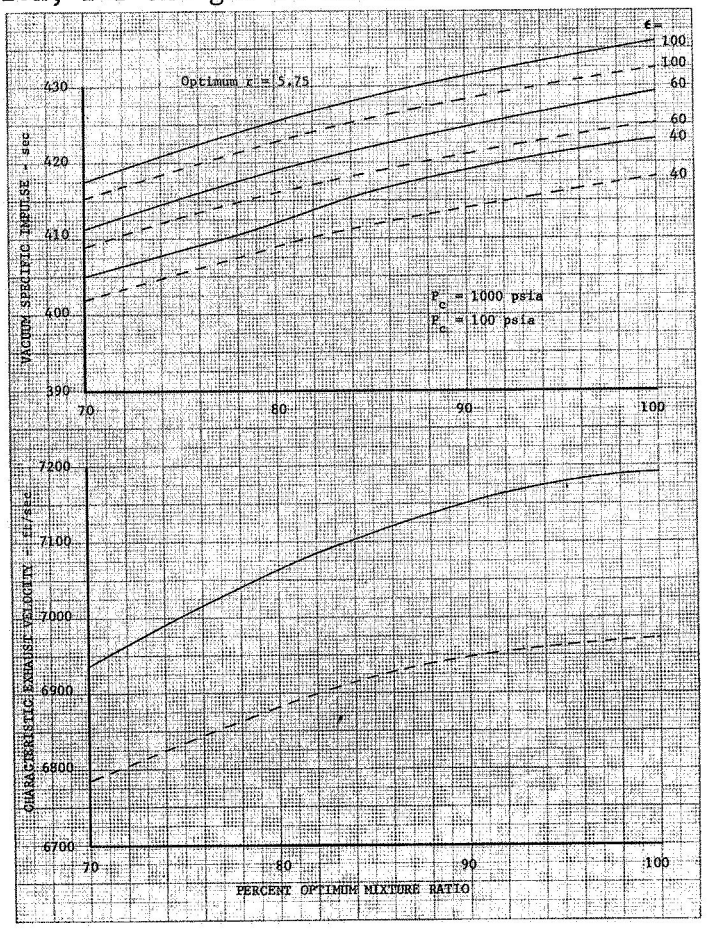


Figure G-1. Theoretical Performance: Flox/Methane DF 60409

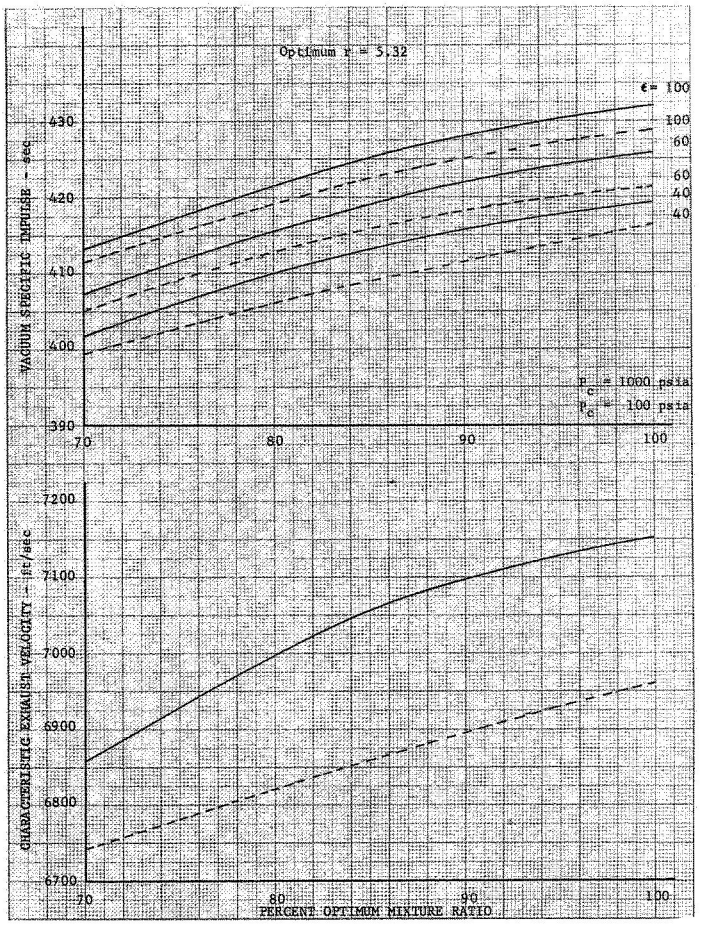


Figure G-2. Theoretical Performance: Flox/55% Methane - 45% Ethane

DF 60410

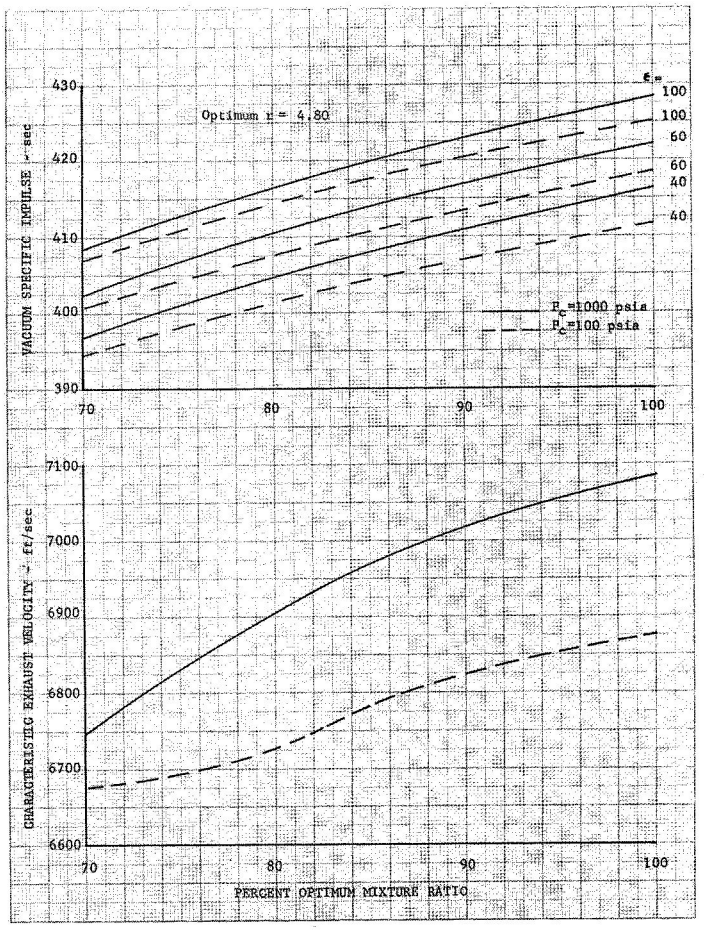


Figure G-3. Theoretical Performance: Flox/Ethane

DF 60411

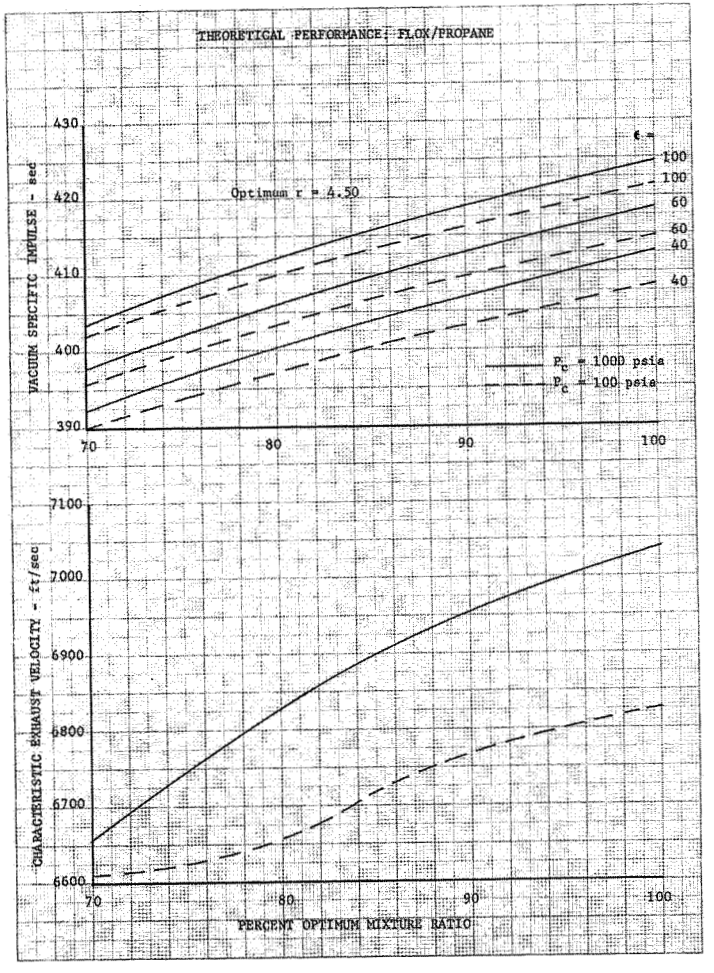


Figure G-4. Theoretical Performance: Flox/Propane

DF 60412

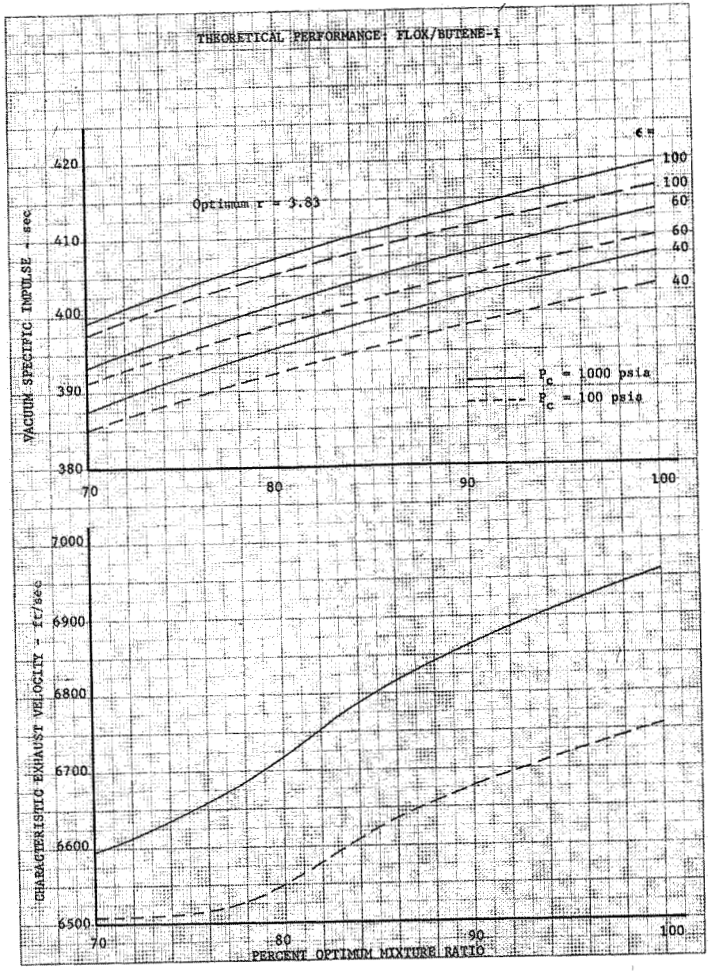


Figure G-5. Theoretical Performance: Flox/Butene-1

DF 60413

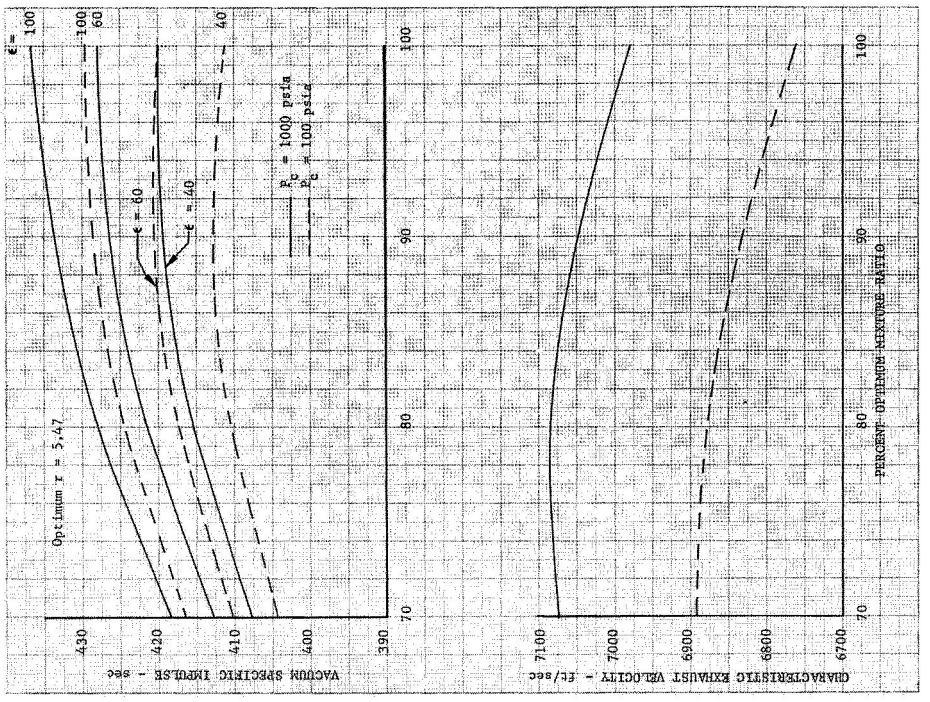


Figure G-7. Theoretical Performance: DF 60415
OF_2/55% Methane - 45% Ethane

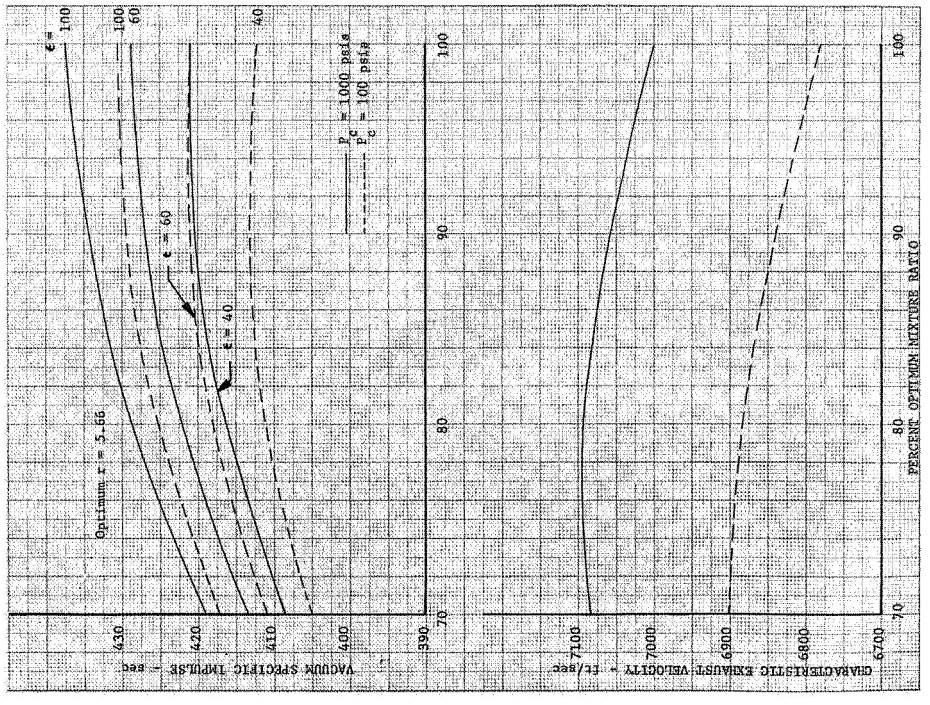


Figure G-6. Theoretical Performance: DF 60414
OF_2/Methane

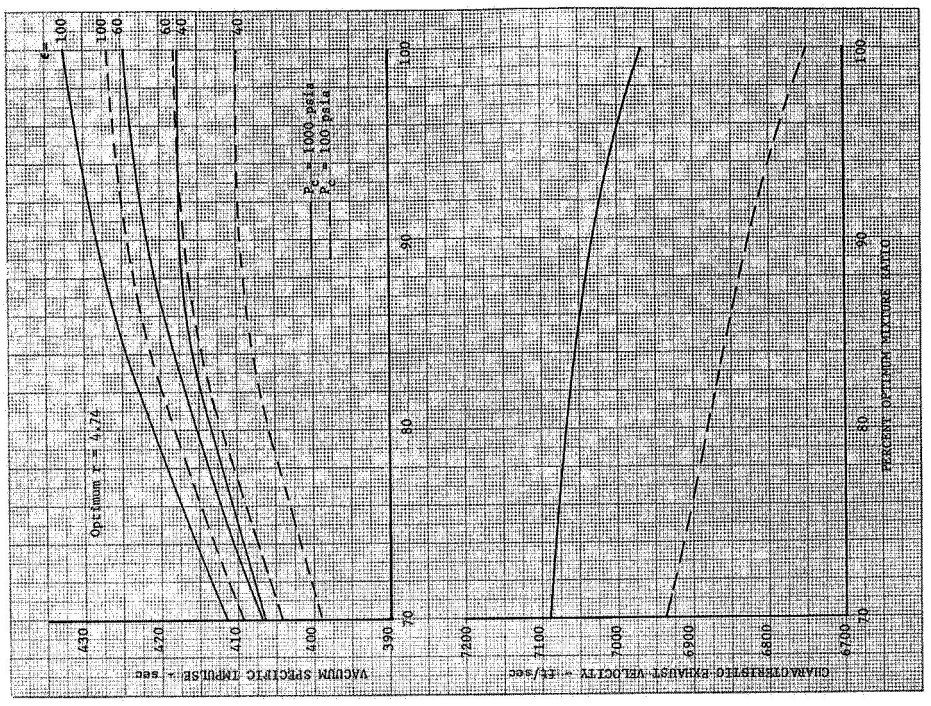


Figure G-9. Theoretical Performance DF 60417
OF_2/Propane

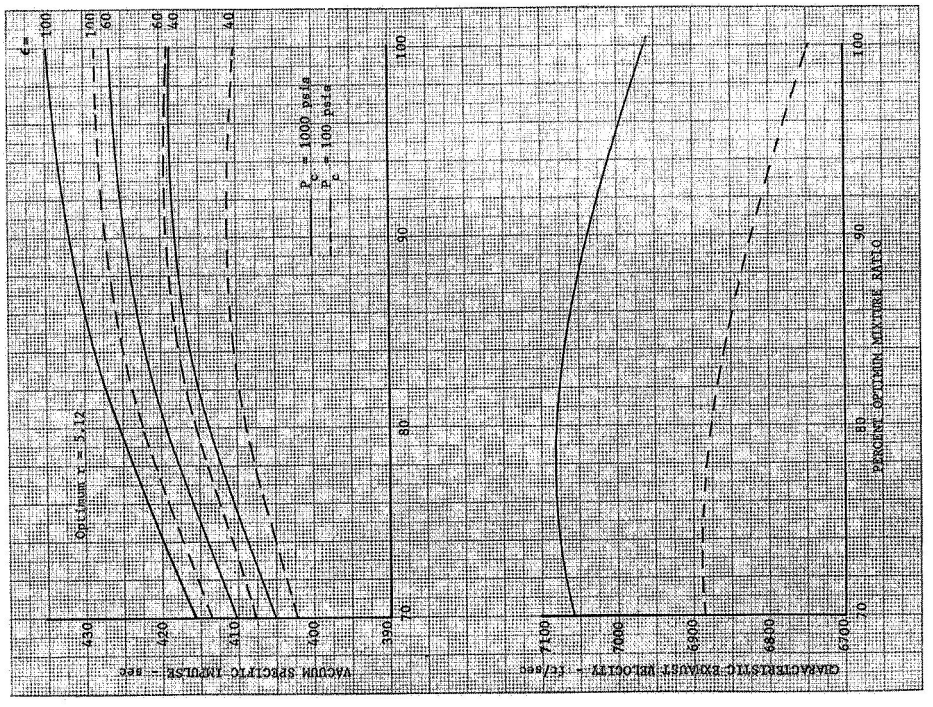


Figure G-8. Theoretical Performance: DF 60416
OF_2/Ethane

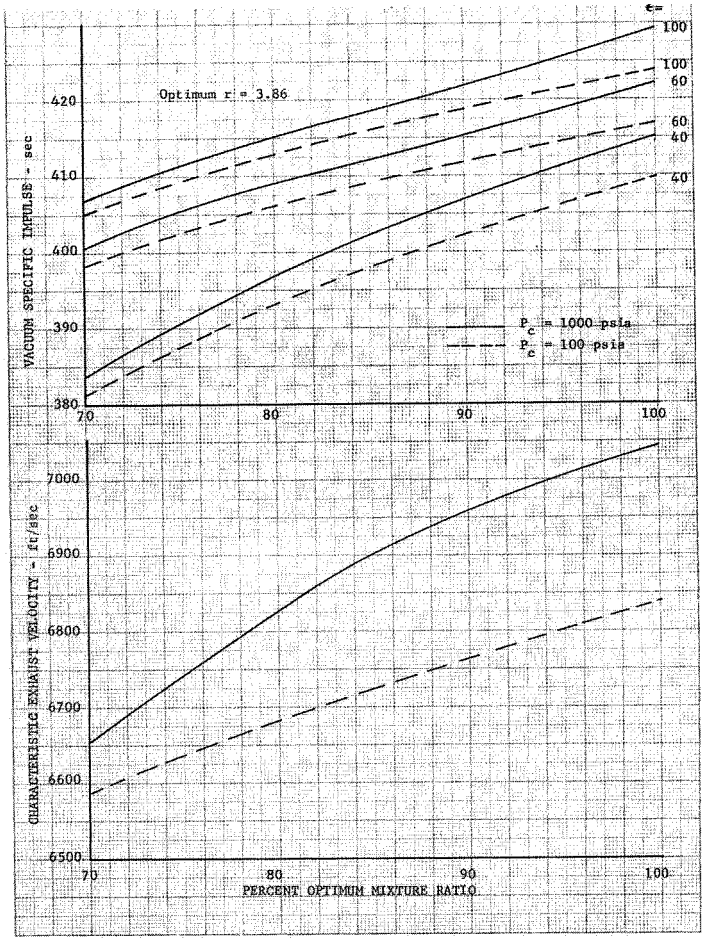


Figure G-10. Theoretical Performance: OF_2/Butene-1 DF 60418

APPENDIX H
DISTRIBUTION LIST FOR INTERIM REPORT NASA CR-72341
CONTRACT NAS3-11190

NASA Lewis Research Center (1)
21000 Brookpark Road
Cleveland, Ohio 44135
Attention: Contracting Officer
MS 500-210

NASA Lewis Research Center (8)
21000 Brookpark Road
Cleveland, Ohio 44135
Attention: Liquid Rocket
Technology Branch
MS 500-209

NASA Lewis Research Center (1)
21000 Brookpark Road
Cleveland, Ohio 44135
Attention: Technical Report Control Office
MS 5-5

NASA Lewis Research Center (1)
21000 Brookpark Road
Cleveland, Ohio 44135
Attention: Technology Utilization Office
MS 3-16

NASA Lewis Research Center (2)
21000 Brookpark Road
Cleveland, Ohio 44135
Attention: AFSC Liaison Office
MS 4-1

NASA Lewis Research Center (2)
21000 Brookpark Road
Cleveland, Ohio 44135
Attention: Library

NASA Lewis Research Center (1)
21000 Brookpark Road
Cleveland, Ohio 44135
Attention: Carl Aukerman
MS 86-1

NASA Lewis Research Center (1)
21000 Brookpark Road
Cleveland, Ohio 44135
Attention: Office of Reliability
& Quality Assurance
MS 500-203

NASA Lewis Research Center (1)
21000 Brookpark Road
Cleveland, Ohio 44135
Attention: Donald L. Nored
MS 500-209

NASA Lewis Research Center (1)
21000 Brookpark Road
Cleveland, Ohio 44135
Attention: E. W. Conrad
MS 100-1

NASA Lewis Research Center (1)
21000 Brookpark Road
Cleveland, Ohio 44135
Attention: W. E. Roberts
MS 3-17

NASA Lewis Research Center (1)
21000 Brookpark Road
Cleveland, Ohio 44135
Attention: Harold Valentine
MS 501-2

NASA (1)
Washington, D. C. 20546
Attention: Code MT

NASA (2)
Washington, D. C. 20546
Attention: RPX

NASA (2)
Washington, D. C. 20546
Attention: RPL

NASA (1)
Washington, D. C. 20546
Attention: SV
Robert F. Schmidt

NASA (1)
Washington, D. C. 20546
Attention: RPX
Frank W. Stephenson, Jr.

Scientific and Technical Informa- (6)
tion Facility
P. O. Box 33
College Park, Maryland 20740
Attention: NASA Representative
Code CRT

NASA Ames Research Center (1)
Moffett Field, California 94035
Attention: Library

NASA Ames Research Center (1)
Moffett Field, California 94035
Attention: C. A. Syvertson

NASA Flight Research Center (1)
P. O. Box 273
Edwards, California 93523
Attention: Library

NASA Goddard Space Flight Center (1)
Greenbelt, Maryland 20771
Attention: Library

NASA Goddard Space Flight Center (1)
Greenbelt, Maryland 20771
Attention: C. R. Gunn
Delta Propulsion Office

NASA John F. Kennedy Space Center (1)
Cocoa Beach, Florida 32931
Attention: Library

NASA John F Kennedy Space Center (1)
Cocoa Beach, Florida 32931
Attention: A. R. Raffaelli

NASA Langley Research Center (1)
Langley Station
Hampton, Virginia 23365
Attention: Library

NASA Manned Spacecraft Center (1)
Houston, Texas 77001
Attention: Library

NASA Manned Spacecraft Center (1)
Houston, Texas 77001
Attention: H. J. Brasseaux
PESD-Propulsion

NASA Manned Spacecraft Center (1)
Houston, Texas 77001
Attention: W. Hammock

NASA George C. Marshall Space (1)
Flight Center
Huntsville, Alabama 35812
Attention: Library

NASA George C. Marshall Space (1)
Flight Center
Huntsville, Alabama 35812
Attention: Keith Chandler,
R-PVE-PA

NASA George C. Marshall Space (1)
Flight Center
Huntsville, Alabama 35812
Attention: Lee W. Jones,
R-PVE-PAS

NASA Western Operations Office (1)
150 Pico Boulevard
Santa Monica, California 90406
Attention: Library

Jet Propulsion Laboratory (1)
4800 Oak Grove Drive
Pasadena, California 91103
Attention: Library

Jet Propulsion Laboratory (1)
4800 Oak Grove Drive
Pasadena, California 91103
Attention: W. B. Powell

Office of the Director of (1)
Defense Research & Engineering
Washington, D. C. 20301
Attention: Dr. H. W. Schulz,
Office of Assistant
Director (Chem.
Technology)

Defense Documentation Center (1)
Cameron Station
Alexandria, Virginia 22314

RTD(RTNP) (1)
Bolling Air Force Base
Washington, D. C. 20332

Arnold Engineering Development Center (1)
Air Force Systems Command
Tullahoma, Tennessee 37389
Attention: AEOIM

Advanced Research Projects Agency (1)
Washington, D. C. 20525
Attention: D. E. Mock

Aeronautical Systems Division (1)
Air Force Systems Command
Wright-Patterson Air Force Base
Dayton, Ohio
Attention: D. L. Schmidt,
Code ASRCNC-2

Air Force Missile Test Center (1)
Patrick Air Force Base, Florida
Attention: L. J. Ullian

Air Force Systems Command (1)
Andrews Air Force Base
Washington, D. C. 20332

Air Force Rocket Propulsion Laboratory (RPR) (1)
Edwards, California 93523

Air Force Rocket Propulsion Laboratory (RPM) (1)
Edwards, California 93523

Air Force Office of Scientific Research (1)
Washington, D. C. 20333
Attention: SREP, Dr. J. F. Masi

U. S. Air Force (1)
Washington 25, D. C.
Attention: Col. C. K. Stambaugh,
Code AFRST

Commanding Officer (1)
U. S. Army Research Office (Durham)
Box CM, Duke Station
Durham, North Carolina 27706

U. S. Army Missile Command (1)
Redstone Scientific Information Center
Redstone Arsenal, Alabama 35808
Attention: Chief, Document Section

U. S. Army Missile Command (1)
Redstone Scientific Information Center
Redstone Arsenal, Alabama 35808
Attention: Dr. W. Wharton

Bureau of Naval Weapons (1)
Department of the Navy
Washington, D. C.
Attention: J. Kay,
Code RTMS-41

Commander (1)
U. S. Naval Missile Center
Point Mugu, California 93041
Attention: Technical Library

Commander (1)
U. S. Naval Ordnance Test Station
China Lake, California 93557
Attention: Code 45

Commander (1)
U. S. Naval Ordnance Test Station
China Lake, California 93557
Attention: Code 753

Commander (1)
U. S. Naval Ordnance Test Station
China Lake, California 93557
Attention: W. F. Thorm,
Code 4562

Commanding Officer (1)
Office of Naval Research
1030 E. Green Street
Pasadena, California 91101

Director (Code 6180) (1)
U. S. Naval Research Laboratory
Washington, D. C. 20390
Attention: H. W. Carhart

Picatinny Arsenal (1)
Dover, New Jersey
Attention: I. Forsten, Chief
Liquid Propulsion
Laboratory

Air Force Aero Propulsion (1)
Laboratory
Research & Technology Division
Air Force Systems Command
United States Air Force
Wright-Patterson AFB, Ohio 45433
Attention: APRP (C. M. Donaldson)

Aerojet-General Corporation (1)
P. O. Box 296
Azusa, California 91703
Attention: Librarian

Aerojet-General Corporation (1)
11711 South Woodruff Avenue
Downey, California 90241
Attention: F. M. West,
Chief Librarian

Aerojet-General Corporation (1)
P. O. Box 1947
Sacramento, California 95809
Attention: Technical Library
2484-2015A

Aerojet-General Corporation (1)
P.O. Box 1947
Sacramento, California 95809
Attention: Dr. C. M. Beighley

Aerojet-General Corporation (1)
P. O. Box 1947
Sacramento, California 95809
Attention: D. T. Bedsole

Aeroprojects, Incorporated (1)
310 East Rosedale Avenue
West Chester, Pennsylvania 19380
Attention: C. D. McKinney

Aerospace Corporation (1)
P. O. Box 95085
Los Angeles, California 90045
Attention: J. G. Wilder,
MS-2293

Aerospace Corporation (1)
P. O. Box 95085
Los Angeles, California 90045
Attention: Library-Documents

Arthur D. Little, Inc. (1)
Acorn Park
Cambridge 40, Massachusetts
Attention: A. C. Tobey

Astropower, Incorporated (1)
Subs. of Douglas Aircraft
Company
2968 Randolph Avenue
Costa Mesa, California
Attention: Dr. George Moc
Director, Research

Astrosystems, Incorporated (1)
1275 Bloomfield Avenue
Caldwell Township, New Jersey
Attention: A. Mendenhall

ARO, Incorporated (1)
Arnold Engineering Development
Center
Arnold AF Station,
Tennessee 37389
Attention: Dr. B. H. Goethert
Chief Scientist

Atlantic Research Corporation (1)
Shirley Highway & Edsall Road
Alexandria, Virginia 22314
Attention: A. Scurlock

Atlantic Research Corporation (1)
Shirley Highway & Edsall Road
Alexandria, Virginia 22314
Attention: Security Office
for Library

Battelle Memorial Institute (1)
505 King Avenue
Columbus, Ohio 43201
Attention: Report Library,
Room 6A

Beech Aircraft Corporation (1)
Boulder Facility
Box 631
Boulder, Colorado
Attention: J. H. Rodgers

Bell Aerosystems, Inc. (1)
Box 1
Buffalo, New York 14205
Attention: T. Reinhardt

Bell Aerosystems, Inc. (1)
Box 1
Buffalo, New York 14205
Attention: W. M. Smith

Bendix Systems Division (1)
Bendix Corporation
Ann Arbor, Michigan
Attention: John M. Bureger

The Boeing Company (1)
Aero Space Division
P. O. Box 3707
Seattle, Washington 98124
Attention: Ruth E. Peerenboom
(1190)

The Boeing Company (1)
Aero Space Division
P. O. Box 3707
Seattle, Washington 98124
Attention: J. D. Alexander

Chemical Propulsion Information (1)
Agency
Applied Physics Laboratory
8621 Georgia Avenue
Silver Spring, Maryland 20910

Chrysler Corporation (1)
Missile Division
Warren, Michigan
Attention: John Gates

Chrysler Corporation (1)
Space Division
New Orleans, Louisiana
Attention: Librarian

Curtiss-Wright Corporation (1)
Wright Aeronautical Division
Woodridge, New Jersey
Attention: G. Kelley

University of Denver (1)
Denver Research Institute
P. O. Box 10127
Denver, Colorado 80210
Attention: Security Office

Douglas Aircraft Company, Inc. (1)
Santa Monica Division
3000 Ocean Park Blvd.,
Santa Monica, California 90405
Attention: J. L. Waisman

Douglas Aircraft Company, Inc. (1)
Santa Monica Division
3000 Ocean Park Blvd.,
Santa Monica, California 90405
Attention: R. W. Hallet

Douglas Aircraft Company, Inc. (1)
Santa Monica Division
3000 Ocean Park Blvd.,
Santa Monica, California 90405
Attention: G. W. Burge

General Dynamics/Astronautics (1)
P. O. Box 1128
San Diego, California 92112
Attention: F. Dore

General Dynamics/Astronautics (1)
P. O. Box 1128
San Diego, California 92112
Attention: Library & Information Services
(128-00)

Convair Division (1)
General Dynamics Corporation
P. O. Box 1128
San Diego, California 92112
Attention: Mr. W. Fenning
entaur Resident
Project Office

General Electric Company (1)
Re-Entry Systems Dept.
P. O. Box 8555
Philadelphia, Pennsylvania 19101
Attention: F. E. Schultz

General Electric Company (1)
Flight Propulsion Lab Dept.
Cincinnati 15, Ohio
Attention: D. Suichu

Grumman Aircraft Engineering (1)
Corporation
Bethpage, Long Island, New York
Attention: Joseph Gavin

Hercules Powder Company (1)
Allegheny Ballistics Laboratory
P. O. Box 210
Cumberland, Maryland 21501
Attention: Library

IIT Research Institute (1)
Technology Center
Chicago, Illinois 60616
Attention: Library

Kidde Aero-Space Division (1)
Walter Kidde & Company, Inc.
675 Main Street
Belleville 9, New Jersey
Attention: R. J. Hanville,
Director of Research
Engineering

Lockheed Missiles & Space (1)
Company
P. O. Box 504
Sunnyvale, California
Attention: Y. C. Lee,
Power Systems R&D

Lockheed Missiles & Space (1)
Company
P. O. Box 504
Sunnyvale, California
Attention: Technical Information
Center

Lockheed-California Company (1)
10445 Glen Oaks Blvd.,
Pacoima, California
Attention: G. D. Brewer

Lockheed Propulsion Company (1)
P. O. Box 111
Redlands, California 92374
Attention: Miss Belle Berlad,
Librarian

Lockheed Missiles & Space (1)
Company
Propulsion Engineering Division
(D.55-11)
1111 Lockheed Way
Sunnyvale, California 94087

Marquardt Corporation (1)
16555 Saticoy Street
Box 2013 - South Annex
Van Nuys, California 91404
Attention: Librarian

Marquardt Corporation (1)
16555 Saticoy Street
Box 2013 - South Annex
Van Nuys, California 91404
Attention: W. D. Boardman, Jr.

Martin-Marietta Corporation (1)
Martin Division
Baltimore 3, Maryland
Attention: John Calathes
(3214)

McDonnell Aircraft Corporation (1)
P. O. Box 6101
Lambert Field, Missouri
Attention: R. A. Herzmark

North American Aviation, Inc. (1)
Space & Information Systems
Division
12214 Lakewood Boulevard
Downey, California 90242
Attention: Technical Information
Center,
D/096-722 (AJ01)

North American Aviation, Inc. (1)
Space & Information Systems
Division
12214 Lakewood Boulevard
Downey, California 90242
Attention: H. Storms

Northrop Space Laboratories (1)
1001 East Broadway
Hawthorne, California
Attention: Dr. William Howard

Purdue University (1)
Lafayette, Indiana 47907
Attention: Technical Librarian

Radio Corporation of America (1)
Astro-Electronics Division
Defense Electronic Products
Princeton, New Jersey
Attention: S. Fairweather

Republic Aviation Corporation (1)
Farmingdale, Long Island
New York
Attention: Dr. William O'Donnell

Rocket Research Corporation (1)
520 South Portland Street
Seattle, Washington 98108

Rocketdyne Division of (1)
North American Aviation, Inc.
6633 Canoga Avenue
Canoga Park, California 91304
Attention: Library,
Department 596-306

Rocketdyne Division of
North American Aviation, Inc. (1)
6633 Canoga Avenue
Canoga Park, California 91304
Attention: R. P. Pauckert

Rocketdyne Division of
North American Aviation, Inc.
6633 Canoga Avenue
Canoga Park, California 91304 (1)
Attention: E. V. Zettle

Rohm and Haas Company
Redstone Arsenal Research
Division
Huntsville, Alabama 35808 (1)
Attention: Librarian

Space-General Corporation
777 Flower Street
Glendale, California
Attention: C. E. Roth (1)

Stanford Research Institute
333 Ravenswood Avenue
Menlo Park, California 94025 (1)
Attention: Thor Smith

Texaco Experiment, Incorporated
P. O. Box 1-T
Richmond, Virginia 23202 (1)
Attention: E. B. Monteath

Texaco Experiment, Incorporated
P. O. Box 1-T
Richmond, Virginia 23202 (1)
Attention: Librarian

Thiokol Chemical Corporation
Reaction Motors Division
Denville, New Jersey 07834 (1)
Attention: A. Sherman

Thiokol Chemical Corporation (1)
Reaction Motors Division
Denville, New Jersey 07834
Attention: Librarian

Thiokol Chemical Corporation (1)
Alpha Division, Huntsville Plant
Huntsville, Alabama 35800
Attention: Technical Director

Thiokol Chemical Corporation (1)
Redstone Division
Huntsville, Alabama (1)
Attention: John Goodloe

TRW Systems, Incorporated (1)
1 Space Park
Redondo Beach, California 90200 (1)
Attention: G. W. Elverum

TRW Systems, Incorporated (1)
1 Space Park
Redondo Beach, California 90200
Attention: STL Tech. Lib. Doc. (1)
Acquisitions

TRW, Incorporated (1)
TAPCO Division
23555 Euclid Avenue
Cleveland, Ohio 44117 (1)
Attention: P. T. Angell

United Aircraft Corporation (1)
Corporation Library
400 Main Street (1)
East Hartford, Connecticut 06118
Attention: Dr. David Rix

United Aircraft Corporation (1)
Corporation Library (1)
400 Main Street
East Hartford, Connecticut 06118
Attention: Erle Martin

United Aircraft Corporation (1)
United Technology Center
P. O. Box 358
Sunnyvale, California 94088
Attention: Librarian (1)

Vought Astronautics (1)
Box 5907
Dallas 22, Texas
Attention: Warren C. Trent

Commander (1)
Office of Research Analysis (OAR)
Attention: RRRD
Holloman AFB,
N. M. 88330

Union Carbide Corporation (1)
Nuclear Division
ORGDP Records Department
P.O. Box P
Oak Ridge, Tennessee 37830
Attention: A. P. Huber,
Superintendent
Technical Division
ORGDP

Aeronutronic Division of (1)
Philco Corporation
Ford Road
Newport Beach, California 92600
Attention: Dr. L. H. Linder,
Manager
Technical Information
Department

Aerospace Corporation (1)
2350 East El Segundo Blvd
El Segundo, California 90045
Attention: Toru Iura
Applied Mechanics Div